Issues with the delivery of power quality in wind farms

A THESIS SUBMITTED TO

FACULTY OF ENGINEERING AND INFORMATION TECHNOLOGY

OF UNIVERSITY OF TECHNOLOGY SYDNEY

FOR THE DEGREE OF

DOCTOR OF PHILOSOPHY

Massood Keshavarz Siahpoosh

May 2019

CERTIFICATE OF ORIGINAL AUTHORSHIP

This thesis is the result of a research candidature conducted jointly with another University as part of a collaborative Doctoral degree. I certify that the work in this thesis has not previously been submitted for a degree nor has it been submitted as part of requirements for a degree except as part of the collaborative doctoral degree and/or fully acknowledged within the text.

I also certify that the thesis has been written by me. Any help that I have received in my research work and the preparation of the thesis itself has been acknowledged. In addition, I certify that all information sources and literature used are indicated in the thesis.

Signature of Student:

Production Note:
Signature removed prior to publication.

Massood Keshavarz Siahpoosh

Date: 12/05/2019

Acknowledgements

This thesis is a culmination of a perfect working relationship with my university supervisors, Dave Dorrell and Li Li and my mentor in Aurecon Company Jeffery Russell that I am eternally grateful to. Dave, Li and Jeff provided unreserved support during my PhD and generously guided me during my research development.

I am also greatly in debt to the Safe Engineering Services for CDEGS software, Power Analytics for Paladin design base software, Manitoba HVDC Research Centre for PSCAD -EMTDC software and EATON for CYMCAP software who have provided me student licence and support during my simulation and enquires.

This research is not entirely a mathematical theory or study. This research is based on actual constructed equipment and components used in wind farms. I have endeavoured to include lessons learnt from several years of construction in wind farms; all the hard work of engineers in this research therefore many people have contributed in this study so I want to thank many people who in some way contributed to the progress and research of the work contained herein.

Last but not the least is the unconditional love and encouragement provided by my wife Maryam and my two beautiful kids Ariana and Aaron who served as a secure anchor during the hard and easy times.

Thank you.

Massood

Table of Contents

Abbreviation

Abbreviation	Description
AC	Alternating Current
AEMO	Australian Energy Market Operator
ASIG	Asynchronous induction generators
CDEGS	Current Distribution, Electromagnetic Fields, Grounding and Soil Structure Analysis
CIT	Current Injection Test
DC	Direct Current
DFIG	Doubly Fed Induction Generator
EPR	Earth Potential Rise
GMR	Geometric Mean Radius
HIFREQ	CDEGS software module for electromagnetic field analysis
HV	High Voltage
LFI	Low Frequency Induction
LPS	Lightning Protection System
LV	Low Voltage
MV	Medium Voltage
NER	Australian Nation Electricity Rules
NSP	Network Service Provider
PCC	Point of Common Coupling
RSM	Rolling Sphere Method
SS	Substation
STTM	Short Term Trading Market
ZEST	Zigzag Switchgear Earth Transformer

List of Figures

List of Tables

Abstract

Wind farms are designed to harvest wind kinetic energy; however, their generated power is dependent on their wind streams, and therefore their operation can impact system stability. Unlike conventional steams (gas or hydro power stations), wind farms normally require vast areas and MV distribution networks to collect generated power from each wind turbine and transfer it to a point of common coupling. Scattered wind turbines with variable generated power and long cable runs or aerial lines can create some power quality issues such as flicker, transients, voltage sags, frequency fluctuation, power factor and voltage fluctuations. Most wind turbines have large power electronic converters to complete the power conversion. Power electronic converters can create harmonics and commutation notches. These aspects are known as power quality issues.

Power quality issues are important because generated power from wind farms should be connected to a power grid to be delivered to the end user. To connect and operate wind farms, the generated power by wind farms should meet network service provider (NSP) and national codes. In Australia, the Australian Energy Market Operator (AEMO) defines nationwide power quality requirements for power stations including wind farms.

In this research the intention is to use real data extracted from established wind farms to assess turbines and power network operation. Real data are used as inputs for software simulation and power quality assessment for steady state and transient conditions. The following software is used:

- EDSA-Paladin software is used for detailed power system analysis, fault condition assessment and harmonic assessment.
- PSCAD-EMTDC software is used for wind farm steady state and transient operation assessment including turbine behaviour during the fault and inrush current (during turbine start –up).

During the analysis most of the power distribution components are modelled. The cable impedances including capacitance of cables are included in the power system analysis for both steady state and transient condition assessment.

Some manual calculation methods are proposed to calculate some of the power quality aspects such as flicker, fault levels and commutation notches. Manual calculations are used to validate software simulation as well.

The transient operation of a wind farm power distribution system is another important topic which is assessed in this research. Ferroresonance can be critical during wind turbine switching or fault conditions. This results in ferroresonant harmonics and overvoltages in the system.

The ferroresonance does not have a linear nature; therefore, it cannot be predicted by analytical methods. PSCAD-EMTDC software is used to analyse the behaviour of a wind farm power network in ferroresonant states. Results prove that ferroresonance is a function of the network components, specifically the length of cables and transmission lines. A detailed study should be conducted during the design stage prior to system installation.

The earthing system of a wind turbine and its interconnection can play an important role in wind farm power system failure. The settings of protection relays should be selected with respect to human and farm animal safety and equipment protection. In this research the following issues are discussed, and improved methods are presented:

- Soil resistivity test;
- Lightning protection system analysis;
- Lightning strikes earth potential rise;
- Earth fault analysis; and
- Current injection test.

To conclude this research some of the issues which have resulted in voltage sag, interruption, turbine failure and wind farm outage are presented with root cause analysis discussions.

This research is an attempt to assess different wind farm components and fundamental considerations which should be considered during planning, design, construction and operation in order to minimize power quality issues. The state of problems has been provided in Section 1-2 of this thesis.

This research brings together several analysis techniques and real wind farm scenarios to address power quality issues. Claims are made to originality in terms of bringing together several studies to get an overall power quality assessment of a wind farm and claims are made for some new techniques. These claims are summarized in Section 1-3 of this thesis and made for work in Chapters 2 and 3.

Chapter 1: Introduction

1.1 Introduction

This research addresses quality issues with the delivery of power from wind farms. Wind farms are more popular today and are part of the power system development plans in most countries. They are one of the main renewable energy assets with low-carbon emission and economic viability. A wind farm normally has a large foot print and requires a dispersed distribution system to collect generated power from each wind turbine. The generated power from a wind turbine is dependent on the wind stream which is very variable; therefore, wind farm operation as a part of a power system requires power quality consideration.

As the worldwide popularity of wind energy increases, several problems began to immerge concerning the behaviour of a wind turbine during both steady state and transient conditions, which directly affects grid stability. As an example, after South Australia's major blackout event which occurred at 16:18 on Wednesday 28 September 2016, where a severe storm caused wind farms to be disconnected from the electricity network, wind farms were blamed in the first instance. Preliminarily investigations revealed that high winds, thunderstorms, lightning strikes, hail, and heavy rainfall resulted in multiple transmission system faults. In the two minutes between 16:16 and 16:18, system faults caused loss of three major 275 kV transmission lines north of Adelaide. Generation initially rode through the faults, but at 16:18, following an extensive number of faults in a short period of time, 315 MW of wind generation disconnected (one group at 16:18:09, a second group at 16:18:15). The uncontrolled reduction in generation resulted in increased flow on the main Victorian interconnector (Heywood) to make up the deficit. This resulted in the Heywood Interconnector overloading. To avoid damage to the interconnector, the automatic-protection mechanism activated, tripping the interconnector. In this event, this resulted in the remaining customer load and electricity generation in SA being lost (referred to as a system blackout). This automatic protection operated in less than half a second at 16:18. The event resulted in the SA regional electricity market being suspended [51].

These types of events led to grid operators in many countries to review their system stability assessments at the interconnection of wind farms with the network. This was to ensure the stability of their network in both steady state and transient conditions remains intact. There are different guidelines and grid code requirements in different parts of the world, but they have common aims: to permit the development, maintenance and operation of a coordinated, reliable and economical transmission and distribution system. Some of the grid code requirements are assessed in this

work. A detailed wind farm power system analysis is presented in Chapter Two. Different parts of a wind farm power network are considered, and the system interactions are assessed.

Unlike conventional steam, gas or hydro power generation stations, wind farms consist of many scattered turbines which are spread over a considerable area. They are generally up to only 2 or 3 MW in size, so this will result in a MV distribution system in the form of underground cables or overhead lines or combination of both. Therefore, wind farm power system behaviour will be impacted by turbine interconnection methods and characteristics. Accordingly, transmission lines or cables play a major role in the network stability in both steady state and transient conditions since these dictate the system impedances. Long cable runs between generators make wind farm power system analysis more complicated. Transmission line or cable impedances are functions of physical configuration, load current, and soil thermal and electrical resistivity. These should be considered in wind farm power analysis. This is a topic which has not been previously investigated in depth. They are is presented in this research for power quality assessment. A brief discussion about how these characteristics should be considered for wind farm power quality is presented here. Multi-core MV cables are usually used for turbine tower base connections (with a voltage range of 11 kV to 33 kV). Cable impedances including cable capacitance should be considered in steady-state and transient power system analyses (refer to Table 2-5 for 33 kV cable characteristics). This analysis cannot be done with manual calculation for a large wind farm; therefore, a power system analyser software package is used in this research for analysis. The following software is used in this research for wind farm power quality assessment for steady state and transient conditions:

- EDSA-Paladin software is used for detailed power system analysis, fault condition assessment, flicker and harmonic assessment; and
- PSCAD-EMTDC software is used for wind farm steady state and transient operation assessment including turbine behaviour during the fault and inrush current (during turbine start-up).

In Chapter Two wind turbine fundamentals are discussed. Wind turbine types are defined according to the Australian Energy Market Operator (AEMO) and different generators and associated technologies are summarized:

Case Study 1: Doubly Fed Induction Generators (DFIGs).

Case Study 2: Asynchronous induction generators with external variable resistor and Doubly Fed Induction Generators (ASIGs and DFIGs).

The DFIG is a common choice for multi-MW wind turbines due to their long life, rigid structure, variable speed operation, and active and reactive power control ability [12]. The rotor of a DFIG is connected via slip rings to a converter that is formed from back-to-back 3-phase pulse wave modulation (PWM) inverters. This converter allows bi-directional power flow and it can control the reactive power to the machine to control its excitation, and the generation or absorption of reactive power. They have been used in many wind farms over several decades including the types presented in Case Studies 1 and 2. Therefore, DFIG is discussed in section two of this research briefly. The term "doubly-fed" reflects the fact that the stator voltage is applied from the grid via a transformer, whereas the rotor voltage is controlled by a bi-directional electronic converter fed from the grid. This converter will handle up to about 25 % of the total generator power. When operating subsynchronously, power flows into the rotor and out of the stator with the power amplified across the airgap so that there is net generation. At higher wind speeds the generator operates super-synchronously and electrical power flows out of both the stator and rotor.

Case Study 1 (DFIG) is an existing wind farm although the turbine and wind farm details are restricted due to commercial-in-confidence issues. Therefore, the parameters and turbine number have been modified here though they still reflect a realistic case. Case Study 2 (DFIG) is presented in this research to address details which cannot be revealed from Case Study 1. Both wind farms have 690 V wind turbines with 690 V / 33 kV tower base transformers. It is assumed that wind farm Case Study 1 is connected to a 330 kV transmission line via a step-up substation. It is assumed that wind farm Case Study 2 is connected to a 132 kV transmission line via a step-up substation.

In Chapter Two, the power systems of wind farm Case Studies 1 and 2 were modelled in Paladin software for load flow using the Fast Decoupled Newton Raphson method. This includes short circuit and transient analyses. The fault level of Case Study 2 was calculated manually to validate the software simulation. This practice can be included in technical guidelines and standards.

The load flow and power quality of wind farm Case Studies 1 and 2 were conducted considering the following:

- 3 phase fault level at each bus bar or specific equipment.
- Phase-to-earth fault level at each bus bar or specific equipment (the 33 kV system has delta winding transformer. A zig-zag transformer was used to provide a low zero-sequence impedance and high positive and negative sequence impedances to fault currents [20].
- Power factor analysis.

- Voltage fluctuation in different locations of system.
- Cable loading.

The analysis of the Case Study 1 system during significant network load variation and busbar fault is simulated for voltage and frequency at the point of common coupling (PCC). The wind turbine generator is analysed using a DFIG generator dynamic model.

The power quality aspects in actual wind farms are under investigation which is reflected in standards and guidelines. In this work aspects of power quality are simulated to study how a wind farm can be integrated smoothly into power grid. Firstly, the Australian Nation Electricity Rules (NER) for wind farm power quality assessment are briefly discusses. These cover the planning stage to the actual wind farm operation. The Australian Energy Market Operator (AEMO) and the Network Service Providers (NSPs) assess the proposed wind farm performance standards against the technical requirements and need to be satisfied with the levels of performance.

After discussion regarding the network access level and expected emission level by the AEMO and NSPs, the following main power quality issues for wind farm Case Study 2 are conducted using Paladin software and PSCAD software:

- Harmonics;
- Flicker;
- Unbalance;
- Voltage fluctuations;
- Wind gust impact on voltage;
- Transient analysis and ferroresonance; and
- Interruption.

The harmonic emission levels of Case Study 2 are assessed for two different types of wind turbines (ASIG and DFIG). DFIGs and asynchronous generators with an external variable resistor are simulated for comparison in terms of their harmonic emission. The comparison and analysis of two different turbines is an area that can be studied more.

Flicker simulation for wind farms is not defined clearly in standards and other resources; therefore, a manual calculation method is presented in this work which is developed from existing standards and guidelines.

Voltage unbalance and commutation notch issues as well as the simulation methods are presented in this thesis. It is then proposed to mitigate these power quality issues.

System fault ride through (FRT) and short voltage dip for Case Study 2 with respect to the system protection relay configuration, online tap changer (OLTC) response time, and wind farm

behaviour, for the following operation scenarios, are simulated using Paladin software in order to analyse the reliability of system:

- Steady state response of the network; and
- Dynamic response of the network.

In the last section of Chapter Two, Case Study 2 and the connected sub-transmission system are modelled in PSCAD for transient analysis and ferroresonance assessment. The wind turbine operation during low wind speed (cut-in speed and turbine group starting) has the most concern in terms of the understanding of ferroresonance which could be excited under these conditions. Therefore, modelling is undertaken using PSCAD/EMTDC software.

In Chapter 3 the wind turbine lightning and earthing system is briefly discussed. The earthing and lightning protection system defines the earth fault clearance times and interruptions. The protection setting of each wind turbine is related to the earthing system total impedance. The following topics are discussed in Chapter 3:

- Soil resistivity test;
- Lightning protection system analysis;
- Lightning strike earth potential rise;
- Earth fault analysis; and
- Current injection test.

An actual soil resistance test is conducted in this work. The test results are interpreted according to IEEE standard guidelines.

The lightning protection system for a wind turbine is briefly discussed. Lightning strike conditions are simulated using the inverse Fourier transformation method with strike frequency analysis. The lightning strike earth potential rise is simulated.

Following on from the lightning strike simulations, the step and touch voltage calculation for humans and farm animals is discussed. The farm animal safe voltage limits calculation method is presented along with the earth fault analysis at a wind turbine tower base. This is new work since usually only human safe voltage limits are addressed.

In Chapter 4 wind turbine failures related to operation and construction issues are discussed. The purpose of this section is to highlight issues which can create interruptions in power supply in wind farm networks.

1.2 Statement of Problem

This research is an attempt to assess different wind farm components and fundamental considerations which should be considered during planning, design, construction and operation in order to minimize power quality issues. The highlighted issues in this research can be used by a designer at the planning and detailed design stage to improve system power quality and reliability. Following aspects can be considered as problems topics:

1. The impact of an actual constructed power distribution system on power system parameters such as impact of soil characteristics on system impedances. By including realistic system data, and data taken from measurement, this emphasises the validity of the system simulation.
2. Wind farm power system analysis using the Newton-Raphson method and proposed validation method by manual calculation.
3. Fault analysis and impact of faults on the wind farm power system.
4. Wind farm power quality requirements from the national power system operator.
5. Wind farm power quality aspects for normal operation, and turbine switching transient and during fault scenarios.
6. Wind farm ride through assessment.
7. Wind farm frequency fluctuation requirement based on Australian and international requirements.
8. Wind turbine generator behaviour during fault conditions.
9. Wind farms soil resistivity tests.
10. Wind turbine lightning impact analysis and turbine high frequency response.
11. Safe step and touch voltage for wind turbines including human and animals.
12. In service wind farm failures and root cause analysis.
13. Ferroresonance issues are addressed when fault conditions occur in the simulations and these are investigated to see if it makes a contribution to poor power quality.

The issues raised in this research are based on fundamental aspects and are continuing issues. This research can be used as a guideline for system engineering and can be considered as a revision to the existing engineering practice, power quality assessment and earthing system design.

1.3 Claims to Originality

This work brings together several analysis techniques and real wind farm scenarios to address power quality issues. Claims are made to originality in terms of bringing together several studies

to get an overall power quality assessment of a wind farm and claims are made for some new techniques. These claims are made for work in Chapters 2 and 3.

Chapter 2

This thesis investigates two types of wind turbines; these are assessed for load flow and power quality aspects. Case Study 1 (DFIG) and Case Study 2 (DFIG + ASIG) are simulated using actual wind farm components for the turbines in terms of the transient and sub-transient impedances and interaction between the underground cables in terms of both positive and negative sequence MV cable impedances in respect to the power quality issues in various locations of wind farm turbines. This level of detailed study is not presented in most existing studies.

Consideration of the Zigzag Switchgear Earth Transformer (ZSET) to provide star point (neutral connection) for an ungrounded 3-phase system to permit the grounding of that neutral to an earth reference point and harmonic mitigation application to suppress triplet (3rd, 9th, 15th and 21st) harmonic currents is not presented in existing studies to the author's knowledge.

Based on this study simulation results the voltage and frequency of the point of common coupling (PCC) can change due to the DFIG generators dynamic response in the event of significant network load variation or fault situations. This can be used for fault ride through (FRT) assessment to prevent nuisance outage same as South Australia's major blackout event. The validation method presented in this research can be used to validate software simulation and models.

In this research, one week with significant wind speed values, between 4 and 11 m/s, was selected. The flicker simulation results indicate that generated flicker, when all eight wind turbines start at the same time at cut-in wind speed, is not acceptable according to IEC and local service provider standards. However, it is very unlikely to have the same wind stream simultaneously hitting wind turbines which are scattered across the field. This gives an insight into possible issues related to flicker.

Wind farm behaviour for the following operation scenarios is assessed to ensure reliability of system:

- Steady-state response of network; and
- Dynamic response of network.

The voltage drop (for the continuous operation) is assessed for peak load and low summer and winter loads. This dept of analysis assessment appears not to be available in the existing published studies. The following assessments are included:

- Voltages over 110 % for the durations permitted under clause S5.1a.4 NER (refer to Figure 2-60 later);

- 90 % to 110 % of normal voltage continuously;
- 80 % to 90 % of normal voltage for a period of at least 10 s; and
- 70 % to 80 % of normal voltage for a period of at least 2 s.

Experience leads to the identification of specific practical scenarios in which ferroresonance should be considered. Wind farm Case Study 2 and the sub-transmission system are modelled in PSCAD for transient analysis and ferroresonance assessment. The wind turbine operation during low wind speed has the most concern in order to understand if ferroresonance can be excited, therefore modelling is undertaken using PSCAD/EMTDC software. Different fault scenarios are assessed. Based on assessments, the fault on the MV system are reflected on to the 132 kV side of the step-up transformer with over voltage, current and power waves. This shows signs of ferroresonance. This is a specific assessment is not common in this type of study.

Chapter 3

The common method for soil electrical measurement is the equally-spaced Wenner-Array method. In this research a few methods are proposed to validate the software simulation results.

As a case study, more than 50 wind turbine foundations are modelled in the software with a site-specific soil model. For lightning transient analysis, the turbines blades, nacelle and mast are modelled using lightning protection zone 1 (LPZ1) and zone 2 (LPZ2) according to IEC TR 61400-24: 2002 [46] and Australian standard AS/NZS 1768:2007 [47] requirements. Lightning shielding protection systems are analysed. Accordingly, the rolling sphere method (RSM) with a strike distance of 45 m is applied to the model and the results are presented in Figure 3-18 which indicates that the embedded lightning protection conductors on the blades and the lightning protection air terminals of the wind turbine can protect the wind turbine nacelle and tower base transformer from direct lightning contact. This type of assessment is not presented in similar studies.

The performance of a wind turbine earthing system is analysed when a lightning stroke current waveform with a maximum of 30 kA peak (as recommended in Table 1 of IEC 61400-24) strikes the turbine. The lighting strike frequency curves are used for the wind turbine with an inverse Fourier transformation simulation and the responses are presented. The time domain response of the wind turbine strike at the soil surface away from the turbine as well as the centre of the tower time domain are presented. The time domain response of the scalar potential rise along the turbine blades and turbine base is presented in Figure 3-23. This type of simulation is not presented in similar studies.

The IEC60479.1 method is used to calculate a prospective humans touch potential considering the top-layer resistivity and mutual impedance between parallel feet (including the surface layer

reduction factor C_s). The IEEE 80 method is used for person step voltage calculations. Since the IEC 60479.1 values are mainly based on experiments with animals as well as information available from clinical observations (only a few experiments with shock currents of short duration have been carried out on live human beings). The impedances used for human bodies are obtained from the calculation of the prospective body resistances of farm animals. These determine the safe limit of the resulting body current. Using similar values for the human safe limit calculations, the allowable body current limit method is used for step and touch voltage calculations. This a new study in terms of its completeness.

An earth potential rise comparison is made between a wind farm with several turbines and MV cable interconnection only using additional bare conductors alongside the HV cables. The simulation indicates that the earth potential rise can be reduced significantly using additional bare conductors alongside the HV cables. This type of comparison is not presented in other studies. A Current Injection Test (CIT) method is proposed to validate the simulation results as a part of this study.

Chapter 2: Wind Farm Power Quality

2.1 Introduction

In this chapter the power distribution systems of two wind farms (Case Studies 1 and 2) are discussed and simulated. These two wind farms will be referred to as Case Studies since they should remain anonymous. The purpose of this chapter is to assess the power quality issues and actual generated power of each Case Study. The limitations of the power quality at the Point of Common Coupling (PCC are assessed for different operation scenarios and compared with IEC standard limits and Australian Energy Market Operator (AEMO) limits.

Both wind farms have variable wind speed turbines which utilize DFIGs. The power quality issues for system operation during short circuits, earth faults and wind fluctuation are assessed. The power distribution system of both wind farms consists of 33 kV / 690 V transformers and 33 kV underground cables and overhead lines. Since some components, such as the DFIGs and underground cables, directly affect the power quality of the entire system, they are discussed in detail. The outcomes of this chapter can be summarised as:

- Power quality aspects in various locations of existing wind farms;
- Transient assessment of turbines on system power quality delivery;
- Assessment of fundamental improvement (the impact of different system reticulation such as usage of underground and above ground installation); and
- Load flow aspects.

2.2 Wind Turbine Fundamentals

Prior to examining the behaviour of Case Studies 1 (DFIG) and 2 (ASIG and DFIG), the following discussions are presented to summarize the differences between the wind turbines, particularly in terms of the electrical generation. In general, turbines can be divided into two groups: fixed speed and variable speed turbines. However, the Australian Energy Market Operator (AEMO), which defines the power quality requirements, has divided wind turbines into four types [30].

2.2.1 Fixed Speed Wind Turbine Generator (Type 1)

Fixed speed wind turbines use squirrel-cage induction generators (SCIGs), for conversion of the mechanical energy extracted from the wind into electrical energy. All grid-connected wind

turbines, from the first in 1939 until the development of variable-speed grid-connected wind turbines in the 1970s, were fixed-speed wind turbines [10]. The simplicity, toughness and their relative cost-effectiveness are the main advantages of fixed speed SCIG wind turbines. The arrangement is shown in Figure 2-1. These generators are generally run at close to unity power factor, so that the reactive power flow at the turbine LV transformer terminals is almost zero. These generators require reactive power to support the field so that capacitors are used to provide the VARs and an additional dynamic reactive support plant is often installed at the wind farm collection grid to enable the wind farm to meet technical performance requirements.

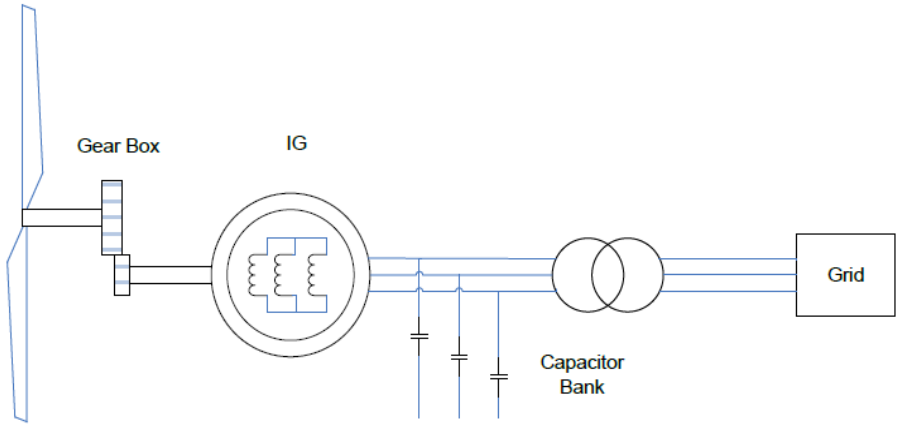

Figure 2-1: Schematic diagram of Type 1 wind turbine generator [32].

2.2.2 Variable Speed Wind Turbine Generator (Types 2, 3 and 4)

At least in principle, there are different solutions which allow the rotor to run at variable speeds, keeping the frequency constant. These solutions can be both of mechanical as well as electrical nature, even if the most used ones are electrical, in particular when using one of the following configurations:

- Asynchronous AC generators with external variable resistor (Type 2) with the stator connected to the grid and rotor resistance used for limited speed control;
- Asynchronous AC generators with a power converter interposed between the rotor and grid; these are known as a doubly-fed configuration (Type 3); and
- Generators (synchronous generators – SGs – brushless permanent magnet or wound field, or asynchronous induction generators – ASIGs – cage induction machines) with a power electronic converter interposed between the stator and grid (Type 4).

A schematic diagram of a typical semi-variable speed wind turbine, referred to as a Type 2 wind turbine, is shown in Figure 2-2. A wound rotor induction generator is used for all practical installations. This machine construction allows access to the rotor windings, enabling connection

of a thyristor-controlled variable resistance to the machine rotor. By adjusting this variable rotor resistance, the machine operating point can be adjusted across the torque-speed curve of the machine, which then allows a 'semi variable' speed operation of up to 10 % above the synchronous speed. The thyristor rectifier which is in parallel to the rotor-connected resistors is uses to short the resistors and phase-angle control allows this to be done in a controlled manner. A blade pitch controller is used to control the active power. Type 2 wind turbines are generally superior to Type 1 with regards to converting a given wind resource into energy [32].

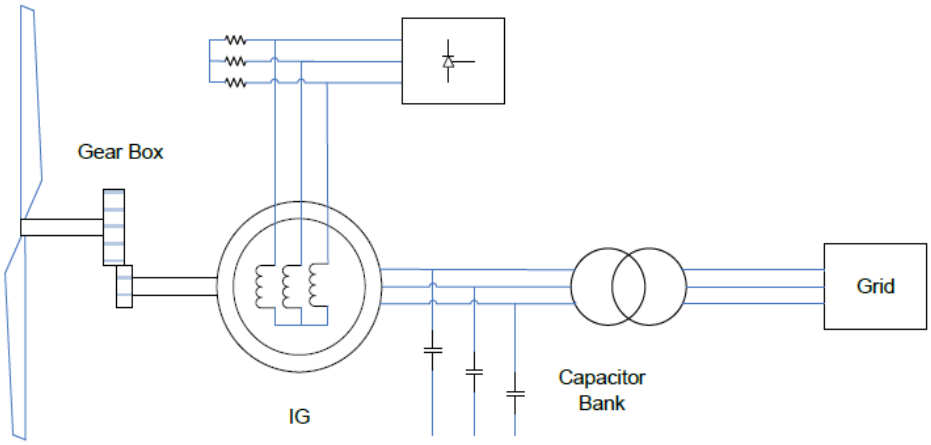

Figure 2-2: Schematic diagram of Type 2 wind turbine generator [32].

A schematic diagram of a typical variable-speed Type 3 wind turbine is shown in Figure 2-3. These are sometimes referred to as doubly-fed induction generators (DFIG). A wound rotor induction generator is used for all practical installations. Type 3 wind turbines have a connection between the machine rotor windings and the power system through a back-to-back voltage source converter. The key difference between Types 2 and 3 wind turbines is the replacement of the controlled resistance used in Type 2 with a four-quadrant (not SCR bridge), back-to-back voltage source converter. This gives the Type 3 system the capability of transmitting rotor active power in either direction and generating or absorbing reactive power in a controlled manner on both the rotor and grid sides. Hence, this rotor converter allows independent control of the wind turbine active and reactive power. It eliminates the need for reactive compensation equipment as installed at the terminals of type 1 and 2 wind turbines. Bi-directional flow of active power through the rotor converter allows Type 3 turbines to operate both above and below the synchronous speed. Above the synchronous speed, the rotor converter injects active power to the grid, whereas below the synchronous speed power is consumed in the rotor from the grid. The operating speed range depends on the back-to-back converter ratings with respect to the generator ratings. For economic reasons it has been a common practice to size the rotor power electronic converter at around 25

to 35 % of the generator rating, which provides an operating speed range of around ± 25 to 35 % of the rated speed.

Another advantage of the Type 3 turbine is that the mechanical drive train is largely decoupled from the electrical system via the back-to-back converter. This means that variations in the prime mover do not have a noticeable impact on the grid, resulting in lowered flicker levels. The control of reactive power is managed by the rotor power electronic converter. For active power control, a combination of the converter control and turbine blade pitch controllers is used. The blade pitch controller is much slower than the rotor converter controls and does not respond to first swing stability type events.

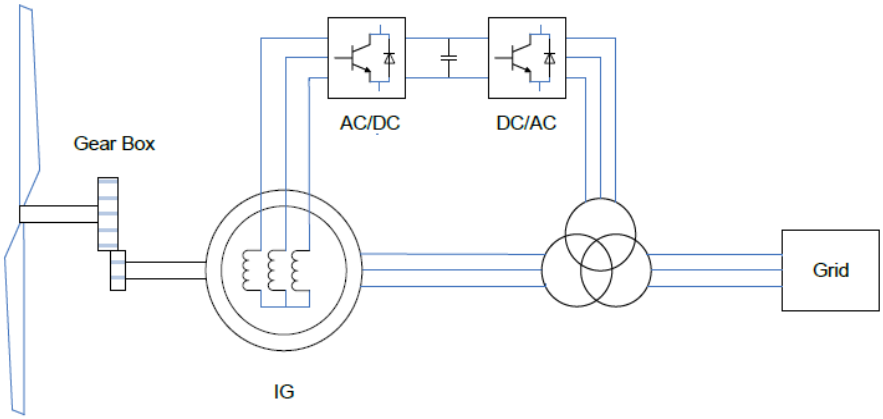

Figure 2-3: Schematic diagram of Type 3 (DFIG) wind turbine generator [32].

A disadvantage of the Type 3 turbine is the use of brushes and slip rings to connect the rotor with the converter, resulting in higher maintenance requirements compared to a simple squirrel cage induction machine. However, this does not affect the grid performance capability.

A schematic diagram of a typical variable-speed, full rated converter Type 4 wind turbine is shown in Figure 2-4. Squirrel cage induction machines, wound field synchronous machines, and permanent magnet synchronous machines have all been used in practice for these turbines, with both geared and gearless (direct drive) options. Figure 2-4 shows the geared version. The back-to-back voltage source power converter has the same rating as the generator, and the generator has no direct connection to the power system. This allows operation of the generator at any speed from zero to maximum rated speed, and provides an improved reactive power capability range compared with the type 3 wind turbines.

An advantage of a Type 4 wind turbine is that the power system and the generator are completely decoupled, unlike Type 3 machines, where there is a loose coupling between the generator and grid through stator windings. The control of active and reactive power is completely determined

by the converter and can be performed faster than a Type 3 wind turbine. The impact of power system voltage and frequency disturbances on the generator and mechanical drive train are minor. Most commercial Type 4 turbines use a DC braking chopper resistor in parallel with the DC-link capacitor inside the power converter (refer to Figure 2-4). This resistor can dissipate excess energy caused by temporary imbalances in the electrical and mechanical power during network fault conditions, when grid-side active power may temporarily need to drop to near zero.

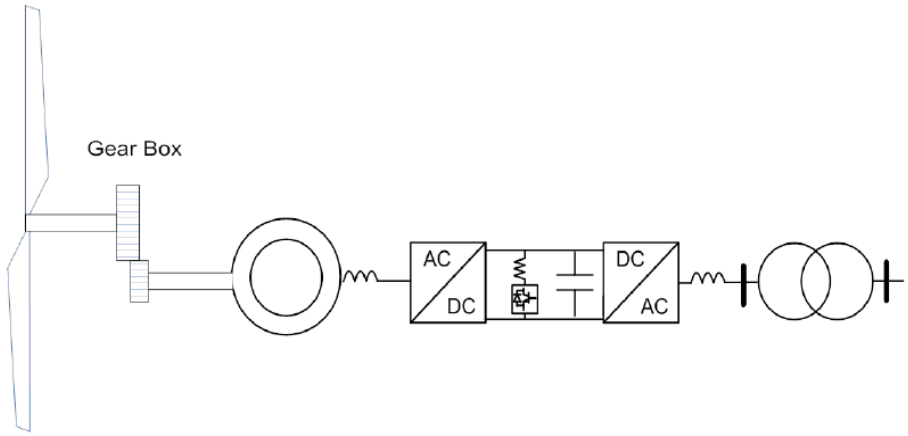

Figure 2-4: Schematic diagram of Type 4 wind turbine generator [32].

The above generators and associated technologies are well known in this industry however there is no consensus on what the best choice is from a wide technical perspective. The Doubly Fed Induction Generator (DFIG) is the choice for multi-MW wind turbines due to their long life, rigid structure, variable speed operation, and active and reactive power controllability [12]. They have been used in many in-service wind farms in the last decade including Case Studies 1 and 2 presented in this research. Therefore, DFIG has been discussed in this section briefly. The term "doubly-fed" reflects the fact that the stator voltage is applied by the grid, whereas the rotor voltage is applied by the electronic converter from the grid.

2.2.3 Doubly Fed Induction Generator (DFIG)

One of the main requirements of the wind turbine is the capability of operating over a wide wind speed range in order to achieve optimum aerodynamic efficiency by tracking the optimum tip-speed ratio. Therefore, the generator's rotor must be able to operate at a variable rotational speed. The DFIG system therefore operates in both sub- and super-synchronous modes with a rotor speed range around the synchronous speed. The stator circuit is directly connected to the grid while the rotor winding is connected via slip-rings to a three-phase converter. For variable-speed systems where the speed range requirements are small, for example ± 30 % of synchronous speed, the

DFIG offers adequate performance and is sufficient for the speed range required to exploit typical wind resources.

The back-to-back inverter converter is in the induction generator rotor circuit. This is only rated to handle a fraction of the total power – the rotor power – which is typically about 30% nominal generator power. Therefore, the losses in the power electronic converters are reduced, compared to a system where the converter must handle the entire power, and the system cost is lower due to the partially-rated converter [13].

Thus, it is possible to supply the rotor with voltages with the correct magnitude and frequency from the converter with the purpose of compensating for the difference of frequency between the angular velocity of the stator rotating magnetic field and the effective angular velocity of the rotor.

The block diagram and equivalent electrical circuit of the DFIG are shown in Figures 2-5 to 2-7.

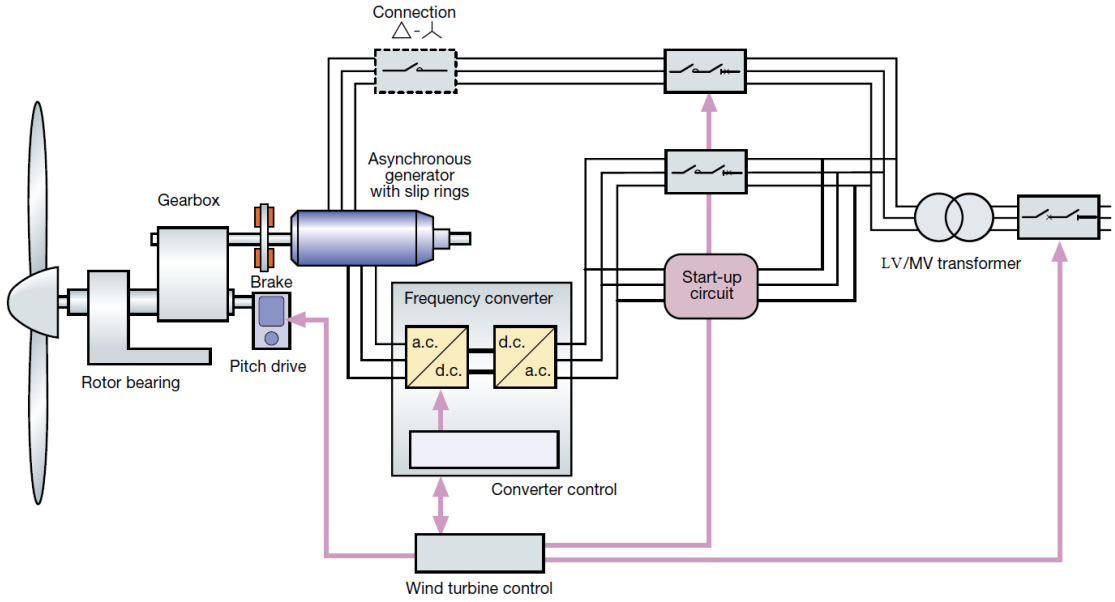

Figure 2-5: Wind Turbine component block diagram [10] (courtesy of ABB).

In general, DFIG turbines will operate in two modes, subsynchronous mode when the rotor absorbs power from grid (via convertor) to compensate the slip as shown in Figure 2-6 (a). Other operation mode is super-synchronous mode when both rotor and stator are generating power as shown in Figures 2-6 (b).

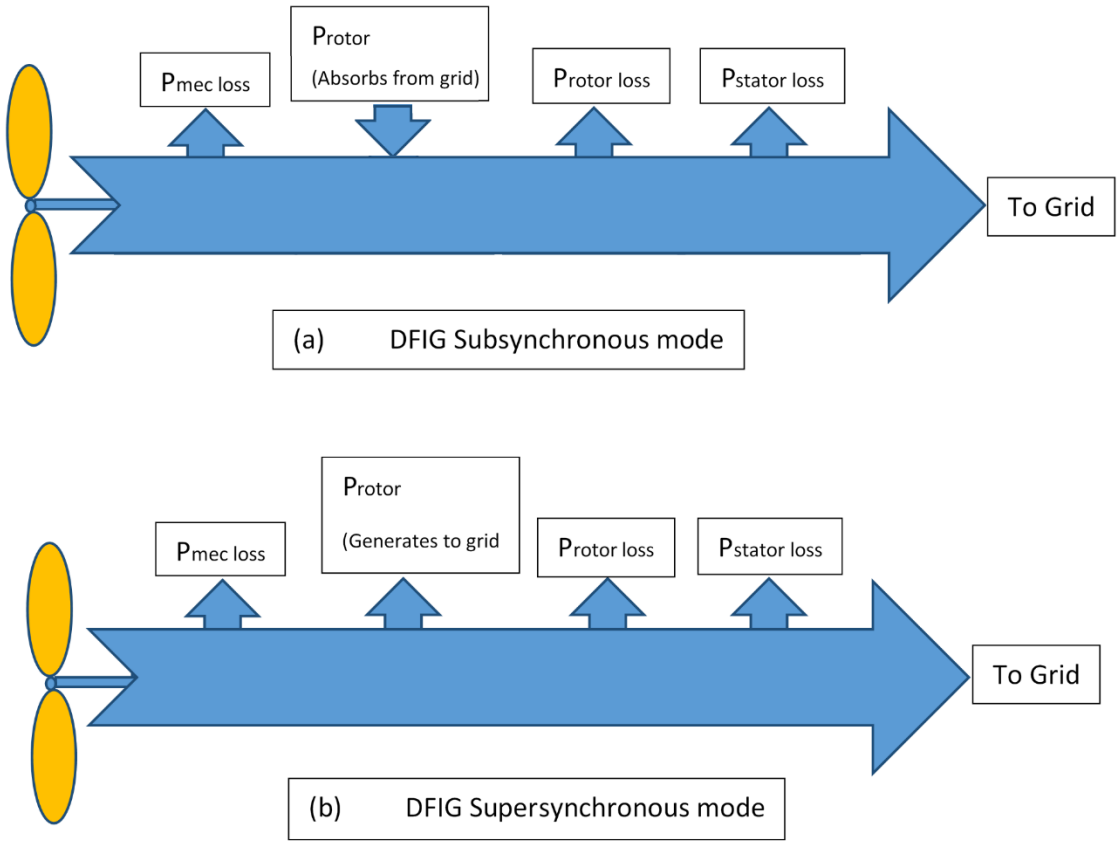

Figure 2-6: DFIG Wind Turbine energy conversion block diagram.

The doubly fed asynchronous generator was first used with a direct frequency converter made up of thyristors in the Growian Wind Turbine, which was installed in Kaiser-Wilhelm-Koog at the beginning of the 1980s. During the operation of the turbines it was possible to demonstrate the regulation characteristic with well smoothed output power [6].

In the past, most national network design codes and standards did not require wind farms to support the power system during a disturbance. For example, during a network fault or sudden drop in frequency wind turbines were tripped off the system. However, with the increased use of wind energy, wind farms will have to continue to operate during system disturbances and support the network voltage and frequency. Network design codes are now being revised to reflect new requirements and it is mandatory to carry out simulation studies to understand the impact of system disturbances on wind turbines and consequently on the power system itself. These studies require accurate steady-state and dynamic models of wind turbines and their associated control and protection.

2.2.3.1 DFIG Steady-State Model

In the steady-state, the DFIG active and reactive generated power is decoupled from the rotor slip using the converter. The rotor mechanical power through the shaft and electrical power through slip rings and stator power distributions are modelled and this is quite a complex problem.

The steady-state models of DFIG wind turbines are similar to asynchronous machine equivalent circuits as shown in Figure 2-7 for sub-synchronous and super-synchronous speeds. These models are based on a per-phase representation of the rotor referred to the stator with power flow into and out of the rotor controlled using the voltage source in the rotor part of the circuit. For correct representation of the DFIG wind turbine, it is important to model the control system used which will be discussed in the dynamic model.

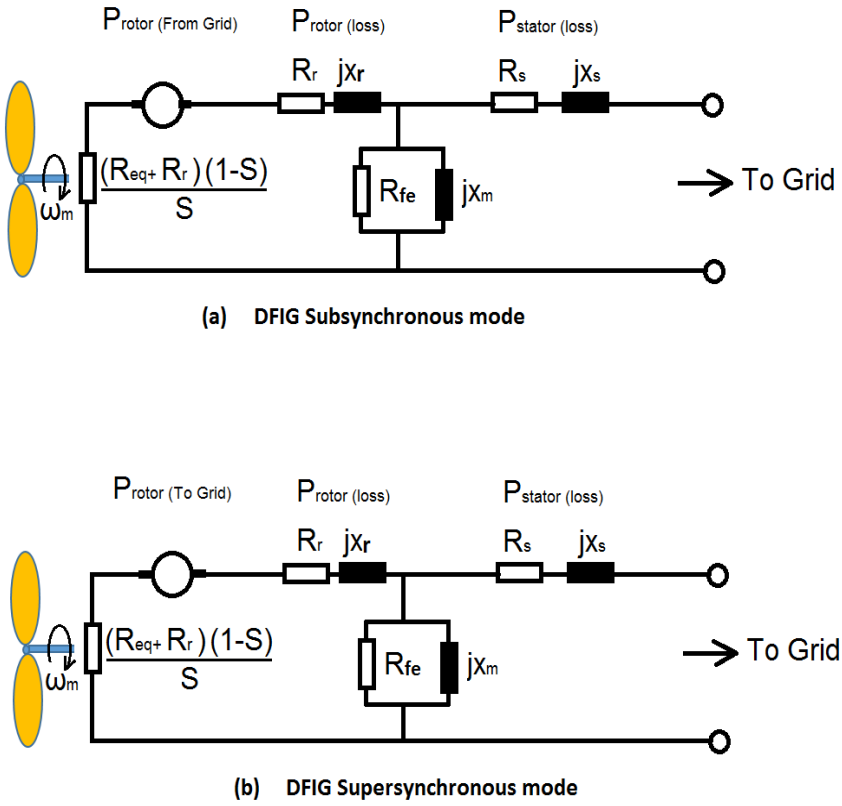

Figure 2-7: DFIG Wind Turbine equivalent circuit diagrams.

As shown in the above model the rotor torque is controlled by field-oriented control (FOC) in the dq stator flux reference frame. This reference frame, known as the synchronous reference frame (SRF), is useful in order to reduce partially the complexity of the mathematical equations that describe the system [18]. There are many widely used control philosophies for DFIG and the voltage-oriented control technique is one of them. The principle of voltage-oriented control is to

use a d-axis in reference frame aligned with the stator voltage, then the active and reactive power flows of the DFIG can be controlled independently [23]. This method has been explained in the dynamic modelling section briefly.

The vectorial diagram of the DFIG can provide better understanding of generator operation. The DFIG stator voltage (V_s) can be considered to be 90° leading with respect to the stator flux as shown in Figure 2-8.

The stator voltage is almost aligned with the in-quadrature axis, q (synchronous reference frame), while the magnetizing current in the stator has a single component in the d-axis.

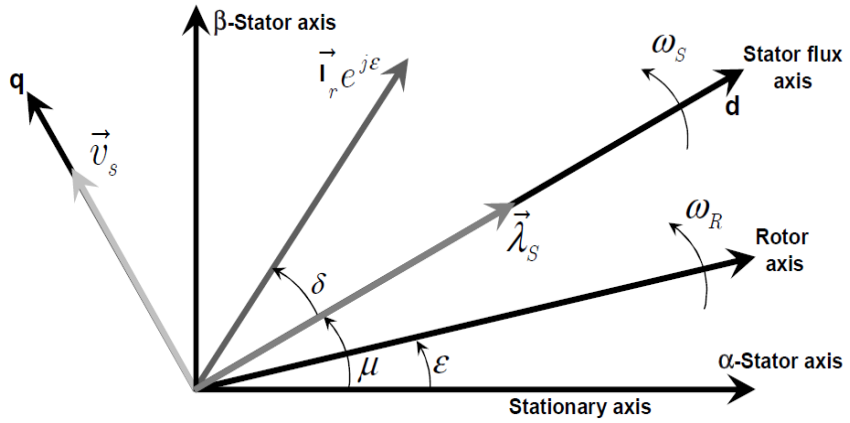

Figure 2-8: DFIG vectorial diagram in the dq reference frame [18].

Figure 2-8 diagram represents the vector diagram for both sub and super synchronous operation. The parameters for both sub and super synchronous operation are presented below:

ω_m: Rotor angular frequency in mechanical radians per second

ω_s: Synchronous angular frequency [rad/s]

$p_{machine}$: machine pole-pair number

E_m: magnetizing voltage across X_m [V]

s: Rotor slip [p.u.]

λ: Flux linkage [Wb]

V_s, V_r: Stator and Rotor voltage [V]

I_s, I_r: Stator and Rotor current [A]

L_s, L_r: Stator and rotor machine inductance [H]

L_{ss}, L_{rr}: Stator and rotor machine self-inductance [H]

T_m, T_e, T_{sp}: Mechanical, electromagnetic, set point torque [Nm]

The equivalent circuit parameters for the DFIG wind turbines in Case Studies 1 is given in Table 2-1, where;

$X_S = \omega_S(L_S)$ and $X_r = \omega_r(L_r)$

R_s, R_{fe} , R_r: Stator , iron loss and rotor resistance [Ω]

X_s, X_m , X_r: Stator , magnetizing and rotor reactance [Ω]

Table 2-1: Equivalent Circuit Parameters for the DFIG in Case Study 1 and 2.

DFIG wind turbines used at Wind Farm (Capacity about 2 MW)	**Parameter**	**4 pole generator - value**
Stator resistance	R_s [Ω]	0.0042
Stator leakage reactance	X_s [Ω]	0.0625
Magnetizing reactance	X_m [Ω]	3.5809
Iron loss resistance	R_{fe} [Ω]	131
Rotor leakage reactance	X_r [Ω]	0.0674
Rotor resistance	R_r [Ω]	0.0047

For DFIG, the mechanical power is given by

$$P_m = T_{mech}\omega_r = \frac{T_{mech}\omega_s(1-s)}{p_{machine}}$$

where $p_{machine}$ is the machine pole-pair number. The power is amplified across the airgap and the airgap power is given by

$$P_{airgap} = \frac{T_{mech}\omega_s}{p_{machine}} = \mathrm{Re}\left[3\bar{E}_m\bar{I}_s^*\right] \approx 3\left|\bar{E}_m\right|\left|\bar{I}_s\right|_{p.f.\approx 1}$$

In this equation it is assumed that the machine field is supplied by the rotor so that the power factor at the machine stator terminals is close to unity. Carrying out further manipulation to get E_m in terms the stator current and terminal voltage by again assuming unity p.f. and neglecting the voltage drop across L_s since it is small and in quadrature to the terminal voltage then

$$\frac{T_{mech}\omega_s}{p_{machine}} = 3E_mI_s = 3I_s\left(V_s - I_sR_s\right)$$

This uses simply the rms voltages and current and assumes a motoring convention for power flow. After more manipulation then

$$I_s^2R_s - I_sV_s + \frac{T_{mech}\omega_s}{3p_{machine}} = 0$$

and this quadratic can be solved as shown in (2.1). The stator current can be calculated from

$$I_s = \frac{V_s - \sqrt{V_s^2 - \left(\frac{4R_s T_m \omega_s}{3p_{machine}}\right)}}{2R_s} \quad \text{p.f. } \approx 1 \tag{2.1}$$

This analysis has several approximations. The magnetizing voltage can be more accurately calculated from

$$\bar{E}_m = \bar{V}_s - \bar{I}_s(R_s + j\omega_s L_s)\,, \tag{2-2}$$

which can give the true magnetizing current

$$\bar{I}_m = \frac{\bar{E}_m}{j\omega_s L_m} \tag{2-3}$$

And the rotor current:

$$I_r = I_s - I_m\,. \tag{2-4}$$

The equivalent circuit applied rotor voltage is then

$$\bar{V}_r = s\bar{E}_m - \bar{I}_r(R_r + js\omega_s L_s) \tag{2-5}$$

And the equivalent rotor impedance is

$$\bar{Z}_{eq} = \frac{\bar{V}_r}{\bar{I}_r}\,. \tag{2-6}$$

Mechanical power and generated power through the DFIG generator based on the simplified steady state equivalent circuit can be calculated via the induction motor equations.

2.2.3.2 DFIG Dynamic Model

To model the DFIG wind turbine, it is important to correctly represent the wind turbine generator and associated control system. Dynamic models of DFIG wind turbines have been published in various papers and books. DFIG dynamic models are based on different control system used to operate induction motor with equivalent circuits like Figure 2-7. The sub- and super-synchronous operation of induction machine via slip control requires closed loop control circuits to adjust rotor excitation via the rotor converter. This uses pulse wave modulation (PWM) of the DC link voltage to produce the correct AC voltages to control the DFIG. It usually requires current, speed and position feedback for full control. One advantage the DFIG has over the cage induction generator is that the rotor current is easily measured and therefore known. This makes it more straightforward to control; the cage induction generator current must be estimated. This means the stator and rotor current can be controlled in a dynamic fashion so that they are orthogonal which maximizes the generator torque per amp performance. The regulating blocks of a full system are shown in Figure 2-9.

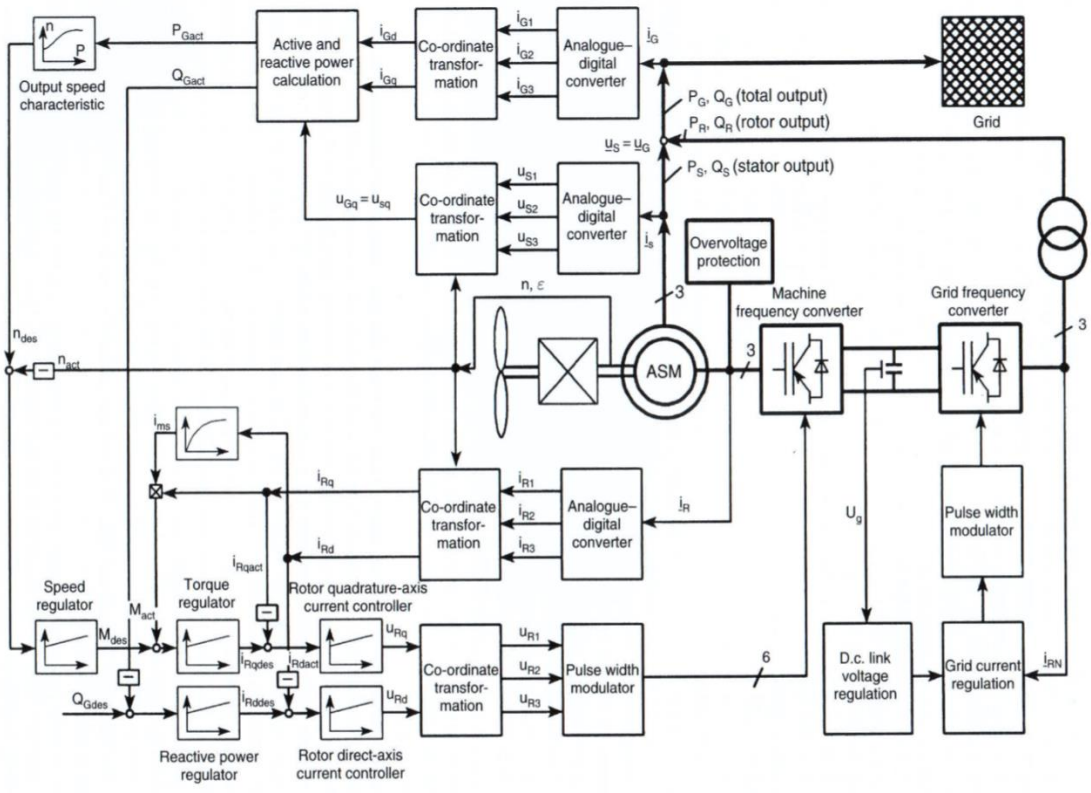

Figure 2-9: DFIG Wind Turbine control system block diagram [6].

The power quality aspects of DFIG turbines will be considered in Case Studies 1 and 2; however, in order to model the DFIG dynamic system, some of the power quality issues have to be discussed and this is done in this section. The Australian Energy Market Operator (AEMO) and other grid operators have concerns regarding the capability and stability of wind power generators connected to the grid when grid voltage sags occur. This feature, known as the fault ride-through (FRT) capability, states the fault condition boundaries where a wind turbine (WT) should be disconnected from the grid. In some cases, as with the Spanish and German GC, give the operation pattern for the system under such conditions [18].

DFIG wind turbines consist of back-to-back PWM inverter converters as their control system. In such systems fulfilling the FRT requirements is not straightforward due to its connection topology; they are especially sensitive to any voltage sag. The reason is that a DFIG generator, when the voltage at the stator windings drops (due to grid voltage fluctuation), a sudden over-current appears in the stator that, in turn, induces voltages into the rotor windings. This over-current can damage the machine, and the rotor side converter and as a consequence, so that protection is required.

There have been many studies and projects focused on improving DFIG fault ride-through capabilities. The following methods have been proposed for FRT improvements:

- Crowbar circuits;

- Careful airgap flux control; and
- Static switching with breakers.

One of the proposed solutions is based on limiting the over-currents in the rotor converter by means of connecting crowbar circuits during the fault. This kind of solution requires the installation of extra hardware in the system, something that increases the costs and hinders its reliability since the control system should become more complex. Moreover, and despite the fact that a crowbar is able to reduce the current peaks under sag conditions, this device does not avoid the disconnection of the rotor side converter after the fault is detected.

In addition, the design of such protection is calculated considering the present features of the wind power system, so any future change of its configuration would affect its performance [18].

The voltage and airgap magnetic flux can be calculated from the equations below based on the following assumptions as explained in reference [19]:

a) The stator current is assumed positive when flowing toward the machine (sub-synchronous).

b) The equations are derived from the synchronous reference frame using direct (d) and quadrature (q) axis representation.

c) The q-axis is assumed to be 90° ahead of the d-axis in the direction of rotation.

d) The component of the stator voltage used within the model is rated to the highest generator busbar voltage obtained from the load flow solution that is used to initialize the model.

e) The dc component of the stator transient current is ignored, permitting representation of only fundamental frequency components.

f) The higher order harmonic components in the rotor injected voltages are neglected.

The phasors can be broken down on to the synchronously-rotating reference d-q axes and are rotating so that the d-axis voltage can be written as

$$v_{ds} = \bar{R}_s \bar{i}_{ds} - \bar{\lambda}_{qs} \tag{2-7}$$

This accounts for the stator resistance and the q-axis flux linkage. A similar voltage equation can be obtained for the q-axis:

$$v_{qs} = \bar{R}_s \bar{i}_{qs} - \bar{\lambda}_{ds} \tag{2-8}$$

The rotor windings are rotating so the d-axis rotor voltage also has a third “speed” term and also the frequency of the induced voltages are at slip frequency so that

$$v_{dr} = \bar{R}_r \bar{i}_{dr} - s\bar{\lambda}_{qr} + \frac{1}{\omega_s}\frac{d}{dt}\bar{\lambda}_{dr} \tag{2-9}$$

and

$$v_{qr} = \bar{R}_r \bar{i}_{qr} - s\bar{\lambda}_{dr} + \frac{1}{\omega_s}\frac{d}{dt}\bar{\lambda}_{qr} \tag{2-10}$$

The rotor is often short-circuited so that

$$v_{dd} = \bar{R}_d \bar{i}_{dd} - s\bar{\lambda}_{qd} + \frac{1}{\omega_s}\frac{d}{dt}\bar{\lambda}_{dd} = 0 \tag{2-11}$$

$$v_{qd} = \bar{R}_d \bar{i}_{qd} - s\bar{\lambda}_{dd} + \frac{1}{\omega_s}\frac{d}{dt}\bar{\lambda}_{qd} = 0 \tag{2-12}$$

These can be solved as matrix form:

$$\begin{pmatrix} \bar{\lambda}_{ds} \\ \bar{\lambda}_{dr} \\ \bar{\lambda}_{dd} \end{pmatrix} = \begin{pmatrix} \bar{L}_{ss} & \bar{L}_m & \bar{L}_m \\ \bar{L}_m & \bar{L}_{rr} & \beta\bar{L}_m \\ \bar{L}_m & \beta\bar{L}_m & \bar{L}_{dd} \end{pmatrix} \begin{pmatrix} \bar{i}_{ds} \\ \bar{i}_{dr} \\ \bar{i}_{dd} \end{pmatrix} \tag{2-13}$$

$$\begin{pmatrix} \bar{\lambda}_{qs} \\ \bar{\lambda}_{qr} \\ \bar{\lambda}_{qd} \end{pmatrix} = \begin{pmatrix} \bar{L}_{ss} & \bar{L}_m & \bar{L}_m \\ \bar{L}_m & \bar{L}_{rr} & \beta\bar{L}_m \\ \bar{L}_m & \beta\bar{L}_m & \bar{L}_{dd} \end{pmatrix} \begin{pmatrix} \bar{i}_{qs} \\ \bar{i}_{qr} \\ \bar{i}_{qd} \end{pmatrix} \tag{2-14}$$

where in (2-13) and (2-14):

$$\beta = 1 + \frac{\bar{L}_{rm}}{L_m} \tag{2-15}$$

$$\bar{L}_{ss} = \bar{L}_s + \bar{L}_m \tag{2-16}$$

$$\bar{L}_{rr} = \bar{L}_r + \beta\bar{L}_m \tag{2-17}$$

$$\bar{L}_{dd} = \bar{L}_d + \beta\bar{L}_m \tag{2-18}$$

Accordingly based on matrix (2-10) and (2-11), the stator current can be calculated from the following in per unit form.

$$\bar{i}_{ds} = \left(\frac{\bar{\lambda}_{ds} - \bar{L}_m \bar{i}_{dr} - \bar{L}_m \bar{i}_{dd}}{\bar{L}_{ss}} \right) = \frac{\bar{v}_{ds}}{\bar{L}_{ss}} - \frac{\bar{L}_m}{\bar{L}_{ss}} \bar{i}_{dr} - \frac{\bar{L}_m}{\bar{L}_{ss}} \bar{i}_{dd} \tag{2-19}$$

$$\bar{i}_{qs} = \left(\frac{\bar{\lambda}_{qs} - \bar{L}_m \bar{i}_{qr} - \bar{L}_m \bar{i}_{qd}}{\bar{L}_{ss}} \right) = \frac{\bar{v}_{ds}}{\bar{L}_{ss}} - \frac{\bar{L}_m}{\bar{L}_{ss}} \bar{i}_{qr} - \frac{\bar{L}_m}{\bar{L}_{ss}} \bar{i}_{qd} \tag{2-20}$$

The rotor current can be calculated by considering the above equations:

$$p\bar{i}_{dr} = \frac{\bar{X}_3}{\sigma_1}\bar{v}_{dr} - \frac{\bar{R}_r \bar{X}_3}{\sigma_1}\bar{i}_{dr} + \frac{\bar{R}_r \bar{X}_2}{\sigma_1}\bar{i}_{dd} + s\omega_s \bar{i}_{qr} + \frac{\bar{L}_m}{L_{ss}}\sigma_2 \left[s\bar{v}_{ds} + \frac{1}{\omega_s} p\bar{v}_{qs} \right] \tag{2-21}$$

$$p\bar{i}_{qr} = \frac{\bar{X}_3}{\sigma_1}\bar{v}_{qr} - \frac{\bar{R}_r\bar{X}_3}{\sigma_1}\bar{i}_{qr} + \frac{\bar{R}_d\bar{X}_2}{\sigma_1}\bar{i}_{dd} - s\omega_s\bar{i}_{dr} + \frac{\bar{L}_m}{L_{ss}}\sigma_2\left[s\bar{v}_{qs} - \frac{1}{\omega_s}p\bar{v}_{ds}\right] \quad (2\text{-}22)$$

$$p\bar{i}_{dd} = \frac{\bar{X}_2}{\sigma_1}\bar{v}_{qr} + \frac{\bar{R}_r\bar{X}_2}{\sigma_1}\bar{i}_{dr} - \frac{\bar{R}_d\bar{X}_1}{\sigma_1}\bar{i}_{dd} + s\omega_s\bar{i}_{qd} + \frac{\bar{L}_m}{L_{ss}}\sigma_3\left[s\bar{v}_{ds} + \frac{1}{\omega_s}p\bar{v}_{qs}\right] \quad (2\text{-}23)$$

$$p\bar{i}_{qd} = \frac{\bar{X}_2}{\sigma_1}\bar{v}_{qr} + \frac{\bar{R}_r\bar{X}_2}{\sigma_1}\bar{i}_{qr} - \frac{\bar{R}_d\bar{X}_1}{\sigma_1}\bar{i}_{qd} + s\omega_s\bar{i}_{dd} + \frac{\bar{L}_m}{L_{ss}}\sigma_3\left[s\bar{v}_{qs} + \frac{1}{\omega_s}p\bar{v}_{ds}\right] \quad (2\text{-}24)$$

where in (2-21) to (2-24):

$$\bar{X}_1 = \left[\bar{L}_{rr} + \frac{\bar{L}_{m,}^2}{\bar{L}_{ss}}\right] \quad (2\text{-}25)$$

$$\bar{X}_2 = \left[\beta\bar{L}_m + \frac{\bar{L}_m^2}{\bar{L}_{ss}}\right] \quad (2\text{-}26)$$

$$\bar{X}_3 = \left[\bar{L}_{dd} + \frac{\bar{L}_m^2}{\bar{L}_{ss}}\right] \quad (2\text{-}27)$$

$$\sigma_1 = \left[\frac{\bar{X}_1\bar{X}_3 - \bar{X}_2^2}{\omega_s}\right] \quad (2\text{-}28)$$

$$\sigma_2 = \left[\frac{\bar{X}_2 - \bar{X}_3}{\sigma_1}\right] \quad (2\text{-}29)$$

$$\sigma_3 = \left[\frac{\bar{X}_2 - \bar{X}_1}{\sigma_1}\right] \quad (2\text{-}30)$$

As part of the power quality issues studied here it is required to analyse the wind farm voltage fluctuations. Since Case Studies 1 and 2 both include DFIG turbines, analysis of their behaviour is required. According to the above discussion, the DFIG dynamic model should be analysed during the asymmetrical voltage fluctuations. The aim is to maintain the DFIG in normal operation mode. The rotor-side converter (RSC) and grid-side converter (GSC) control the DFIG as shown in Figure 2-9. The control system has five feedback control loops: four current-loops and a DC voltage loop. The GSC controller can keep the DC bus voltage of the DC-link constant and control the reactive power exchange with the grid. The RSC controller can supply the rotor voltage that the DFIG needs.

2.2.4 HV Cables

The majority of wind farms that have wind turbines located several hundreds of metres away from one another with underground cables linking them. This is illustrated in Figure 2-10. Normally the electromechanical energy conversion takes place on lower voltage generators and the

generated power will be transformed to a medium voltage using a step-up transformer substation at the point of common coupling (PCC).

Figure 2-10: Cable installation for wind farm (courtesy of Aurecon)

The cable impedance (especially capacitance) will attenuate generated harmonics and transients caused by power electronic equipment. Therefore, in this section the symmetrical components method will be presented for cable impedance simulation. The symmetrical components method is a simplified analysis for unbalanced three-phase power systems under both normal and abnormal conditions. The basic idea is that an asymmetrical set of N phasors can be expressed as a linear combination of N symmetrical sets of phasors by means of a complex linear transformation.

To use the symmetrical components method of analysis, the network element (transformers, lines, cables and generators) impedances should be calculated or obtained from measurements. In this section, to simplify calculations, transformers are not explicitly modelled in the manual calculation but included in the software analysis. The upstream network impedances are also reflected in the Thevenin model.

The symmetrical components method decomposes the unbalanced network parameters such as voltages and currents of a three-phase system into three separate but balanced symmetrical components, namely positive, negative and zero sequence components. Therefore, to calculate positive, negative and zero sequence voltages and currents, we must first calculate the corresponding positive, negative and zero sequence impedances which will generate and limit

voltages and currents respectively. Extreme unbalances of voltages and currents in the network are caused by system faults such as phase-to-earth faults.

The equations for calculating the series positive and the zero sequence impedance values for a 3 core, insulated metallic sheath covered cables are presented [20].

2.2.4.1 Positive and Negative Sequence Impedances of a Core Cable

In a perfectly balanced three-phase power system, the voltage phasors have equal magnitudes but are 120 degrees apart. In an unbalanced system, the magnitudes and phases of the phasors are different. Decomposing the voltage phasors into their symmetrical components can help in analysing the system as well as visualizing any imbalances. The system impedances for the cable can be calculated. The screen shot in Figure 2-11shows a cross section of a three core 33 kV cable.

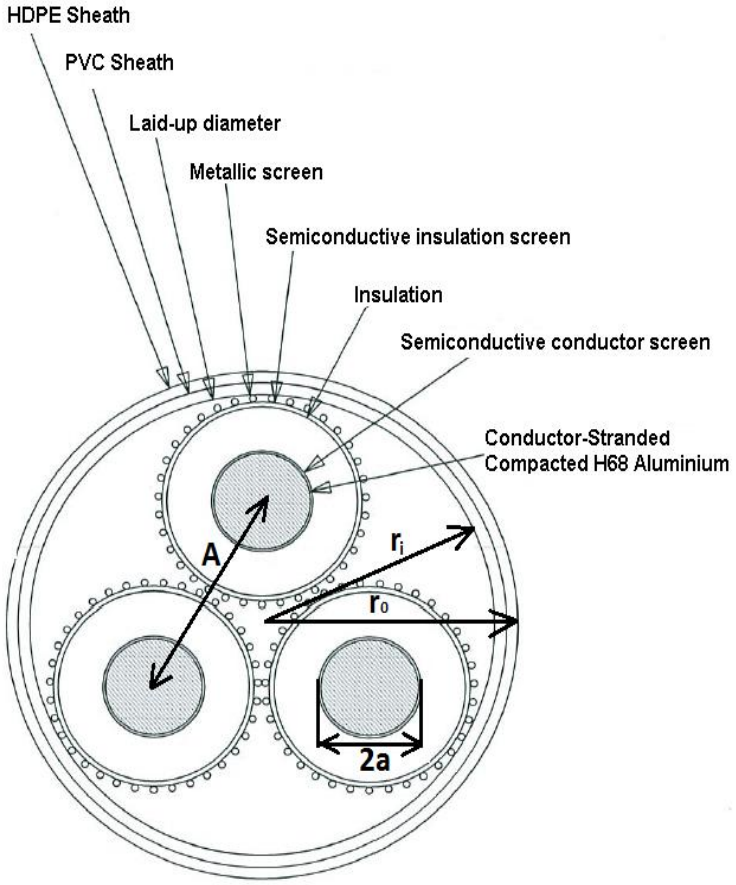

Figure 2-11: Typical 3 core 33 kV Aluminium cable cross-section without armour.

To analyse the positive sequence impedance of a three-core cable at the grid frequency *f* of 50 Hz, it can be assumed that the positive sequence AC resistance of the conductors is equal to the DC resistance of the conductor. This is an approximation at this stage which becomes more inaccurate with larger conductors due to skin and proximity effects. Therefore:

$$R_1 = R_{cond(DC)} \quad \left[\frac{\Omega}{\text{km}}\right] \tag{2-31}$$

The positive sequence reactance of the cable can be calculated from

$$X_1 = 2.893\times10^{-3}\log_{10}\left(\frac{A}{GMR}\right) \qquad \left[\frac{\Omega}{\text{km}}\right] \tag{2-32}$$

where A is the spacing between the centres of two conductors (mm) as shown in Figure 2-11, and GMR is the Geometric Mean Radius of one conductor (mm) and is calculated using:

$$GMR = aK \quad \text{[mm]} \tag{2-33}$$

where a is the radius of the conductor (mm) as shown in Figure 2-11 and K is a converting factor from radius to the Geometric Mean Radius (GMR) and varies for different types of cables (e.g., for stranded cable with 37 strands is 0.768). Hence, the positive sequence impedance of a 3-core cable is given by:

$$Z_1 = R_1 + jX_1 \quad \left[\frac{\Omega}{\text{km}}\right] \tag{2-34}$$

Long cables may also have capacitance and data sheets can be used to look up the cable impedances. The negative sequence impedance of the cable is equal to the positive sequence impedance so that

$$Z_2 = Z_1 = R_1 + jX_1 \qquad \left[\frac{\Omega}{\text{km}}\right] \tag{2-35}$$

2.2.4.2 Zero Sequence Impedance of a Three-Core Cable

To calculate the zero sequence self-impedance of the cable, the conductors in the cable must be considered as a group, and the equivalent GMR for the group of conductors must be calculated. The three-core cables will be replaced by a single conductor with an equivalent GMR and resistance of 3 parallel conductors considered as a group thereafter. This is obtained from [20]:

$$Z_0 = 3\left[\frac{R_{cond}}{3} + 988.2\times10^{-6} f + j2.893\times10^{-3} f\log_{10}\left(\frac{658368\sqrt{\frac{\rho}{f}}}{GMR_{3con}}\right)\right] \qquad \left[\frac{\Omega}{\text{km}}\right] \tag{2-36}$$

where R_{cond} is the DC resistance of one conductor provided by the cable supplier in Ω/km and ρ is the deep layer soil resistivity in Ω-m. GMR_{3con} is the Geometric Mean Radius of three conductors and calculated from:

$$GMR_{3con} = \sqrt[3]{aKA^2} \tag{2-37}$$

The zero sequence self-impedance of the sheath of cable is calculated using [20]:

$$Z_{ss0} = 3\left[R_{sh} + 988.2\times10^{-6} f + j2.893\times10^{-3} f \log_{10}\left(\frac{658368\sqrt{\frac{\rho}{f}}}{GMR_{sh}} \right) \right] \left[\frac{\Omega}{\text{km}} \right] \tag{2-38}$$

where R_{sh} is the cable sheath resistance and can be calculated by:

$$R_{sh} = \frac{\rho_{sh}\times10^{9}}{\pi\left(r_0^2 - r_i^2\right)} \qquad \left[\frac{\Omega}{\text{km}} \right] \tag{2-39}$$

where ρ_{sh} is the resistivity of the cable sheath material in (Ω-m). Screened 3-core aluminium cables have been used for both case studies. For aluminium cables, $\rho_{sh} = 2.84\times10^{-8}$ (Ω-m), r_0 and r_i are the outer and inner radius of the cable in (mm) as shown in Figure 2-11. GMR_{sh} is the *GMR* of the sheath and can be obtained from:

$$GMR_{sh} = \frac{r_0 + r_i}{2} \quad \text{[mm]} \tag{2-40}$$

Since armoured cable was not used in Case Studies 1 and 2, the zero-sequence mutual impedance between the group of 3 cores and the cable armour is not presented here (refer to NZCCPTS Application Guide for more details [20]). This analysis can be extended to include a parallel earth conductor that is often used in these applications.

2.2.5 Load Flow and Power System Study

The topic this research is issues with the delivery of power quality in wind farms. The power quality of a wind farm depends on the behaviour of each individual turbine as well as impact of group operation and the power distribution network. Load flow and power system study assessment is essential for power quality assessment.

The short circuit manual calculation presented in Australian Standard AS3851 which is generally based on IEC 60909 has been used in this research to compare the fault levels of the software model. This is to validate the model component are modelled correctly and can be used for load flow study.

The load flow and power system studies normally provide following information:

- 3 phase fault level at each bus bar or specific equipment;
- Fault levels at each bus bar or padmount;
- Power factor analysis;
- Voltage fluctuation at different locations;
- Current flow in the system; and
- Cable loading.

Case Studies 1 (DFIG) and 2 (DFIG and ASIG) are simulated using the Paladin Design Base software package. The same model has been used for power quality analysis and transient simulation. Paladin Design Base software is widely recognised as a robust and accurate modelling system for large networks. The software has the provision to perform both load flow and fault studies. There are several fault study algorithms available to comply with specific international standards. In this modelling, all fault studies were performed with the IEC 60909 algorithm set. The results of simulation are verified by comparing the results with "As Built" information.

The results of the load flow and power system study confirm the power factor correction details such as location and ratings. They confirm the equipment fault withstand characteristics.

2.3 Power Quality Assessment

Power quality can be defined as the comparison of the actual voltage and current waveforms with their "clean" sinusoidal waveforms. Pure sine waves that are free of distortion are sometimes referred to as clean power. Many papers have been written on this subject, so only a brief review of the subject will be presented here. The main intent of this research is to discuss some design ideas that should be considered during wind farm system studies. Also what mitigation method is necessary, and if so, what type should be implemented [21].

In this research the following items are highlighted as the main power quality items for wind farms:

- Harmonics;
- Flicker;
- Unbalance;
- Voltage fluctuation;
- Wind gust impact on voltage;
- System fault ride through (FRT);
- Network Loading / Interaction with nearby power plants;
- System frequency fluctuation; and

- System stability and intra-regional impact.

Power quality aspects are discussed at each case study based on the simulations and readings.

2.4 Network Connection Requirement

Each country has its own network standards and requirement for grid connection and operation. In Australia the National Electricity Market Management Company Limited (NEMMCO) was the market operator for the Australian National Electricity Market (NEM). It was established in 1996 to administer and manage the NEM. On 1 July 2009, NEMMCO was succeeded by the Australian Energy Market Operator (AEMO).

The Australian Energy Market Operator (AEMO) manages the National Electricity Market (NEM) and the Victorian gas transmission network. AEMO also facilitates electricity and gas full retail contestability, overseeing these retail markets in eastern and southern Australia. It is additionally responsible for national transmission planning for electricity and the establishment of a Short Term Trading Market (STTM).

Wind farm grid connection requires AEMO compliance assessment according to the technical requirements set out in the National Electricity Rules. Normally the wind farm operator and Network Service Providers will complete this document jointly and submit it with the registration application to AEMO. Technical items associated with wind farm power quality issues are presented below:

- Reactive Power Capability (for rated active power);
- Quality of Electricity Generated;
- Generating Unit Response to Frequency Disturbances;
- Generating System Response to Voltage Disturbances;
- Generating System Response to Disturbances following Contingency Events;
- Partial Load Rejection; and
- Protection of Generating Units from Power System Disturbances

These requirements will be assessed for each case study.

2.5 Wind Farms Case Study 1

In this research two wind farms have been assessed. The actual wind farm remains anonymous; therefore Case Study 1 (DFIG) and Case Study 2 (DFIG + ASIG) have been used to reference each wind farm.

Case Study 1 comprises more than fifty wind turbines. These wind turbines are scattered in even collection groups in an area of about 10 km². The turbines have 33 kV interconnection with a minimum separation distance of 200 m and maximum separation distance of 1300 m between the turbines.

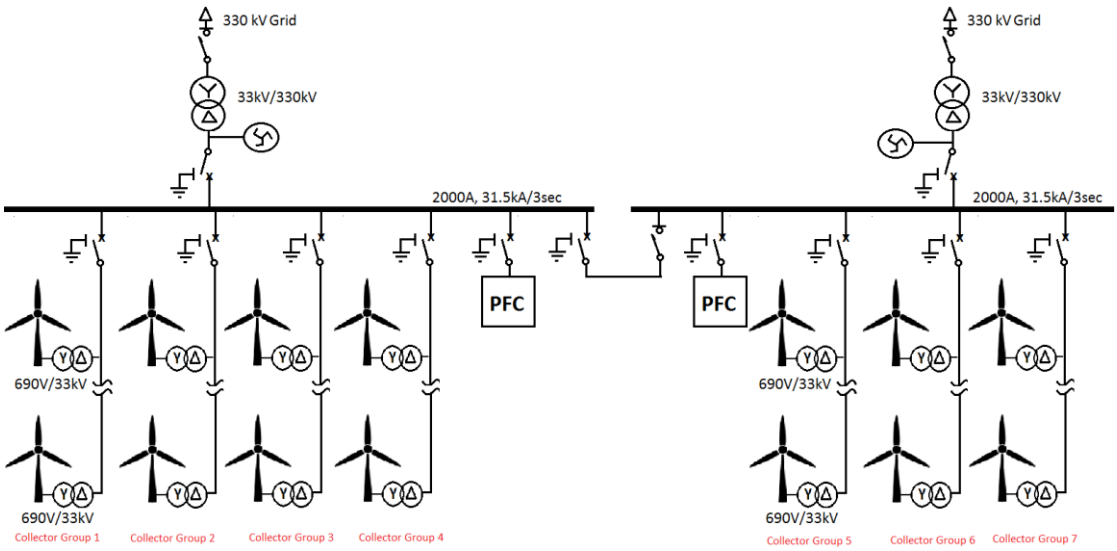

Figure 2-12: System reticulation of wind farm Case Study 1.

Each turbine has internal controls that monitor the wind direction and speed, with power production beginning at winds above 14 km/h (4 m/s). The power produced continues to increase until the turbines reach maximum or 'rated' capacity at wind speeds of around 40 km/h (11 m/s).

Stronger winds do not make the blades turn faster. The blades rotate at a regular 15 to 18 rpm and operate at rated capacity until the wind speed reaches 90 km/h (25 km/s). The turbines automatically shut down and turn out of the wind when the wind speed goes beyond 90 km/h (25 km/s).

Wind turbines in Case Study 1 (DFIG) have been designed and constructed with 690 V / 33 kV step up transformers that supply the 33 kV switchgear via 33 kV / 690V transformers. The wind turbine rated voltage is 690 V (refer to Figure 2-13).

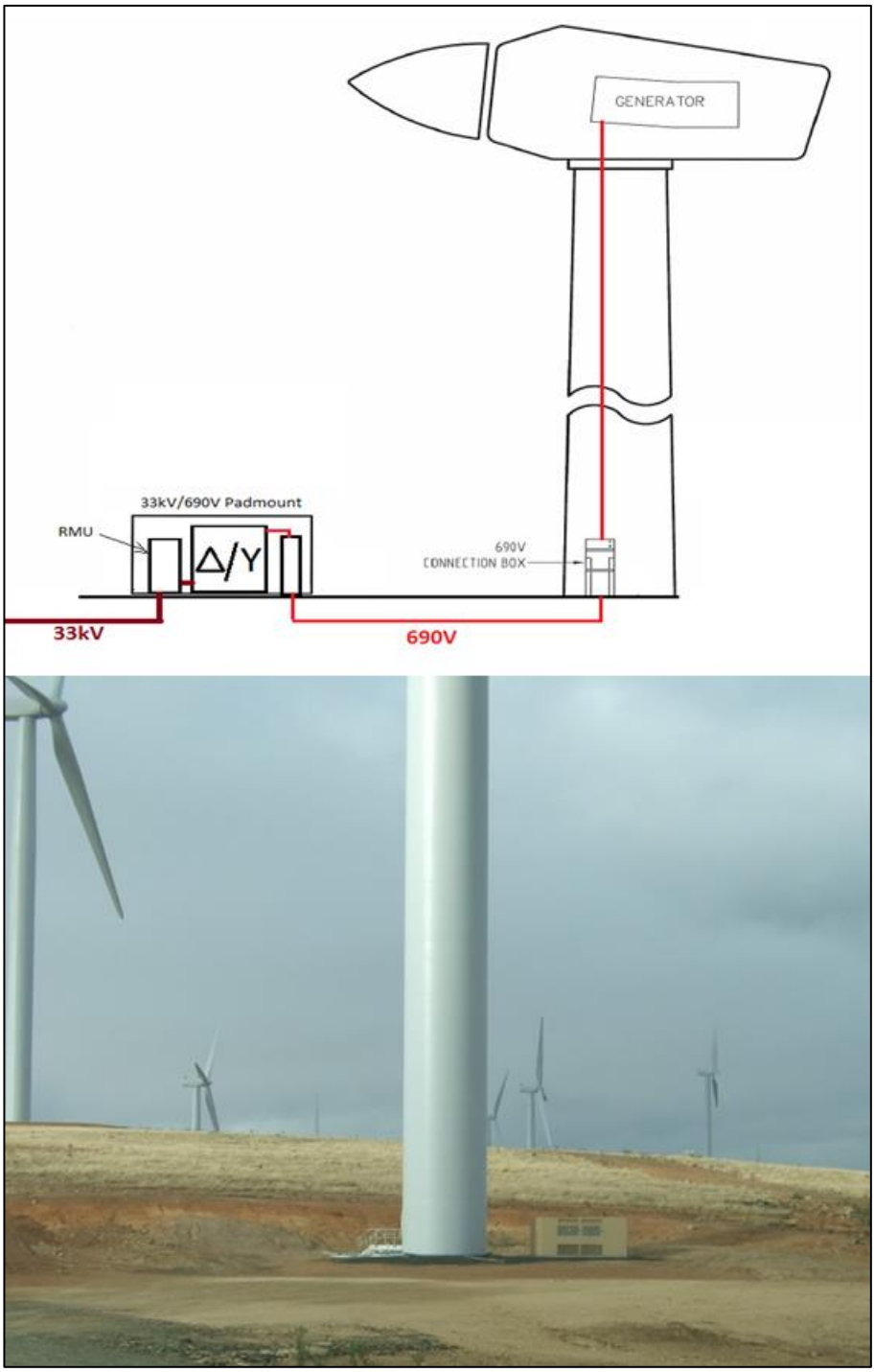

Figure 2-13: Wind Turbine and step-up transformer arrangement.

The tower height is assumed to be 80 m with a diameter of 4.3 m at ground level and 4 m at the top of the tower. The turbine characteristics are shown in Table 2-2.

Table 2-2: Technical data of Wind Turbines for Case Study 1 (DFIG).

General	
Rated power	1 pu
Hub type	Horizontal Axis
Hub height (above ground)	80 m
Rated wind speed	12 m/s
Cut-in wind speed	4 m/s
Cut-out wind speed	25 m/s
Recut-in wind speed after over speed	23 m/s
Short circuit ratio without soft starter (Isc/In)	5.2
Rotor	
Swept diameter	88.90 m
Swept area	6207.16 m²
Number of blades	3
Relative Position to tower	Upwind
Rotor blade pitch setting	Slew bearings
Rated speed	15.79 rpm
Blade length	43.25 m
Cone angle	5°
Tilt angle	4°
Gearbox	
Gearbox ratio	1:98.828
Generator	
Rated power	approximately 2MW
Type	Doubly Fed Induction Generator
Number of poles	4
Synchronous speed	1500 rpm
Rated speed	1511 rpm
Voltage	690 V AC
Frequency	50 Hz
Tower	
Tower Length	77.5 m

According to the above technical characteristics, wind turbines will convert wind power to 690 V electric power in the rotor circuit. The power curve of wind turbines used in Case Study 1 (DFIG) is presented in Figure 2-14.

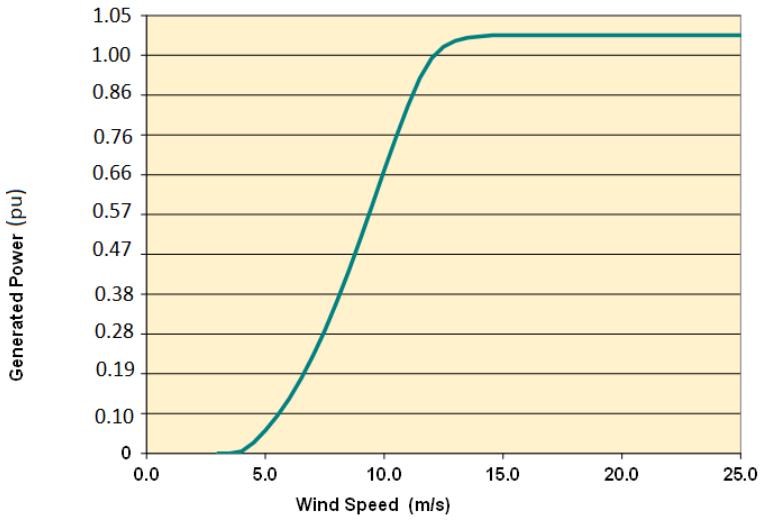

Figure 2-14: Wind Turbine power curve (courtesy of Aurecon)

The power curve in Figure 2-14, is typical for a wind turbine. The wind turbine will cut in at wind speed of 4 m/s and, in order to minimize the inrush current to the generator in a soft starter can be used. For an asynchronous induction generator (ASIG) a soft starter is used because it has a more limited operating range than the DFIG. If the generator speed reaches synchronous speed the soft starter thyristor will connect the generator to the grid by a phase controller with a phase angle of zero degrees. At this point phase and frequency of the generator stator are the same as the grid. Accordingly, the soft starter will be bypassed during normal power generation. This soft starter is a combination of thyristors and a small controller. Below rated speed the phase angle will be adjusted to reduce the inrush current since the machine is not operating at synchronous speed.

The soft starter will improve the starting inrush current but will generate a harmonic which will be considered in the power quality study. The peak inrush current for wind turbines with a soft starter will be less than 27 % of the turbine rated current for wind speeds of 4 m/s (cut-in wind speed) and can be less than 113 % of the turbine rated current for wind speeds of 12 m/s (rated wind speed). ASIGs are used in Case Study 2.

To reduce the impact of the turbine inrush current during starting, a soft start function with the characteristics in Figure 2-15 is proposed. This allows the turbine to be slowly turned on and this rate is variable depending on the wind speed and the turbine can ramp up to the correct speed in a controlled manner.

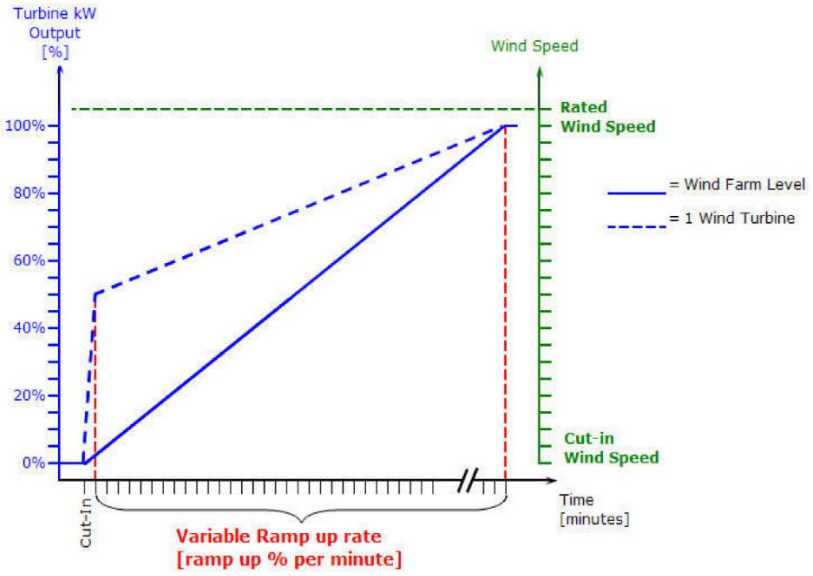

Figure 2-15: Wind Turbine ramp-up function in respect to wind farm (courtesy of Aurecon and turbine supplier)

The wind turbines in Case Study 1 have a power factor compensation unit of 1050 kVAr (14 steps power factor correction – PFC) with control range of 0.92 lagging to 0.997 leading.

To analyse the wind farm power quality and load flow issues, wind turbines and power distribution system components, such as the step-up transformers and collector cables, are modelled in Paladin software. This is used to model Case Studies 1 and 2 electrical distribution systems with different arrangements. It is used to perform various calculations such as system fault levels, load flow, cable ampacity, turbine transient studies and cable voltage drops. The results generated are compared against operation records.

Manual calculations are used to validate the software simulation results.

Case Study 1 has following main characteristics:

- Wind turbines (as explained above);
- Step up transformer and collector switchgear (690 V/33 kV);
- 33 kV three core cables directly buried; and
- Step up Substation and Transformers (33 kV /330 kV).

Generated power by wind turbine is at 690 V, which is transferred to point of common coupling via 690V/33kV transformer with the specifications given in Table 2-3.

Table 2-3: Technical data of Step up transformer for Case Study 1 (DFIG).

Technical Parameter	Requirement
Rated Power	2500 kVA
Primary Voltage	33 kV (ph - ph)
Secondary Voltage	690 V (ph - ph)
Vector Group	Dyn11
Frequency	50 Hz
Primary Rated Line Current	43.7 A
Secondary Rated Line Current	2092 A
Impedance Voltage @75°C	6.6 %
No Load Loss @75°C	2900 W
Full Load Loss @75°C	17900 W
LV Fault level	31.7 kA
Resistance Voltage (Re %)	0.72 %
Reactance Voltage (Xe %)	6.56 %
X/*R* Ratio	9.16
Zero Sequence Impedance	5.28 %
HV/LV Conductor	Aluminium/ Aluminium

2.5.1 Wind Farm Connection to Grid

Case Study 1 (DFIG) wind farm, is connected to the 330 kV transmission system via two feeders. Accordingly, the source impedance is provided by the grid operator. The positive and zero sequence impedance values for the existing 330 kV transmission line are as follows:

Positive Sequence Impedance:
$0.76 + j5.85$ %
Zero Sequence Impedance:
$5.43 + j17.31$ %
X/*R* ratio of 14 has been assumed for the transformer.

The grid characteristics from the connection point of the wind farm have been modelled for minimum short circuit (Min SC) and maximum short circuit (Max SC) as given in Table 2-4.

Table 2-4: Grid Characteristics.

Grid Condition	Voltage	Positive Sequence		Negative Sequence		Zero Sequence	
		R	***X***	***R***	***X***	***R***	***X***
	kV	%	%	%	%	%	%
Normal Grid connection Min SC	330	0.1354	1.8952	0.1354	1.8952	0.1567	2.1944
Normal Grid connection Max SC	330	0.0926	1.2967	0.0926	1.2967	0.0855	1.1970

2.5.2 MV Cable Characteristics

As described above, each turbine is connected to a 33 kV system via directly buried three core 33 kV cables. The following cable data was obtained from the cable manufacture handbook. The cable resistances were adjusted within the model to accurately simulate both load flow and fault conditions at actual temperatures. The cables have been laid approximately 800 mm below ground level. According to thermal soil resistivity, the average recorded in-ground temperature on site was 20.9°C (in summer) and it is believed that the soil temperature in the winter season will be much lower, which would indicate the utilised figure of 25°C is very conservative. The measurement is illustrated in Figure 2-16.

The thermal soil resistivity test has indicated that the soil moisture content will not reach zero at the burial depth of 800 mm.

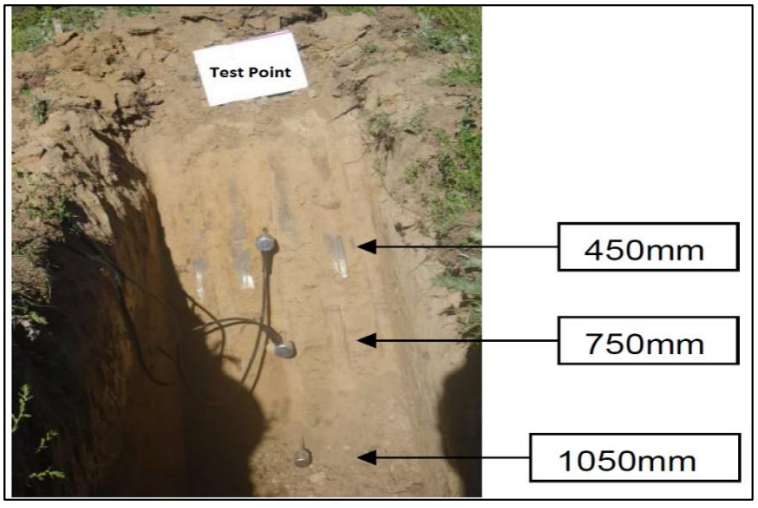

Figure 2-16: Site thermal resistivity test photo for Case Study 1 (courtesy of Aurecon).

Variations in appearance of the soil have indicated different thermal resistivity for various locations. Soil appearance has been monitored during excavation of the cable trenches. The cable characteristics are given in Table 2-5.

Table 2-5: Olex 33 kV Cable Characteristics.

Nominal Conductor Area	Conductor DC Resistance at 20°C	Cond. AC Resistance at 50 Hz and 90°C	Cond. Inductive Reactance at 50 Hz	Insulation Resistance at 20°C	Conductor to Screen Capacitance	Charging Current Per Phase	Screen DC Resistance at 20°C	Zero Sequence Resistance at 20°C
[mm^2]	[Ω/km]	[Ω/km]	[Ω/km]	[MΩ/km]	[µF/km]	[A/km]	[Ω/km]	[Ω/km]
120	0.253	0.325	0.121	14000	0.178	1.06	0.272	1.07
150	0.206	0.264	0.117	13000	0.190	1.14	0.272	1.02
185	0.164	0.211	0.114	12000	0.203	1.21	0.272	0.980
240	0.125	0.161	0.109	11000	0.224	1.33	0.272	0.941
300	0.100	0.129	0.106	9800	0.245	1.46	0.272	0.917
400	0.0778	0.102	0.102	9000	0.270	1.61	0.272	0.895
500	0.0628	0.0814	0.106	8200	0.296	1.77	0.272	0.680

2.5.3 Transformers

Wind farm Case Study 1 (DFIG) includes three different types of transformers as below:

- Turbine tower base 690 V / 33 kV transformer;
- Grid connection 33 / 330 kV transformer; and
- Zigzag Switchgear Earth Transformer (ZSET) at 33kV network.

The turbine base and grid connection transformers were used to step-up the voltage for transmission and distribution and are well known in the industry. However the Zigzag Switchgear Earth Transformer (ZSET) has a specific use and is not common equipment in power grids. The Zigzag transformer has a special purpose, the transformer with a zigzag or "interconnected star" winding connection creates an output source with voltage vector sum of two (2) phases offset by 120°.The ZEST provides a missing neutral connection from an ungrounded 3-phase system to permit the grounding of that neutral to an earth reference point. The ZEST also has a harmonic mitigation application, as it can suppress triplet (3rd, 9th, 15th and 21st) harmonic currents [24].

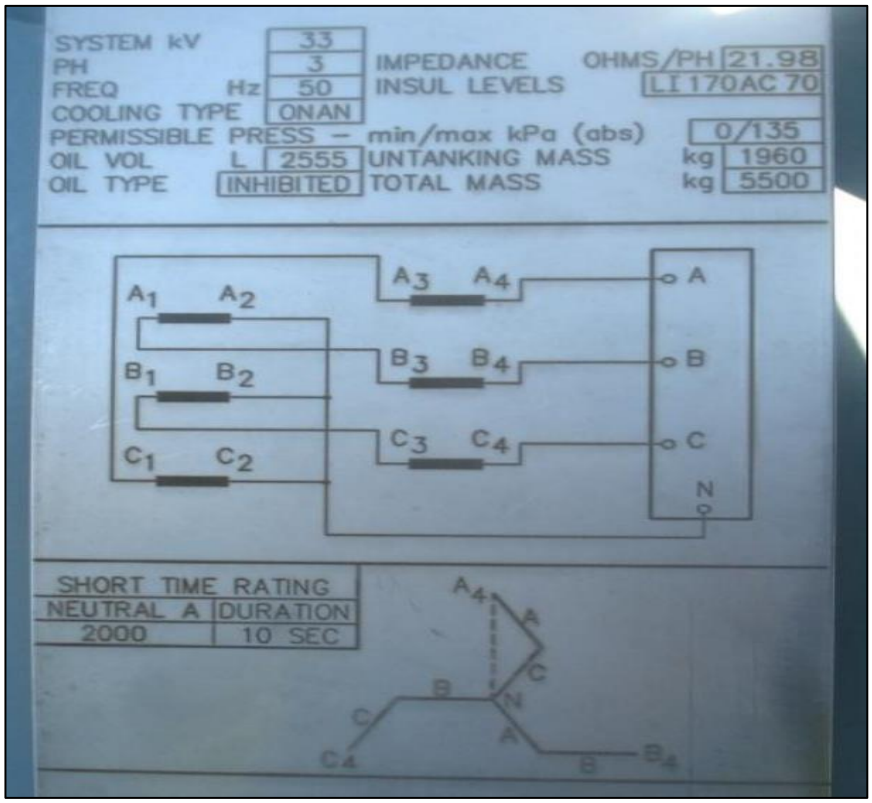

Figure 2-17: ZEST name plate photo for Case Study 1 (courtesy of Aurecon)

Table 2-6: Transformer Characteristics.

Type of Transformer	Rating	Primary Winding	Secondary Winding	Positive Sequence		Negative Sequence		Zero Sequence	
				R	***X***	***R***	***X***	***R***	***X***
	MVA	V	V	%	%	%	%	%	%
Turbine Base LV/MV	2.5	690	33000	0.716	6.56	0.716	6.56	∞	∞
Grid Connection MV/HV	80	33000	330000	0.28	13.49	0.28	13.49	∞	∞
Switchgear Earth Transformer	1	1000	33000	NA				11.47	16.08

Figure 2-17 presents screen shot of the ZEST nameplate, the impedance of each phase of the above ZEST transformer is 21.98 Ω with a neutral current rating of 2000 A for 10 s. To correctly model the network impedance, percentages of transformer impedance should be calculated. According to IEEE C57.32:2015 [25] for grounding transformers zero sequence impedance should be rated in ohms per phase on the name plate of grounding transformers, also when sequence impedances for the system are not specified, the ratio X/R should be taken to be the

ratio of Ohms reactance to Ohms resistance in the winding of the ZEST through which the current flows. The impedance of the ZSET is assumed to be 1.25 + j17.51 Ω.

The data in Table 2-6 are used in the system model.

2.5.4 Generator

The transient and subtransient impedances data in Table 2-7 is used to model the wind turbine generators. This is based on the supplier information.

Table 2-7: Case Study 1 (DFIG) Generator Characteristics.

WTG Nacelle Generators									
Duty	**Output Voltage**	**Sub Transient**				**Transient**			
		Positive Sequence		**Negative Sequence**		**Positive Sequence**		**Negative Sequence**	
		X″	***X″/R***	***X″***	***X″/R***	***X′***	***X′/R***	***X′***	***X′/R***
	V	%		%		%		%	
4 Pole	690	20	9.1	13.6	9.1	36	9.1	-	-

2.5.5 Wind Farm Load Flow Analysis

The different power systems representing each Case Study wind farm are modelled in Paladin design base software. Wind farm models are used for load flow studies and power quality assessment. Manual calculation presented in Section 2.5.5.2 is used to validate the software model. The purpose of the load flow and power study is to provide the following information. The following parameters have direct impact on the quality of delivered power to grid:

- 3 phase fault level at each bus bar or specific equipment;
- Phase to earth fault level at each bus bar or specific equipment;
- Power factor analysis;
- Voltage fluctuation on different locations of system; and
- Cable loading.

The grid connection and each component of Case Study 1 are modelled as per the specifications presented in Section 2.6.4. This is shown in Figure 2-18.

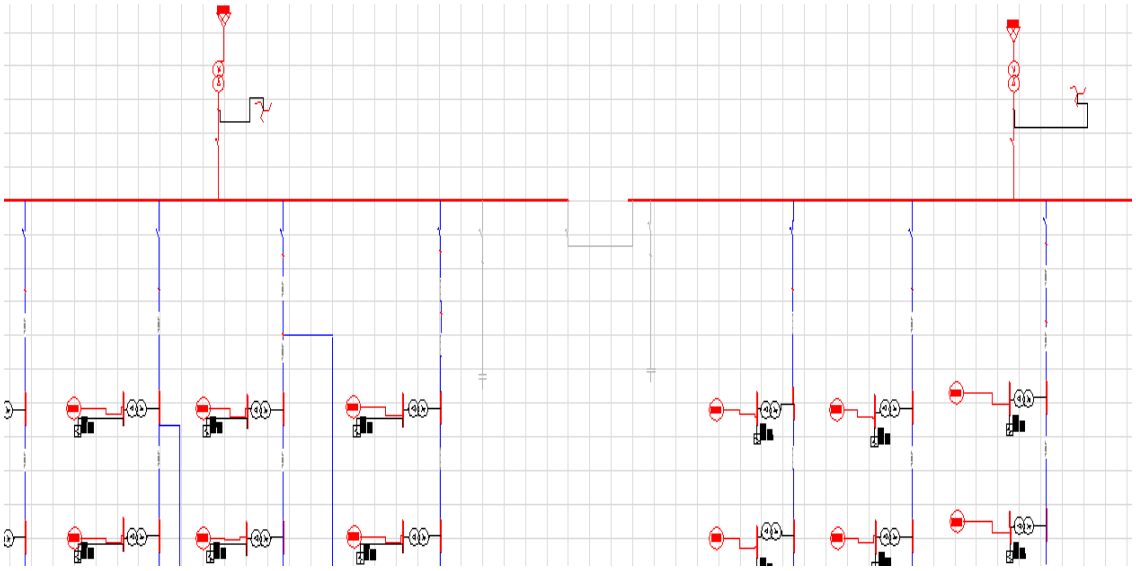

Figure 2-18: Wind farm Case Study 1 in Paladin software.

2.5.5.1 Load Flow Assessment

There are several mathematical methods for power network system study and load flow analyses. Among these methods, iterative methods are widely used. From these methods, the Newton–Raphson power flow method is preferred and has become a reference method for calculating power flow. Along with this, Gauss-Seidal is used for load flow solutions. Here, a fast-decoupled Newton-Raphson load flow analysis method is used to compute Case Study 1 (DFIG) steady-state (voltages magnitudes and angles) and the real and reactive power flows into every line and transformer. The power system model generates non-linear algebraic equations and to solve these equations, two solution algorithms based on power equations of the methods are adopted. Experiment results show that the number of iterations increases proportionally with the number of buses for the Gauss-Seidel technique while that of the Newton–Raphson method remains almost constant even with a varying number of buses. Gauss-Seidal is best suited for systems with a small number of buses because it does not converge with large bus systems. The Gauss-Seidel method was widely used before the introduction of the Newton-Raphson method (NR) which is more reliable but has higher computation memory requirements. The method was made practical by using optimally ordered Gaussian elimination and special programming techniques. Performance of the conventional NR method has continued to receive attention. In 2009, Yuo et al. [55] proposed a method of constructing the Jacobian matrix for Newton power flow expressed in rectangular form. The small impedance branch may result in the non-convergence of the Newton-Raphson power flow method in both rectangular form and polar form. Analysis shows the configuration of the Jacobian matrix plays a big part in the convergence of the Newton-

Raphson power flow in rectangular form particularly when it is applied in systems with small impedance branches.

Normally load flow analysis can be conducted for systems operating under balanced conditions. However in this research unbalanced network frequency load flow is assessed as well. The steady-state solution of an AC electrical network is governed by the matrix equation [29]:

$$\bar{I} = \bar{Y}\bar{V} \tag{2-41}$$

In this equation $\bar{I}$ is an *n*-dimensional vector of network currents injected on each system bus; $\bar{V}$ is an *n*-dimensional vector of system voltages at each system bus; and, $\bar{Y}$ is an $n \times n$ matrix of network admittance; which is a convenient representation of the inverted network complex impedances. The diagonal elements of the admittance matrix are the sum of all the admittances connected to each node, known as the self-admittance:

$$\bar{Y}_{ii} = \sum_{\substack{j=0 \\ j \neq i}}^{n} \bar{Y}_{ij} \tag{2-42}$$

where, as noted, $i \neq j$. The off-diagonal elements are equal to the negative of the mutual admittance between network nodes so that

$$\bar{Y}_{ij} = \bar{Y}_{ji} = -\bar{y}_{ij} \tag{2-43}$$

The network buses connect the impedances of each respective circuit branch so that they are represented by $\bar{Z}_{i1}, \bar{Z}_{i2}, \bar{Z}_{i3}, \ldots \bar{Z}_{in}$. The impedances are inverted to obtain the system admittances where $\bar{y}_{i1}, \bar{y}_{i2}, \bar{y}_{i3}, \ldots \bar{y}_{in}$. Using Kirchhoff's Current Law:

$$\bar{I}_i = \bar{y}_{i0}\bar{V}_i + \bar{y}_{i1}\left(\bar{V}_i - \bar{V}_1\right) + \bar{y}_{i2}\left(\bar{V}_i - \bar{V}_2\right) + \ldots + \bar{y}_{in}\left(\bar{V}_i - \bar{V}_n\right) \tag{2-44}$$

$$\bar{I}_i = \bar{V}_i \sum_{\substack{j=0 \\ i \neq j}}^{n} \bar{y}_{ij} - \sum_{\substack{j=1 \\ i \neq j}}^{n} \bar{V}_j \bar{y}_{ij} \tag{2-45}$$

The formulation of the network equations based on the nodal admittance form results in complex linear simultaneous equations. However, in a power system it is typically the system power injections and absorptions that are known, not the currents. The real and reactive power injections at bus *i* are as follows:

$$P_i + jQ_i = \bar{V}_i \bar{I}_i^* \tag{2-46}$$

$$\frac{\left(P_i + jQ_i\right)}{\bar{V}_i^*} = \bar{V}_i \sum_{\substack{j=0 \\ i \neq j}}^{n} \bar{y}_{ij} - \sum_{\substack{j=1 \\ i \neq j}}^{n} \bar{V}_j \bar{y}_{ij} \tag{2-47}$$

Therefore, the system model consists of nonlinear equations which can only be solved by iterative means subject to the nodal power balance criteria. The real power losses and reactive power charge in HV cables and transformers are then deduced from the sum of the determined power flows. For larger power systems such as Case Study 1, particularly for high resolution time sequential solutions, this is only feasible by computational methods [29]. Therefore, the Paladin Design base software is used for power system analysis and the Figures 2-23 to 2-25 below and Table 2-8 present the results of the study. In this model, all fault studies were performed with the IEC 60909 algorithm set.

The load flow and fault current studies are all steady-state and do not attempt to predict system transients caused by faults, switching and changes in generation dispatch. The OLTCs of the 330 V / 33 kV power transformers are not enabled during any of the Load Flow scenarios and are set to the primary tap. Switchgear was not modelled in the load flow and short circuit studies as its inclusion adds a lot of complexity and does not affect the results in any measurable way.

Each wind turbine in Case Study 1 (DFIG) generates power at power factor between 0.74 and 0.92 depending on the generator current. Each tower is fitted with a 14 step 1050 kVAr capacitor bank to compensate generated power. This capacitor bank can be switched to adjust the WTG Reactive Power Dispatch at the 690 V connection point. The 33 kV cabling system is therefore required to operate continuously over a range of 0.95 lagging to 0.97 leading power factor swings.

Table 2-8: Load flow computation results. (This is not for full load conditions, partial loadings are simulated.)

Scenario		**Grid Condition 1**			**Grid Condition 2**		
		***P* [pu]**	***Q* [pu]**	**Losses [pu]**	***P* [pu]**	***Q* [pu]**	**Losses [pu]**
Normal Operation Grid connection Voltage 1 pu	Planned	0.92	0.3	0.00273	0.43	0.14	0.0013
	As-Built	0.71	0.32	0.00286	0.64	0.28	0.00337
Under Voltage Operation Grid connection Voltage 0.9 pu	Planned	0.91	0.29	0.00274	0.44	0.14	0.0013
	As-Built	0.69	0.41	0.00458	0.63	0.37	0.00527
Higher Voltage Operation Grid connection Voltage 1.1 pu	Planned	0.92	0.54	0.0023	0.43	0.26	0.00109
	As-Built	0.71	0.35	0.0032	0.65	0.30	0.00258

Figure 2-19 shows the turbine output and operational losses integrated over a yearly cycle based on the available wind data and the wind curve of the turbines for wind farm Case Study 1.

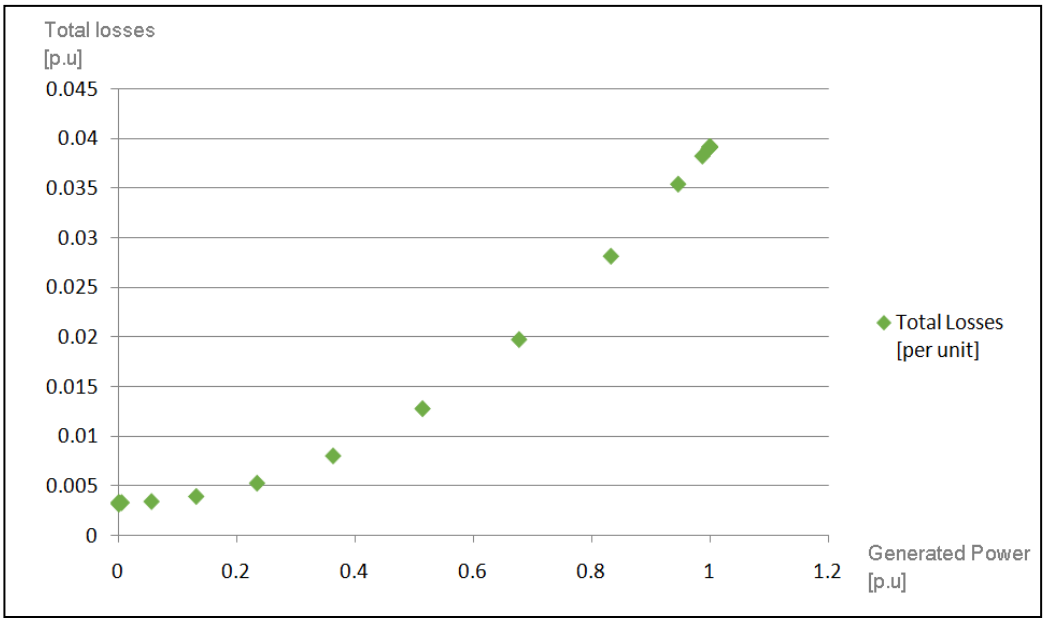

Figure 2-19: Total loss based on generated power over yearly cycle for Case Study 1.

The 690 V cable losses from the DFIG generator terminals to the tower base step up transformers have not been included in the wind farm total loss rate. Figure 2-20 shows the duration of wind speeds recorded over a yearly cycle (8760 hrs).

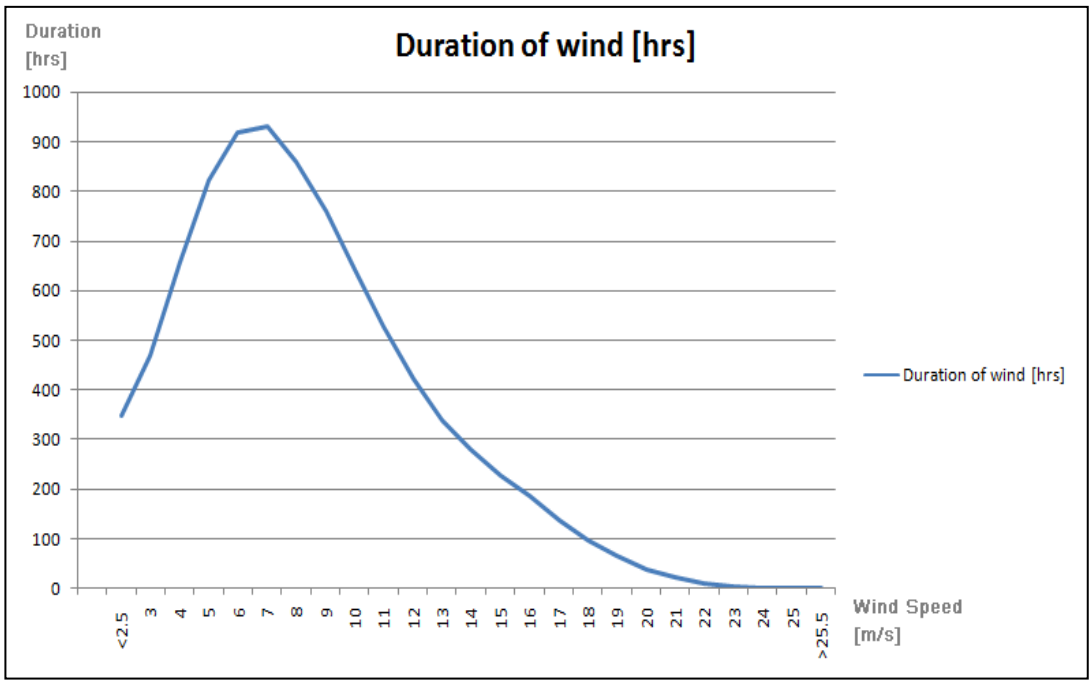

Figure 2-20: Wind duration record over a yearly cycle for Case Study 1.

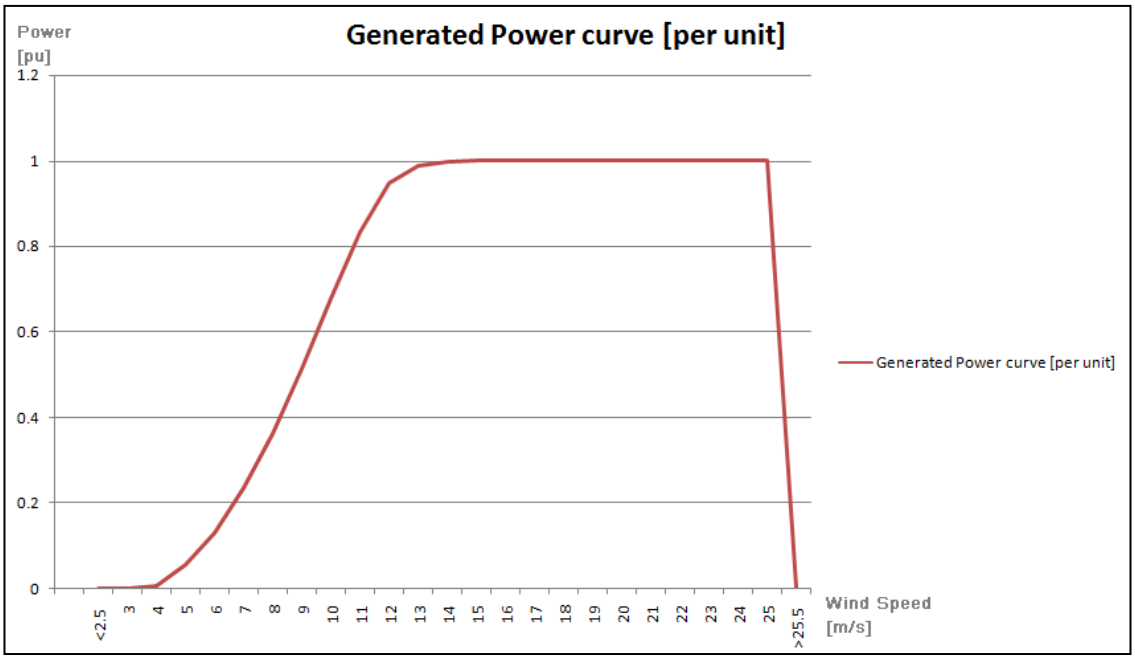

Figure 2-21: Power generation record for DFIG wind turbines at wind farm Case Study 1.

The power system study is the basis of network power system operation. The power study defines minimum requirement of power factor correction system and SCADA skeleton. This is shown in Figure 2-22 for Case Study 1.

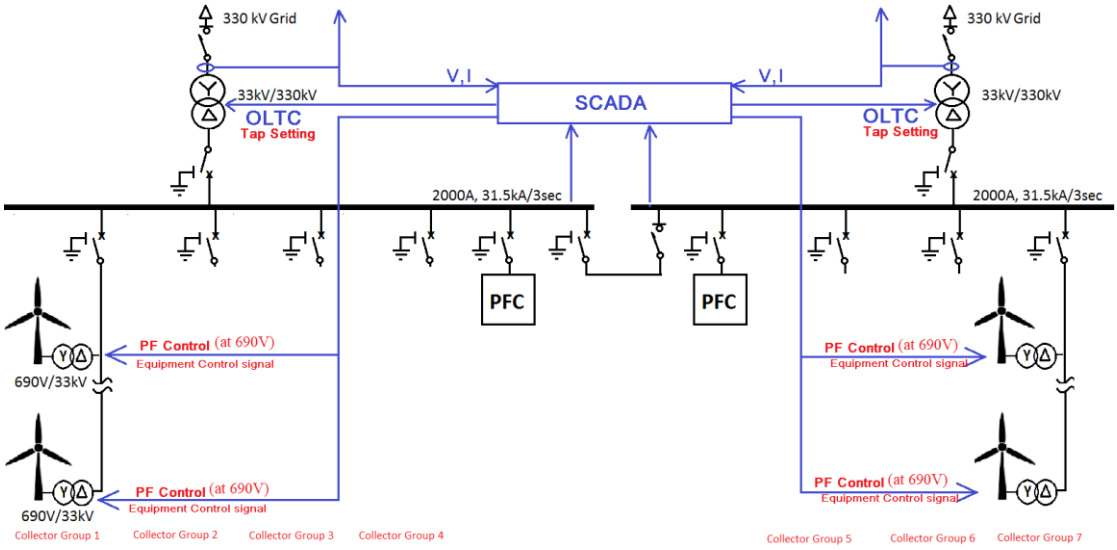

Figure 2-22: Wind farm Case Study 1 SCADA block diagram.

The load flow analysis was used to design the wind farm power system at the design stage. However, during operation, the P, Q and V of the wind farm will be controlled via the SCADA system. Additional power factor correction units (PFCs) are shown in Figure 2-22.

Simulation results indicate that during significant network load variation the voltage and frequency of the point of common coupling (PCC) can change due to the DFIG generators dynamic response. Figures 2-23 and 2-24 present the PCC voltage and frequency response during major load switching at the assumed nearby industrial park with large size induction motors. Note that the pu voltage fluctuation in Figure 2-23 is small and this is for a 10 MW load switch.

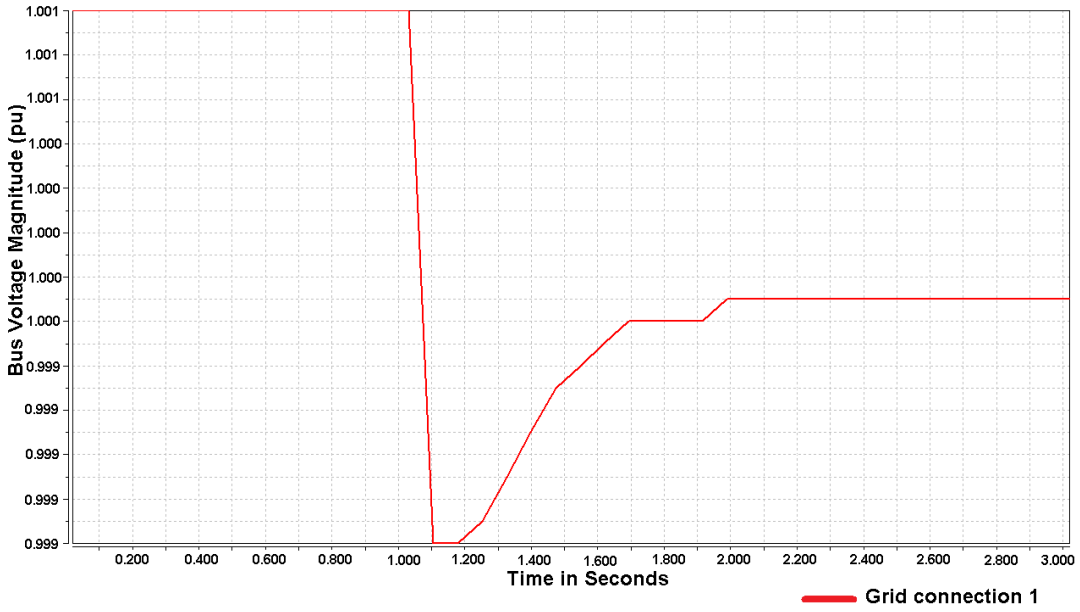

Figure 2-23: Voltage fluctuation for Case Study 1 PCC for 10 MW load switching.

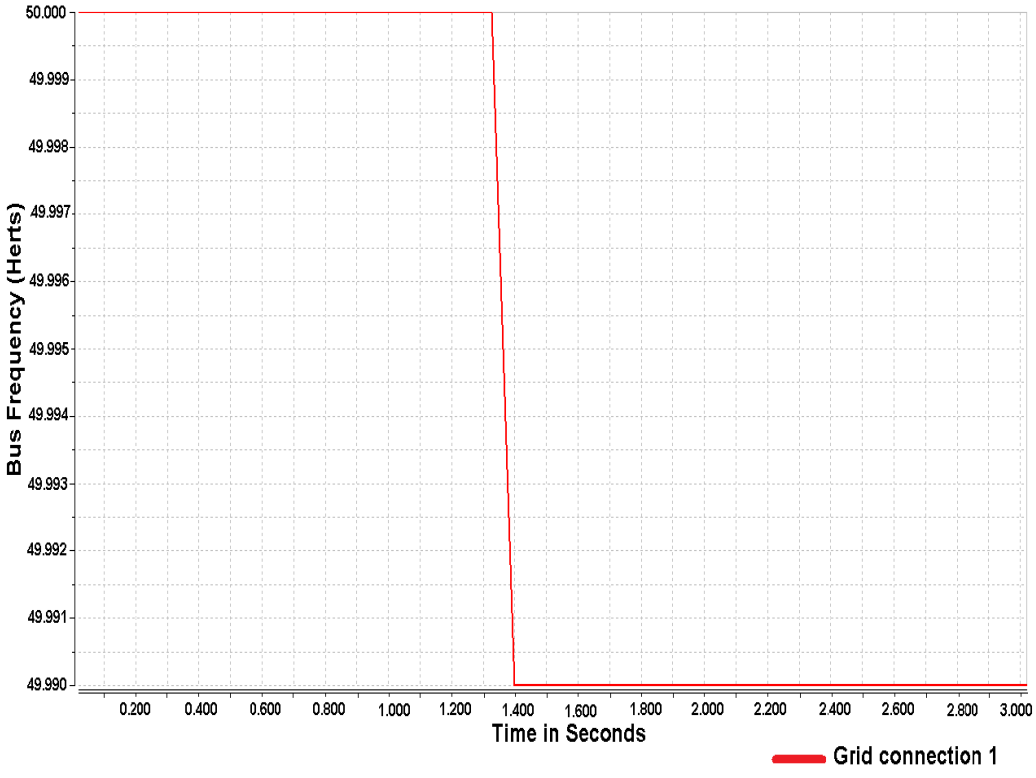

Figure 2-24: Frequency fluctuation for Case Study 1 PCC for 10 MW load switching.

The system study indicates that during 10 MW load switching due to the On-Line Tap Changer (OLTC) response the DFIG will be impacted by a load fluctuation which results in frequency fluctuation. Figure 2-25 shows the voltage curves of the first DFIG located 200 m from the wind farm main substation and second DFIG located 2.5 km away from the main substation.

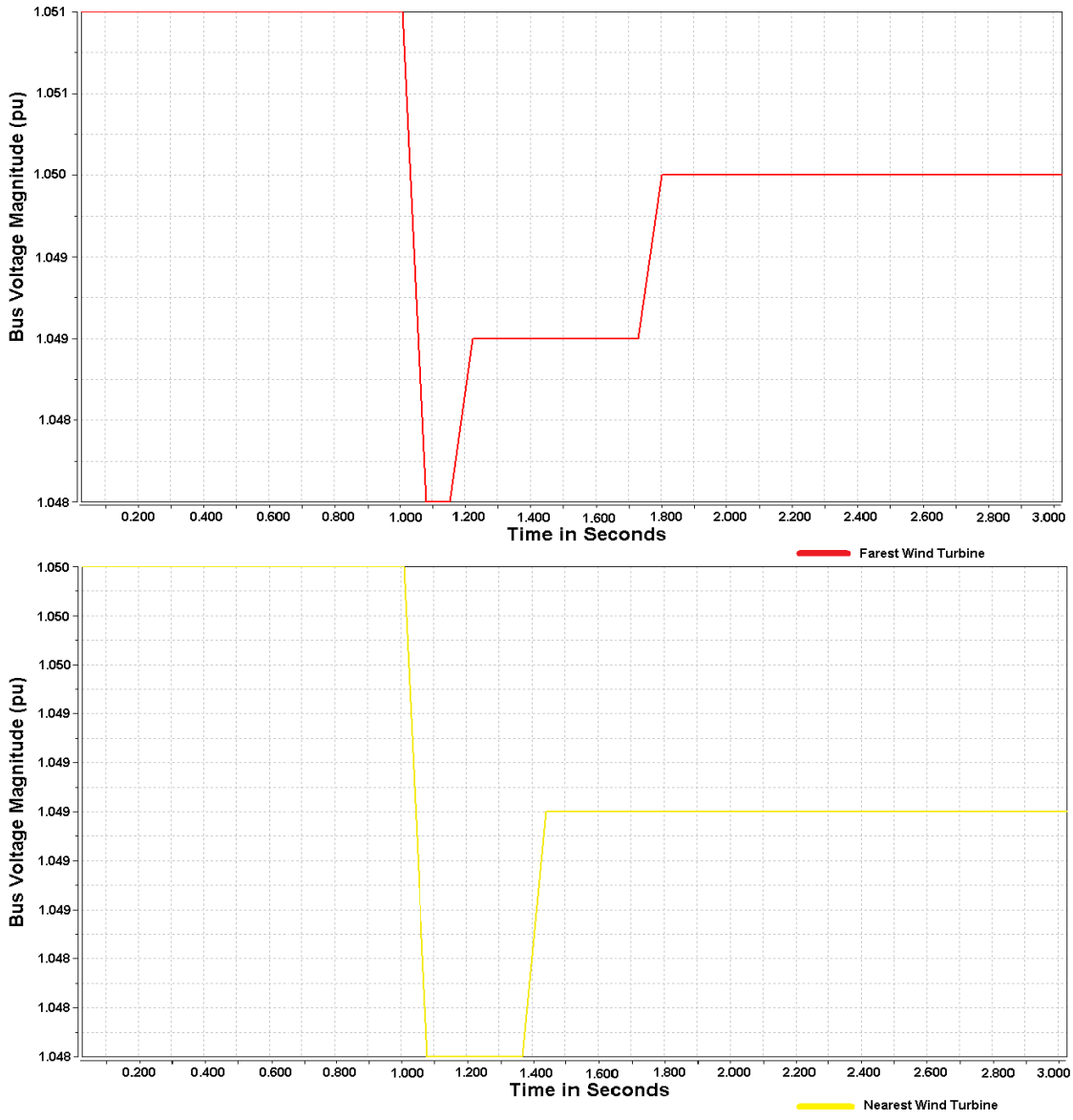

Figure 2-25: Voltage fluctuation at DFIGs for Case Study 1 during 10 MW load switching.

2.5.5.2 Fault Condition Assessment

Power supply interruption is one of the power quality aspects, therefore it is important to consider fault conditions for all power systems. The power system components should be able to handle the expected fault level. This requires accurate fault level calculations based on impedances and

behaviour of system components. The fault condition studies thus need to consider contributions of both within wind turbines and grid point of common coupling (PCC).

The wind farm fault condition is not covered in the standards since the behaviour of the DFIG generator is not well defined. In this research fault transient analysis is conducted for three scenarios:

- Fault supplied by grid assuming DFIG wind turbines do not contribute to the fault level;
- Fault supplied by DFIG wind turbines only; and
- Actual operating system fault analysis when grid and wind turbines are contributing.

The wind turbine and DFIG generator have been modelled in Paladin design base software for Case Study 1. The principal of fault level calculations is presented in IEC 60909 and AS 3851. Three scenarios are considered in the short circuit analysis of Case Study 1. The primary purposes for these scenarios are

- Maximum fault level: To determine the maximum three phase and line to ground fault levels at bus locations throughout the wind farm for the purpose of equipment selection (Refer to Figure 2-30).
- Minimum fault level: To determine the minimum fault levels at bus locations throughout the wind farm to ensure definite operation of protection devices and adequate clearing times.

As presented in Australian Standard AS 3851and IEC 60909 there is a distinction between short-circuit impedances at short-circuit location and short-circuit impedances of individual electrical equipment. According to the calculation with symmetrical components, there can be positive-sequence, negative-sequence and zero-sequence short-circuit impedances. In most cases the negative sequence impedances are equal to the positive-sequence impedances when calculating the initial short-circuits currents. The following sections provide the main element modelling method for short circuit analysis:

I. DFIG generator model

Figure 2-26 demonstrates the meaning and the principal measurement of the positive-sequence and the zero-sequence impedances of the DFIG generator power system.

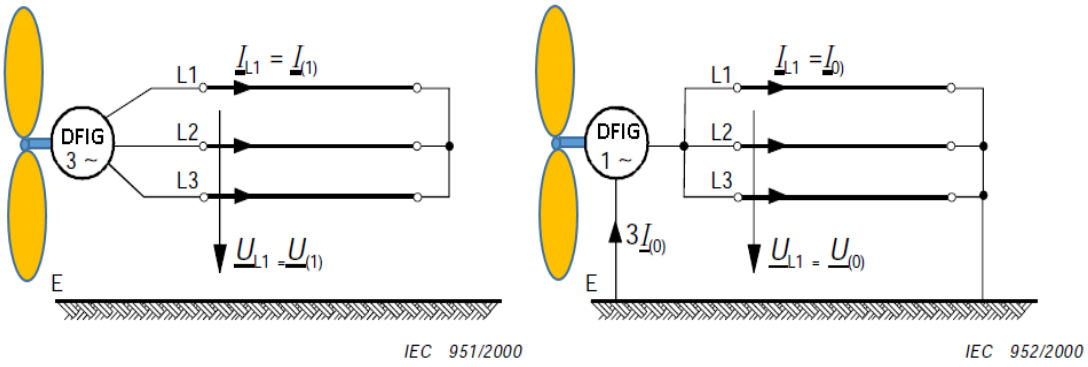

a) positive-sequence b) zero-sequence

Figure 2-26: Positive-sequence and zero-sequence impedances of a DFIG for Case Study 1 (courtesy of IEC).

In practice, the measurement of voltage U_{L1} and current I_{L1} leads to the absolute value Z of the impedance. The impedances are shown in Figure 2-27 where

$$Z_{(1)L} = \left(\frac{U_{L1}}{I_{L1}}\right) = \left(\frac{U_{(1)}}{I_{(1)}}\right) \tag{2-48}$$

$$Z_{(0)L} = \left(\frac{U_{L1}}{I_{L1}}\right) = \left(\frac{U_{(0)}}{I_{(0)}}\right) \tag{2-49}$$

The DFIG generator impedances for Case Study 1 were provided by the turbine supplier and included in the software model for the network fault level study.

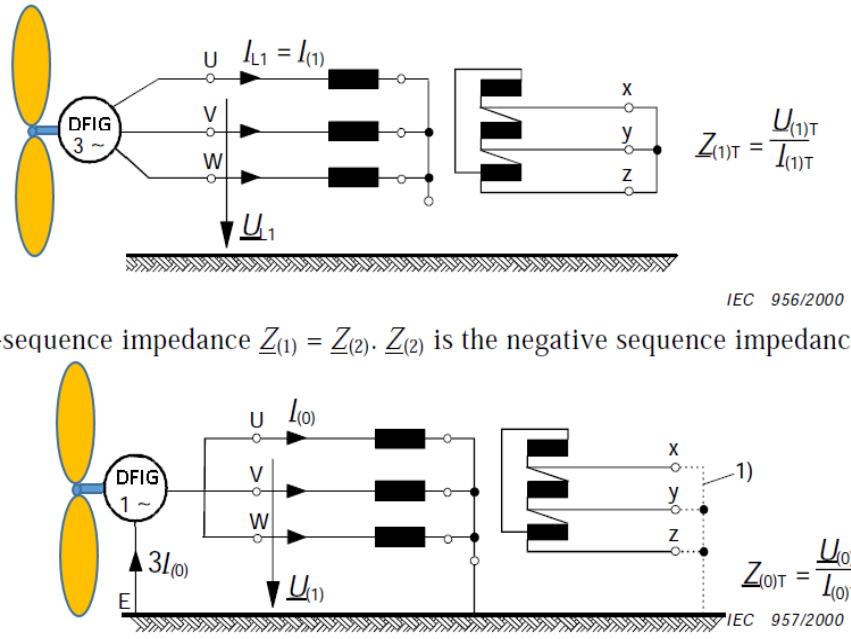

a) Positive-sequence impedance $\underline{Z}_{(1)} = \underline{Z}_{(2)}$. $\underline{Z}_{(2)}$ is the negative sequence impedance

b) Zero-sequence impedance $\underline{Z}_{(0)}$

Figure 2-27: Positive-sequence and zero-sequence impedances of transformer for Case Study 1 (courtesy of IEC).

I. Transformers model

Transformers with the vector group YNd are typical in high-voltage networks, with neutral point earthing, normally only on one side. Transformer impedances are normally provided by the supplier which should be included in the software model for the network fault level study.

II. Grid PCC model

The fault level of the transmission and distribution system at the proposed location for wind farms normally will be provided by the network operator during the wind farm detailed design. The fault level can be used to calculate the grid source impedances according to the Thevenin equivalent voltage method. The following calculations were adopted from Australian Standard AS 3851:

$$\text{Positive Sequence Impedance } Z_{(1)S} = \frac{cV}{\sqrt{3}I_{3\phi}} \tag{2-50}$$

Where $I_{3\phi}$ is network short circuit provided by the EHV grid operator. The c is voltage factor and has been chosen to be representative of Australian practice. The voltage factor represents a conservative method of taking into account the effects of shunt admittances including passive loads and transformer tap positions. The introduction of a voltage factor (c) is necessary for the following reasons:

(a) Voltage variations depending on time and place;

(b) Changing of transformer taps;

(c) Neglecting loads and capacitances by calculations; and

(d) The sub-transient behaviour of generators and motors.

The voltage factor (c) for systems with nominal system voltage U_n is presented in Table 2-9 for maximum and minimum fault level calculation.

Table 2-9 Voltage factor levels [36].

Nominal system voltage U_n	**Voltage factor (c)**	
	Maximum short- circuit	**Minimum short- circuit**
$U_n \le 690$ V	1.09	0.94
$U_n > 690$ V	$\frac{U_h}{U_n}$	$\left(\frac{\text{Lowest operating voltage}}{U_n}\right)^*$

*This is a line-to-line voltage. In the absence of an established value, assume c = 0.9.

U_h is the highest voltage of the system as per standard limit.

Separating $Z_{(1)S}$ into the real and imaginary components yields:

$$Re_{z_{(1)S}} = Z_{(1)S} \cos\left| a\tan\left(\frac{X}{R_{3\phi}}\right)\right| \tag{2-51}$$

$$Im_{z_{(1)S}} = Z_{(1)S} \sin\left| a\tan\left(\frac{X}{R_{3\phi}}\right)\right| \tag{2-52}$$

$$\text{Negative Sequence Impedance, } Z_{(2)S} = Z_{(1)S} \tag{2-53}$$

The zero sequence impedance (including reactance) can be calculated by following equations:

$$I_{1\phi} = \frac{\sqrt{3}cV}{\left|Z_{(1)S} + Z_{(2)S} + Z_{(0)S}\right|} \tag{2-54}$$

$$Z_{(0)S} = \frac{\sqrt{3}cV}{I_{1\phi E}} - 2Z_{(1)S} \tag{2-55}$$

Separating them into the real and imaginary components yields:

$$Re_{z_{(0)S}} = \left(\frac{\sqrt{3}cV}{I_{1\phi E}}\right)\cos\left| a\tan\left(\frac{X}{R_{1\phi E}}\right)\right| - 2Re_{z_{(1)S}} \tag{2-56}$$

$$Im_{z_{(0)S}} = \left(\frac{\sqrt{3}c.V}{I_{1\phi E}}\right)\sin\left| a\tan\left(\frac{X}{R_{1\phi E}}\right)\right| - 2Im_{z_{(1)S}} \tag{2-57}$$

$$Z_{(0)S} = Re_{z(0)s} + jIm_{z(0)s} \tag{2-58}$$

III. Cable model

A method of cable impedance calculation is presented in above Section 2.5.5.2-II. Normally cables impedances will be provided by the supplier which should be included in the software model for the network fault level study.

The short circuit studies performed for Case Study 1 (DFIG) considered contributions from both within the wind farm and from the network. The results from the study together with the equipment data and selection criteria demonstrate the suitability of specified cables and

switchgear for the collector system. The short circuit study provides the necessary information required to design the protection system.

Practical Example - Case Study 2:

Due to several commercial restrictions for Case Study 1, a second wind farm - Case Study 2 - is used to demonstrate wind farm behaviour during fault conditions. Case Study 2 is not a real installation. It is assumed that Case Study 2 includes eight units of 2 MW wind turbines and a 33 kV network as shown in Figure 2-28.

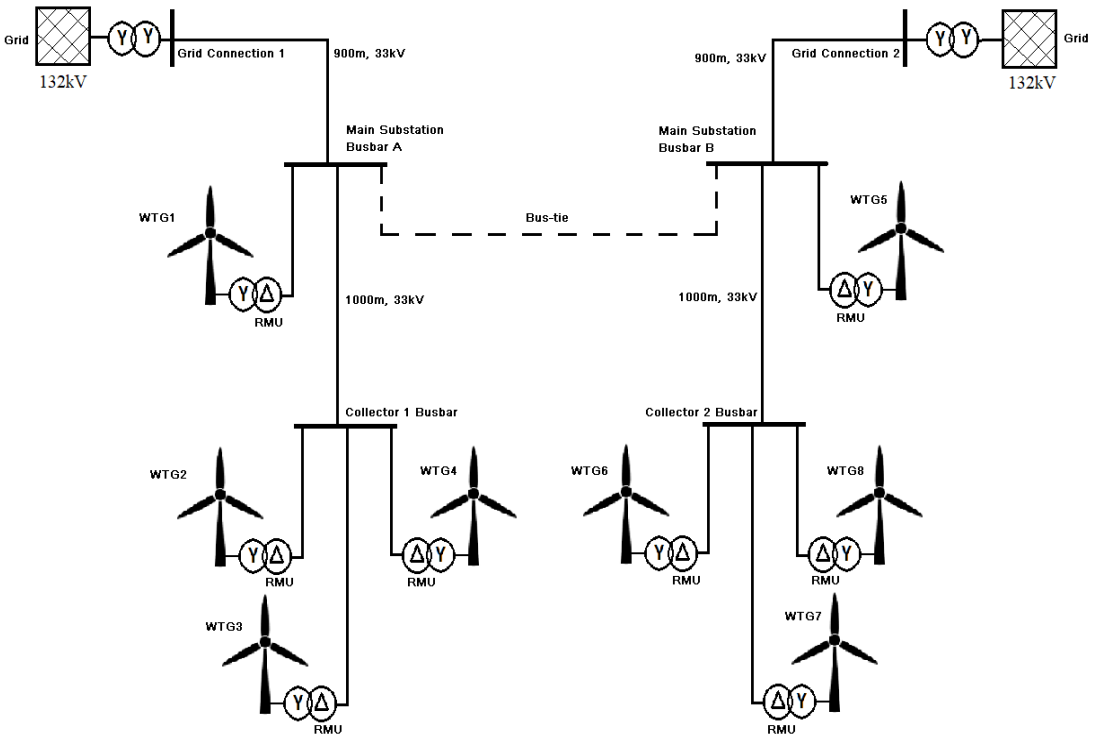

Figure 2-28: Wind farm Case Study 2 power system.

The DFIG generator technical data assumed for the 2MW turbines is presented in Figure 2-29. The following fault scenarios are considered for Case Study 2:

- Fault supplied by grid assuming DFIG wind turbines does not contribute to fault level;
- Fault supplied by DFIG wind turbines only; and
- Actual operating system fault analysis when grid and wind turbines are contributing.

The fault analysis results are presented in the Figure 2-30. The 33 kV circuit breakers of the wind turbines are left in the open position for first round of simulations to analyse grid and turbine fault levels independently.

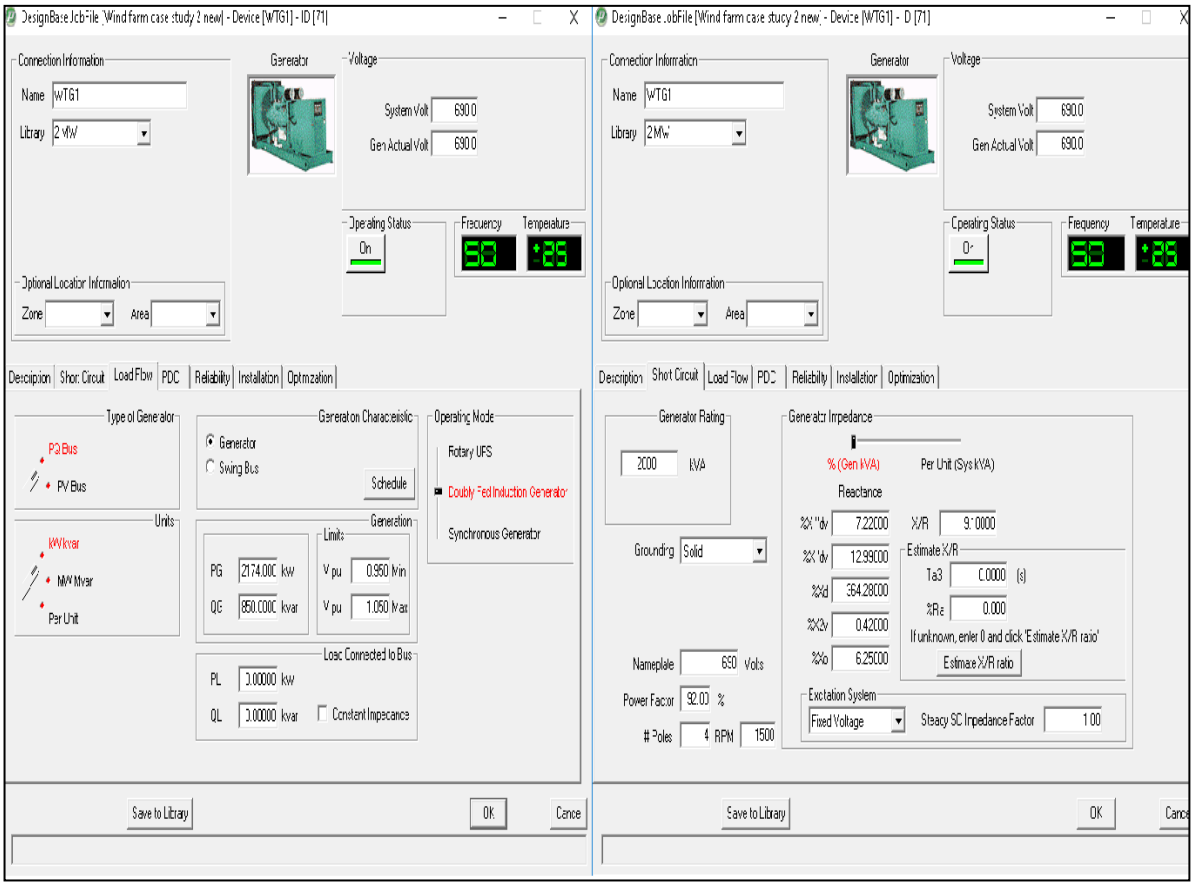

Figure 2-29: Case Study 2 DFIG technical data.

Bus Results: 0.5 Cycle--Symmetrical

Bus Name	Pre-Flt V	3P Flt. A	LL Flt. A	LG Flt. A	LLG Flt A	Thevenin Imped. Complex Z+(pu)	Zo(pu)	3P X/R	Cd	Bus Description
Collector 01 Bus	33000	15070	13206	6665	13426	0.1161	0.5582	7.3614		
Collector 02 Bus	33000	15010	13152	6649	13336	0.1166	0.5590	6.1197		
Grid Connection 1	33000	18100	15900	7400	16044	0.0967	0.5187	20.000	PC	
Grid Connection 2	33000	18100	15900	7400	16044	0.0967	0.5187	20.000	PC	
HVS 01A Bus	33000	16543	14514	6961	14723	0.1058	0.5454	10.693		
HVS 01B Bus	33000	16489	14466	6953	14718	0.1061	0.5457	8.0888		
WTG1	690	29464	48227	45946	46945	143.285	2.4584	9.1000	GI	DFIG
WTG1 LV MSB	690	21800	28726	21461	28224	144.244	6.6714	3.8311		
WTG2	690	29464	48227	45946	46945	143.285	2.4584	9.1000	GI	DFIG
WTG2 LV MSB	690	21800	28726	21461	28224	144.244	6.6714	3.8311		
WTG3	690	29464	48227	45946	46945	143.285	2.4584	9.1000	GI	DFIG
WTG3 LV MSB	690	21800	28726	21461	28224	144.244	6.6714	3.8311		
WTG4	690	29464	48227	45946	46945	143.285	2.4584	9.1000	GI	DFIG
WTG4 LV MSB	690	21800	28726	21461	28224	144.244	6.6714	3.8311		
WTG5	690	29464	48227	45946	46945	143.285	2.4584	9.1000	GI	DFIG
WTG5 LV MSB	690	21800	28726	21461	28224	144.244	6.6714	3.8311		
WTG6	690	29464	48227	45946	46945	143.285	2.4584	9.1000	GI	DFIG
WTG6 LV MSB	690	21800	28726	21461	28224	144.244	6.6714	3.8311		
WTG7	690	29464	48227	45946	46945	143.285	2.4584	9.1000	GI	DFIG
WTG7 LV MSB	690	21800	28726	21461	28224	144.244	6.6714	3.8311		
WTG8	690	29464	48227	45946	46945	143.285	2.4584	9.1000	GI	DFIG
WTG8 LV MSB	690	21800	28726	21461	28224	144.244	6.6714	3.8311		

Fault supplied by grid only

Fault supplied by DFIG turbines only

Figure 2-30: Case Study 2 fault levels independently.

To validate the software simulation, manual calculations have been conducted. It is assumed the fault level of 33 kV grid connection 1 and 2 is 18.1 kA for 3-phase fault and 7.4 kA for earth fault. The X/R ratio of 42 has been provided by service provider of the wind farm Case Study 1 (DFIG) and have been used as an input for both studies.

The positive sequence impedance can be calculated using above the equations presented in this section where the voltage factor (c) is 1.091.

$$Z_{(1)S} = \frac{1.091 \times 33000}{\sqrt{3} \times 18100} = 1.15 \quad [\Omega]$$

$$Re_{z(1)S} = 1.15 \cos\left(a \tan(42)\right) = 0.03 \quad [\Omega]$$

$$Im_{z(1)S} = 1.15 \sin\left(a \tan(42)\right) = 1.15 \quad [\Omega]$$

Therefore, the source positive sequence impedance is:

$$Z_{(1)S} = 0.03 + j1.15 \quad [\Omega]$$

Accordingly, the source zero sequence impedance is:

$$Z_{(0)S} = 0.14 + j6.12 \quad [\Omega]$$

Case Study 2 has 900 m of underground cable between the grid connection point (PCC) and the wind farm main substation. The short circuit level at the wind farm main substation is calculated from

$$Z_{(1)} \text{ (at wind farm substation)} = Z_{(1)S} + Z_{(1)} \text{(conductor)}$$

The conductor impedances have been provided by the cable manufacturer for 3-core, 500 mm², 33 kV cable for the 900 m length is

$$Z_{(1)500 \text{ sq conductor}} = 0.0628 + j0.106 \quad \left[\frac{\Omega}{\text{km}}\right]$$

$$Z_{(0)500 \text{ sq conductor}} = 0.0680 + j0.0606 \quad \left[\frac{\Omega}{\text{km}}\right]$$

$$Z_{(1) \text{ at wind farm substation}} = \left(0.03 + j1.15\right) + \left(\left(0.0628 + j0.106\right) \times 0.9\right) = 0.09 + j1.25 \quad [\Omega]$$

$$Z_{(0) \text{ at wind farm substation}} = \left(0.14 + j6.12\right) + \left(\left(0.0680 + j0.0606\right) \times 0.9\right) = 0.2 + j6.18 \quad [\Omega]$$

$$I_{3\phi \text{ at PCC}} = \frac{cV}{\sqrt{3} \times \left| Z_{(1)\text{at}} \right|} = \frac{1.091 \times 33000}{\sqrt{3} \times 1.25} = 16629 \quad [\text{A}]$$

$$I_{1\phi \text{ at PCC}} = \frac{\sqrt{3}\, cV}{\left| Z_{(1)at} + Z_{(2)\text{at}} + Z_{(0)\text{at}} \right|} = \frac{\sqrt{3} \times 1.091 \times 33000}{\sqrt{0.38^2 + 8.68^2}} = 7177 \quad [\text{A}]$$

The same calculations have been done for Collector 1 and 2 substations located 1000 m from the wind farm main substation so that

$$I_{3\varphi} = \frac{1.091 \times 33000}{\sqrt{3} \times 1.37}$$

$$I_{3\,\phi \text{ collector}} = \frac{cV}{\sqrt{3} \times \left| Z_{(1)\text{col}} \right|} = \frac{1.091 \times 33000}{\sqrt{3} \times 1.37} = 15191 \quad [\text{A}]$$

$$I_{1\,\phi \text{ collector}} = \frac{\sqrt{3}\, cV}{\left| Z_{(1)col} + Z_{(2)col} + Z_{(0)col} \right|} = \frac{\sqrt{3} \times 1.091 \times 33000}{\sqrt{1.18^2 + 8.92^2}} = 6930 \quad [\text{A}]$$

Table 2-10 shows the comparison between software simulation and manual calculation.

Table 2-10: Fault level calculation validation by software and manual method for Case Study 2.

Location of fault	Software calculation		Manual calculation	
	3 Phase fault level [A]	Earth fault level [A]	3 Phase fault level [A]	Earth fault level [A]
Grid connection 1	18100	7400	18100	7400
Grid connection 1	18100	7400	18100	7400
Main substation Busbar A	16543	6961	16629	7177
Main substation Busbar B	16489	6953	16629	7177
Collector 1 Busbar	15070	6665	15191	6930
Collector 2 Busbar	15010	6649	15191	6930

These calculations validate the software model so the transient simulation can be confidently accepted. Figures 2-31 to 2-38 have been plotted by the Paladin Design Base transient analysis module for the following scenarios. It is assumed the primary protection will clear the fault within 100ms (without auto re-closing) and the back-up protection clearance time is 450 ms.

Scenario 1: A 3 phase fault occurs at Case Study 2 main substation with a clearance time of 100 ms; the impact of the fault on network voltage and wind turbine operation are presented in Figures 2-31 to 2.34. It is assumed that the fault has occurs at 1 s.

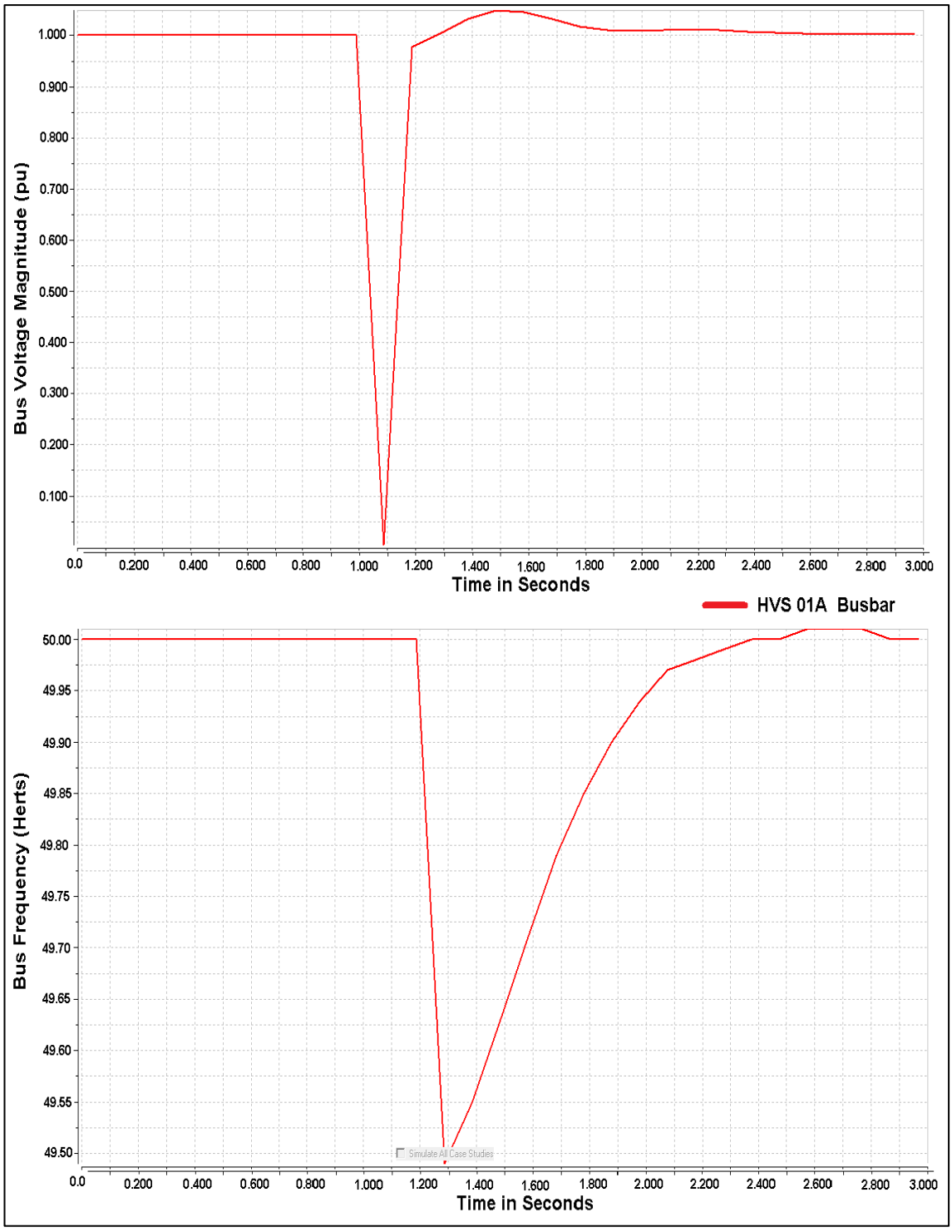

Figure 2-31: Voltage and frequency during 3-phase fault at main substation (100 ms clearance time).

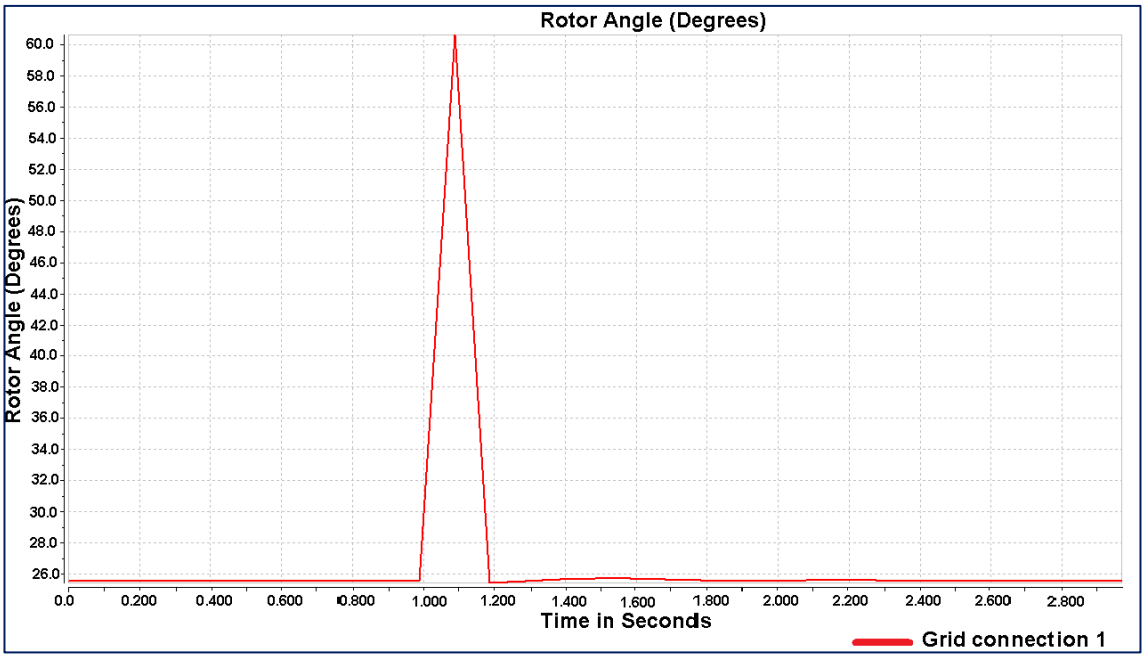

Figure 2-32: DFIG WTG1 rotor angle behaviour during 3-phase fault at main substation (100 ms clearance time).

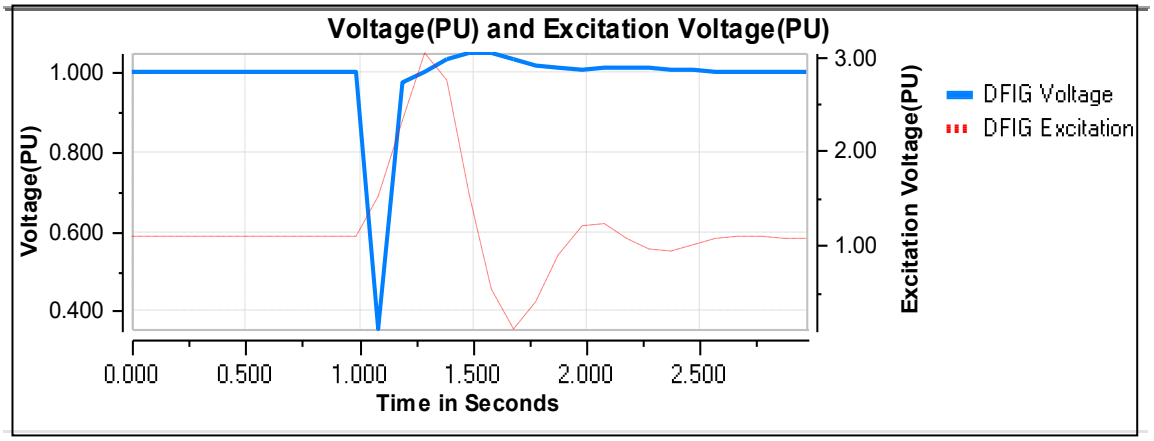

Figure 2-33: DFIG WTG1 voltage behaviour during 3-phase fault at main substation (100 ms clearance time).

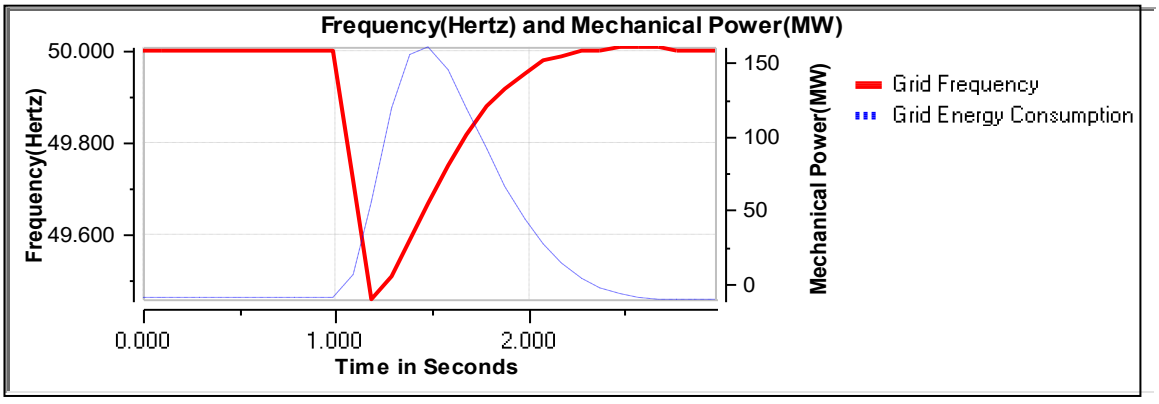

Figure 2-34: Grid power consumption behaviour during 3-phase fault at main substation (100 ms clearance time).

Scenario 4: A 3-phase fault at the Case Study 2 main substations busbar with 450 ms duration. The impacts of fault on network voltage and wind turbine operation are presented in Figures 2-35 to 2-38. It is assumed that the fault occurs at 1 s.

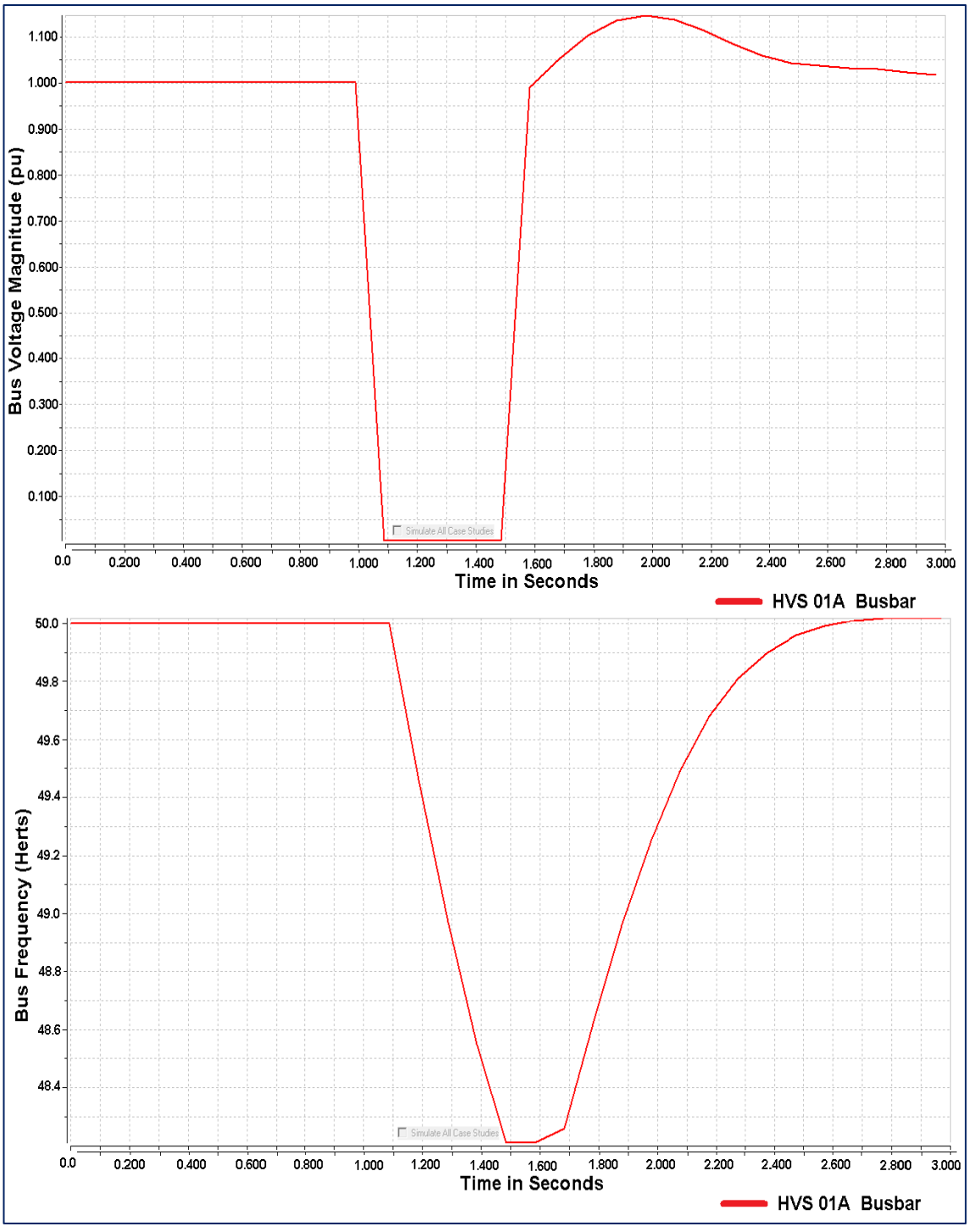

Figure 2-35: Voltage and frequency behaviour during 3-phase fault at main substation (450ms clearance time).

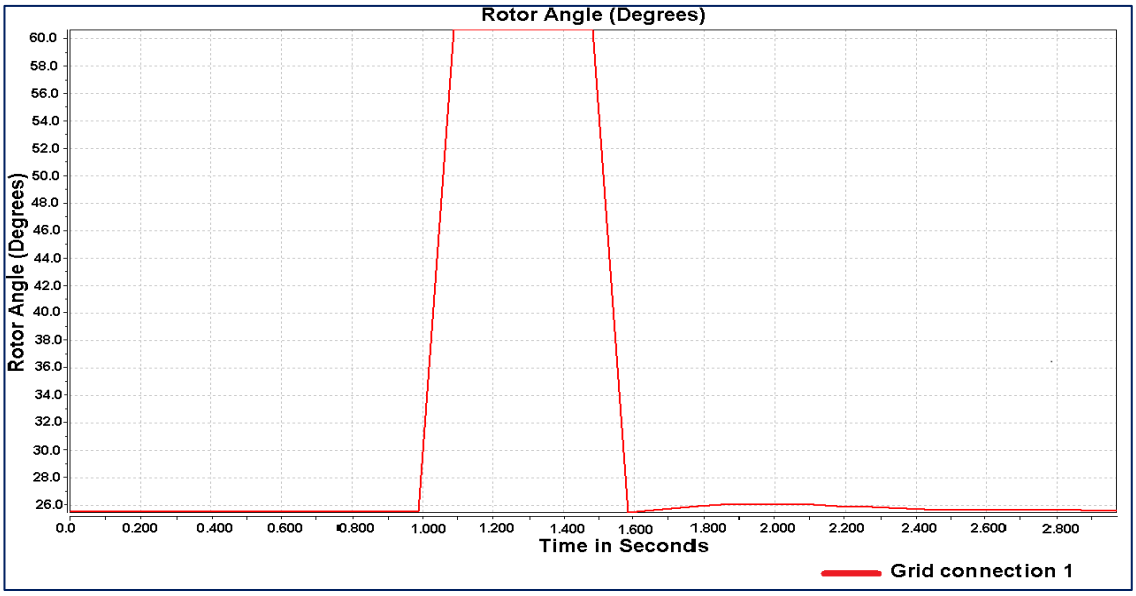

Figure 2-36: DFIG WTG1 rotor angle behaviour during 3-phase fault at main substation (100ms clearance time).

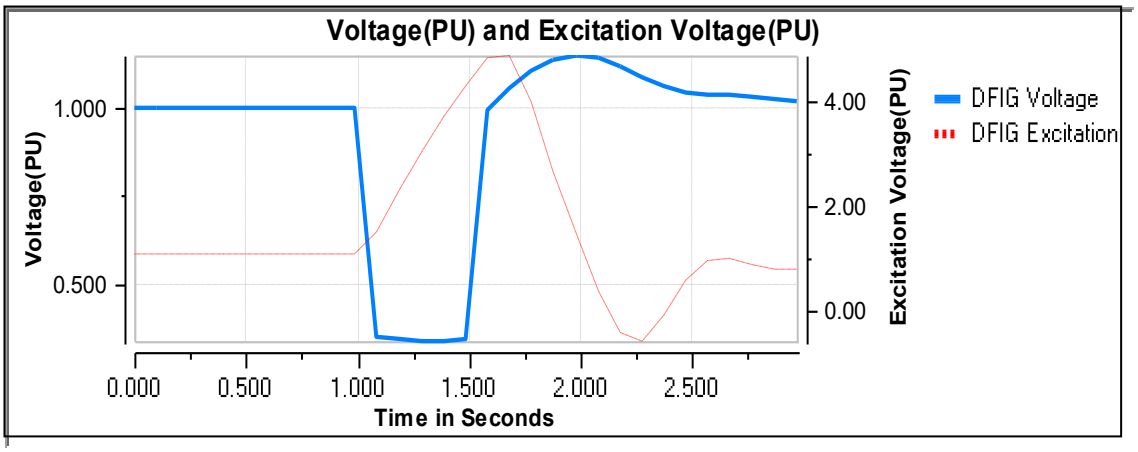

Figure 2-37: DFIG WTG1 voltage behaviour during 3-phase fault at main substation (450ms clearance time).

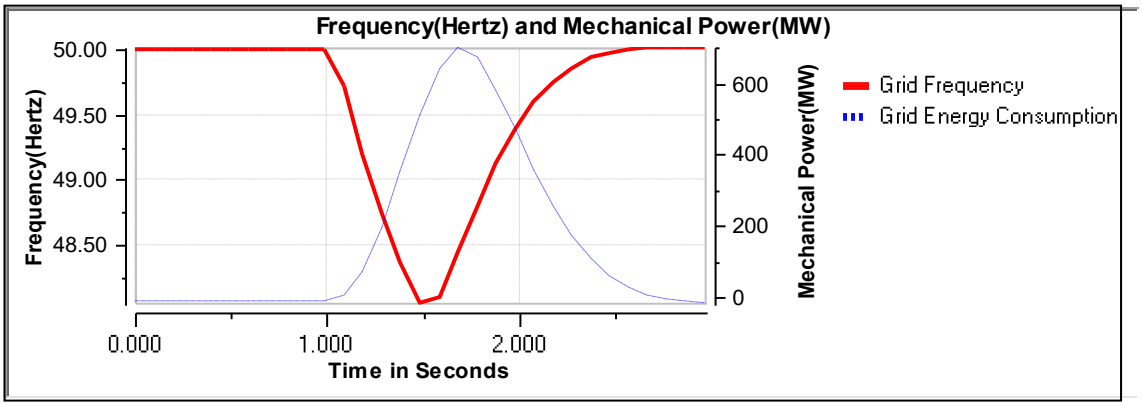

Figure 2-38: Grid power consumption behaviour during 3-phase fault at main substation (450ms clearance time).

As shown in the above fault scenarios, the duration of the fault can impact the wind farm voltage stability. The location of the fault is critical since it will impact on nearby DFIG operation which will impact on the system stability.

2.6 Wind Farm Power Quality Analysis

Power quality can be defined as the comparison of the actual voltage and current waveforms with their "clean" sinusoidal waveforms. Pure sine waves that are free of distortion are sometimes referred to as clean power. Many papers have been written on this subject, so only a brief review of the subject will be presented here. The main intent of this research is to discuss some design ideas that should be considered during wind farm project system study. Also what mitigation method is necessary, and if so, what type should be implemented [21].

In this research the following items are highlighted as the main power quality items for wind farms:

- Harmonics;
- Flicker;
- Unbalances;
- Voltage fluctuation; and
- Wind gust impact on voltage.

The following power quality aspects are considered in the discussion of the main power quality items:

- System stability and intra-regional impact;
- System fault ride through (FRT);
- Network Loading / Interaction with nearby power plants; and
- System frequency fluctuation.

Wind farm power quality assessment is a vital requirement from the planning stage to the actual wind farm operation as it will define whether the wind farm can be connected to the national electricity grid. In Australia, the definition of access limit has been presented by the Australian National Electricity Rules (NER) [30]. The access limits under "NER acceptance of performance Standards" are

- **Automatic Access:** The highest level of performance which is required by the Network Service Provider (NSP) to allow wind farm connection to their network.
- **Minimum Access:** The worst level of performance that can be tolerated by the NSP at the connection point of the wind farm to their grid.

- **Negotiated Access:** Falls between Automatic and Minimum levels

The Australian Energy Market Operator (AEMO) and Network Service Provider (NSP) are assessing proposed wind farm performance standards against the technical requirements and will need to be satisfied that the levels of performance of wind farms are considered not to have a detrimental effect on power system quality and security. These technical requirements consider the quality of the electricity generated by a generating system at its connection point that can have a detrimental effect on other network users [31]. Each connection point is assigned (by the connecting NSP) an automatic access standard for allowable levels of voltage fluctuation, harmonic voltage distortion and voltage unbalance. If the wind farm operator wishes to have a performance standard that is lower than the automatic access standard, this will be a matter for negotiation with the connecting NSP.

The automatic access emission limits are described in the NER as emission limits no more than acceptance levels determined in accordance with either of the stage 1 or the stage 2 evaluation procedures.

This is AEMO's or NSP's responsibility to provide a minimum negotiated harmonic emission limit that is allowable for that location while still ensuring that AEMO can meet the planning limits. The wind farm may be required to provide reports or other evidence to AEMO as to how its generating system will comply with the agreed levels.

If wind farm harmonic emissions, flicker, voltage unbalance and voltage fluctuation fall between automatic and minimum levels, then access to the network can be allowed under a set of emission levels and under a set of conditions negotiated between the wind farm operator and NSP. In general, the closer the wind farm power quality emission is to the Automatic Access standards, the easier it is to create a Negotiated Access. Negotiated Access is usually granted as a Temporary Access based on the availability of "unused" emission allocations which the customer can "borrow". NSP will often require that a customer bring their installation close to the Automatic Access standard and reserve the right to reclaim the "borrowed" allocation if network conditions change.

The determination of the amount of present power quality emission allocation normally is based on at least a week of measurement data under wind farm normal operation at the PCC.

2.6.1 Harmonics

A harmonic is a wave whose frequency is an integer multiple of the fundamental frequency. Harmonics can be caused by magnetic saturation of the cores of transformers. They are also caused by the power electronic devices such as diodes, thyristors, IGBTs and other switching devices which are found in convertors used in DFIG wind turbines [7].

As mentioned above, the harmonic emission limit for wind farms will be defined by AEMO or NSP. It is assumed that the harmonic voltage distortion is equal to or less than the limits shown in Table 2-11 as a percentage of the fundamental voltage shall be used for Case Study 1.

Table 2-11: Allowable harmonic emission level for Case Study 1.

Harmonic Order	% Network Voltage	Harmonic Order	% Network Voltage	Harmonic Order	% Network Voltage
1	100	18	0.08	35	0.21
2	0.12	19	0.38	36	0.08
3	0.17	20	0.08	37	0.20
4	0.08	21	0.08	38	0.08
5	0.41	22	0.08	39	0.08
6	0.10	23	0.27	40	0.08
7	0.41	24	0.08	41	0.19
8	0.08	25	0.27	42	0.08
9	0.21	26	0.08	43	0.19
10	0.08	27	0.08	44	0.08
11	0.57	28	0.08	45	0.08
12	0.08	29	0.24	46	0.08
13	0.57	30	0.08	47	0.18
14	0.08	31	0.23	48	0.08
15	0.11	32	0.08	49	0.17
16	0.08	33	0.08	50	0.08
17	0.038	34	0.08	THD	0.53

Since Case Study 1 performance results cannot be presented in this research, the Case Study 2 model is used for harmonic analysis.

Accordingly, two scenarios were simulated for Case Study 2 (ASIG and DFIG):

- **Scenario 1:** it is assumed that all turbines are 2 MWA synchronous generators (ASIG) with external variable resistor (Type 2).
- **Scenario 2:** it is assumed that all turbines ae 2 MW DFIG generators of Type 3.

Paladin software is used to simulate harmonic emission for wind farm Case Study 2. It is assumed that Table 2-12 represents the generated current and voltage harmonic by a 2 MW asynchronous generator (ASIG) with external variable resistor.

Table 2-12: Assumed harmonics on 2 MW Asynchronous generators with external variable resistor.

Harmonic Order	**1**	**3**	**5**	**7**	**9**	**11**	**13**	**15**
% Current	100	19.63*	17.8	12.59	1.43	2.97	0.60	0.38
% Voltage	100	0.03	0.24	0.21	0.01	0.00	0.08	0.00

*Based on the private communication with a turbine manufacturer

Accordingly, Table 2-13 represents the generated current and voltage harmonics from a 2 MW DFIG generator.

Table 2-13: Assumed harmonics on 2 MW DFIG generators.

Harmonic Order	**% Current**	**Harmonic Order**	**% Current**	**Harmonic Order**	**% Current**
1	100.000	18	0.010	35	0.550
2	0.052	19	1.766	36	0.008
3	0.329	20	0.012	37	0.428
4	0.042	21	0.049	38	0.002
5	30.055*	22	0.010	39	0.019
6	0.013	23	0.991	40	0.006
7	8.736	24	0.011	41	0.385
8	0.008	25	0.916	42	0.006
9	0.071	26	0.013	43	0.322
10	0.019	27	0.035	44	0.005
11	6.251	28	0.011	45	0.021
12	0.005	29	0.714	46	0.002
13	3.401	30	0.012	47	0.261
14	0.007	31	0.544	48	0.009
15	0.055	32	0.006	49	0.232
16	0.014	33	0.021	50	0.008
17	2.226	34	0.007	THD	32.28

The harmonic analyses for both generators are shown in Figures 2-39 and 2-40 (at 690 V bus bar).

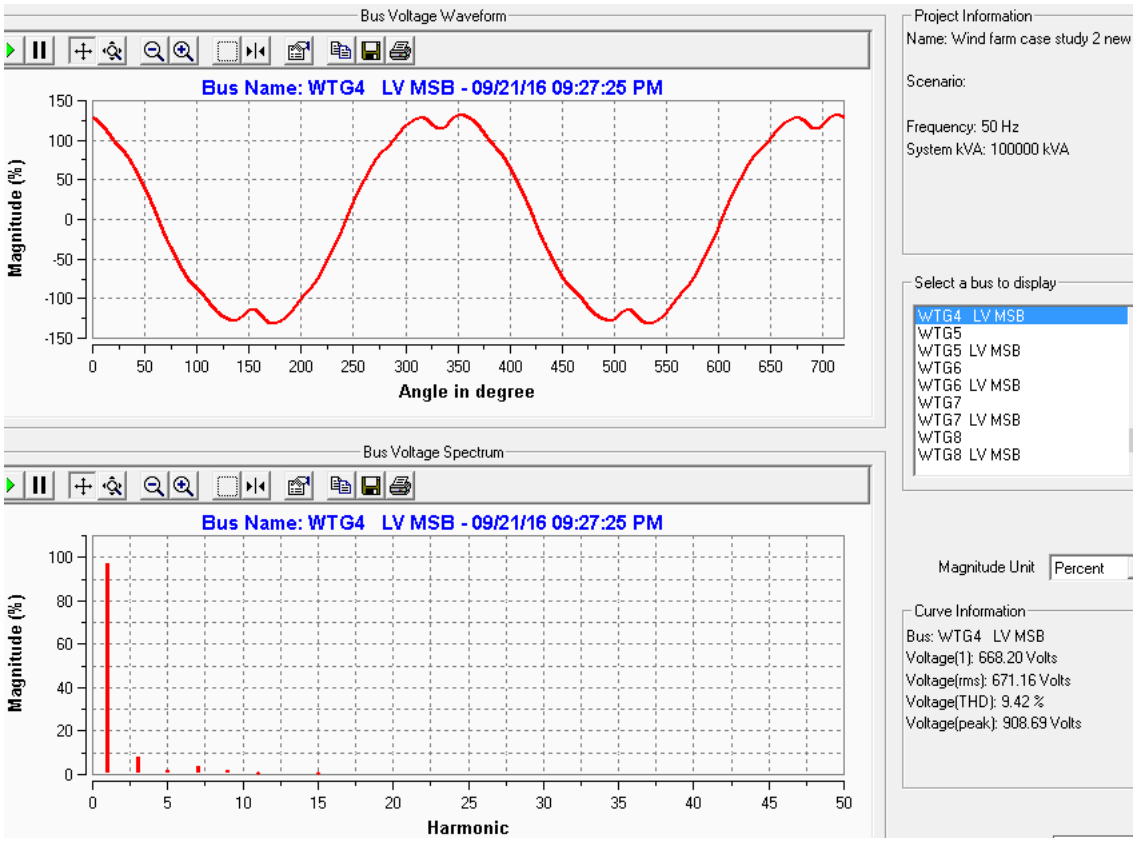

Figure 2-39: Harmonic Voltage for WTG04 - 2MW Asynchronous generators with external variable resistor.

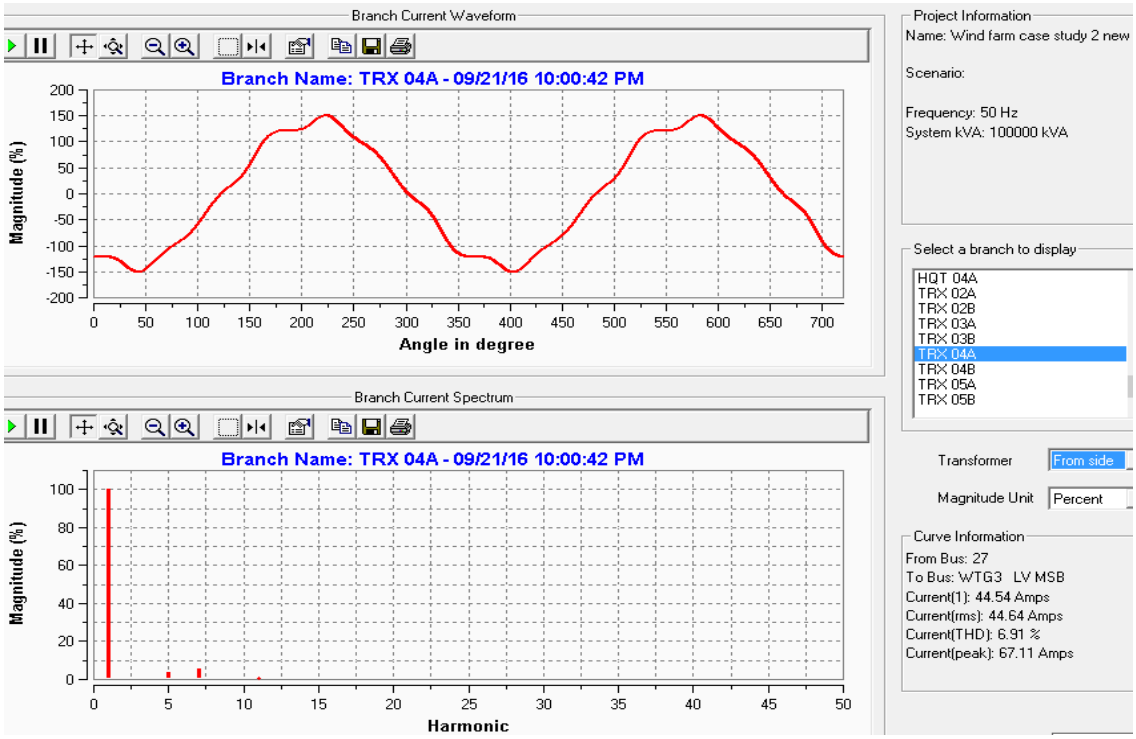

Figure 2-40: Harmonic Current for WTG04 - 2MW asynchronous generators with external variable resistor.

The wind turbine WTG 04 is located 1.9 km away from the grid connection. The total generated harmonics from eight wind turbines at grid connection 1 are shown in Figures 2-41 and 2-42.

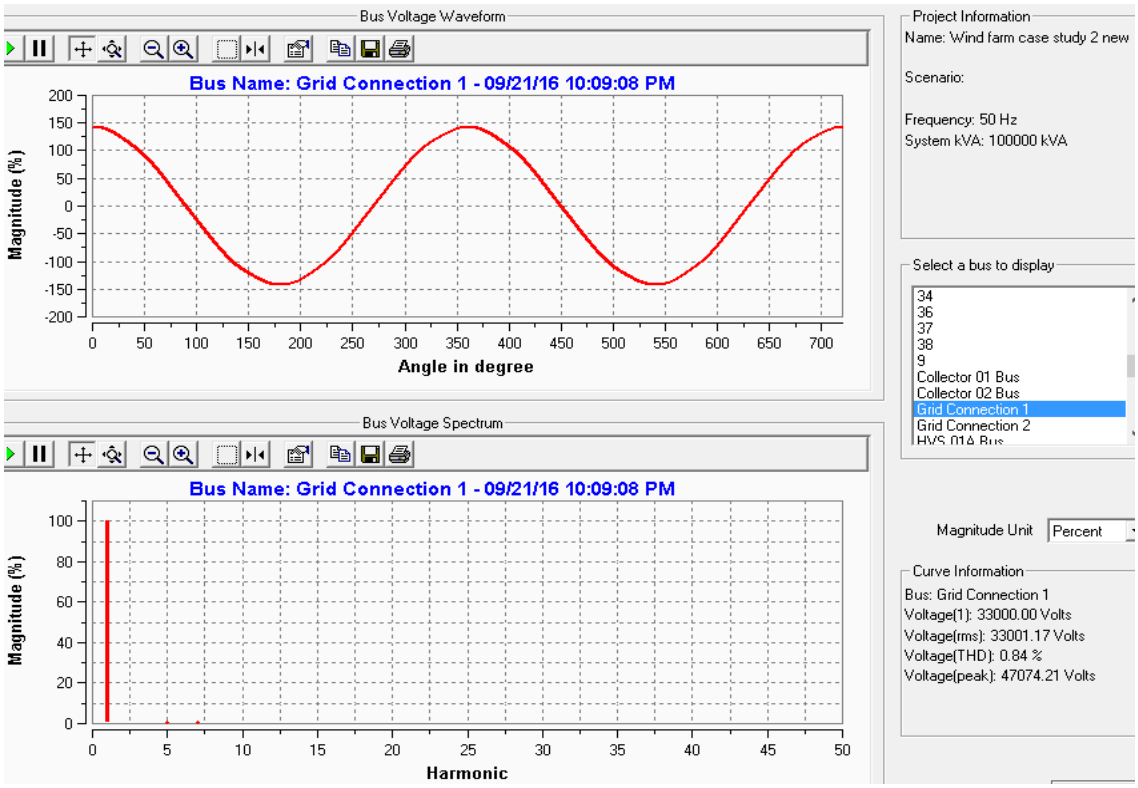

Figure 2-41: Harmonic Voltage for Case Study 2.

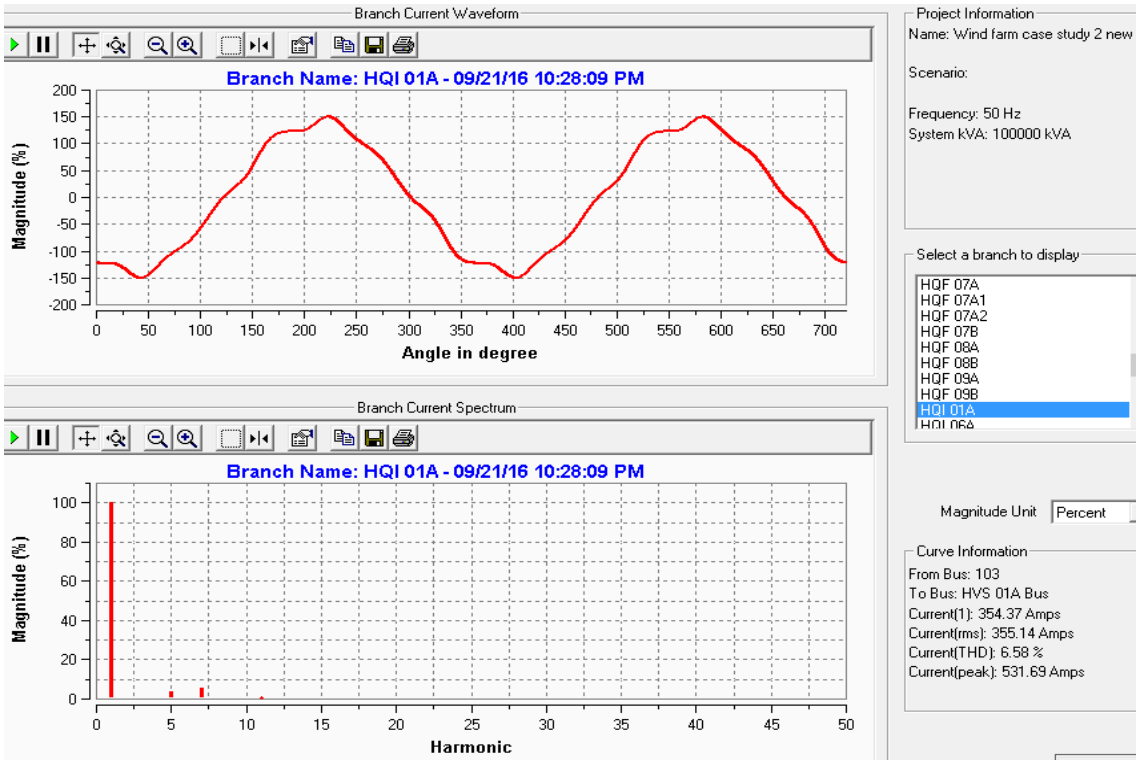

Figure 2-42: Harmonic Current for Case Study 2.

It is expected that 33 kV cables will contribute to filter generated harmonics due to their capacitive nature. Based on analysis and as shown in Figures 2-41 and 2-42 at the grid connection point, a voltage THD % of 0.84 % can appear which is above the allowable limit and needs adjustment.

The expected harmonic levels at the main 33 kV bus is presented in Figure 2-43 which can be used for harmonic filter selection as shown in the figure.

Harmonic Voltages

Bus Name	Frequency (Hz)	Vh (Volts)	Deg	Vh / V1 (%)
Collector 01 Bus				
	50.00	32,996.46	0.17	100.00
	150.00	0.00	0.00	0.00
	250.00	120.31	13.73	0.36
	350.00	285.43	26.52	0.87
	450.00	0.00	0.00	0.00
	550.00	44.60	-138.85	0.14
	650.00	25.84	-128.77	0.08
	750.00	0.00	0.00	0.00

Harmonic Currents

Branch Name:	Frequency (Hz)	Ih (Amps)	Deg	Ih / I1 (%)
HQI 01A				
	50.00	354.37	-146.45	100.00
	150.00	0.00	0.00	0.00
	250.00	12.01	105.07	3.39
	350.00	19.84	117.46	5.60
	450.00	0.00	0.00	0.00
	550.00	2.02	-48.24	0.57
	650.00	0.97	-38.27	0.27
	750.00	0.00	0.00	0.00

Figure 2-43: Detailed harmonic voltage and current for Case Study 2.

It is assumed that a 2 MW DFIG has a 700 kW inverter to convert generated energy from the rotor to the grid and vice versa. Accordingly, Case Study 2 is simulated and the results are presented in Figures 2-44 and 2-45.

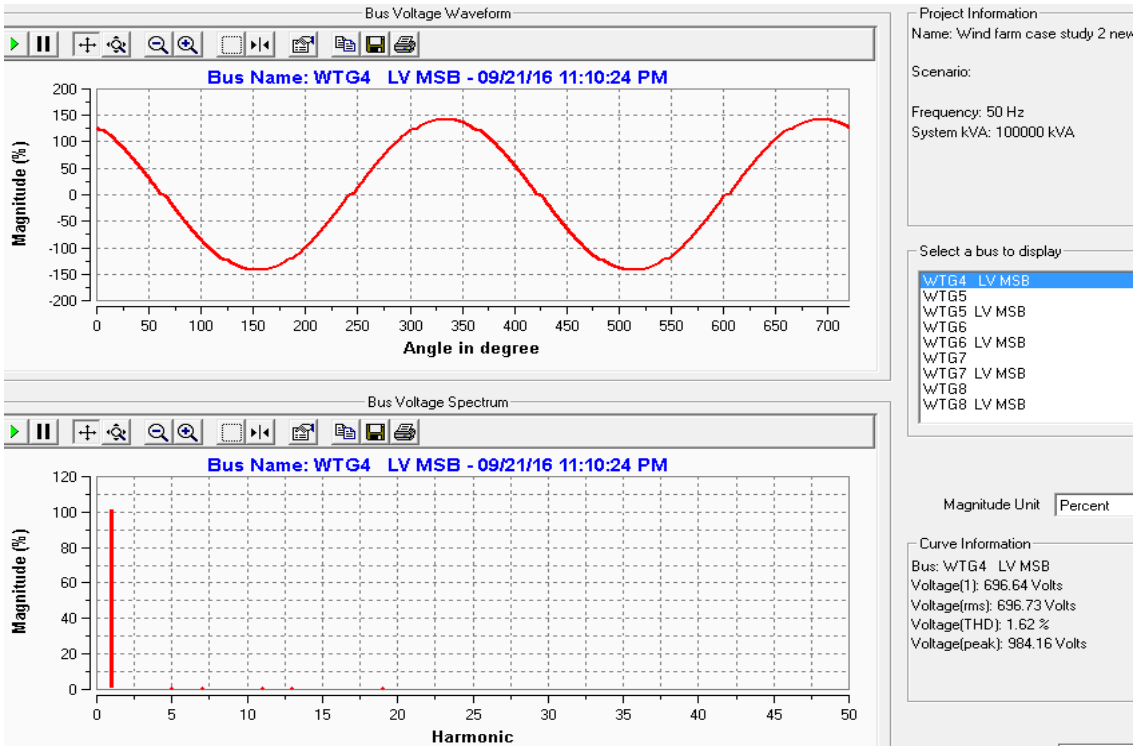

Figure 2-44: Harmonic Voltage for WTG04 - 2MW DFIG.

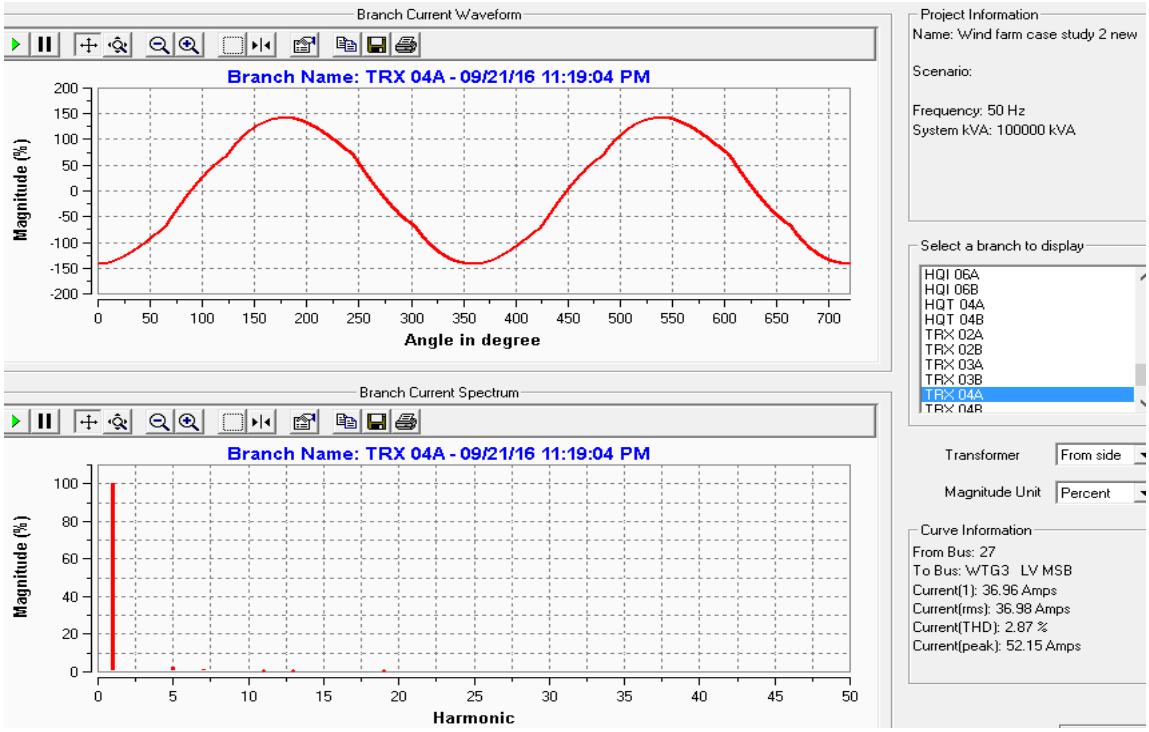

Figure 2-45: Harmonic current for WTG04 - 2MW DFIG.

The total generated harmonics from eight wind turbines at grid connection 1 is shown in Figures 2-45 and 2-47. The harmonics are tabulated in Figures 2-48 and 2-49.

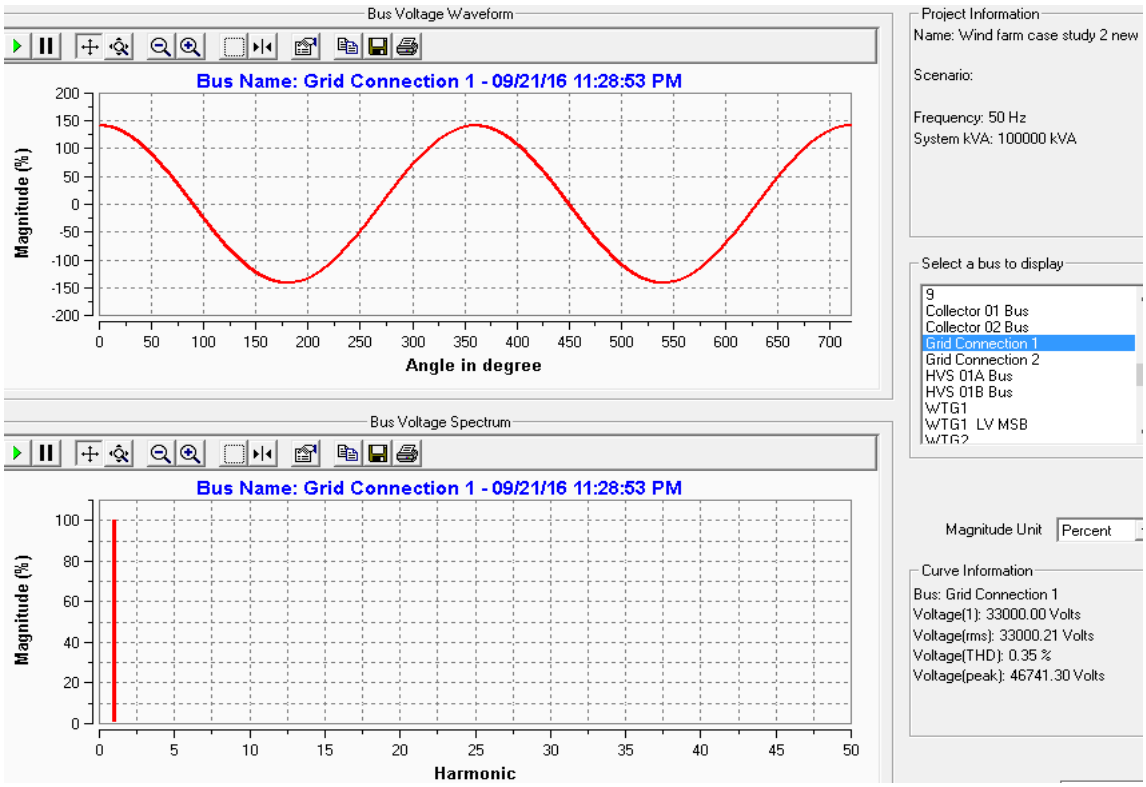

Figure 2-46: Harmonic Voltage for wind farm Case Study 2 with DFIG.

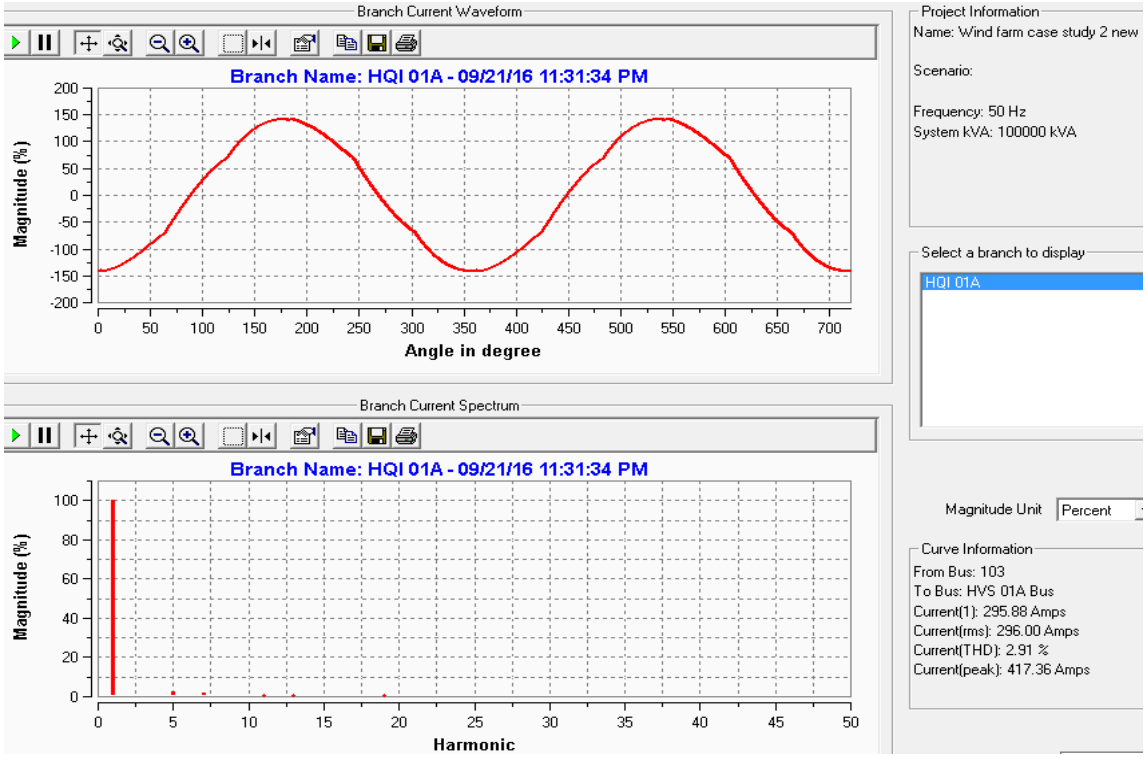

Figure 2-47: Harmonic Voltage for Case Study 2 with DFIG.

Harmonic Voltages

Bus Name	Frequency (Hz)	Vh (Volts)	Deg	Vh / V1 (%)	Frequency (Hz)	Vh (Volts)	Deg	Vh / V1 (%)
Collector 01 Bus								
	50.00	33,042.98	0.12	100.00	1,300.00	0.17	105.19	0.00
	100.00	0.05	173.02	0.00	1,350.00	0.00	0.00	0.00
	150.00	0.00	0.00	0.00	1,400.00	0.39	-65.78	0.00
	200.00	0.18	13.76	0.00	1,450.00	10.74	117.59	0.03
	250.00	67.71	14.18	0.20	1,500.00	0.00	0.00	0.00
	300.00	0.00	0.00	0.00	1,550.00	21.98	-53.47	0.07
	350.00	66.02	-152.85	0.20	1,600.00	0.10	129.97	0.00
	400.00	0.03	-151.20	0.00	1,650.00	0.00	0.00	0.00
	450.00	0.00	0.00	0.00	1,700.00	0.32	-41.17	0.00
	500.00	0.21	39.88	0.00	1,750.00	10.80	142.33	0.03
	550.00	31.29	42.15	0.09	1,800.00	0.00	0.00	0.00
	600.00	0.00	0.00	0.00	1,850.00	22.76	-28.87	0.07
	650.00	48.82	-127.60	0.15	1,900.00	0.04	154.67	0.00
	700.00	0.05	55.04	0.00	1,950.00	0.00	0.00	0.00
	750.00	0.00	0.00	0.00	2,000.00	0.37	-16.57	0.00
	800.00	0.25	-115.17	0.00	2,050.00	9.80	167.01	0.03
	850.00	17.71	67.71	0.05	2,100.00	0.00	0.00	0.00
	900.00	0.00	0.00	0.00	2,150.00	22.63	-4.28	0.07
	950.00	38.47	-102.79	0.12	2,200.00	0.15	179.33	0.00
	1,000.00	0.11	80.27	0.00	2,250.00	0.00	0.00	0.00
	1,050.00	0.00	0.00	0.00	2,300.00	0.16	8.00	0.00
	1,100.00	0.26	-90.44	0.00	2,350.00	8.70	-168.36	0.03
	1,150.00	11.14	92.75	0.03	2,400.00	0.00	0.00	0.00
	1,200.00	0.00	0.00	0.00	2,450.00	22.08	20.28	0.07
	1,250.00	27.72	-78.10	0.08	2,500.00	0.31	-156.05	0.00

Figure 2-48: Detailed harmonic Voltage for Case Study 2 with DFIG.

Harmonic Currents

Branch Name:	Frequency (Hz)	Ih (Amps)	Deg	Ih / I1(%)	Frequency (Hz)	Ih (Amps)	Deg	Ih / I1(%)
HQI 01A								
	50.00	295.88	-179.76	100.00	1,300.00	0.00	-164.56	0.00
	100.00	0.01	-93.63	0.00	1,350.00	0.00	0.00	0.00
	150.00	0.00	0.00	0.00	1,400.00	0.01	24.44	0.00
	200.00	0.02	105.41	0.01	1,450.00	0.19	-152.19	0.06
	250.00	6.76	105.52	2.28	1,500.00	0.00	0.00	0.00
	300.00	0.00	0.00	0.00	1,550.00	0.35	36.73	0.12
	350.00	4.59	-61.90	1.55	1,600.00	0.00	-139.83	0.00
	400.00	0.00	-60.37	0.00	1,650.00	0.00	0.00	0.00
	450.00	0.00	0.00	0.00	1,700.00	0.00	49.02	0.00
	500.00	0.01	130.54	0.00	1,750.00	0.15	-127.49	0.05
	550.00	1.42	132.75	0.48	1,800.00	0.00	0.00	0.00
	600.00	0.00	0.00	0.00	1,850.00	0.30	61.30	0.10
	650.00	1.83	-37.10	0.62	1,900.00	0.00	-115.16	0.00
	700.00	0.00	145.51	0.00	1,950.00	0.00	0.00	0.00
	750.00	0.00	0.00	0.00	2,000.00	0.00	73.58	0.00
	800.00	0.01	-24.76	0.00	2,050.00	0.12	-102.84	0.04
	850.00	0.52	158.10	0.18	2,100.00	0.00	0.00	0.00
	900.00	0.00	0.00	0.00	2,150.00	0.26	85.86	0.09
	950.00	0.99	-12.45	0.33	2,200.00	0.00	-90.53	0.00
	1,000.00	0.00	170.60	0.00	2,250.00	0.00	0.00	0.00
	1,050.00	0.00	0.00	0.00	2,300.00	0.00	98.13	0.00
	1,100.00	0.01	-0.14	0.00	2,350.00	0.09	-78.23	0.03
	1,150.00	0.24	-176.96	0.08	2,400.00	0.00	0.00	0.00
	1,200.00	0.00	0.00	0.00	2,450.00	0.22	110.40	0.07
	1,250.00	0.54	12.15	0.18	2,500.00	0.00	-65.93	0.00

Figure 2-49: Detailed harmonic Current for wind farm Case Study 2 with DFIG.

Based on the simulation harmonic results (Figures 2-39 and 2-40) for a wind farm with 2 MW asynchronous generators with external variable resistor (Type 2), it can be stated that these turbines will generator more harmonics than a similar wind farm with the same sized DFIGs. This is very much a function of the particular generators and control simulated. DFIGs use back-to-back PWM inverters, usually formed from IGBTs. These switch at tens of kHz and these harmonics are far higher than the low frequency harmonics that are investigated for power quality. Asynchronous generators are older technology and the rotor resistances may be controlled by thyristor rectifiers which use phase angle control. Since there is no PWM then the switching frequency is much lower and therefore more liable to induce low frequency harmonics into the stator which will lead to degraded power quality. More modern PWM switching of the resistor may well reduce harmonic content of an asynchronous generator.

The harmonic currents in the range 50 Hz to 5 kHz may induce interference into communication systems. This phenomenon is more pronounced at higher order harmonic frequencies because of increased coupling between circuits and because of higher sensitivity of the communication circuits in the audible range. Since wind farms are normally located in the remote areas the low induction interference into communication systems should not exist. The wind farms communication systems consist of fibre optic (single mode fibre optic) as shown in Figure 2-10, and therefore the low induction interference should not exist.

2.6.2 Voltage Fluctuation and Flicker

In this section of research wind turbines and wind turbines voltage fluctuation will be discussed. The voltage fluctuation can be considered as flicker for the following conditions:

- Voltage Fluctuations; and
- Wind gust impact on voltage.

Power-line flicker is a visible change in brightness of a lamp due to rapid fluctuations in the voltage of the power supply. The voltage fluctuation with certain time domain can be considered as flicker. Voltage fluctuation is generated over the source impedance change or variable generated power by wind turbines. The effects can range from disturbance to epileptic attacks of photosensitive persons. Flicker may also affect sensitive electronic equipment such as television receivers or industrial processes relying on constant electrical power [1].

As explained in TR IEC 61000.3.7:2012 [33], the international flickermeter provides two quantities to characterize the flicker severity:

- **Short Term Flicker** P_{st} : The flicker measurement is obtained for each 10 min period.
- **Long Term Flicker** P_{lt} : The flicker value is obtained for each 2 h period). The flicker related voltage quality criteria are generally expressed in terms of P_{st} and/or P_{lt} .The long term flicker typically being derived from groups of 12 consecutive P_{st} values.

$$P_{lt} = \sqrt[3]{\frac{1}{12} \times \sum_{j=1}^{12} P_{st_j}^3} \tag{2-59}$$

IEC 61400-21 has provided a uniform methodology for measurement and assessment of power quality characteristics of grid connected wind turbines. The aim of this standard is to provide consistency and accuracy for all the assessments. In this respect the term power quality includes those electrical characteristics of the WT that influence the voltage quality of the grid to which the wind turbine is connected. IEC 61400-21 procedures for assessing compliance with power quality requirements are valid for wind turbines with PCC at MV or HV in power systems with fixed frequency within ±1 Hz, and sufficient active and reactive power regulation capabilities and sufficient load to absorb the wind power production.

The measurements aim in general to verify the characteristic of power quality parameters for the full operational range of the assessed wind turbine or wind farm. Measurements are however not required for wind speeds above 15 m/s. This is because requiring measurements at higher wind speeds would normally give a significant longer measurement period due to the rare appearance of higher wind speeds, and are not expected to give significantly better verification of the characteristic power quality parameters of the assessed wind turbine [34].

Two different scenarios are defined by IEC 61400.21 for flicker calculation:

- Continuous operation flicker; and
- Switching operation flicker.

2.6.2.1 Continuous operation flicker

The measurement and assessment procedures for flicker during continuous operation of a wind turbine are shown in Figure 2-50. The same method was used for assessment of the wind farm.

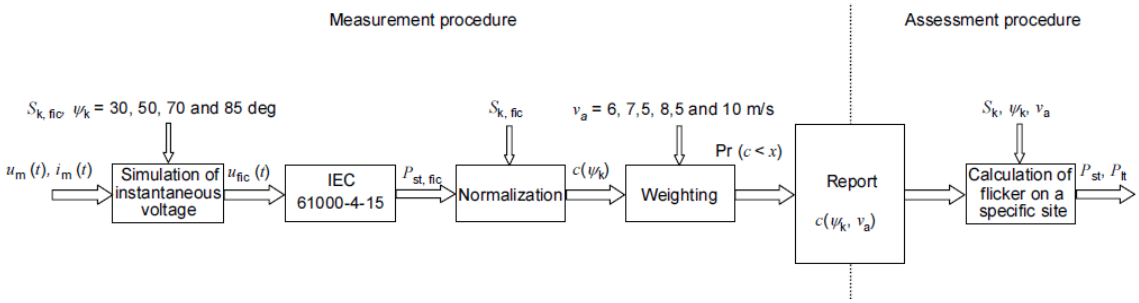

Figure 2-50: Flicker measurement and assessment procedures during continuous operation of a wind turbine [34] (courtesy of IEC).

Measurement of power quality:

The measurement process is presented in IEC 61400-21. This standard specifies the assessment method that uses current and voltage time-series measured at the wind turbine terminals, $U_m(t)$ and $I_m(t)$. For the wind turbine flicker measurement, it is presented as a current source $I_m(t)$. The voltage fluctuation at the terminals of wind turbine is $U_{fic}(t)$ so that

$$U_{fic}(t) = U_0(t) + R_{fic} \times I_m(t) + L_{fic} \times \frac{dI_m(t)}{\mathrm{dt}} \tag{2-60}$$

where the grid impedance is given as a resistance R_{fic} in series with an inductance of L_{fic}. Normally the grid impedance can be obtained from the network operator. When the value of resistance is not known, a typical *X/R* ratio of 10 should be used for ratings less than 10 MVA. For ratings above 10 MVA up to 400 MVA, the *X/R* ratio should be taken as [36]:

$$\frac{X_k}{R_k} = 30 \log_{10}(\text{MVA rating}) - 20 \tag{2-61}$$

The grid voltage is:

$$U_0(t) = \sqrt{\frac{2}{3}} \times U_n \times \sin(\propto_{\mathrm{m}}(t)) \tag{2-62}$$

where U_n is the r.m.s. value of the nominal voltage of the grid and

$$\propto_m (t) = 2\pi \times \int_0^t f(t)dt + \propto_0 \tag{2-63}$$

where

$f(t)$ is the frequency (that may vary over time);

t is the time since the start of the time-series;

$\propto_0$ is the electrical angle at $t = 0$.

As shown in Figure 2-50, the output of the flicker measurement will be the flicker coefficient $C_{(\psi k)}$. The flicker coefficient $C_{(\psi k)}$ is a normalized measure of the flicker emission during continuous operation of the wind turbine so that

$$C_{(\psi k)} = P_{st} \times \frac{S_k}{S_n} \tag{2-64}$$

where S_n is the rated apparent power of the wind turbine and S_k is the rated short circuit level at the wind farm grid. The Ψ_k is the phase angle of network short circuit impedance:

$$\Psi_k = \text{atan}\left(\frac{X_k}{R_k}\right) \tag{2-65}$$

where X_k is the network short circuit reactance and R_k is the network short circuit resistance.

Assessment of power quality:

The IEC 61400.21 states that the 99th percentile flicker emission from a single wind turbine during continuous operation shall be estimated applying following equation:

$$P_{st} = P_{lt} = C_{(\psi,V_a)} \times \frac{S_n}{S_k} \tag{2-66}$$

where $C_{(\psi,V_a)}$ is the flicker coefficient of the wind turbine for the given network impedance phase angle Ψ_k at the PCC and for the given annual average wind speed V_a at the hub of the wind turbine on site. The flicker coefficient of the wind turbine for the actual Ψ_k and V_a at the site may be found from the table of data produced as a result of the measurements described above.

Wind farm flicker emission can be estimated by the sum of individual turbine flicker emission:

$$P_{st\Sigma} = P_{lt\Sigma} = \frac{1}{S_k} \times \sqrt{\sum_{i=1}^{Nwt} \left(C_{i(\psi,V_a)} \times S_{ni}\right)^2} \tag{2-67}$$

where N_{wt} is the number of wind turbines operating in the wind farm of the Case Study.

2.6.2.2 Switching operation flicker

The start-up or switching between generators can be considered as switching operation. The switching operation flicker should consider the following operation scenarios:

- Wind turbine start-up at cut-in wind speed;
- Wind turbine start-up at rated wind speed; and
- The worst case of switching between generators (applicable to wind farms).

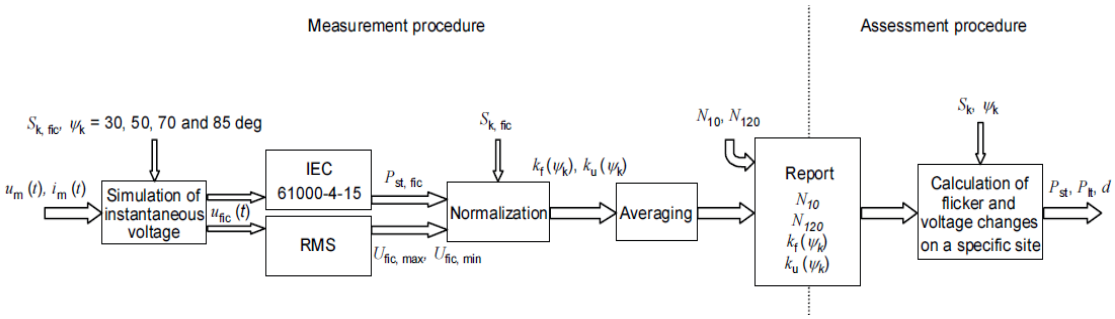

Figure 2-51: Flicker measurement and assessment procedures during switching operations of a wind turbine [34] (courtesy of IEC).

Measurements of power quality:

To measure the switching flicker first we need to understand wind turbine behaviour. Normally the manufacturer can provide the maximum number of switching operations:

1) The maximum number of the switching operation within a 10 min period N_{10};
2) The maximum number of the switching operation within a 2 hr period N_{120};
3) The flicker step factor $K_{f(\psi_k)}$ or the network impedance phase angles ψ_k = 30°, 50°, 70° and 85°; and
4) The voltage change factor $K_{u(\psi_k)}$ for the network impedance phase angles ψ_k = 30°, 50°, 70° and 85°.

The flicker step factor $K_{f(\psi_k)}$ can be calculated using [34]:

$$K_{f(\psi_k)} = \frac{1}{130} \times \frac{S_n}{S_k} \times P_{st} \times T_p^{0.31} \tag{2-68}$$

where:

T_p is the measurement period, long enough to ensure that the transient of the switching operation has abated, though limited to exclude possible power fluctuations due to turbulence;

P_{st} is the flicker emission from the wind turbine on the grid;

S_n is the rated apparent power of the wind turbine;

S_k is the short-circuit apparent power of the grid.

Accordingly, the voltage change factor $K_{u(\psi_k)}$ can be calculated from [34]:

$$K_{u(\psi_k)} = \sqrt{3} \times \frac{U_{max} - U_{min}}{U_n} \times \frac{S_k}{S_n} \tag{2-69}$$

where U_{max} and U_{min} are the maximum and minimum of one period RMS values of the phase-to-neutral voltage on the grid during the switching operation.

Assessment of power quality:

The flicker emission due to switching operations of a single wind turbine shall be estimated applying the following equation [34]:

$$P_{st} = 18 \times N_{10}^{0.31} \times K_{f(\psi_k)} \times \frac{S_n}{S_k} \tag{2-70}$$

$$P_{lt} = 8 \times N_{120}^{0.31} \times K_{f(\psi_k)} \times \frac{S_n}{S_k} \tag{2-71}$$

For wind farms with several wind turbines connected to the PCC, the flicker emission from the sum of them can be estimated using the following equation [34]:

$$P_{st\Sigma} = \frac{18}{S_k} \times \left[\sum_{i=1}^{Nwt} N_{10,i} \times \left(K_{f,i(\psi_k)} \times S_{n,i} \right)^{3.2} \right]^{0.31} \tag{2-72}$$

$$P_{lt\Sigma} = \frac{8}{S_k} \times \left[\sum_{i=1}^{Nwt} N_{120,i} \times \left(K_{f,i(\psi_k)} \times S_{n,i} \right)^{3.2} \right]^{0.31} \tag{2-73}$$

2.6.2.3 Case Study 2 flicker assessment

In this research, both continuous and switching operation flicker scenarios were assessed for Case Study 2 which consists of eight 2 MW wind turbines connected to a 33 kV network. The network connection diagram is presented in Figure 2-52.

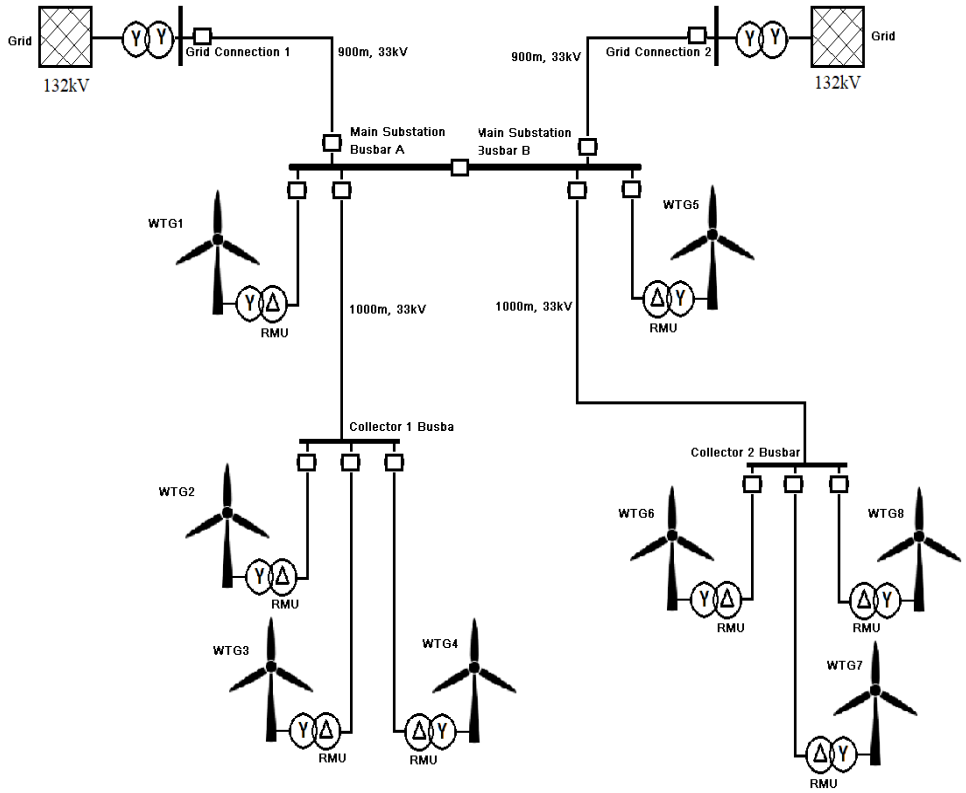

Figure 2-52: Case Study 2 network connection diagram.

Case Study 2 is a fictitious wind farm with following short circuit conditions:

A. When grid connection 1 and 2 are in-service: $I_k = 29855\,\text{A}$ with $\frac{X_k}{R_k} = 8.92$

B. When grid connection 1 is in-service only: $I_k = 12333\ \text{A}$ with $\frac{X_k}{R_k} = 11.17$

C. When grid connection 2 is in-service: $I_k = 17528\ \text{A}$ with $\frac{X_k}{R_k} = 7.81$

The above fault levels were calculated using the Paladin Design base software as briefly explained in Section 2.5.5.2.

Wind Farm continuous operation:

The rated short circuit level of wind farm grid S_k can be calculated from:

$$S_k = \sqrt{3}\, x V_n \times I_k \tag{2-74}$$

Therefore:

A. $S_k = \sqrt{3}\ \text{x}33000 \times 29855 = 1706$ MVA

B. $S_k = \sqrt{3}\ \text{x}33000 \times 12333 = 705$ MVA

C. $S_k = \sqrt{3}\ \text{x}33000 \times 17528 = 1002$ MVA

And the phase angle of network short-circuits impedances are:

A. $\Psi_k = \text{atan}\left(\frac{X_k}{R_k}\right) = 83.6^{\circ}$

B. $\Psi_k = \text{atan}\left(\frac{X_k}{R_k}\right) = 84.9^{\circ}$

C. $\Psi_k = \text{atan}\left(\frac{X_k}{R_k}\right) = 82.7^{\circ}$

It can be assumed that the phase angle for all three scenarios is 85°.

It is assumed that Figure 2-53 represents the wind speed and generated power at the turbine 690 V terminals for a three-month period, where a scatter plot shows 10 min mean values of the electric power as a function of the wind speed.

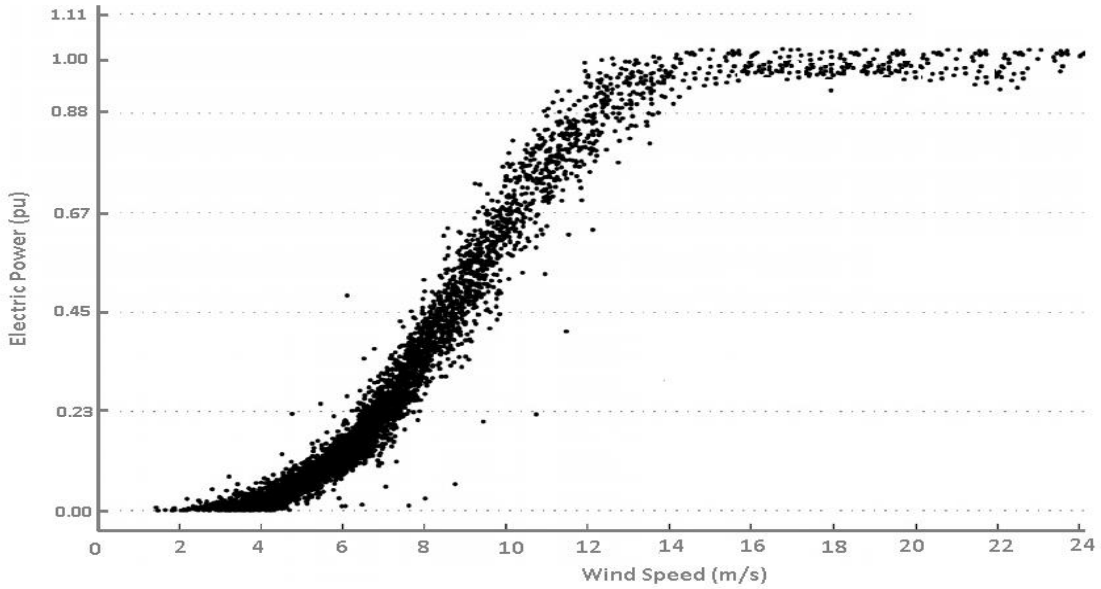

Figure 2-53: Power performance curve of a 2 MW Wind turbine at Case Study 2.

One week with significant wind speed values, between 4 and 11 m/s, was selected. Periods of 10 min are prefiltered removing those containing cut-in or cut-out wind speeds, or switching operations. Figure 2-54 presents a histogram of the 10 min periods analysed [35].

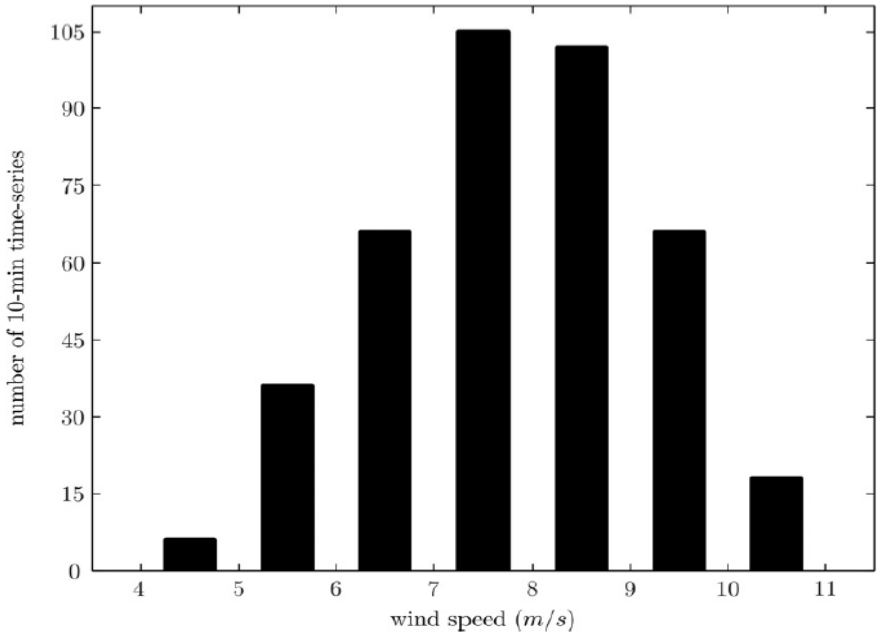

Figure 2-54: 10-min time-series per wind speed bins for Case Study 2.

Figure 2-55 represents measured flicker coefficients $C_{(\psi k)}$ for wind farm Case Study 2 with network impedance phase angle $\Psi_k = 85°$.

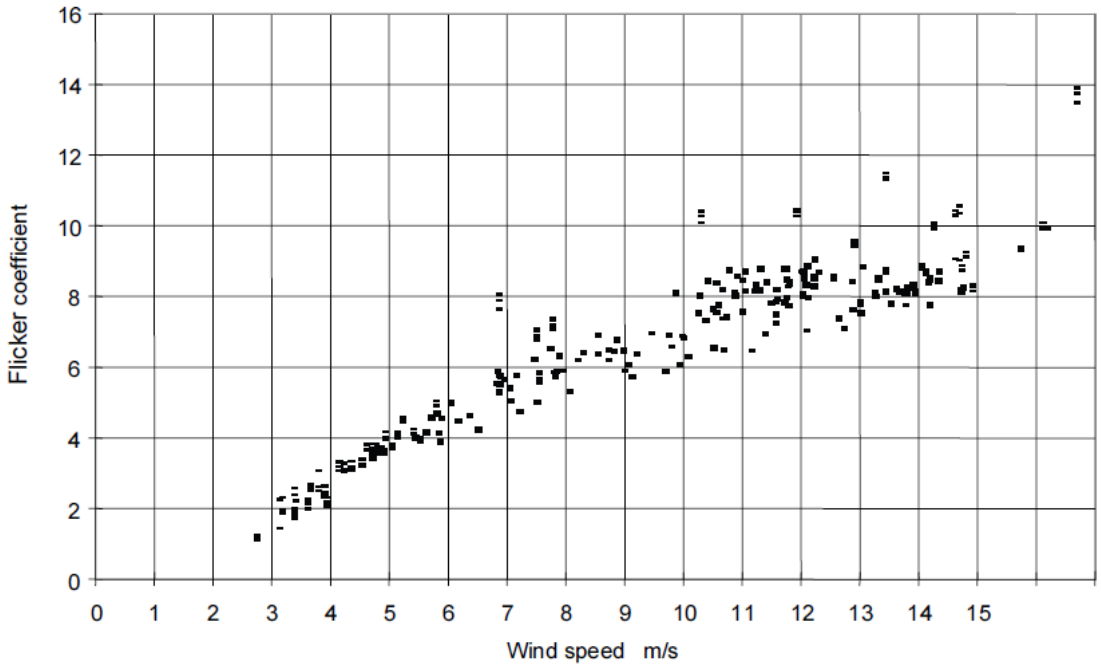

Figure 2-55: Flicker coefficient as a function of wind speed at Case Study 2.

The flicker coefficients for the most frequent wind speed of 7.5 m/s is $C_{(85°,\,7.5)} = 6$. Since Case Study 2 has eight 2 MW turbines; therefore the network continuous operation flicker can be calculated from

A. When grid connections 1 and 2 are in-service

$$P_{st\Sigma} = P_{lt\Sigma} = \frac{1}{S_k} \times \sqrt{\sum_{i=1}^{Nwt} (C_{i(\psi,V_a)} \times S_{ni})^2}$$

$$P_{st\Sigma} = P_{lt\Sigma} = \frac{1}{1706} \times \sqrt{8 \times (6 \times 2)^2} = 0.020$$

B. When grid connection 1 is in-service only

$$P_{st\Sigma} = P_{lt\Sigma} = \frac{1}{705} \times \sqrt{8 \times (6 \times 2)^2} = 0.049$$

C. When grid connection 2 is in-service only

$$P_{st\Sigma} = P_{lt\Sigma} = \frac{1}{1002} \times \sqrt{8 \times (6 \times 2)^2} = 0.034$$

Wind Farm switching operation:

It is assumed that the flicker step factor $K_{f(\psi_k)} = 0.32$ and voltage change factor $K_{u(\psi_k)} = 0.09$ for the phase angle of $\Psi_k = 85°$ have been tested and measured by the supplier.

Therefore the flicker emission for switching operation under different network scenarios can be calculated as defined in Section 7.6.3 of IEC61400-21. For the maximum number of switching operations N_{10} and N_{120} should be determined for each type of switching operation by the turbine manufacturer. In the event that the wind turbine manufacturer cannot provide these numbers, or the manufacturer cannot provide sufficient specification of the wind turbine control system to support the provided numbers, the following can be assumed:

- **N_{10} = 10 and N_{120} = 120 for wind turbine start-up at cut-in wind speed and the worst case of switching between generators.**

A. When Grid connections 1 and 2 are in-service

$$P_{st\Sigma} = \frac{18}{S_k} \times \left[\sum_{i=1}^{Nwt} N_{10,i} \times \left(K_{f,i(\psi_k)} \times S_{n,i} \right)^{3.2} \right]^{0.31}$$

$$P_{st\Sigma} = \frac{18}{1706} \times \left[8 \times \left(10 \times 0.32 \times 2 \right)^{3.2} \right]^{0.31} = 0.13$$

$$P_{lt\Sigma} = \frac{8}{S_k} \times \left[\sum_{i=1}^{Nwt} N_{120,i} \times \left(K_{f,i(\psi_k)} \times S_{n,i} \right)^{3.2} \right]^{0.31}$$

$$P_{lt\Sigma} = \frac{8}{1706} \times \left[8 \times \left(120 \times 0.32 \times 2 \right)^{3.2} \right]^{0.31} = 0.66$$

B. When Grid connection 1 is in-service only

$$P_{st\Sigma} = \frac{18}{705} \times \left[8 \times \left(10 \times 0.32 \times 2 \right)^{3.2} \right]^{0.31} = 0.31$$

$$P_{lt\Sigma} = \frac{8}{705} \times \left[8 \times \left(120 \times 0.32 \times 2 \right)^{3.2} \right]^{0.31} = 1.60$$

C. When Grid connection 2 is in-service only

$$P_{st\Sigma} = \frac{18}{1002} \times \left[8 \times \left(10 \times 0.32 \times 2 \right)^{3.2} \right]^{0.31} = 0.21$$

$$P_{lt\Sigma} = \frac{8}{1002} \times \left[8 \times \left(120 \times 0.32 \times 2 \right)^{3.2} \right]^{0.31} = 1.13$$

- **N_{10} = 1 and N_{120} = 12 for wind turbine start-up at rated wind speed.**

A. When Grid connection 1 and 2 are in-service

$$P_{st\Sigma} = \frac{18}{S_k} \times \left[\sum_{i=1}^{Nwt} N_{10,i} \times \left(K_{f,i(\psi_k)} \times S_{n,i} \right)^{3.2} \right]^{0.31}$$

$$P_{st\Sigma} = \frac{18}{1706} \times \left[8 \times \left(1 \times 0.32 \times 2 \right)^{3.2} \right]^{0.31} = 0.013$$

$$P_{lt\Sigma} = \frac{8}{S_k} \times \left[\sum_{i=1}^{Nwt} N_{120,i} \times \left(K_{f,i(\psi_k)} \times S_{n,i} \right)^{3.2} \right]^{0.31}$$

$$P_{lt\Sigma} = \frac{8}{1706} \times \left[8 \times \left(10 \times 0.32 \times 2 \right)^{3.2} \right]^{0.31} = 0.056$$

B. When Grid connection 1 is in-service only

$$P_{st\Sigma} = \frac{18}{705} \times \left[8 \times \left(1 \times 0.32 \times 2 \right)^{3.2} \right]^{0.31} = 0.031$$

$$P_{lt\Sigma} = \frac{8}{705} \times \left[8 \times \left(10 \times 0.32 \times 2 \right)^{3.2} \right]^{0.31} = 0.136$$

C. When Grid connection 2 is in-service only

$$P_{st\Sigma} = \frac{18}{1002} \times \left[8 \times \left(1 \times 0.32 \times 2 \right)^{3.2} \right]^{0.31} = 0.022$$

$$P_{lt\Sigma} = \frac{8}{1002} \times \left[8 \times \left(10 \times 0.32 \times 2 \right)^{3.2} \right]^{0.31} = 0.096$$

The voltage flicker levels that can be used for the purpose of determining emission limits have been defined in IEC 61000.3.7 as shown in Table 2-14, taking into consideration all fluctuating installations. Planning levels should allow coordination of voltage fluctuations between different voltage levels. Planning levels also normally are specified by the system operator or owner for all system voltage levels and can be considered as internal quality objectives of the system operator or owner and may be made available to individual customers on request.

Table 2-14: Planning levels for flicker in 33 kV power system.

Flicker	IEC 61000.3.7 Table 2	Typical Flicker limits (by Australian system operator)	
		Automatic Access	Minimum Access
P_{st}	0.9	0.432	0.8
P_{lt}	0.7	0.361	0.6

Table 2-15 shows the comparison between generated flicker for different operational scenarios and acceptable limits.

Table 2-15: Wind farm Case Study 2 flicker assessment result.

Operational Scenario	System Arrangement	Short Term			Long Term		
		P_{st}	Limit	Pass	P_{lt}	limit	Pass
Continuous operation	A. Grid connection 1 and 2	0.020	0.432 - 0.9	Y	0.020	0.361 - 0.7	Y
	B. Grid connection 1only	0.049		Y	0.049		Y
	C. Grid connection 2 only	0.034		Y	0.034		Y
Switching start-up at cut-in wind	A. Grid connection 1 and 2	0.13		Y	0.66		Y
	B. Grid connection 1only	0.31		Y	1.6		N
	C. Grid connection 2 only	0.21		Y	1.13		N
Switching start-up at rated wind	A. Grid connection 1 and 2	0.013		Y	0.056		Y
	B. Grid connection 1only	0.031		Y	0.136		Y
	C. Grid connection 2 only	0.022		Y	0.096		Y

The flicker simulation results indicate that generated flicker, when all eight wind turbines start at the same time at cut-in wind speed, is not acceptable by IEC and local service provider standards.

However, it is very unlikely to have the same wind stream simultaneously hitting wind turbines which are scattered across the field.

To mitigate IEC standard and local service provider flicker limit exceedances for situations like Case Study 2, the following resolution can be adopted:

- Operational procedure via SCADA system shown in Figure 2-22;
- Lowering the impedance of system to increase the fault level of system; and
- Using voltage regulators.

Among the above options, the following operation procedure via SCADA system is the most feasible alternative in terms of upfront cost and operational maintenance. In this method, the control systems can stagger wind turbine operation and grid connection via the SCADA system.

A part of the above power quality issues following power system issues, are considered in Sections 2.6.3 to 2.6.6:

- Voltage Unbalance
- System fault ride through (FRT);
- Network loading / interaction with nearby power plants;
- System frequency fluctuation; and
- System stability and intra-regional impact.

2.6.3 Voltage Unbalance

Voltage unbalance on a three-phase system is generally caused by unequal loading on two of the three phases by single-phase loads. However, in wind farms the unbalance can be caused by unbalance generation caused by transformer or generator failure. The voltage unbalance is directly related to the amount of the single-phase load as a percentage of the rating, and to the impedance of the mains supply. As an example, a three-phase transformer with a defined regulation, with unbalanced transmission lines can create unbalance line impedances on a 3-phase system. If the unbalance is a significant percentage of the transformer rating, it can cause excessive heating in the transformer.

The voltage unbalance in the wind farms can be managed by transposition of transmission lines and cross-bonding of underground single core cables. If unbalances cannot be mitigated due to wind farm construction constraint the manufacturer of the transformer should be consulted to determine if the transformer can operate in unbalanced condition while the condition can result in over-load.

The voltage unbalance as the ratio of the negative sequence voltage amplitude to the positive sequence voltage amplitude is τ which can be calculated by the following equation [38]:

$$\tau \approx \sqrt{6\sum_{1}^{3}\delta_{ij}^{2}} \tag{2-75}$$

$$\delta_{ij} = \frac{\left(U_{ij} - U_{average}\right)}{\left(3 \times U_{average}\right)} \tag{2-76}$$

where U_{ij} is the nominal line-to-line voltage in V.

IEC 61400.21 [34] defines that the voltage unbalance factor should be less than 2 % in 10 min at the wind turbine terminals. The voltage unbalance factor can be determined as described in IEC 61800-3, clause B.3 [38]. If the voltage unbalance factor is known to be well within the above required range, it does not need to be assessed any further. Otherwise, the voltage unbalance factor must be measured during the test, and test data possibly sample during periods with inappropriate voltage unbalance factor must be excluded.

2.6.4 Commutation Notches

As discussed in Section 2.2.2, DFIG wind turbines are wound rotor induction generators with a connection between the machine rotor windings and the power system through back-to-back voltage source inverters. The DFIG convertor normally consists of insulated gate bipolar transistor (IGBT) devices. The commutation notches can occur when current is commutated from one phase of the supply to the next. Voltage notches are deviations of the a.c. mains voltage from the instantaneous value of the fundamental. The magnitude of the commutation notch in the power system depends on the ratio of power impedance and decoupling reactance in the converter.

An analysis of the notches considers a wider range of frequencies than normal harmonic analysis since they switch at a higher frequency. Their time-domain characteristics cause effects which cannot be understood by a simple harmonic analysis. Therefore, they are analysed in the time domain using an oscilloscope [38].

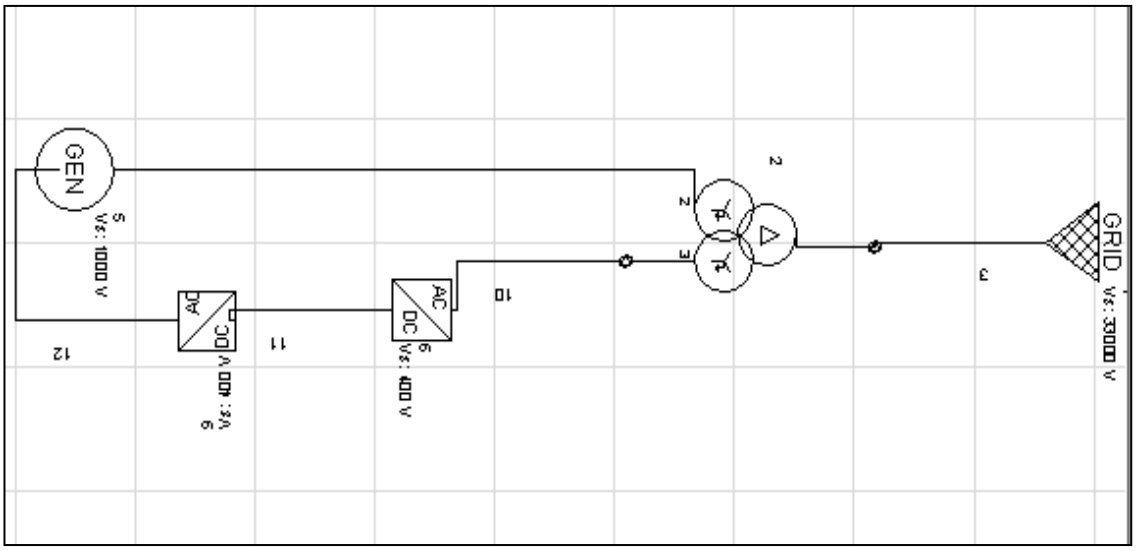

Figure 2-56: DFIG circuit arrangement model in Paladin.

The model is given in Figure 2-56. The typical waveform of commutation notches distinction from non-repetitive transient is shown in Figure 2-57.

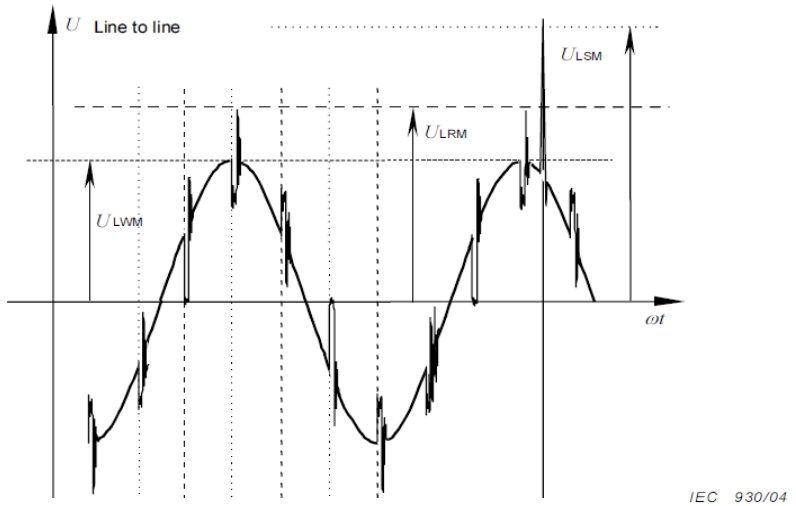

NOTE Typical range of per unit values are provided for reference only.
The figure assumes there is no impedance between PDS terminals and the converter.
Repetitive transients (U_{LRM}/U_{LWM}) = 1,25 to 1,50; depending on the snubber design with respect to d*i*/d*t* and I_{RR} (dynamic reverse current of the semiconductor).
Non-repetitive transients (U_{LSM}/U_{LWM}) = 1,80 to 2,50; depending on additional protective devices.

Figure 2-57: Typical waveform of commutation notches distinction from non-repetitive transient [38].

The IEC standard rules for calculation of notch emission cannot be used for wind farms because of the existence of capacitor banks and long length cables which can cause resonances. Based on practical cases the effect of notches on wind turbines can be much greater than that which would be indicated by a frequency domain analysis of their contribution to the total harmonic distortion. Therefore, a time domain analysis of commutation notches is necessary. The stress due to the

harmonics and commutation notches affects the electronic control and some power devices (such as snubbers circuits) which should be taken into consideration.

The immunity against notches should be considered for wind turbines for the following reasons:

- Wind farm collector synchronisation circuits can be impacted by commutation notches since the zero crossing of voltage is taken as reference for turbine synchronisation; and
- Commutation notches can overload the snubber circuits in the power converter.

The practical mitigation is waveform monitoring and use of filter where the impacts of commutation notches are critical.

2.6.5 System Fault Ride Through (FRT) and Short Voltage Dip

The system stability is a critical aspect which can result in major blackouts. Power system stability and transient behaviour for large scale wind farms is very critical. System stability is largely associated with power system faults in a network such as tripping of transmission lines, loss of production capacity (generator unit failure) and short circuits. These failures disrupt the balance of power (active and reactive) and change the power flow. Though the capacity of the operating generators may be adequate, large voltage drops may occur suddenly. The unbalance and re-distribution of real and reactive power in the network may force the voltage to vary beyond the boundary of stability. A period of low voltage (brownout) may occur and possibly be followed by a complete loss of power (blackout). Figure 2-48 shows a blackout in Australia due to a storm.

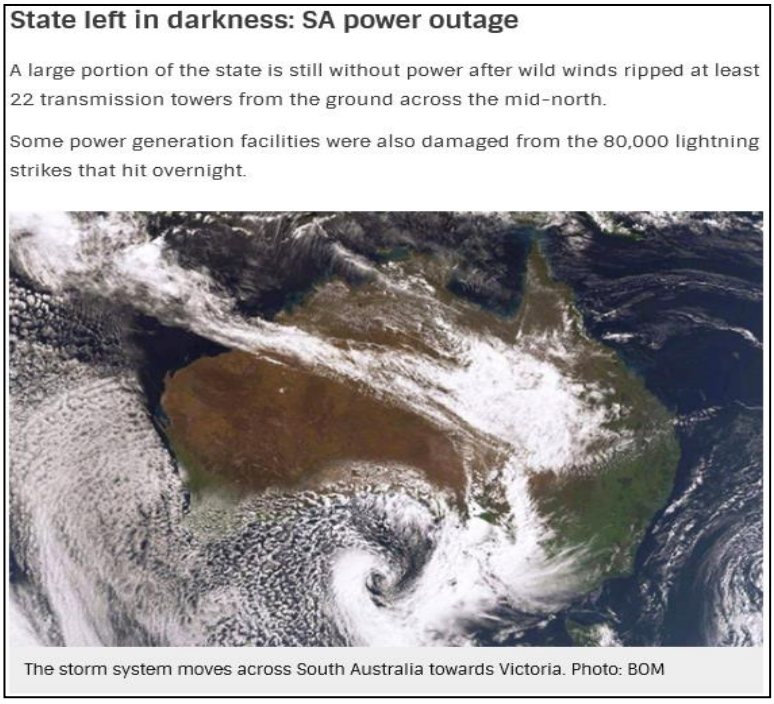

Figure 2-58: South Australia blackout due to storm (screenshot from Yahoo news website 29/09/2016).

The Australian energy market operator (AEMO) and other grid operators have concerns regarding the capability and stability of wind power generators connected to the grid, in case of grid voltage sags which are known as fault ride-through (FRT) capability.

Wind farm Case study 1 FRT and voltage dip assessment:

Since the fault scenario of Case Study 2 has been assessed in Section 2.2, Case Study 1 FRT and voltage dip behaviour are presented in this section.

The main reason for including FRT and voltage dips in power systems is a three-phase short-circuit or earth fault. In both mentioned fault conditions, the protection system which normally consists of primary (instantaneous protection with 120 ms tripping time) and back-up protection (over-current or differential scheme 200 ms tripping time) will protect the system. The upstream protection can be between 200 ms to 400 ms based on the existence of a blocking scheme. Accordingly, the fault duration can be 120 ms to 400 ms. During the fault condition, the system voltage will drop, which can affect wind farm operation due to the system impedance variation and the dynamic response of nearby turbines.

If the fault is nearby, the voltage dip can be more than 10 % of the system voltage. This voltage dip can pass through the conductors and transformers. As an example, in Case Study 1, the service provider grid voltage is 330 kV and wind farm distribution system is 33 kV. The wind turbine generator is rated at 690 V. Therefore, the network fault and FRT voltage dip should pass through two transformers to impact or damage the turbine generators as shown in Figure 2-59. The 330 kV / 33 kV transformer is equipped with an on-load tap changer (OLTC). However, the response time of OLTC is several seconds; therefore, the OLTC may not recover from the FRT voltage dip. The 690 V / 33 kV transformer has an off-load tap changer so it can pass the full ratio of voltage dip to the turbine terminals. This is illustrated in Figure 2-59. The cable capacitance will contribute to compensating the FRT voltage dip; therefore turbines closer to the PCC will be impacted more compared to turbines further away.

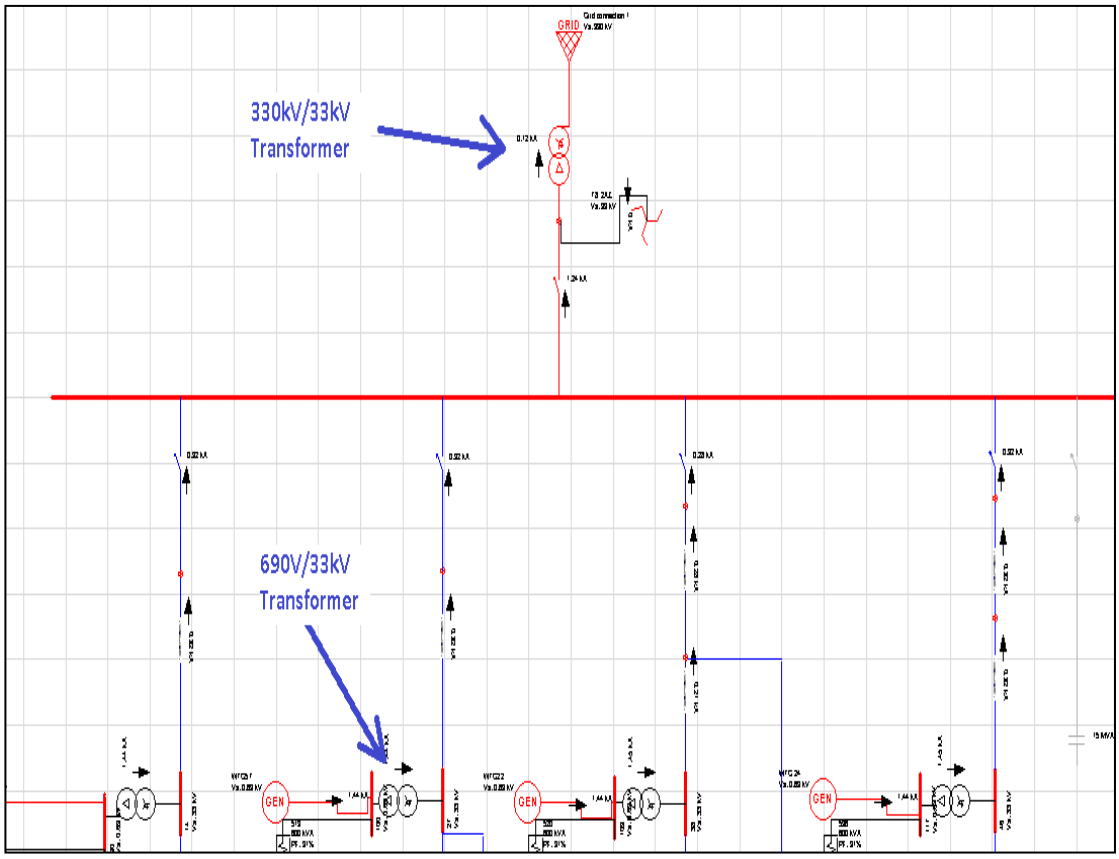

Figure 2-59: Case Study 1 model in Paladin software.

Normally two layers of protection should be in place for wind farms connected to a transmission system:

- Service provider protection system:
  - Over-current / earth fault protection;
  - Differential protection with pilot wire; and
  - Distance protection (EHV transmission lines).
- Wind turbine protection system:
  - Over-current / earth fault protection; and
  - Differential protection with pilot wire.

In FRT the voltage dip situations caused by system faults, nearby wind farms will see this event. In the early days of the development of wind energy, only a few wind turbines were connected to the grid. In this situation, when a fault somewhere on the lines caused the voltage at the wind turbine to drop, the wind turbine was simply disconnected from the grid and was reconnected when the fault was cleared, and the voltage returned to normal. The role of wind farms in supplying system demand was marginal; therefore, the sudden disconnection of a wind turbine or even a wind farm from the grid did not cause a significant impact on the stability of the power system. Today, with multi-MW wind farms on the power system, disconnection of wind farms

from the grid may cause major blackouts. Therefore wind farm behaviour for the following operation scenarios are assessed to ensure reliability of the system:

- Steady-state response of network; and
- Dynamic response of network.

For steady-state and dynamic studies, grid and nearby substations connected to Case Study 1 are modelled. For correct analysis, network elements such as loads and transmission loads are modelled.

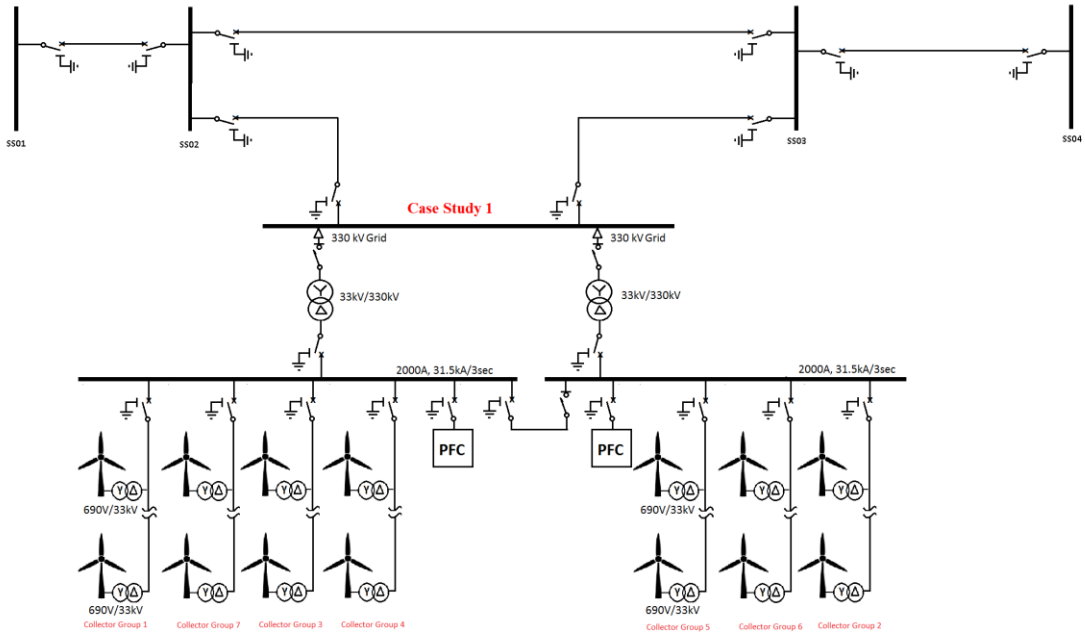

Figure 2-60: Case Study 1 grid connection arrangements.

According to Section S5.2.5.4 of Version 72 of the National Electricity Rules (NER), the Network Automatic Access standard for a generating system and each of its generating units must be capable of continuous uninterrupted operation where a power system disturbance causes the voltage at the connection point to vary within the following ranges:

(1) Voltages over 110 % for the durations permitted under clause S5.1a.4 NER (Figure 2-61);

(2) 90 % to 110 % of normal voltage continuously;

(3) 80% to 90% of normal voltage for a period of at least 10 s; and

(4) 70 % to 80 % of normal voltage for a period of at least 2 s.

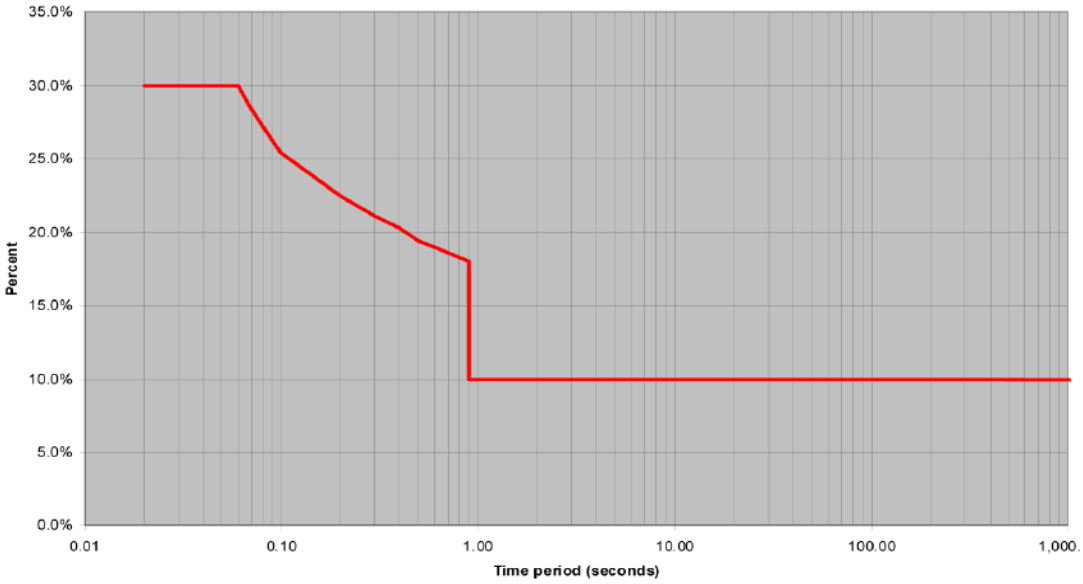

Figure 2-61: Overvoltage percentage for permitted durations [41].

Steady-State:

In the steady-state analysis the network voltage with and without the wind farm should be assessed. The voltage drop (for the continuous operation) with and without the Case Study 1 was assessed and the results are presented in Table 2-16.

Table 2-16: Case Study 1 steady-state voltage assessment result.

Operational Scenario	System Loading	Change in Voltage% at SS busbar			
		SS01	SS02	Case Study 1 (@330 kV)	SS03
Before Case Study 1 connection	Pick load mid season	-1.9	-1.8	NA	-1.2
	Low load mid season	-0.8	-1.3	NA	-0.3
	Pick load mid winter	-1.2	-0.6	NA	-1.2
	Low load mid winter	-0.9	-2	NA	+0.6
	Pick load mid summer	-1.1	-1.0	NA	-0.6
	Low load mid summer	-0.9	-0.9	NA	-0.7
Case Study 1 connection (while SS02 is out of service*)	Pick load mid season	-1.3	-1.2	+3.0	+1.3
	Low load mid season	-1.0	-0.9	+1.9	+0.5
	Pick load mid winter	-0.9	-0.8	+2.6	+1.2
	Pick load mid summer	-0.8	-0.8	+3.1	+1.3
	Low load mid summer	-0.7	-0.7	+1.6	+0.7

*The circuit breaker in substation number SS02 is in open position.

Dynamic response:

In Australia, Section S5.2.5.5 of Version 72 of the National Electricity Rules (NER) defines the requirements for the dynamic behaviour of the generating system response to disturbances following contingency events. The following fault conditions should be considered for dynamic response assessment:

(1) A fault of the relevant type having a metallic conducting path; and

(2) A fault of the relevant type resulting from re-closure onto a fault by the operation of automatic re-closed equipment.

The dynamic response assessment confirms the access level of a wind farm. The Network Automatic Access standard for a generating system and each of its generating units must be capable of continuous uninterrupted operations for the following conditions:

- Unexpected automatic or manual disconnection of, or the unplanned reduction in capacity of one operating generating unit;
- Unexpected disconnection of one major item of transmission plant;
- A three-phase fault in a transmission system cleared by all relevant primary protection systems;
- A two phase to ground, phase to phase, or phase to ground fault in a *transmission system* cleared in:
    i. The longest time expected to be taken for a relevant breaker fail protection system to clear the fault; or
    ii. The longest time expected to be taken for all relevant primary protection systems to clear the fault (if none is specified, 430 milliseconds).
- Power system conditions or energy source availability beyond the Generator's reasonable control.

The Case Study 1 dynamic response cannot be presented in this research due to a confidentiality agreement. However, the results are similar to the simulation presented in Section 2.5.5.2.

2.6.6 Wind Farm Power Frequency Response

One of the critical aspects of wind farms is the dynamic support of the grid, and provision of power frequency response. Figure 2-62 shows the power frequency of power system in a simple way. The system frequency stability depends on the balance between generated and consumed power. This means major system disturbances like the recent storm at South Australia can cause unbalance between generated power and connected load. Normally the following actions are required by system operators [44]:

- Stage 1: Action named inertial frequency response which takes energy from the rotating masses to oppose a frequency deviation from the scheduled frequency.
- Stage 2: The secondary control is performed to restore the used reserves, and the system frequency to its scheduled value.
- Stage 3: Frequency deviation control via governor droop set points.
- Stage 4: Inter states isolation. If the power frequency cannot be restored to the scheduled frequency within allowable time limit, then unbalanced section will be disconnected from other parts of network.

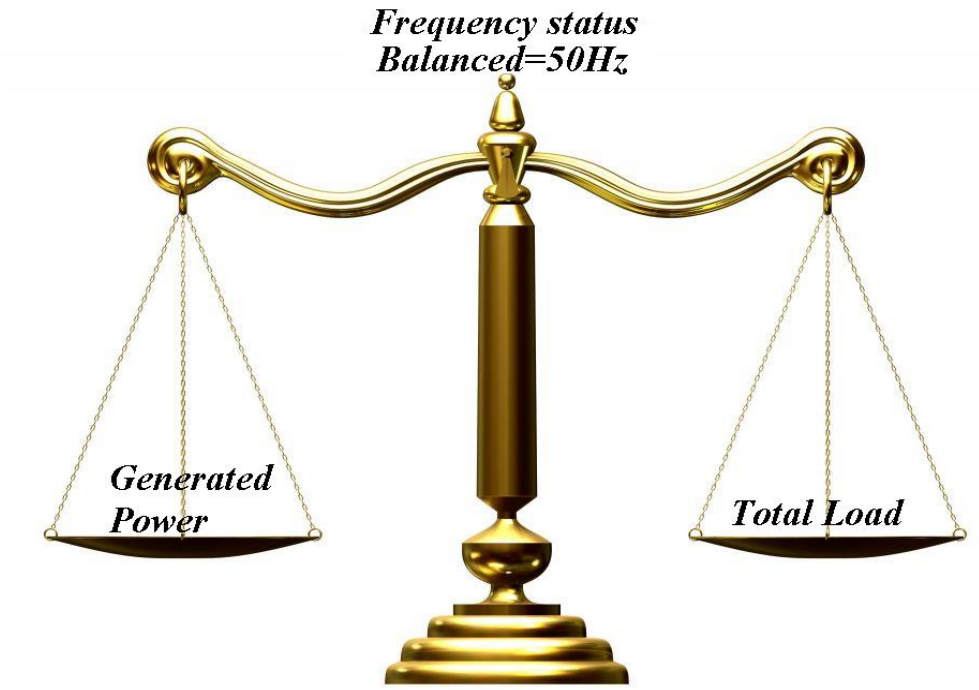

Figure 2-62: Simplified power frequency balance condition

Figure 2-63: Collapsed electricity tower in South Australia (Photo: ABC News, Tom Fedorowytsch 29/09/2016).

Based on the 2010 National Transmission Network Development Plan for Australia, new wind farms with capacity of 7,000 and 8,000 MW could be added to the existing 2,000 MW of wind generation over the next 20 years. Therefore, it is critical to understand the technical performance issues that might arise with this level of wind generation [41]. The large scale penetration and integration of variable speed wind energy can have a significant impact on the system inertia. This is due to the use of power electronic converters with back-to-back Voltage Source Converters (VSC), isolating the wind turbines from the power system and making them insensitive to any change in the system frequency and consequently unable to provide any inertial response [44].
The most common wind turbine generator today is the DFIG which cannot manage to compensate grid frequency fluctuations alone. However, as part of the complete DFIG system, the rotor back-to-back inverter converter allows very flexible control of active and reactive power for both normal and disturbed grid conditions. Currently the following methods are used in different countries for wind farms frequency regulation [42]:

- Limited frequency sensitivity mode;
- Configurable droop characteristic with dead band control; and
- Multi-stage response.

Limited Frequency Sensitivity Mode:

This is a requirement is presented in the German Transmission Code 2007 [45] which defines that all renewable-based generating units must reduce their power generation as per instruction in Figure 2-64 while they are in operation.

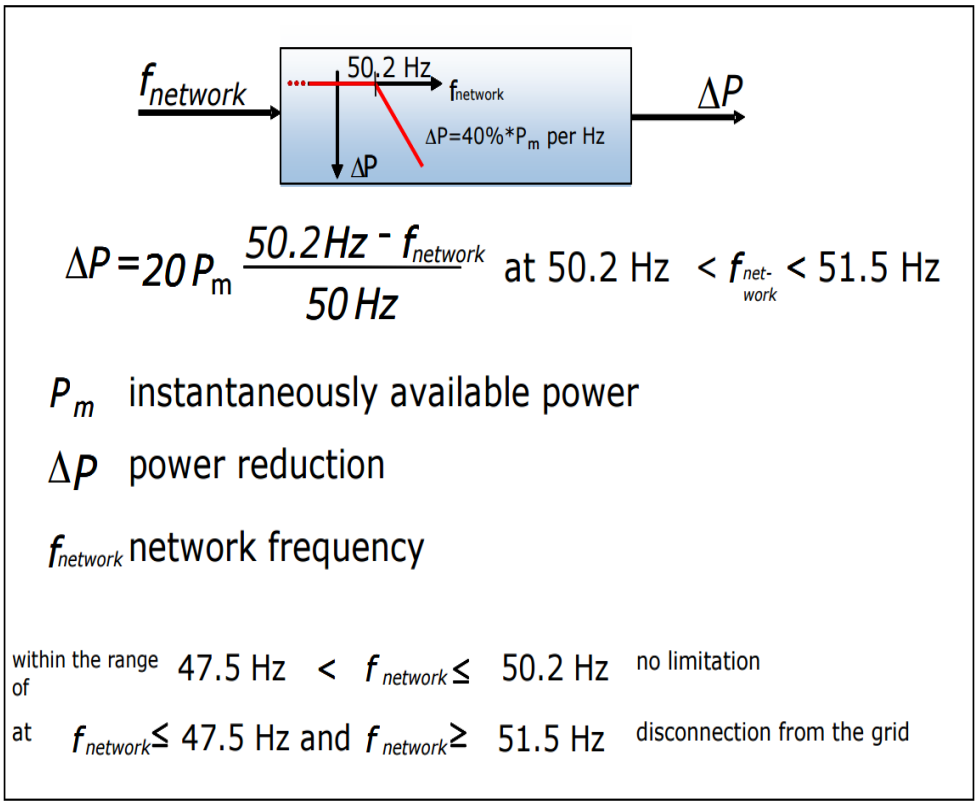

Figure 2-64: Active power reduction of wind turbines in the case of over-frequency in German Transmission Code 2007 [45].

If the frequency returns to a value of $f \leq 50.05$ Hz, the active power output may be increased again as long as the actual frequency does not exceed 50.2 Hz. This control is realized in a decentralized manner (at each individual generator). The neutral zone must be below 10 mHz.

Configurable droop characteristic with dead band control:

This type of control requires a wind farm to operate at a level below its instantaneous available capacity to provide upward and downward frequency regulation capability. Typically, there is a control dead-band which is configured according to the transmission system operator (TSO) requirements within which generator output is independent of frequency. Above this, on the high frequency side, the generator output will decrease linearly with frequency at a rate specified by the TSO until the high frequency limit is reached where it is permissible to disconnect. Similarly, on the low frequency side, the generator output will increase linearly with frequency at a rate specified by the TSO until the low frequency limit is reached or output is limited by primary energy source availability. This type of control capability is required in Ireland, the UK and Spain. The implementation of this requirement is slightly different in the Irish grid code in that the amount of downward regulation required providing under-frequency response in essentially fixed [42].

Multi stage response:

This type of control is like the configurable droop characteristic mentioned above but features additional configurable points which provide for a two-stage response with different droop characteristics and frequency insensitivity ranges. The Danish code allows for 7 TSO-specified frequency points providing for four distinct droop values in total as shown in below Figure 2-65 [42].

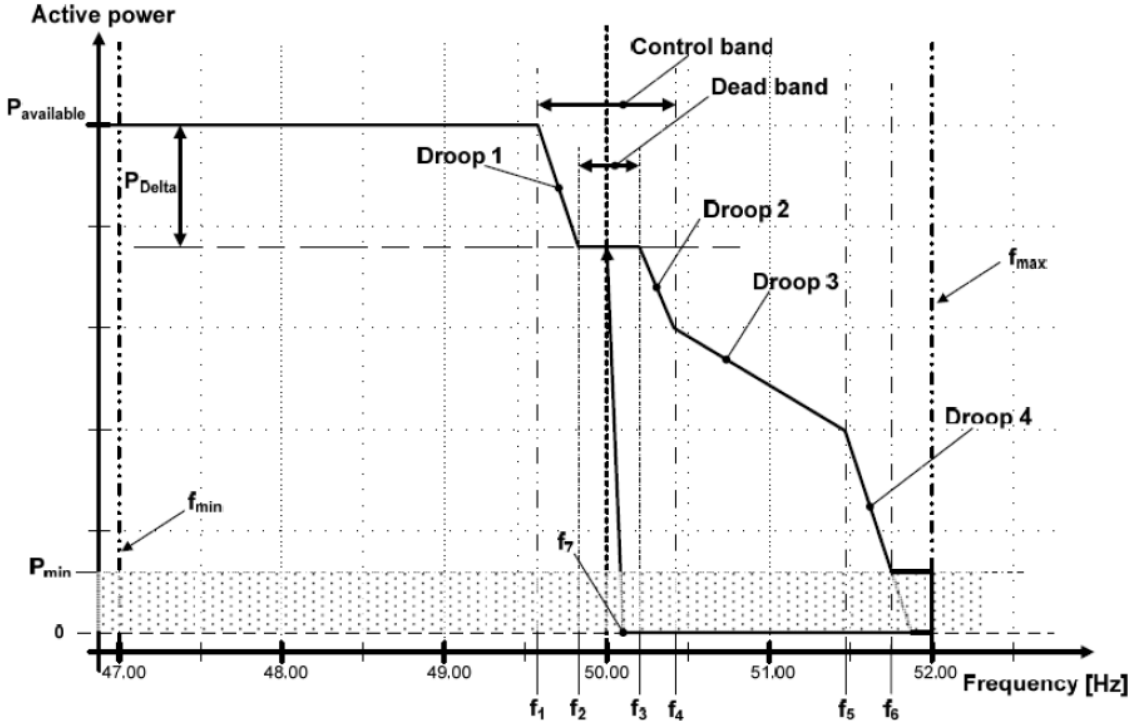

Figure 2-65: Frequency Response Curve from the Danish Grid Code [45].

2.7 Wind Farm Ferroresonance

As well presented in Schneider "Cahier Technique" no 190 [49]. Ferroresonance is a rare phenomenon produced by resonance between capacitances and non-linear inductances in power networks. Ferroresonance causes harmonics and overvoltage to propagate within the power network. The types of ferroresonance can be divided into two categories:

- Transient ferroresonance – generally initiated by switching operations, lightning surges or faults but only lasts for a short period of time. Transient ferroresonance may lead to false protection trips and/or voltage stresses on equipment during the ferroresonant period.
- Sustained ferroresonance – generally initiated by switching operations, lightning surges or faults but sustained by the power network voltage either directly or via coupling. Sustained ferroresonance may lead to uncleared faults and/or damage to electrical equipment.

Sustained ferroresonance is considered to be a more hazardous condition. It is known that ferroresonance cannot be sustained unless the following three conditions exist simultaneously:

1. Presence of capacitances with non-linear inductances under some critical ratios.
2. Presence of at least one point in the system that does not have a fixed potential (isolated neutral, single phase switching, single fuse blowing, etc).
3. Lightly loaded system components or low short-circuit power sources.

The non-linear nature of ferroresonance cannot be predicted by the analytical methods normally employed by design engineers. The likelihood of ferroresonance is sensitive to ratios of system parameters as well as initial conditions, such as the point in the cycle when the initiating event occurs. Accordingly, numerical computational methods using computer models are necessary for predicting the likelihood of ferroresonance and analysing the behaviour of the power network in ferroresonant states.

Ferroresonant waveforms can be classified into four modes:

- Fundamental mode – voltages and currents are periodic with the same period as the power network voltage. The waveform spectrum contains the power frequency and its harmonics;
- Sub-harmonic mode – voltages and currents are periodic with a period equal to an integer multiple of the power network voltage cycle. The waveform spectrum contains a fundamental frequency that is less the power frequency, and the harmonics of this fundamental frequency;
- Quasi-periodic mode – voltages and currents are not precisely periodic but comprise a discontinuous spectrum; and
- Chaotic mode – voltages and currents are not periodic and the spectrum is continuous.

Experience assists in the identification of specific practical scenarios in which ferroresonance should be considered.

Whilst analytical formulae exist for prediction of the likelihood of fundamental and sub-harmonic mode ferroresonance, quasi-periodic and chaotic modes can only be analysed with computer models and numerical simulations.

2.7.1 Wind Farm Ferroresonance

2.7.1.1 Assessment

First step is to assess the existence of three conditions which can create ferroresonance:

Condition 1: Presence of capacitances with non-linear inductances under some critical ratios.

Wind farms including Case Study 1 have long overhead transmission line and/or underground cable between turbines and main substation. Overhead transmission line and underground cables can have significant capacitance. Also the DFIGs and 690 V / 33k V step-up tower base transformers have non-linear inductances.

Condition 2: Presence of at least one point in the system that does not have a fixed potential.

The DFIG rotor is connected to an isolated neutral grid inverter (AC/DC/AC) with variable potential.

Condition 3: Lightly loaded system components or low short-circuit power sources.
Wind turbine generated power depends on the wind speed and the location of the turbine. The wind hitting the turbine and the energy conversion of the turbine for turbines located on the same site will be different for each turbine. Accordingly, the short-circuit impedance can be very low during low wind speed with low power generation.

Based on the above conditions it can be concluded that ferroresonance can exist in Case Study 1. Therefore, we can assess operational scenarios that are likely to produce ferroresonance.

2.7.1.2 Modelling

Case Study 2 and the sub-transmission system are modelled in PSCAD for transient analysis and ferroresonance assessment. The wind turbine operation during low wind speed has the most concern in terms of the understanding of ferroresonance. This is when it can be excited, therefore modelling is undertaken using PSCAD/EMTDC software.

PSCAD is an electro-magnetic transient program which can represent and solve the differential equations of electromagnetic and electromechanical systems in the time domain. The solutions are calculated using a fixed time step. The software allows for the creation and analysis of control systems independent or in conjunction with the electromagnetic or electromechanical systems.
This type of software allows the complex interactions between components to be included and the frequency dependent characteristics of components to be modelled. This is where it

dramatically differs from conventional steady-state load-flow and fault analysis software packages.

PSCAD can be used for various specialised studies including fast front surge studies (lightning surge studies), switching transient studies, transformer inrush and saturation studies and the like. The Case Study 2 power system with a DFIG and tower base transformer are modelled for analysis as shown in Figure 2-66. As stated, This includes saturation effects.

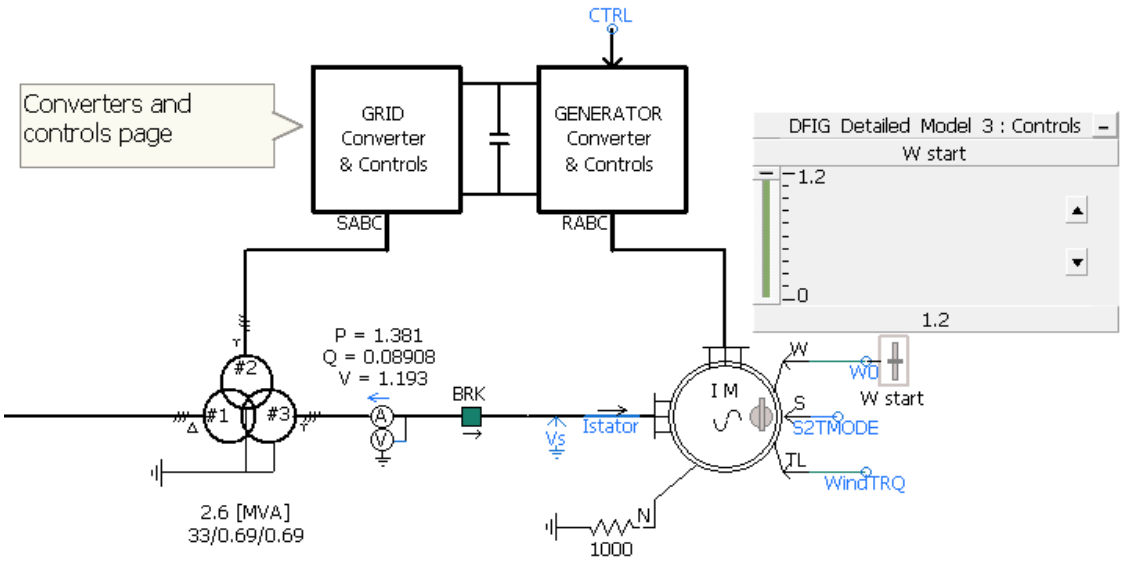

Figure 2-66: DFIG Wind turbine model in PSCAD.

A wind farm with eight 2MW DFIG wind turbines and eight 2.6 MVA three windings transformers are simulated with the following Scenarios:

A. Wind farm with 5 km of aerial line at cut-in wind speed and normal operation;
B. Wind farm Scenario A during a 3-phase-to-earth fault at the 690 V terminals of the LV transformer;
C. Wind farm Scenario A during a 3-phase-to-earth fault at the 33 kV bus bar;
D. Wind farm operation during wind gust; and
E. Wind farm with 100 km of aerial line during a 3-phase-to-earth fault at the 132 kV bus bar.

Scenario A: Wind Turbines Start simultaneously and operates normally

The wind farm PSCAD model arrangement is presented in Figure 2-67. The generated power, voltage and current waveform plots for the wind turbines during cut-in wind speed and normal generation conditions are extracted from the simulation and presented in this section.

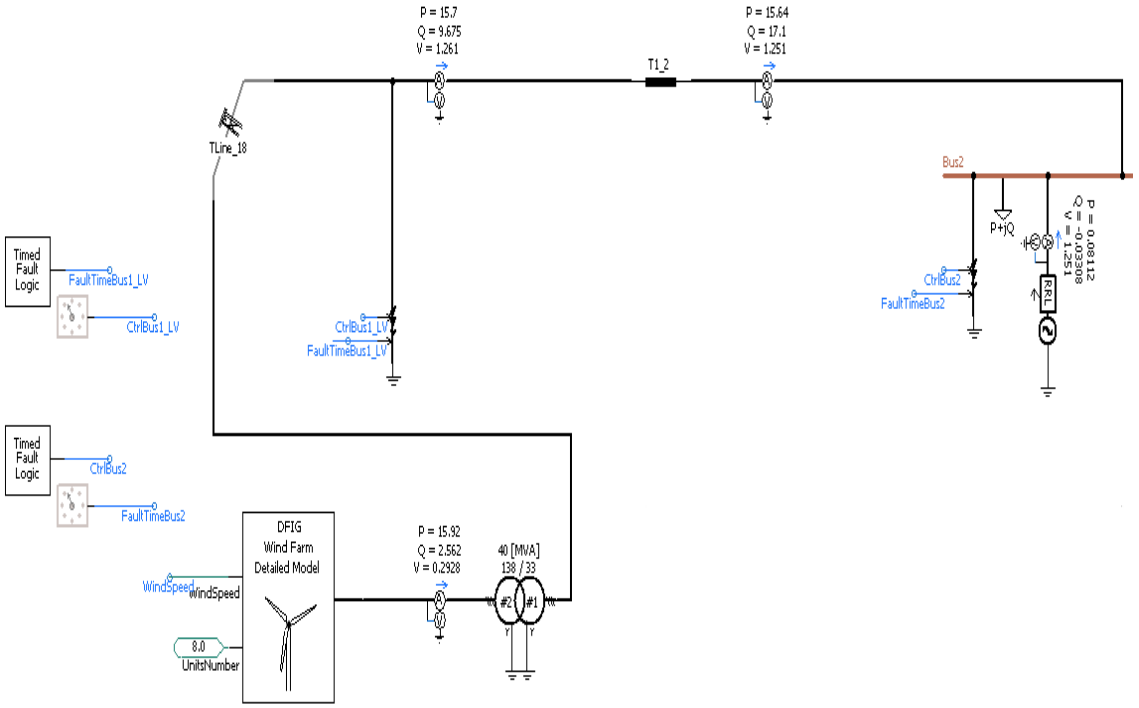

Figure 2-67: Wind farm with 8 DFIG wind turbines in PSCAD.

It is assumed that all eight wind turbines will start simultaneously and the generated power simulated at the 33 kV busbar (distribution system) and LV side of wind farm transformer is presented in Figure 2-68 and Figure 2-69 respectively.

The voltage and current wave curves on the 132 kV busbar at point of connection (upstream transmission system) are presented in Figure 2-70. This simulation shows that the system will reach normal conditions with no evidence of ferroresonance if all the wind turbines start at the same time. The 138kV is the simulated voltage at the bus bar of step-up transformer for Scenario A study.

The nominal voltage system presented in Table 4 of Australian standard AS 60038:2012 [56] have been used for simulation. Accordingly, the maximum voltage level of 145 kV has been used for 132 kV system analysis.

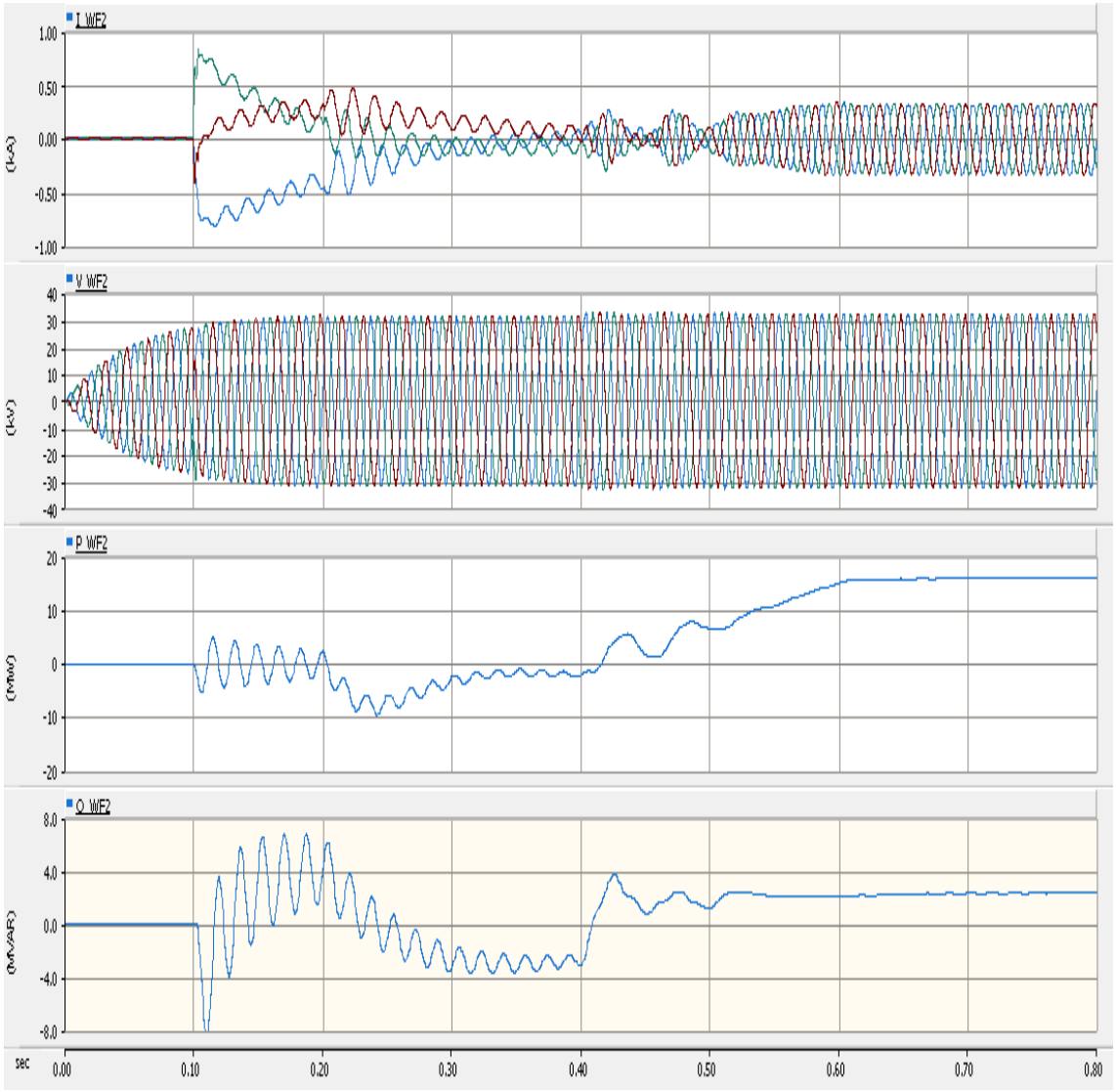

Figure 2-68: Wind farm voltage, current, active power and reactive power generation curve at the 33 kV collector busbar.

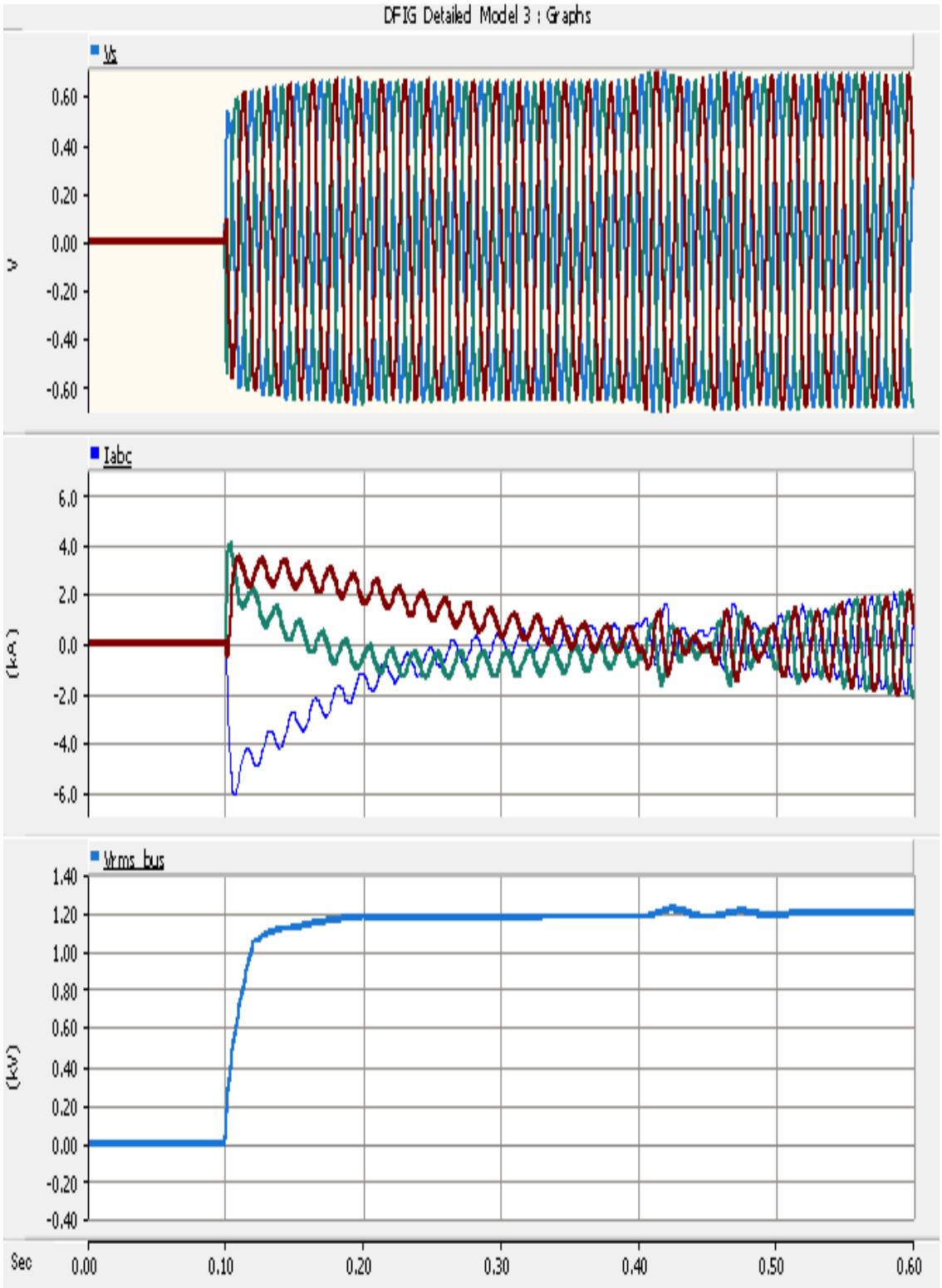

Figure 2-69: Wind farm with eight DFIG wind generators - LV voltage and current waveforms.

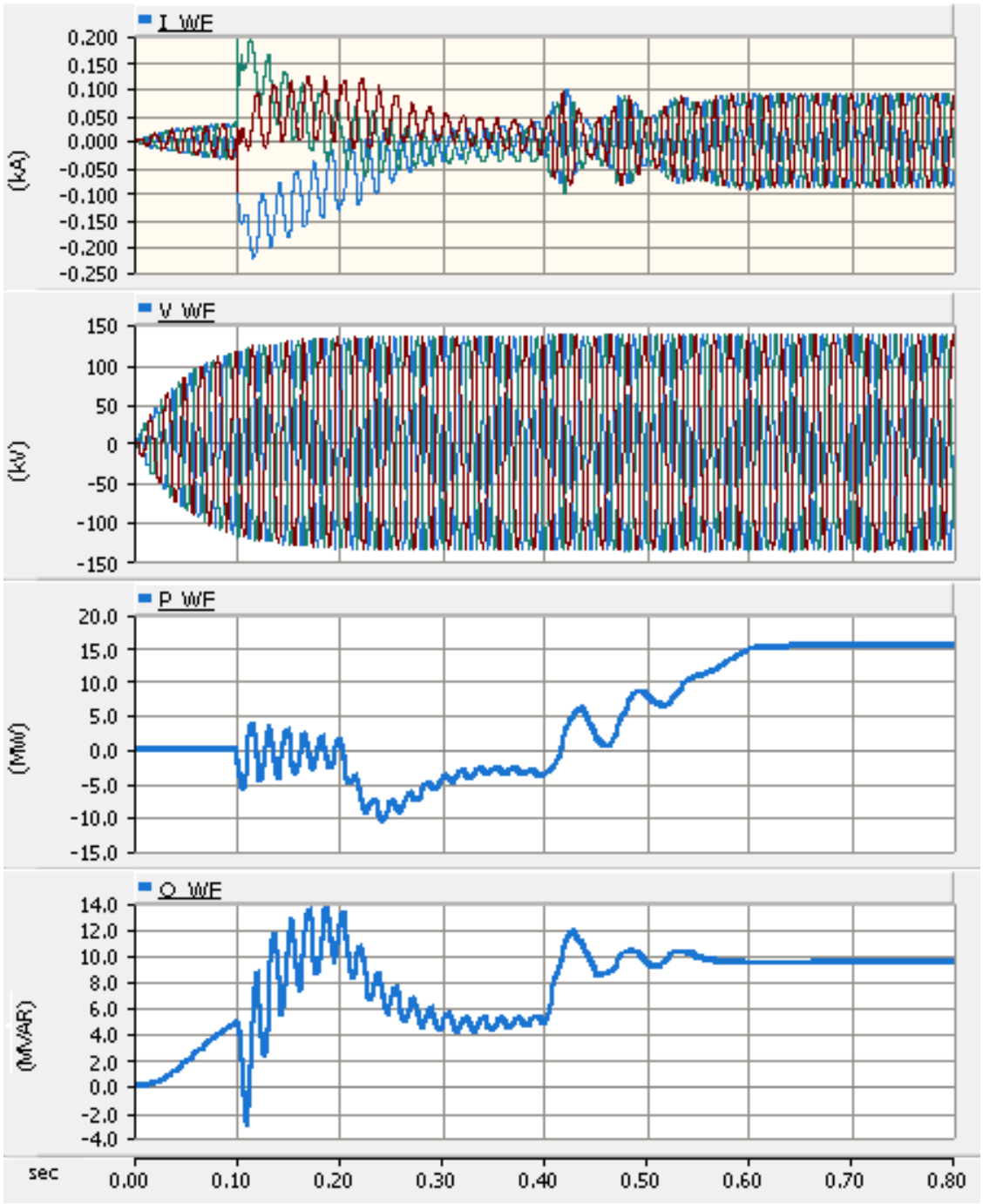

Figure 2-70: Wind farm with eight DFIG wind turbines - 132 kV bus and current waveforms.

Scenario B: Three-phase-to-ground earth fault at wind turbine 690 V transformer terminals

The wind farm PSCAD model arrangement was modified to simulate voltage and current curves of a wind turbine while one of the turbines experiences an earth fault at the 690 V side of the step-up transformer or generator. It is assumed the fault occurs 3 seconds after operation of wind turbine and will be cleared in 0.2 s.

The simulations in Figures 2-71 and 2-72 show that the system will reach normal conditions with no evidence of ferroresonance if there is an LV earth fault on one of the wind turbines. This is the case even with saturation modelling in the system.

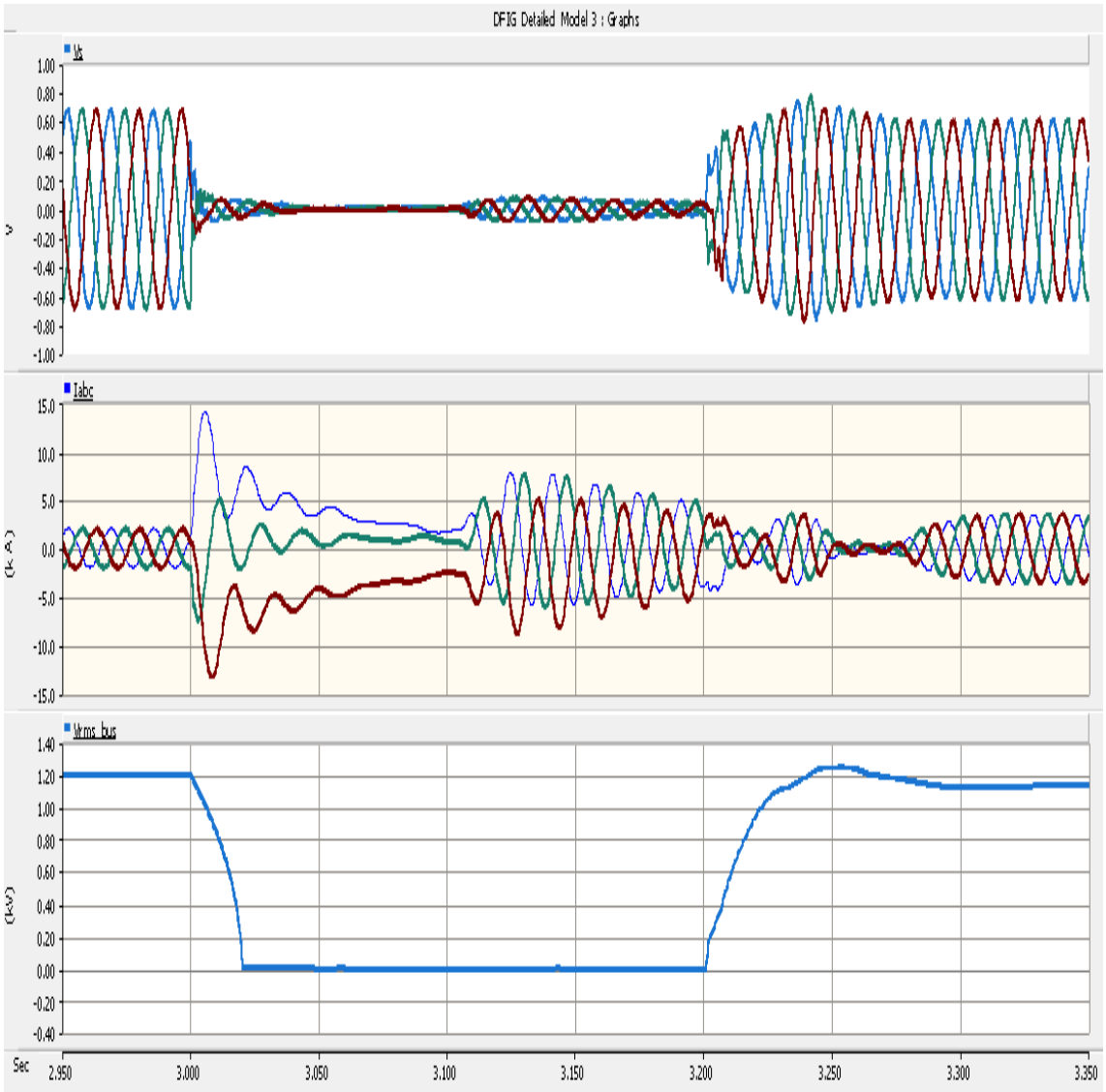

Figure 2-71: Wind turbine (adjacent to faulty turbine) – LV (690 V) voltage and current waveform during the earth fault on nearby wind turbine.

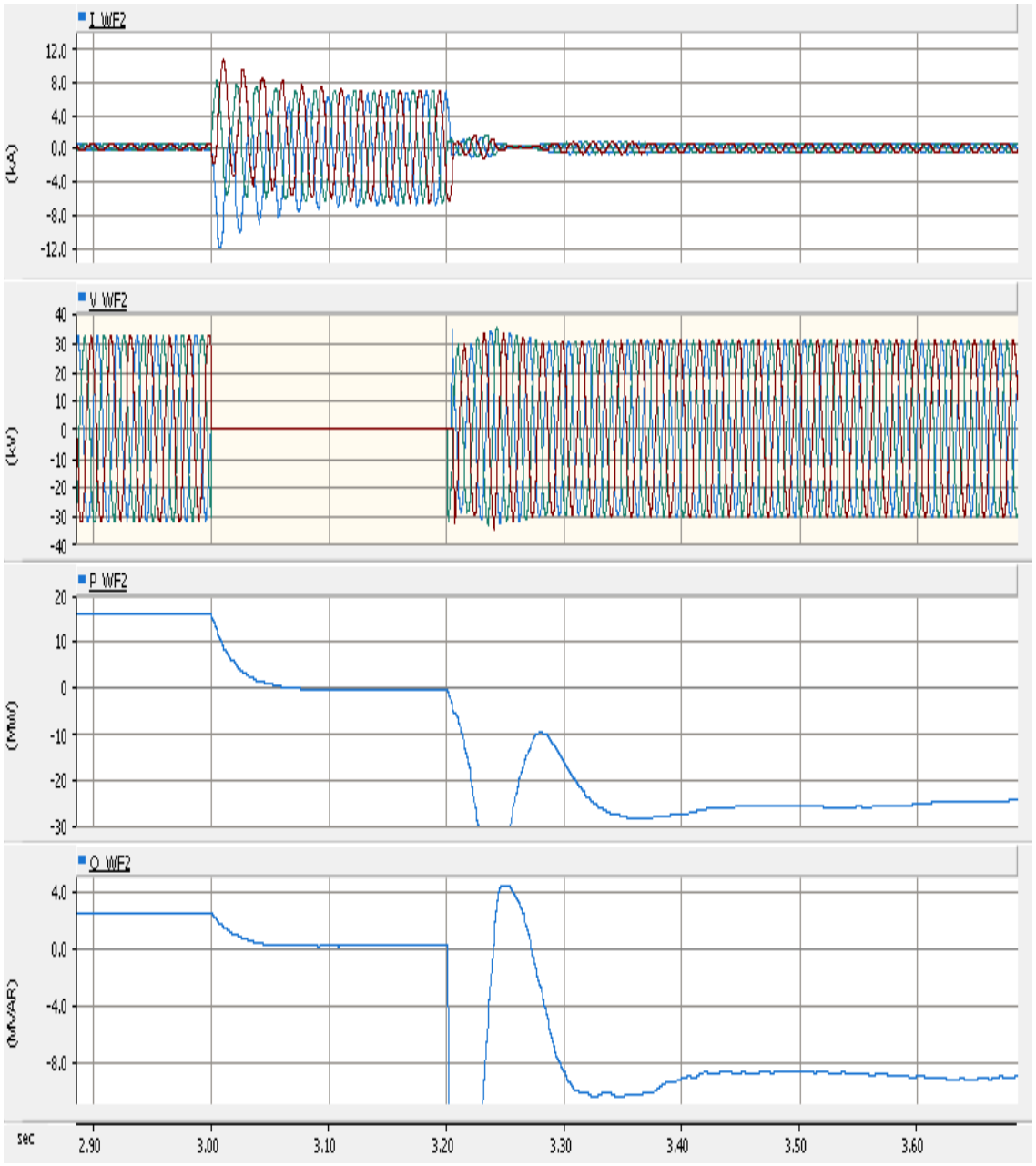

Figure 2-72: Wind farm voltage, current, active and reactive power generation waveform at 33 kV collector busbar.

Scenario C: Single-phase-to-ground earth fault at the wind turbine 33 kV distribution point (5 km aerial).

The wind farm PSCAD model arrangement was modified to simulate the voltage and current curves for the wind farm while there is an earth fault on the 33 kV distribution system which links the wind farm to the power grid. It is assumed that the fault occurs 4 s after operation of the wind turbine and will be cleared in 0.2 s. The aerial line was assumed to be bare Type AAC conductor (refer to Olex supplier catalogue for Mars conductor impedances and technical data).

The fault will be reflected on 132 kV side of the step-up transformer with the voltage, current and power waveforms in Figure 2-73 which shows the presence of some ferroresonance. The 33 kV busbar voltage and current transient during earth fault condition are presented in Figure 2-74. This simulation shows that the system will reach current ferroresonance condition during single-phase-to-ground fault conditions at the wind turbine 33 kV system. This fault could be caused by a cable joint failure.

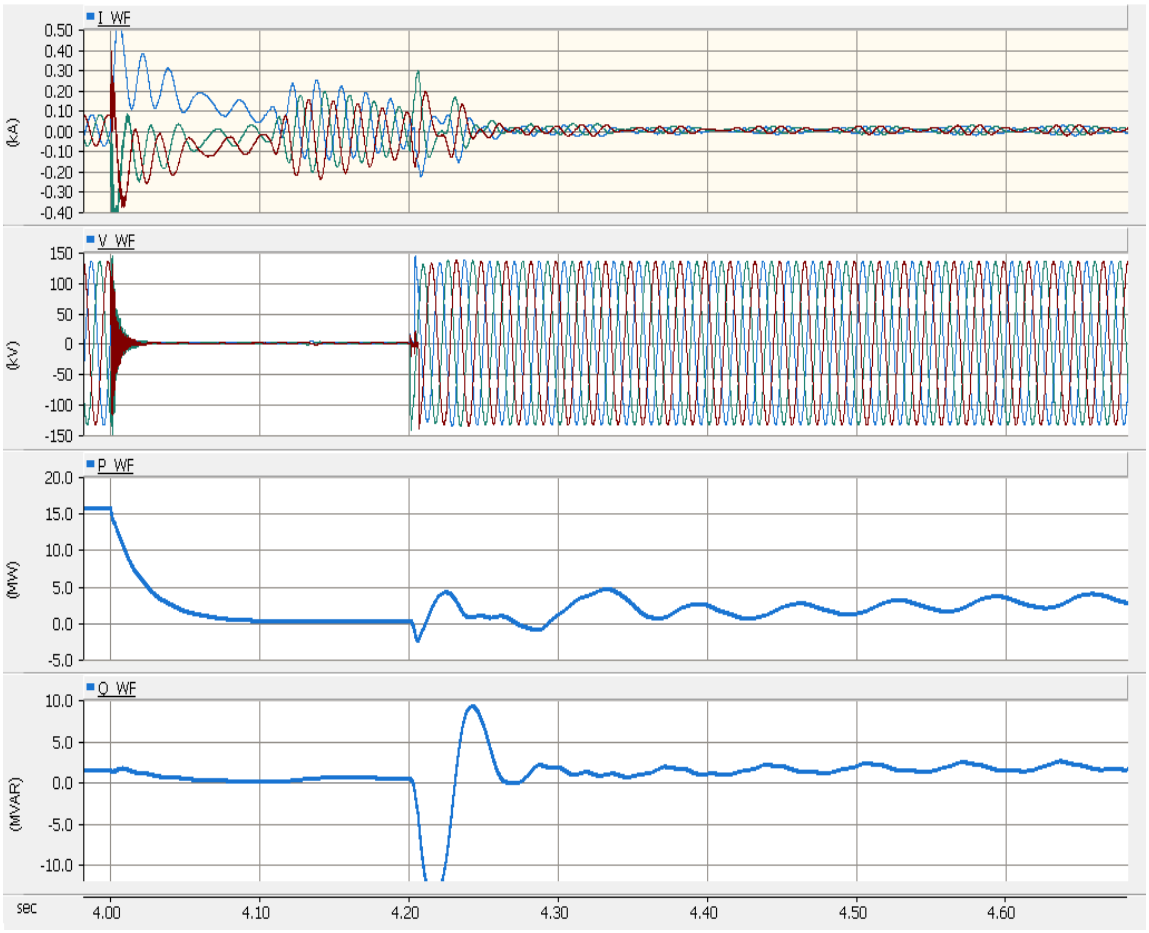

Figure 2-73: Voltage, current and power waveforms of a wind farm connection point to 132 kV grid while there is an earth fault at 33 kV.

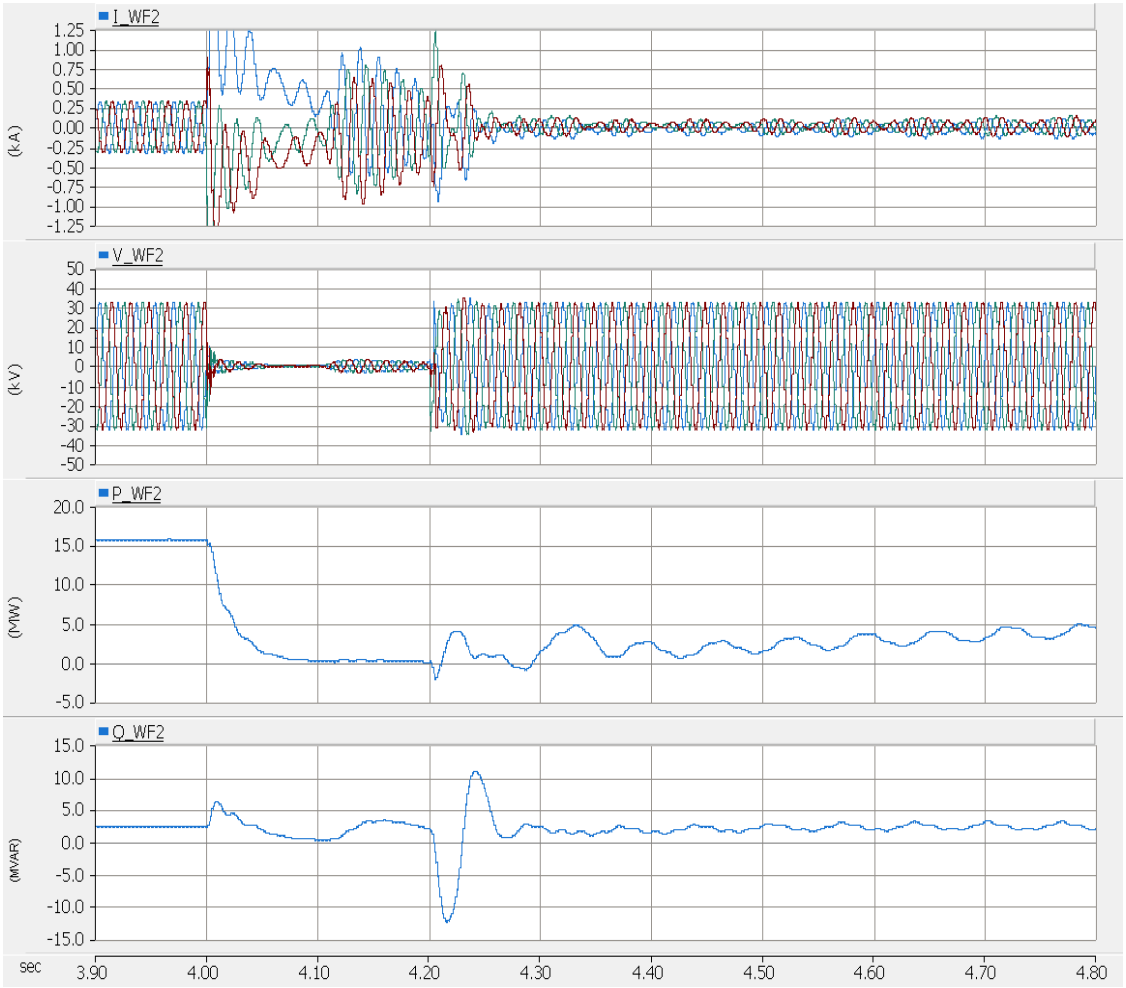

Figure 2-74: 33 kV busbar voltage, and current and power waveforms of a wind farm connection point while there is an earth fault at 33 kV.

Scenario D: Wind Gust impact

The wind farm PSCAD model arrangement was modified to simulate wind gust impact on the voltage and current curves of a wind farm. The worst-case wind gust impact can occur at the turbine starting operation. These waveforms are shown in Figure 2-75. The curves indicate no evidence of ferroresonance in this system with a wind gust impact on wind turbine starting status.

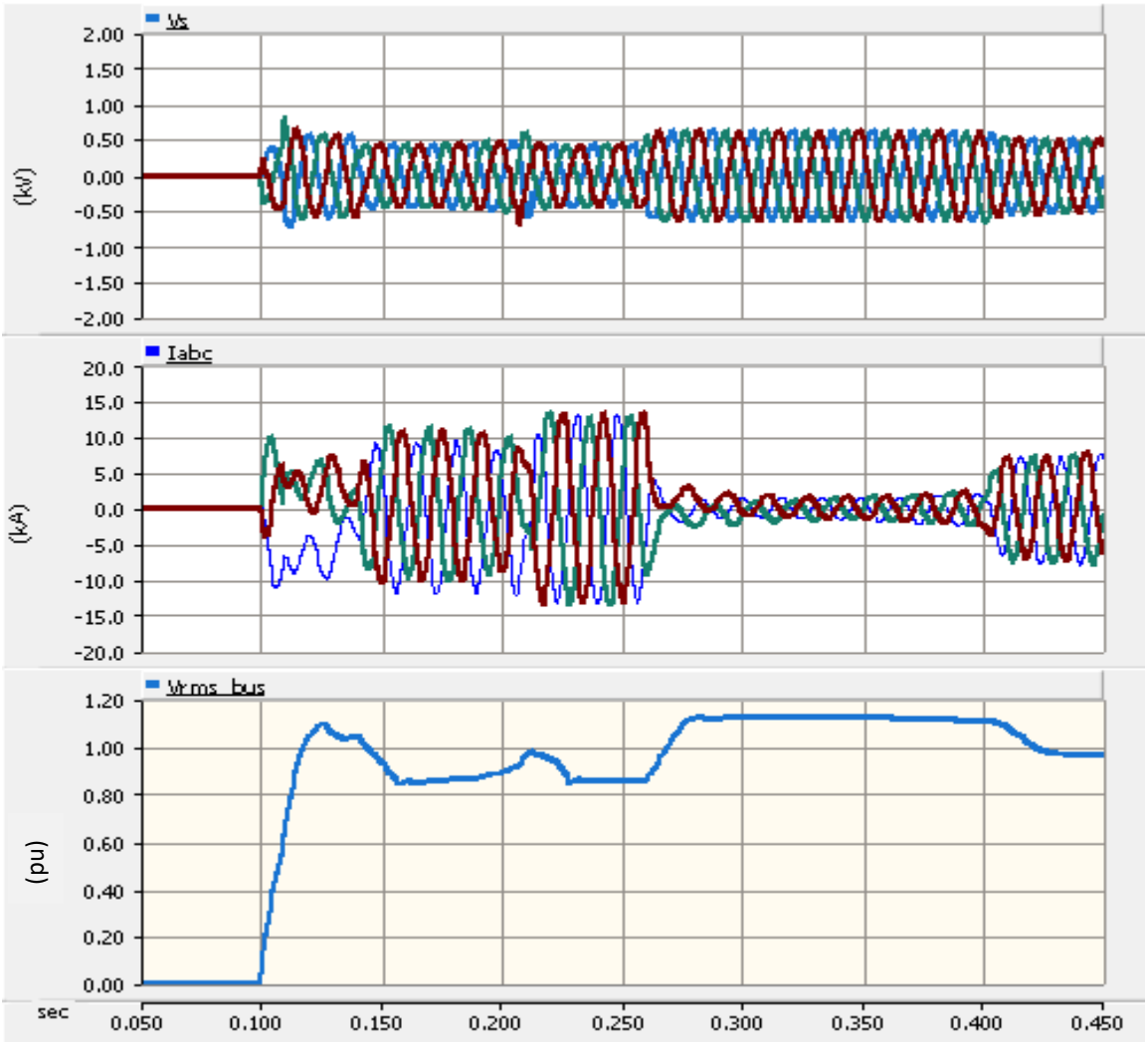

Figure 2-75: LV terminal voltage and current waveforms of a wind turbine while there is a wind gust at 0.1 s after cut-in.

The cut-in assumed to occur at zero second.

Scenario E: Single-phase-to-ground earth fault at the wind turbine 33 kV distribution point (100 km aerial)

The wind farm PSCAD model arrangement was modified to simulate voltage and current curves of a wind farm while there is an earth fault at 33 kV distribution system linking the wind farm to the power grid with 100 km of aerial line between the step-up substation and the grid first substation. It is assumed the fault occurs 4 s after operation of wind turbine and will be cleared in 0.2 s. This seems like a long distance but private conversations suggest these long cables runs are used in Australia. The results for voltage and current on the 33 kV bus are shown in Figure 2-76. The fault will be reflected on 132 kV side of the step-up transformer with the voltage, current and power waves shown in Figure 2-77. Again, for this system, there is no indication of ferroresonance.

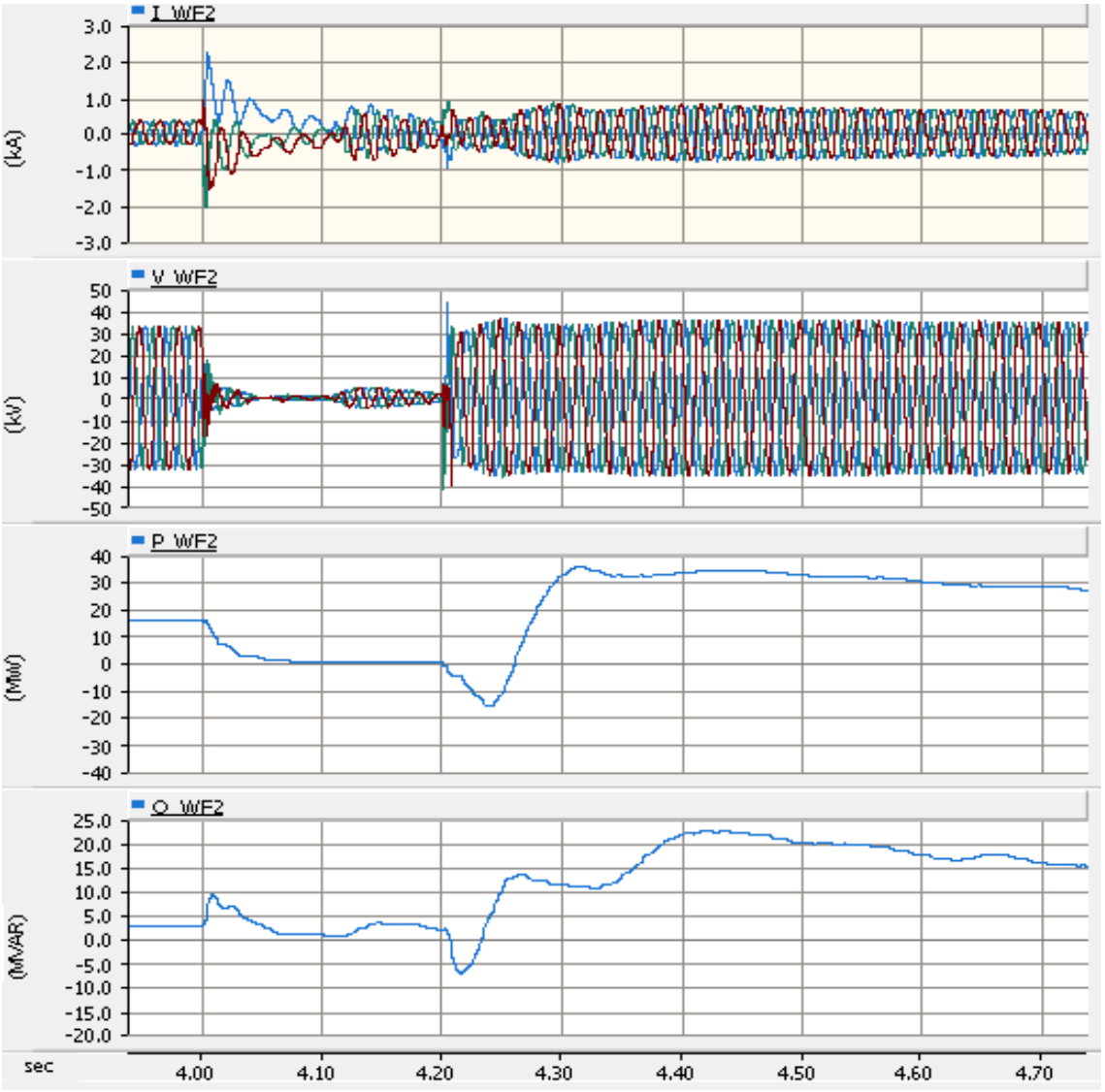

Figure 2-76: Voltage and current waveforms of a wind farm connection point while there is an earth fault at 33 kV.

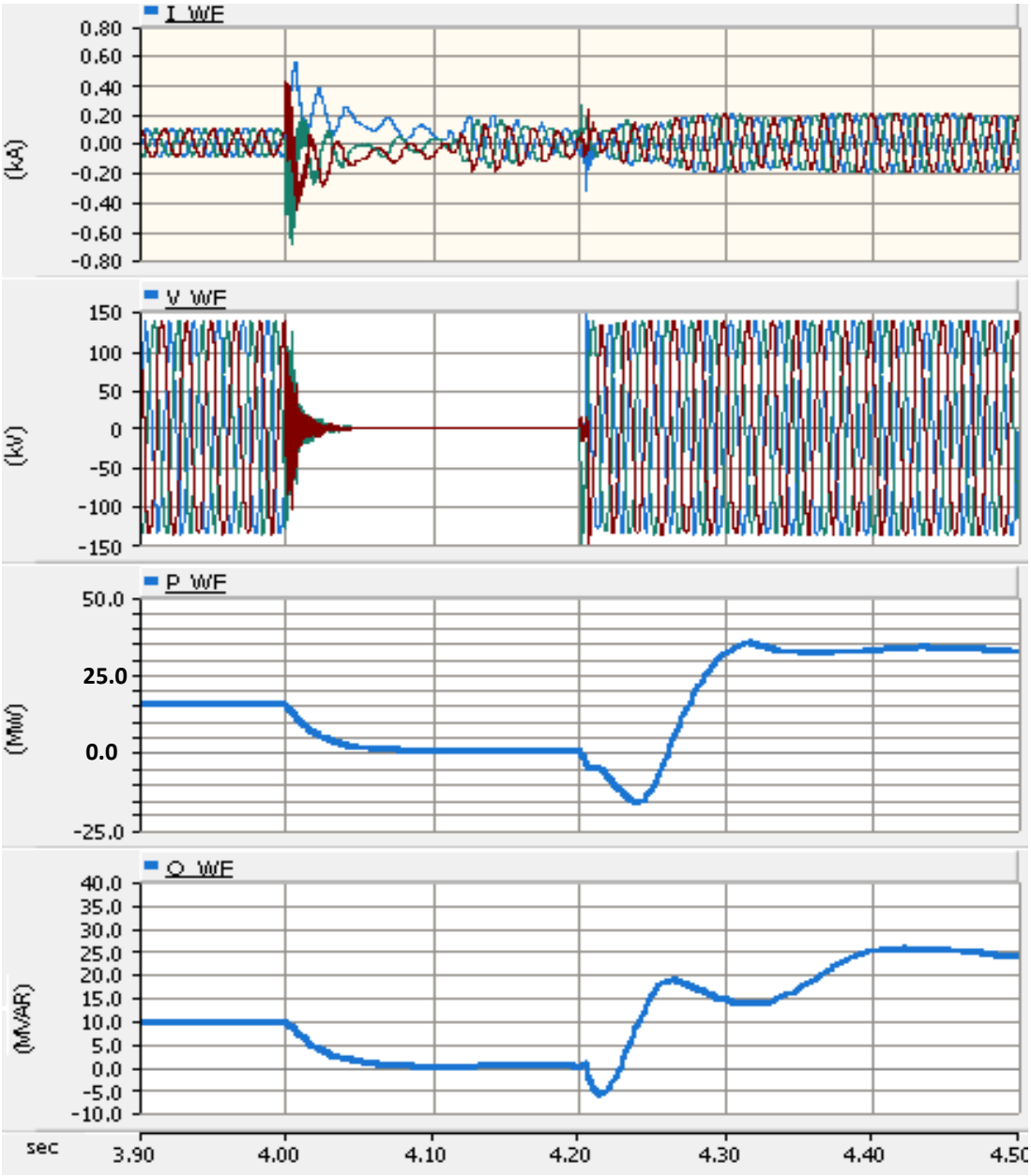

Figure 2-77: Voltage and current waveforms of a wind farm connection point to 132 kV grid.

2.8 Conclusion

In this chapter, load flow and power quality aspects of wind farms have been assessed briefly and these are based on actual installed components. The load flow simulations and manual calculations are used to validate the software model. This can be used as a validation method for future research or actual wind farm design. The validated model is used and the behaviour of the wind turbines under steady-state and transient conditions are assessed. The excitation voltage of a DFIG configuration (Type 3) and asynchronous generators with external variable resistor (Type 2) generators are simulated for different operational scenarios. The frequency responses of these generators for case study arrangement are assessed.

Other power quality aspects, such as the harmonics for Type 2 and Type 3 turbines are assessed. Based on information from turbine manufacturers; Case Study 2 with Type 2 turbine generators appear to have higher harmonic distortion levels compared to Type 3 (DFIG) generators. This is explained – the Type 2 simulation uses phase-angle thyristor control of the external resistors. Other resistor control methods may reduce the harmonic content.

A manual flicker calculation method is proposed which is based on the IEC standard method. The sequence and method of calculation has not been presented in similar research or guidelines elsewhere.

Wind turbine, wind farm and high voltage network responses during switching, steady-state operation and fault location scenarios are presented in the ferroresonance assessment and the simulation plots presented accordingly. The transient behaviour of each component (turbine, wind farm substation and nearby transmission) can be used for protection system design, and current transformer (CT) and capacitor voltage transformer (CVT) saturation studies. It is reported that the implication of ferroresonance includes problems in protection systems, overheating in transformers and reactors, and excessive sound which can lead to equipment failure. It can cause thermal damage to insulators as well as problems in transmission and distribution systems [54].

Simulation results indicate that ferroresonance can be created for certain system configurations. Therefore, to avoid experiencing ferroresonance phenomena on a wind farm grid, similar simulations are recommended at the wind farm design stage.

2.9 Future Work

During this study it is proposed that a comparison of the results for the simulations and findings for the wind farm events, harmonic and transient records, and system losses be carried out to validate the simulation results and power system analysis. Due to a wind farm operator confidentiality agreement the comparisons were not included. This can be considered as another research project and future work.

Chapter 3: Wind Farms Earthing and Lightning Protection Issues

3.1 Introduction

Two of the aspects impacting the performance of electrical systems are the earthing and lightning protection systems. The earthing and lightning protection systems define the earth fault clearance times and interruptions. In this section the earthing system requirement for a wind farm and the ways of improving the earthing system have been discussed briefly and fundamentally. The discussion in this chapter can be summarised in the following theoretical and practical items:

- The soil resistivity test and analysis;
- Earthing system analysis and impact assessment on network fault impedances;
- Earthing system performance test; and
- Lightning strike assessment.

Here, the SES software package is used for simulation of Case Study 1; field test results are given and high frequency analysis is carried out.

3.2 Soil Resistivity

Soil electrical resistance has an important role in earth fault dissipation and fault current return path. As described in IEEE Std 81-2012 [26], there are several methods for estimating the soil characteristics of wind farms. Industry practice is to use the combination of the following standard methods:

- Geological information and soil samples;
- Variation of depth method or three-point method (electrode insertion); and
- Four-point method (current injection method).

The intention of this section is to validate standards and industry practices against practical tests conducted. A good method for measuring the apparent resistivity of large volumes of undisturbed earth is the four-point method. In this method four auxiliary probes are installed in the earth spaced (in a straight line) at intervals and at a certain depth. A test current will be injected by test equipment between the two outer probes and the potential between the two inner probes is measured with the same test equipment (a built-in high-impedance voltmeter). Then, the V/I ratio gives the resistance R in Ω [26].

The following methods are applied for four-point soil resistivity measurements:

1. Equally Spaced or Wenner Arrangement.
2. Unequally Spaced or Schlumberger–Palmer Arrangement.

The common method for wind turbine soil measurement is the equally spaced Wenner Arrangement. Normally the purpose of the soil resistivity testing is to obtain a set of measurements which are then used to develop an equivalent soil model for the electrical earthing system performance but the purpose of the test presented in this section of research is to validate the Wenner Arrangement, and whether or not it is the appropriate method to be followed.

To validate the Wenner soil measurement a test was conducted in the park land adjacent to Penrith Council in NSW (as shown in Figure 3-1). The following instruments were used for the tests:

- Metal detector Minlab XTRA 305; and
- Earth/Ground tester, Saturn GEO X LEM, calibrated.

Existing underground metallic objects can impact on the soil resistivity test; therefore, before carrying out the soil resistivity measurements, a metal detector was used to scan each site for metal pipes, reinforcing steel structures and other metallic objects in the soil. Results from the "Dial Before You Dig" (DBYD) and the metal detector confirmed that there were no metallic objects in the test areas. The DBYD is a referral service for information on locating underground utilities anywhere in Australia.

Figure 3-1: Location of soil resistivity test site.

The Wenner Method involves placing four electrodes in the earth at equal spacing along a straight line. The test set passes current through the two outer electrodes and measures the voltage drop between the inner two electrodes, as shown in Figure 3-2. Using Ohms law, it will calculate a resistance value, which can then be converted to a resistivity.

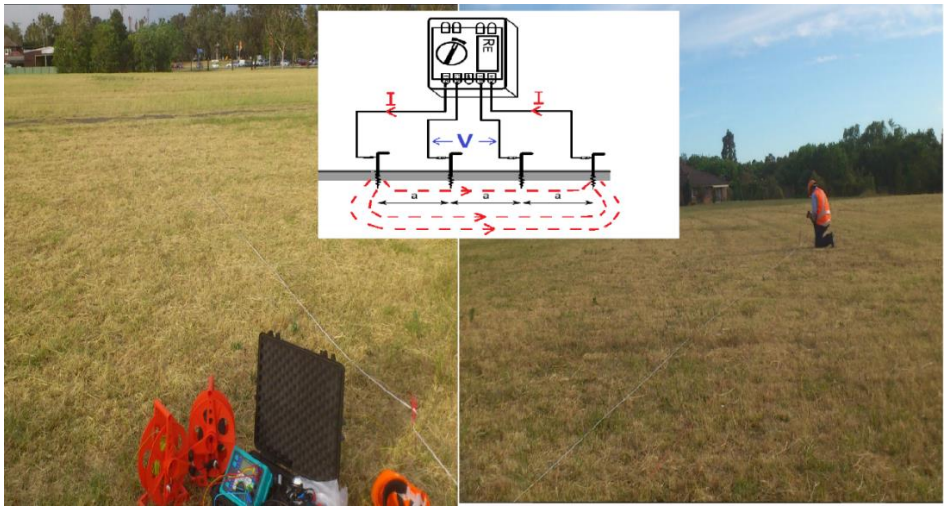

Figure 3-2: Soil resistivity test site.

Wenner array soil resistivity testing should ideally be done with electrode spacing up to 3 times the diagonal of the earthing system (wind turbine foundation). The spacing shall generally cover 1 m, 2 m, 4 m, 8 m, 16 m, 32 m and 50 m. The longest available traverse should be taken as the probe spacing represents the depth of test. Site measurements and pre-simulated value for Traverse 1 is presented in Table 3-1.

Table 3-1: Traverse 1 soil measurements.

Location	Max probe depth [mm]	Probe spacing, a [m]	Resistance			Resistivity [Ωm] $\rho = 2\pi \times a \times RE$	Error due to probe resistance: $1.25\times10^{-6} \times RH \times (RS + 2000) / RE$
			RH [kΩ]	RS [kΩ]	RE [Ω]		
Traverse 1	50	1	4.5	6.8	8.1	50.9**	6.11
	100	2	2.3	6.1	2.75	34.6**	8.47
	200	4	3.3	3.8	1.89	47.5**	12.66
	300	8	2.5	2.2	1.25	62.8**	10.5
	300	16	0.3	1.8	0.868	87.7**	1.64
	300	32	0.2	1.8	0.329	66.1**	2.88
	300	50	1.5	0.4	0.24	75.3**	18.75
	300	100	2.6	2.2	0.09	56.5**	151.67*

*High error due to high probe and ground resistance, less injected current but gives similar soil layer values and model
**Site measurement by Massood Siahpoosh using Saturn GEO X tester

The Wenner method requires at least two traverses which are as near as practicable perpendicular to each other (e.g., North-South and East-West). Each traverse was assessed individually, to check accuracy, before doing any combined data plot. The second traverse set of readings are presented in Table 3-2.

Table 3-2: Traverse 2 soil measurements.

Location	Max probe depth [mm]	Probe spacing, *a* [m]	Resistance			Resistivity [Ωm] $\rho = 2\pi \times a \times RE$	Error due to probe resistance: $1.25\times10^{-6} \times RH \times (RS + 2000) / RE$
			RH [kΩ]	RS [kΩ]	RE [Ω]		
Traverse 2	**50**	**1**	10.3	9.4	7.90	49.64**	18.58
	100	**2**	7.1	7.6	4.90	61.58**	17.39
	200	**4**	3.6	6.3	2.73	68.61**	13.68
	300	**8**	3.6	1	2.12	106.56**	6.37
	300	**16**	1.7	1.3	1.1	110.58**	6.37
	300	**32**	1.1	1.1	0.46	92.49**	9.27
	300	**50**	0.8	1.6	0.21	65.97**	17.14
	300	**100**	0.9	1.9	0.10	62.83**	43.87*

*High error due to high probe and ground resistance, less injected current but gives similar soil layer values and model
**Site measurement by Massood Siahpoosh using Saturn GEO X tester

The measured resistance values presented in Table 3-1 and 3-2 are:

RE: Earthing resistance

RS: Auxiliary earth electrode resistance

RH: Probe resistance

As mentioned above one of the parameters in defining the soil model, is geological information and soil samples. Geological information and soil samples adjacent to the test location show a 3-layer soil configuration at the test location (Figure 3-3). This comparison between soil resistivity test and geotechnical investigation is recommended for interpretation of the test results and soil model simulation.

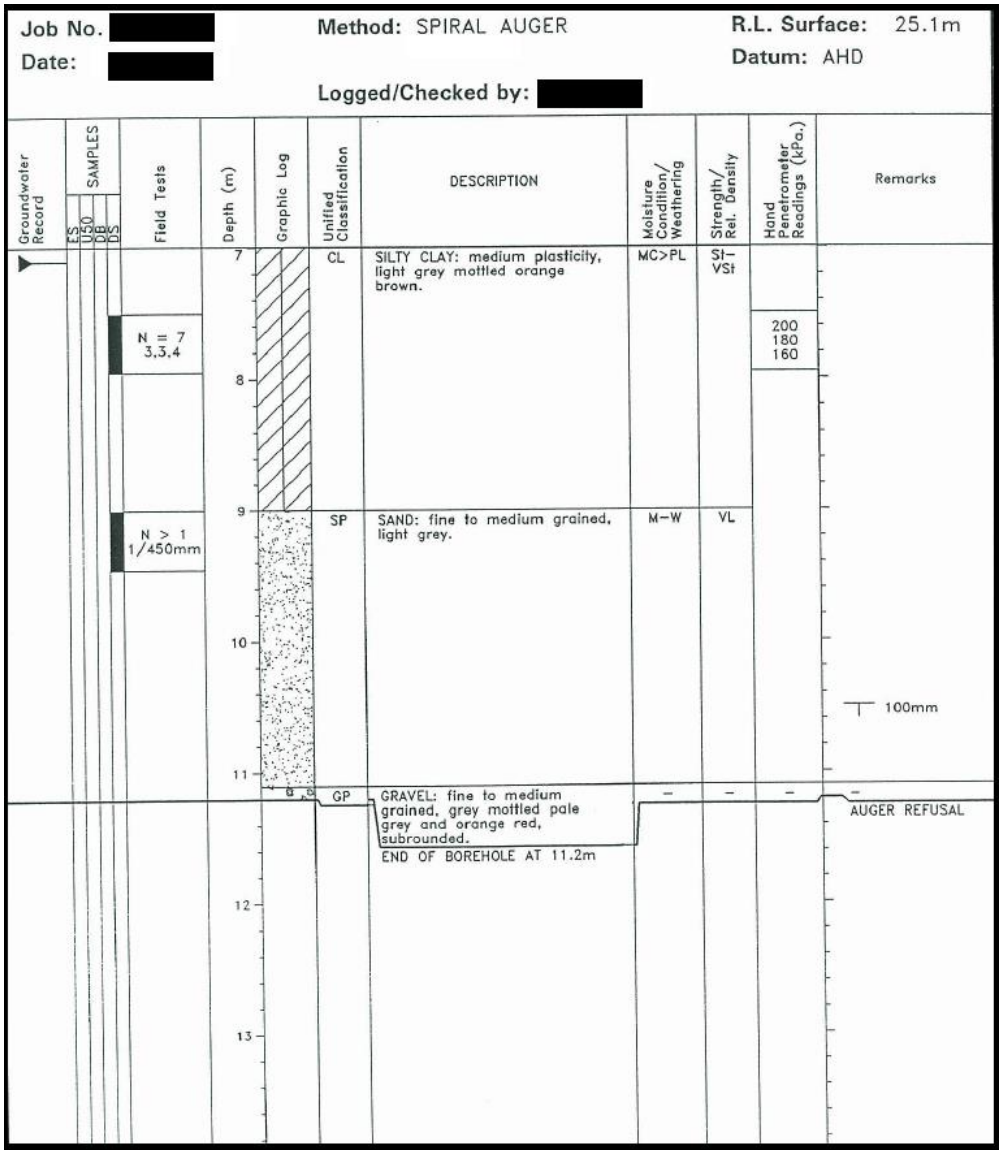

Figure 3-3: Borehole test log (courtesy of Aurecon).

Three-layer soil model analysis is not presented in the current IEEE standard or similar international codes; therefore, in this section, the IEEE 80 two-layer soil model analysis method was used to calculate a three-layer soil model. A two-layer soil model can be approximated according to Blattner and Dawalibi graphical methods using Sunde's graph, which is based on the Wenner four-pin test data. The methods described in IEEE Std 80 [27]. The soil resistivity data plots from Traverse 1 and 2 are presented in Figure 3-4.

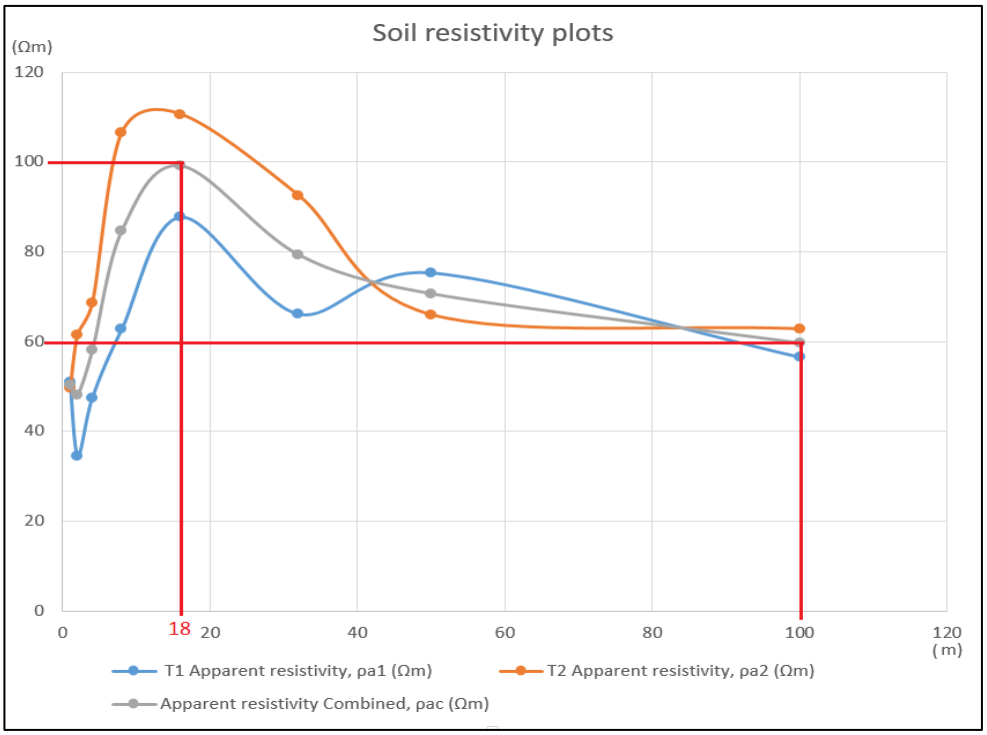

Figure 3-4: Soil resistivity test plots.

Apparent resistivities ρ_1 (50 Ω.m), ρ_2 (100 Ω.m) and ρ_3 (60 Ω.m) are obtained by interpreting the measurements (from a combined model). The depth of each layer of soil can be obtained by Sunde's graphical method. Assumed apparent resistivity will be utilised in layer thickness analysis.

$$\frac{\rho_2}{\rho_1} = \frac{100}{50} = 2 \tag{3-1}$$

From the combined apparent resistivity plot the following points have been selected to be used in Sunde's graphical method to define the thickness of each layer of soil:

$$\rho_{a1} = 100 \quad \Omega.\text{m} \qquad a = 18 \quad \text{m} \tag{3-2}$$

$$\frac{\rho_{a1}}{\rho_1} = \frac{100}{50} = 2 \tag{3-3}$$

$$h_1 = \frac{a_1}{a/h} = \frac{18}{7} = 2.75 \quad \text{m} \tag{3-4}$$

So the top soil layer is calculated to be 2.75 m. At the moment there is no standard method for calculating the thickness of second layer of a three-layer soil, therefore the following method was adopted:

$$\rho_{\text{ave 1 and 2}} = \frac{\rho_1 + \rho_2}{2} = 75 \quad \Omega.\text{m} \tag{3-5}$$

$$\frac{\rho_3}{\rho_{\text{ave 1 and 2}}} = \frac{60}{75} = 0.8 \tag{3-6}$$

$$\rho_{a2} = 60 \quad \Omega.\text{m} \qquad a = 100 \quad \text{m} \tag{3-7}$$

$$\frac{\rho_{a2}}{\rho_1} = \frac{60}{75} = 0.8 \tag{3-8}$$

$$h_2 = \frac{a_2}{a/h} = \frac{100}{7.5} = 13.4 \quad \text{m} \tag{3-9}$$

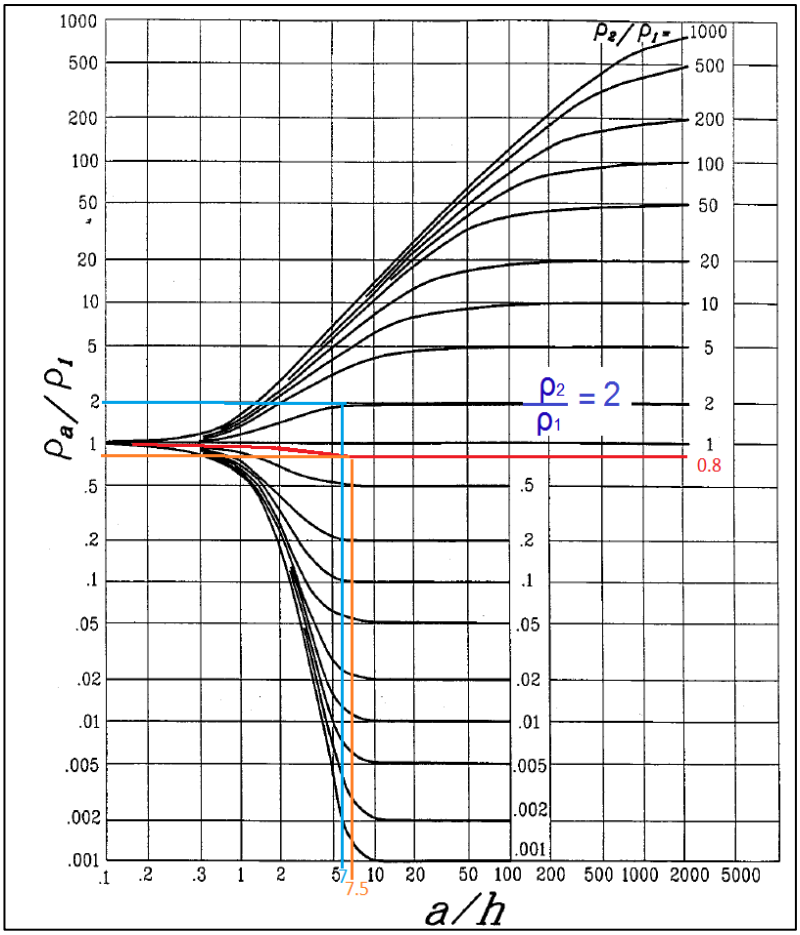

Figure 3-5: Sunde's graph [27].

According to the above discussion the soil model for this test location can be summarised as per Table 3-3.

Table 3-3: Travers 2 soil measurements.

Layer	**Resistivity [Ωm]**	**Depth [m]**
Top	$\rho_1 = 50$	$h_1 = 2.75$
Middle	$\rho_2 = 100$	$h_2 = 13.4$
Bottom	$\rho_3 = 60$	infinite

The soil model was validated by installing two earth electrodes adjacent to the test location. The electrodes were 6m long bare 70 mm² conductors located 300 m away from each other. The

earthing resistance of each electrode was measured by 3 pin fall of potential as per IEEE Std 81-2012 [26] instruction. The first electrode had 10.96 Ω and second earth electrode had 11.66 Ω resistances respectively.

The resistance of installed earth electrodes was calculated according to Appendix A.2 of IEEE Std 81-2012 [26]. The calculation is

$$R = \left(\frac{\rho_1}{2\pi L} \ln\left(\frac{2L}{r} \right) + \sum_{n=1}^{\infty} k^n \ln\left(\frac{2nh+1}{2nh-1} \right) \right) \quad [\Omega] \tag{3-10}$$

where L is the length (which is 6 m) and r is the radius of electrode (which is 6.2 mm based on supplier data). k is the reflection coefficient which can be calculated from

$$k = \frac{\rho_2 - \rho_1}{\rho_2 + \rho_1} \tag{3-11}$$

Accordingly, the resistance of a 6 m earth electrode calculated by equation (3-10) is 13.6 Ω. The measured resistance is about 11 Ω. This value is valid for driven rods as the earth electrode will be in contact with native soil. For the earth electrode installation with boring method, normally a 50 mm diameter bore is made by drilling and earthing compound will be poured during the installation of the earth electrode; however, based on industry practice, and the author's experience, the impact of the earthing compound can be neglected.

3.3 Wind Farm Case Study 1

Case Study 1 has more than fifty wind turbines. The wind turbines are scattered in seven collection groups in an area of about 10 km². The turbines have 33 kV interconnections with minimum separation of 200 m and maximum separation of 1300 m. Case Study 1 was modelled using Safe Engineering Services (SES) CDEGS software package for earthing and lightning protection analysis. The following modules of CDEGS software package were used in this research:

- RESAP – To model equivalent earth structure models based on measured soil resistivity data;
- HiFREQ – To model wind turbines earthing system and simulate voltage gradient for lightning;
- SESShield – 3D - To model turbines LPS and simulate wind turbine shielding; and
- FFTSES – To model lightning stroke current waveform.

3.3.1 Turbine Earthing System Modelling

The earthing system and foundation reinforcement of the wind turbines are modelled using the HiFREQ module of the CDEGS software. A soil resistivity test was conducted at the proposed

location of each wind turbine at the design stage. The test results were revisited and RESAP software module was used to access the soil structures. The three soil models in Figures 3-6 to 3-8 are used for this study.

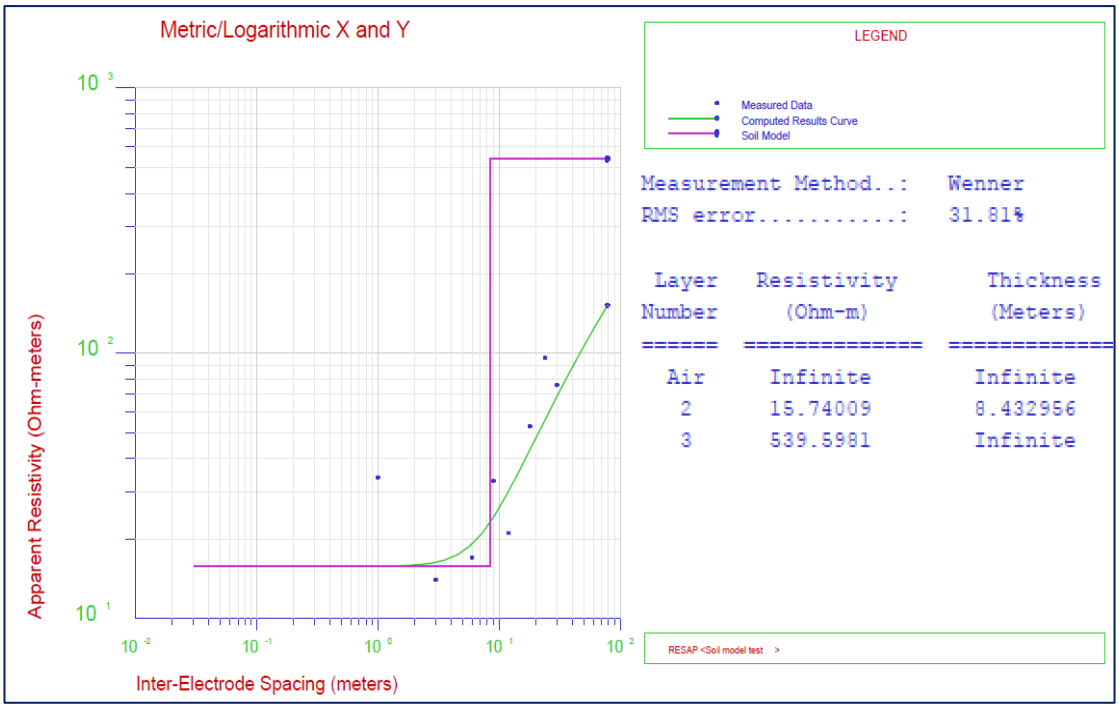

Figure 3-6: Soil model for wind farm Case Study 1 (soil model with lowest resistivity).

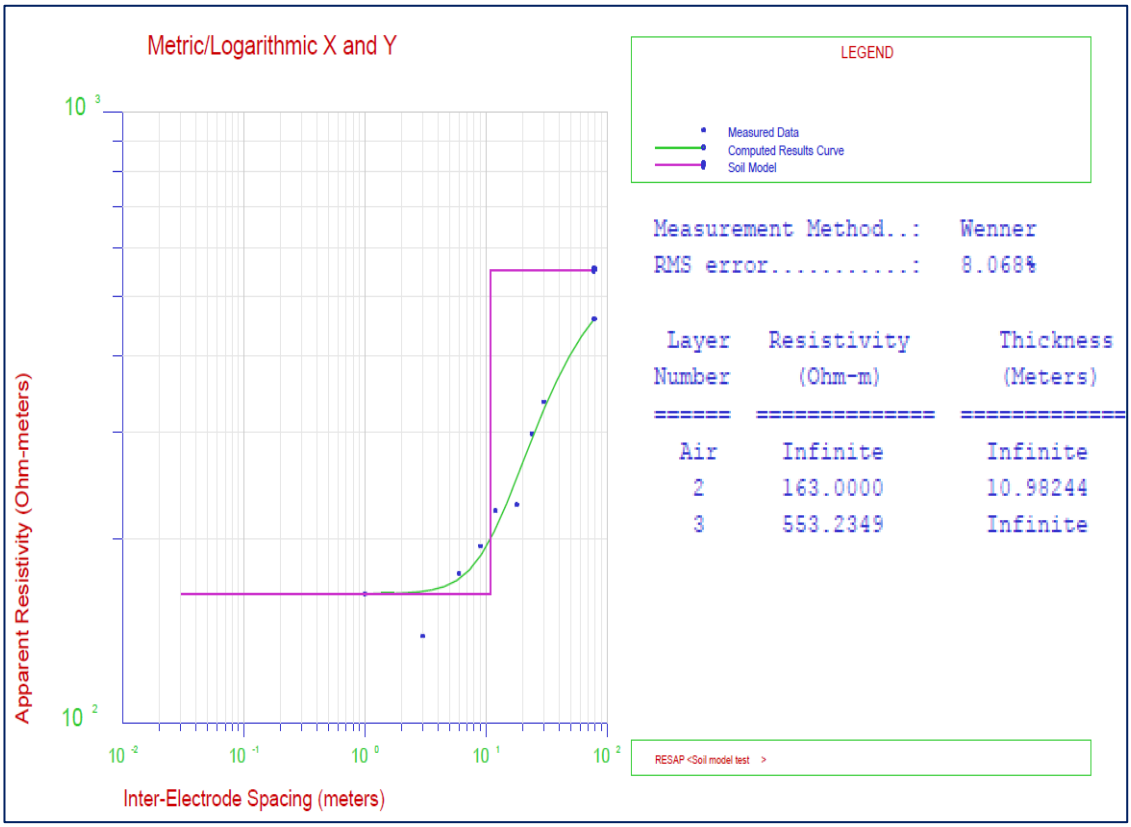

Figure 3-7: Soil model for wind farm Case Study 1 (soil model based on average test results).

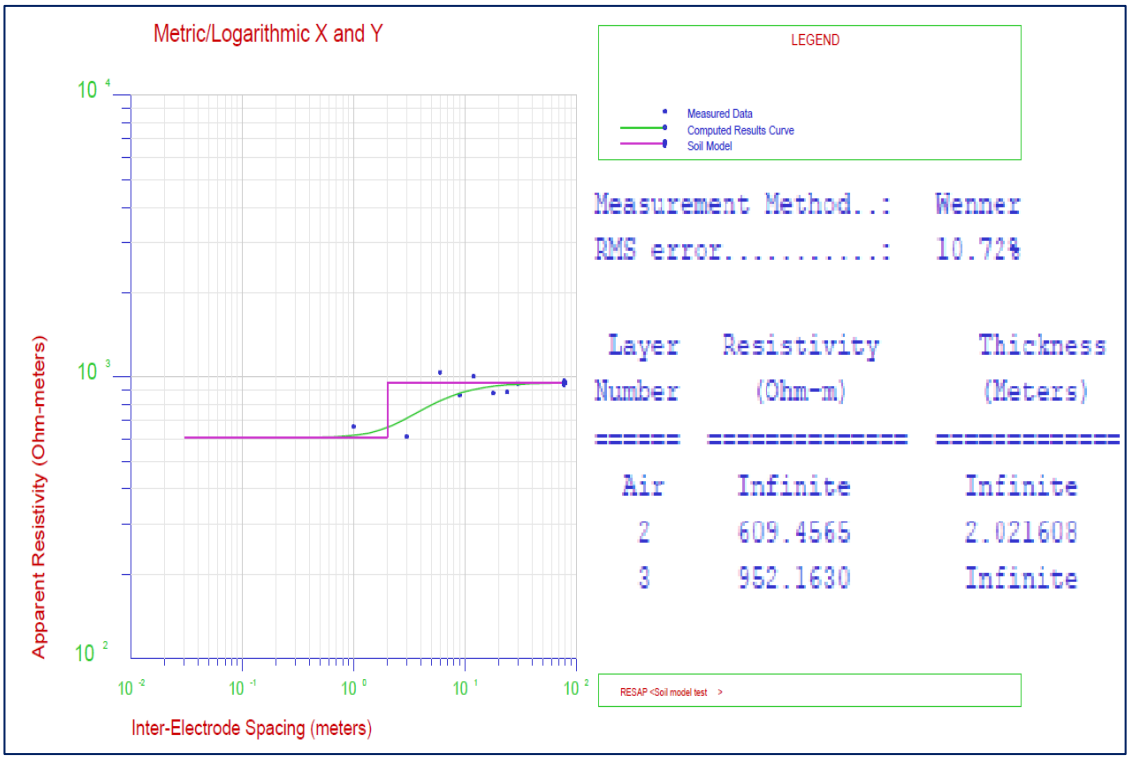

Figure 3-8: Soil model for wind farm Case Study 1 (soil model with highest resistivity).

The turbine foundation of each turbine has been modelled in HiFREQ modules as per As-Built drawings and construction information. Figure 3-9 shows the actual foundations of the installation.

HiFREQ module of CDEGS software are used to model turbines, distribution cables and step up transformers for wind Case Study 1. The SESCAD module of CDEGS are used to model the three-phase transformers and turbines, and the 33 kV network, for the earthing assessment. The turbine towers were modelled as shown in Figure 3-10.

Figure 3-9: Two different type of wind turbine foundations (courtesy of Aurecon).

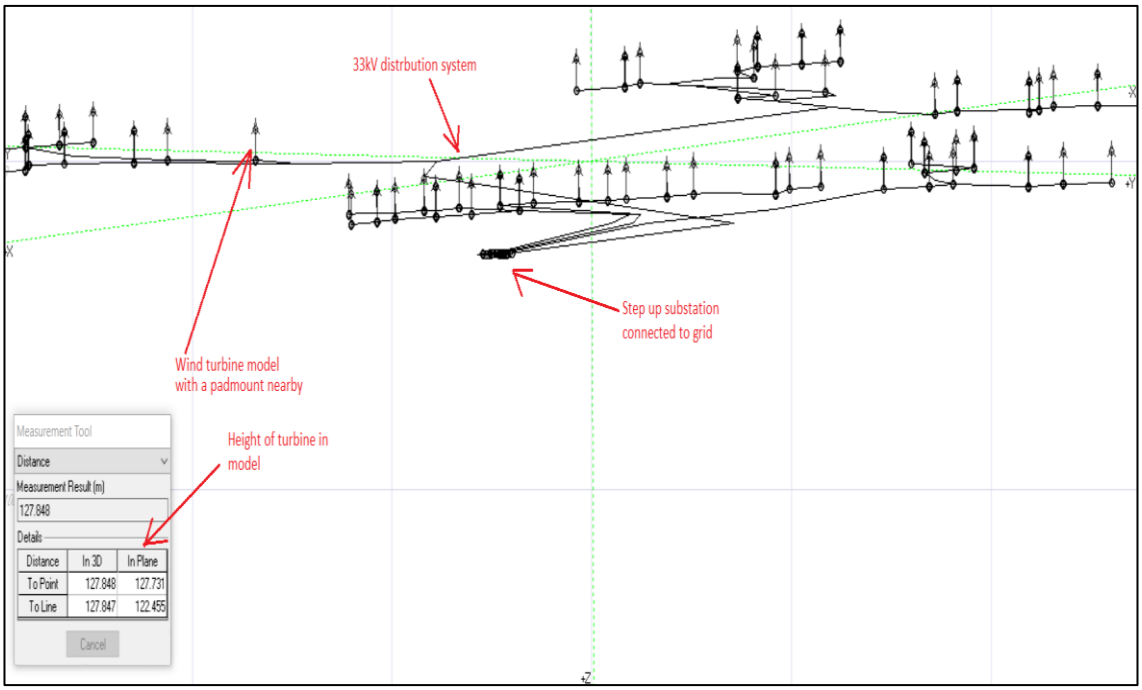

Figure 3-10: Wind farm model in SESCAD of HiFREQ module.

3.3.2 Turbine Lightning Risk Assessment

A lightning stroke can be regarded as a current source. The maximum recorded value of lightning current produced by a single stroke is in the region of 300 kA. Lightning discharges are one of two basic types, downward or upward initiated. A downward initiated discharge starts at the thundercloud and heads towards the earth. In contrast an upward initiated discharge starts at an exposed location on the earth and heads upwards towards a thundercloud [46].

The lightning stroke risk is a common issue for wind farms since the factor of height and standalone conditions can provide good cloud-to-ground discharge path. Wind turbine blades are more likely to be hit by lightning as they are higher than other nearby infrastructures. So it is essential to minimize the impact of lightning on the turbines and their blades. In other words, lightning strikes occur regularly, therefore it is essential that the lightning system functions as it should. Blade damage is shown in Figure 3-11.

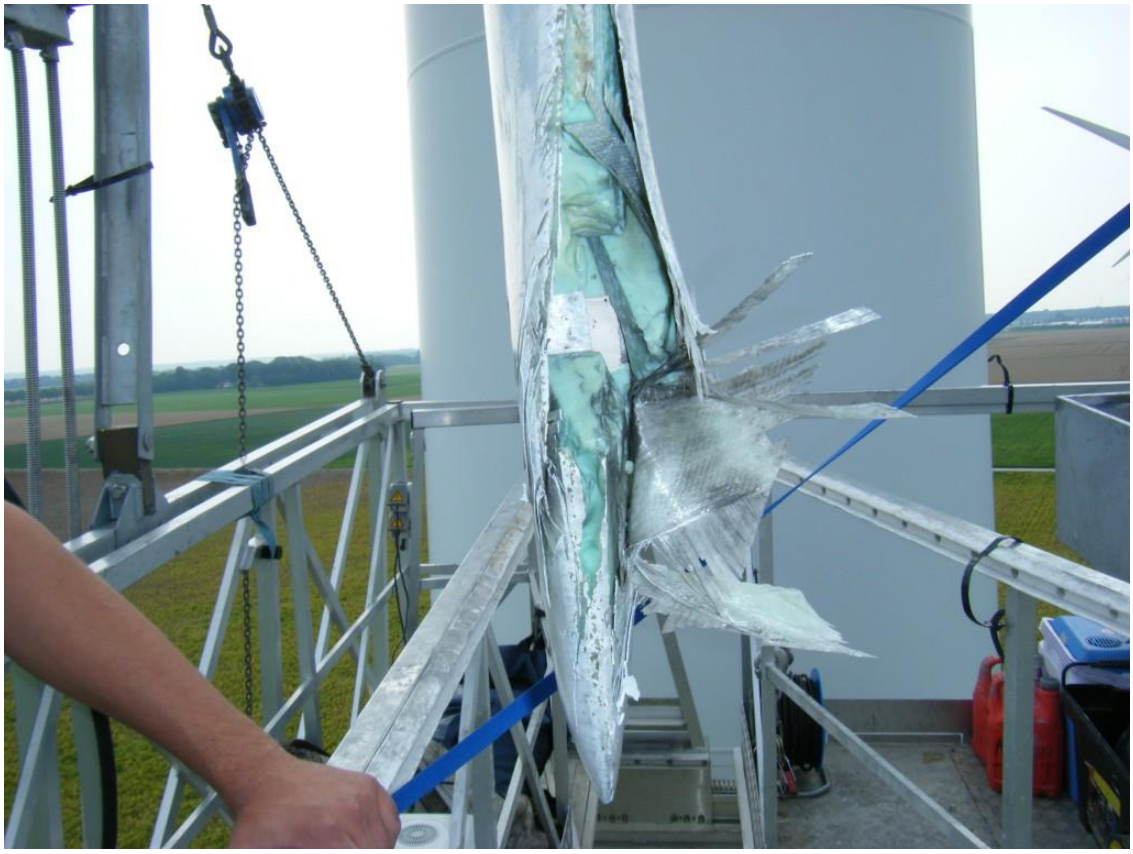

Figure 3-11: Damaged blade by lightning (photo from http://www.globalbladeservice.eu/).

The blades are normally manufactured with lightning protection strips utilizing pre-preg wet laminate process, with a "D" spar. The pre-preg wet laminate process is an interim manufacturing process between wet laminate moulding process and infusion moulding process. The resin is forced into and around the glass using rollers and squeegees. Then often a vacuum bag is applied over the mould to compress the laminate further. The blades consist of several exterior copper "receptor" air terminals [46], which are fastened into interior conductors running the length of the blade. The lightning protection strips are electrically insulated from the blade bearing and hub. The blade arrangements are shown in Figure 3-12.

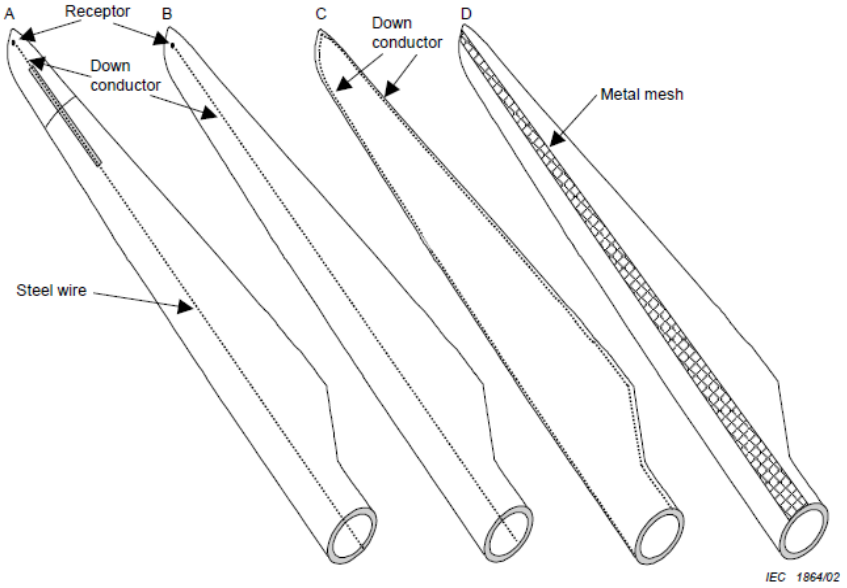

Figure 3-12: Lightning protection for large modern wind turbine blades [46] (courtesy of IEC).

Conductors are fastened to the blade and to one another with steel bolts. Near the blade root a portion of the conductor is imbedded into the fibreglass. The conductor transitions from the blade root area via bonding to the hub and thence to the earth bar. Other components of the lightning protection systems are bonded together.

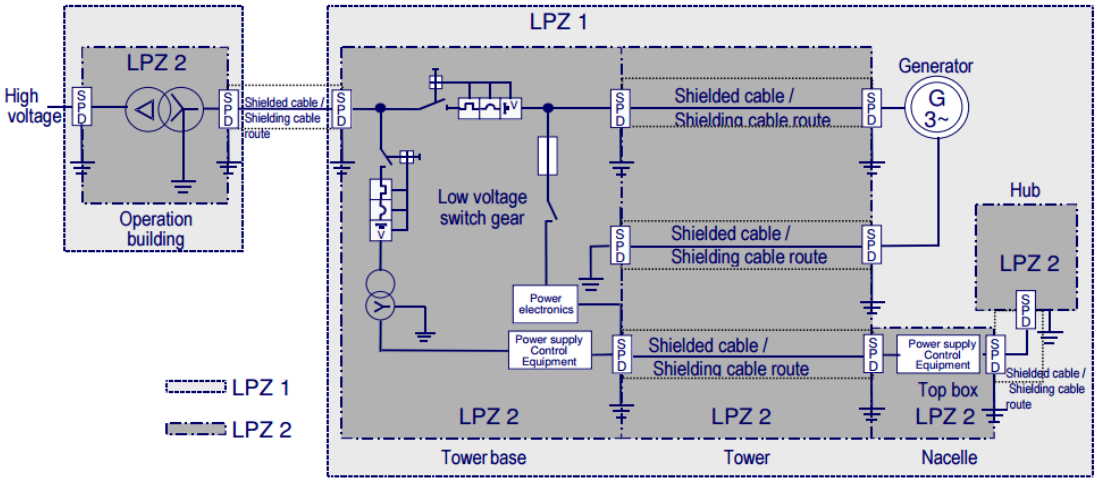

Figure 3-13: Example of lightning protection zones [48].

As shown in Figure 3-13 several surge protection devices will be used in the wind turbine hub, nacelle, tower and step up transformer which has been defined as lightning protection zone 1 (LPZ1) and zone 2 (LPZ2) – Figure 3-14.

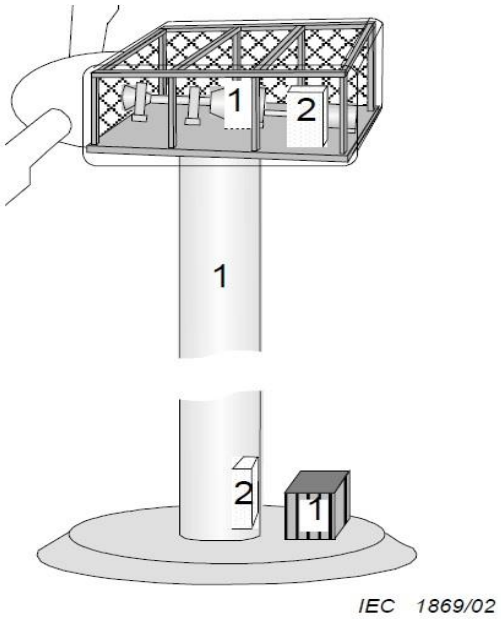

Figure 3-14: IEC Standard lightning protection zones [46] (courtesy of IEC).

In this section, the lightning protection system of a wind turbine has been assessed against shielding requirement and turbines earth grid response to the lightning transients. The assessment is based on IEC TR 61400-24: 2002 [46] and Australian standard AS/NZS 1768:2007 [47] requirements which define the lightning protection level (sphere radius as shown in Figure 3-15).

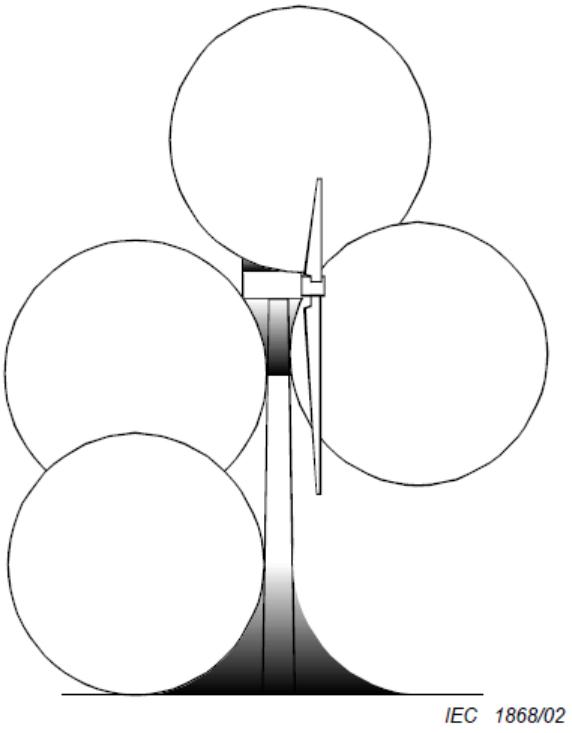

Figure 3-15: IEC Standard Rolling sphere model [46] (courtesy of IEC).

The lightning strike current waveform with the maximum 14 to 30 kA peak current can be used for Case Study 1 as recommended in Table 1 of IEC 61400-24. According to Table 4.2 of standard AS/NZS 1768:2007 [47] this level of current requires the lightning protection to provide Level III lightning protection with effective shielding protection of 45 m (RSM) for turbines. The turbine (Figure 3-16) has been modelled in software package SESShield3D lightning shielding protection systems analysis (Figure 3-17). The rolling sphere method (RSM) with a strike distance of 45 m was applied to the model and the results are presented in Figure 3-18.

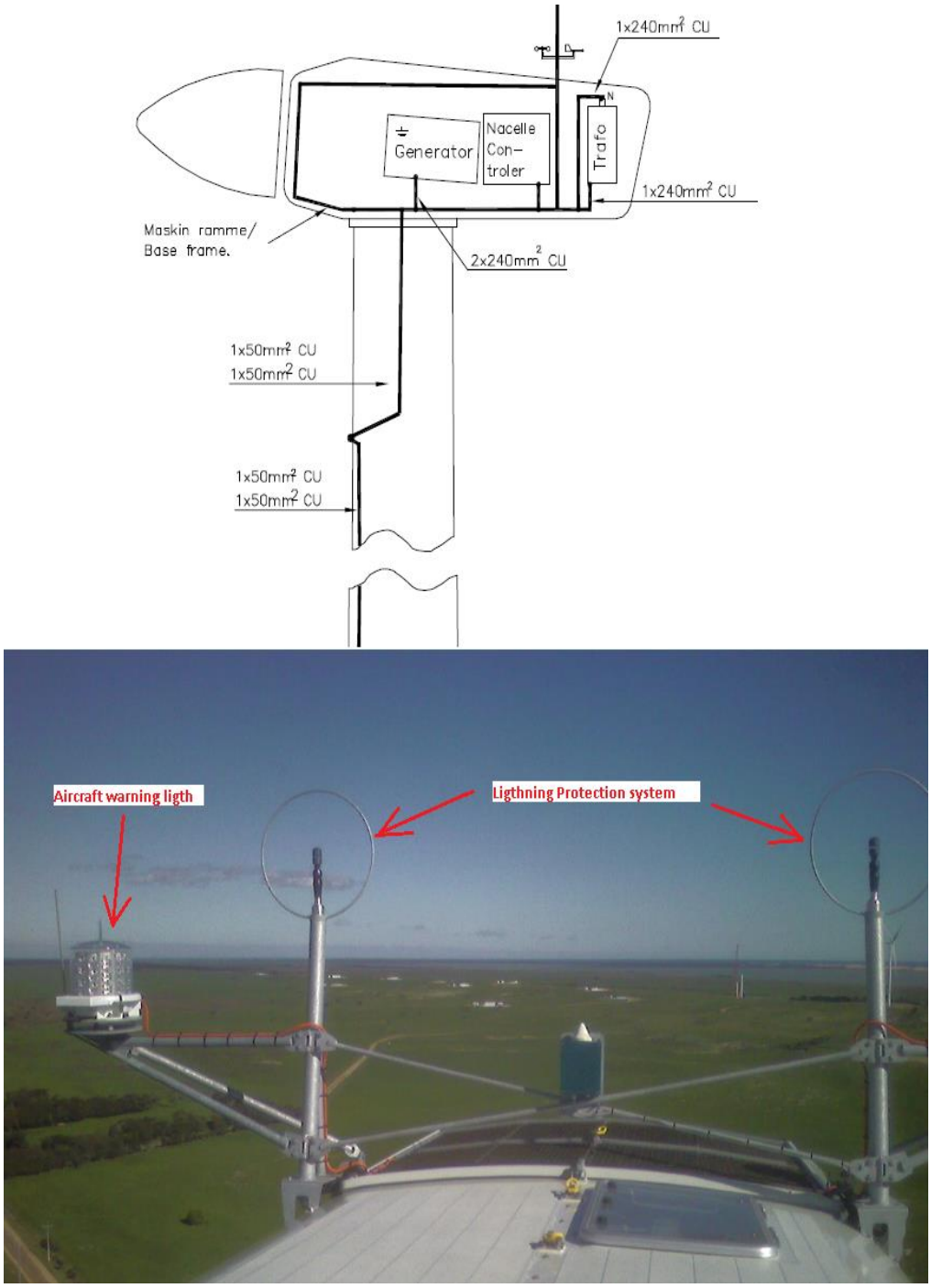

Figure 3-16: Wind turbine typical lightning and earthing system (courtesy of Aurecon).

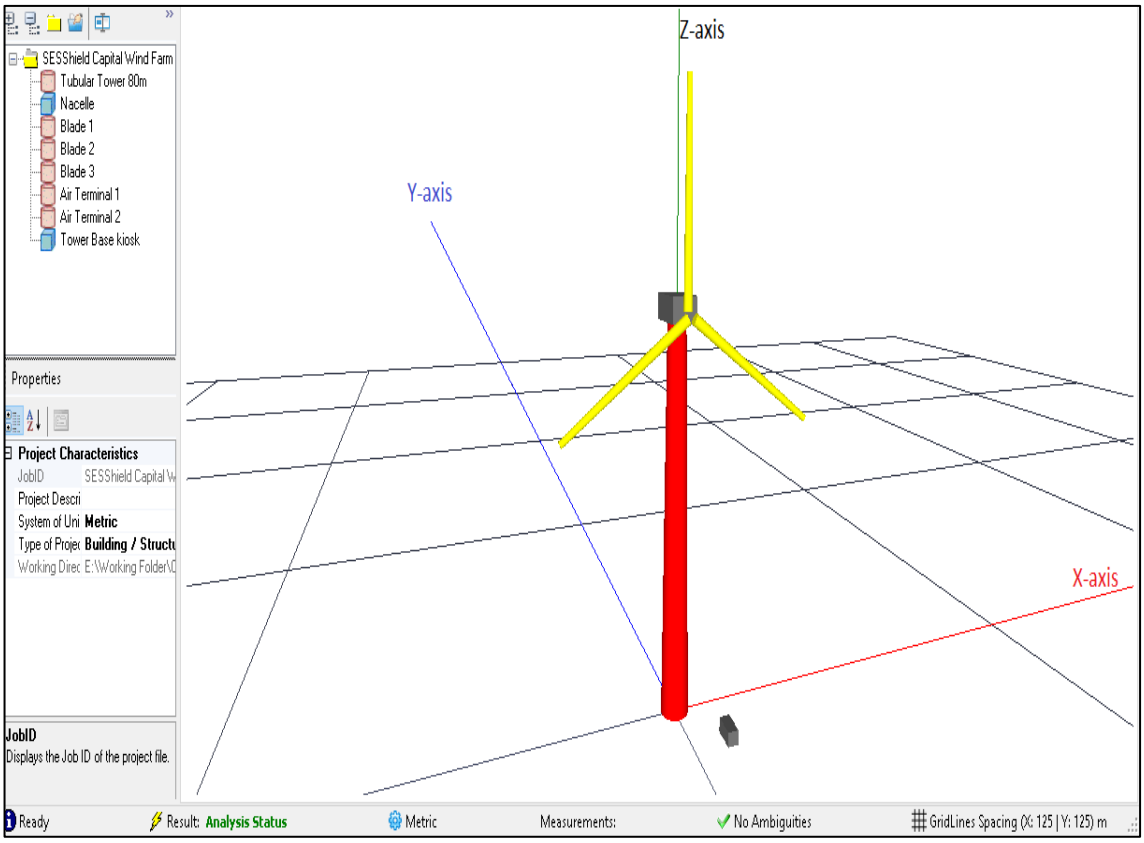

Figure 3-17: An 80 m wind turbine modelled in SESShield-3D.

The Level III lightning protection with effective shielding protection of 45 m (RSM) for turbines simulated by SESShield3D software is presented in Figure 3-18.

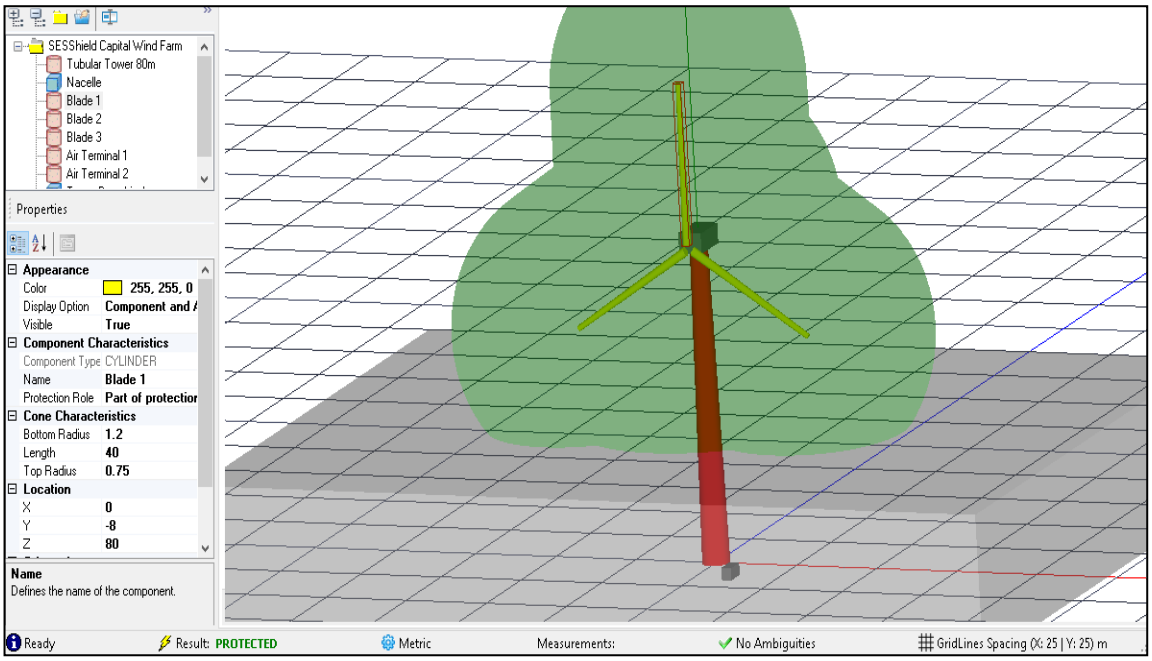

Figure 3-18: Wind turbine lightning protection in SESShield-3D.

The above 3D shielding analysis for the wind turbine model confirms that the embedded lightning protection conductors on the blades and lightning protection air terminals of wind turbine can protect wind turbine nacelle and tower base transformer from direct lightning contact. The green 'bubbles' represent protected areas.

After proving that the lightning protection system will perform adequately to protect the turbines from direct contact, in this section the behaviour of the wind turbine earthing system will be assessed. To simulate the performance of the earthing system when lightning strikes the wind turbines, a lightning stroke current waveform with the maximum 30 kA peak as recommended in Table 1 of IEC 61400-24 has been produced by CDEGS software. The FFTSES module of CDEGS software package was used to generate the waveform and required computation frequencies as shown in Figure 3-19.

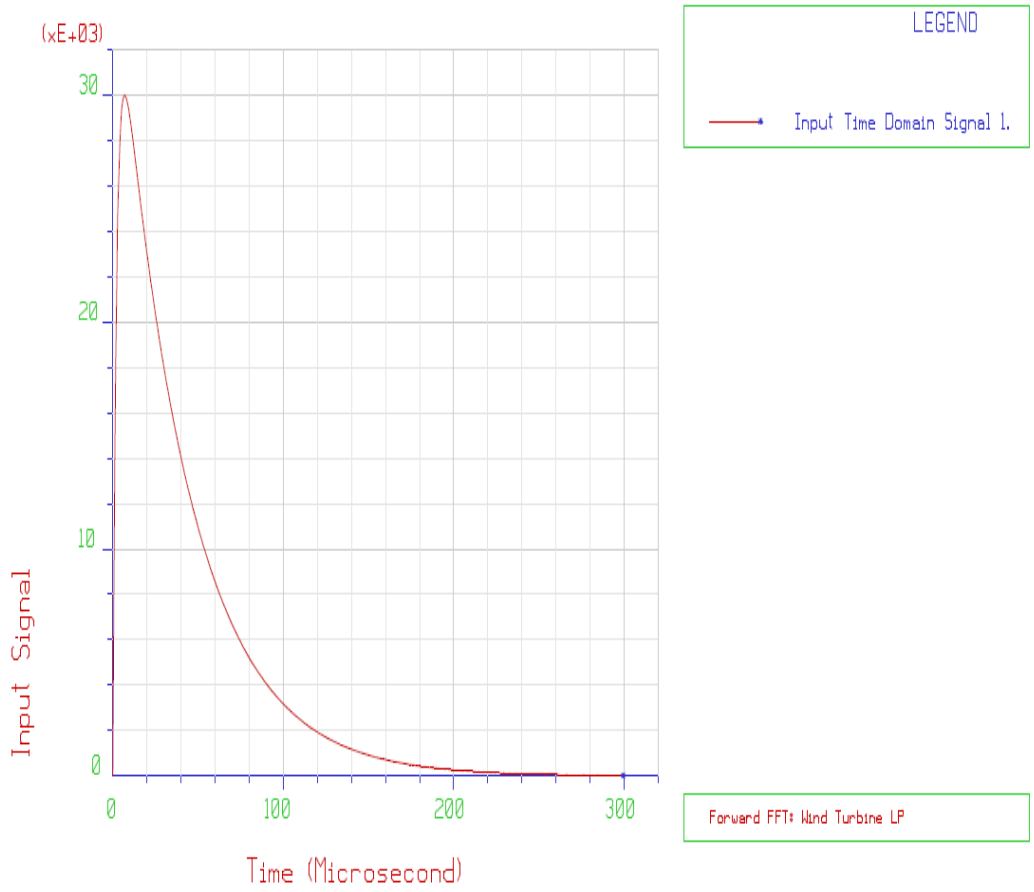

Figure 3-19: Lightning stroke current waveform.

The lightning current modelled in the FFTSES module generated an initial 17 frequencies up to 0.85 MHz (Table 3-4). There are "resonance effects" in the system response of the earthing system. In order to obtain a precise time domain response, additional frequencies are required. Accordingly, wind turbines have been modelled in the HiFREQ module and simulated for all

lightning current wave frequencies. Then the FFTSES module was simulated again with the inverse Fourier transformation using the HiFREQ simulation output to compose the overall time domain response from the individual frequency presented Table 3-4.

Table 3-4: Pre-computed FFTSES recommended frequencies.

Pre-computed Simulation	
Frequency number	**Individual Frequencies [Hz]**
1	00000
2	3333.3335
3	6666.667
4	10000.001
5	13333.334
6	16666.668
7	20000.002
8	23333.334
9	40000.004
10	120000.01
11	240000.02
12	360000.03
13	480000.03
14	600000
15	720000.06
16	840000.06
17	853333.38

The wind turbine was modelled in HiFREQ module and simulated for all lightning current wave frequencies. Then the FFTSES module was simulated again with inverse Fourier transformation using the HiFREQ simulation output to compose the overall time domain response from the individual frequency presented in Table 3-5.

Table 3-5: FFTSES additional frequencies

Additional Frequencies nominated after initial simulation		**Additional Frequencies nominated after Second simulation**
Frequency number	**Individual Frequencies [Hz]**	**Individual Frequencies [Hz]**
1	53333.3	76666.6
2	63333.3	90000.0
3	83333.3	100000.0
4	163333.0	136667.0

The lighting strike presented in Figure 3-19 with the lightning curve frequencies in Tables 3-4 and 3-5 is applied to a standalone wind turbine as shown in Figure 3-20 with inverse Fourier transformation simulation.

Figure 3-21 demonstrates the time domain response of the wind turbines at two different locations of the observation profile. The green curve represents the soil profile away from the turbine and the red curve represents the time domain response at the centre of the tower.

The time domain response of the scalar potential rise along different parts of the turbine is presented in Figure 3-22.

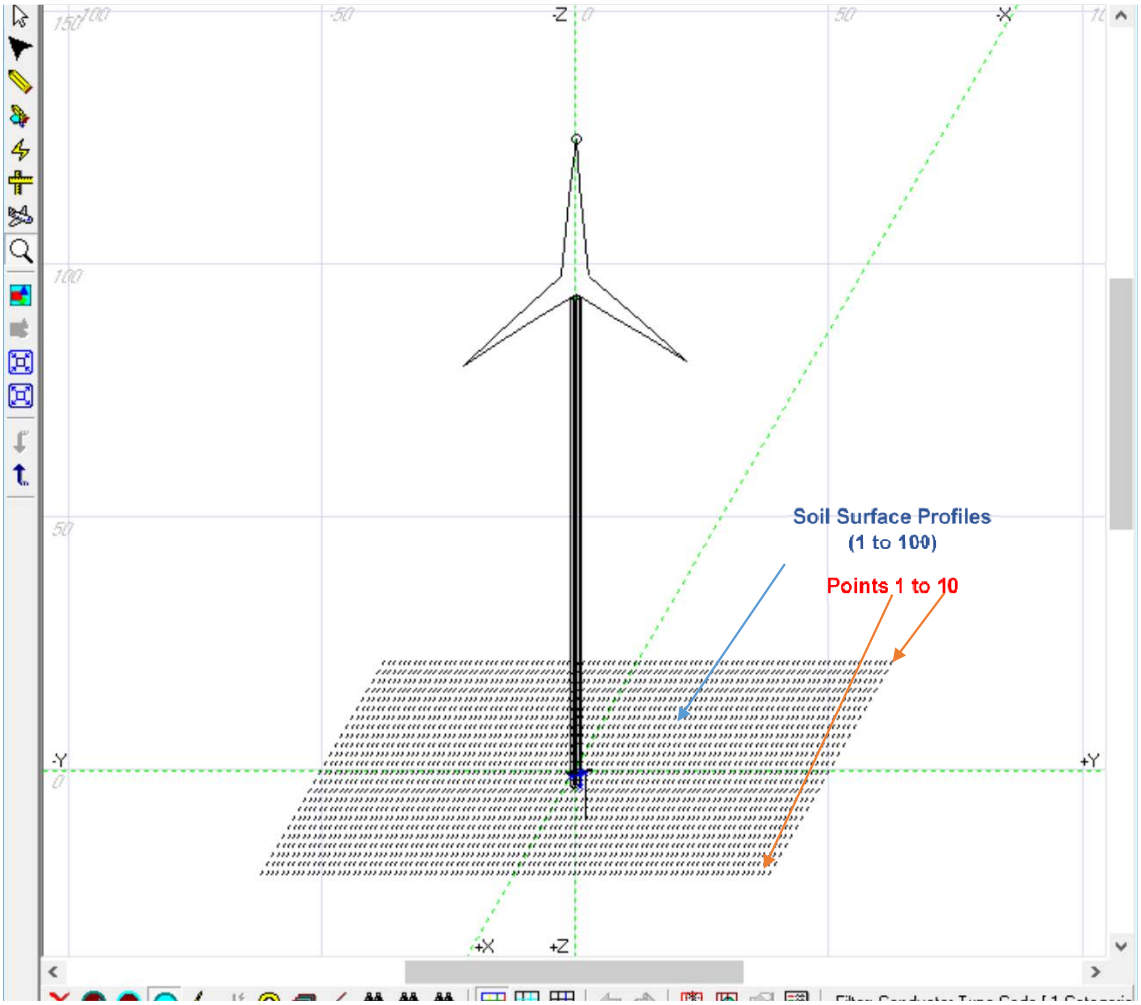

Figure 3-20: Wind turbine model and soil surface profiles with a three-layer soil model.

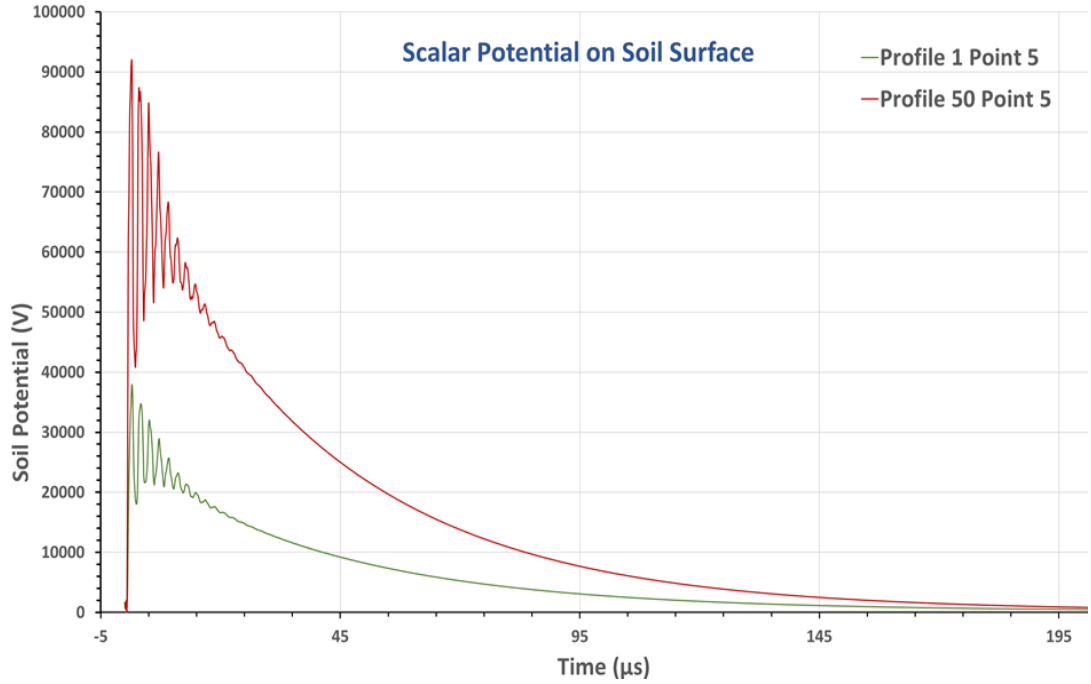

Figure 3-21: Wind turbine response to lightning stroke potential waveform.

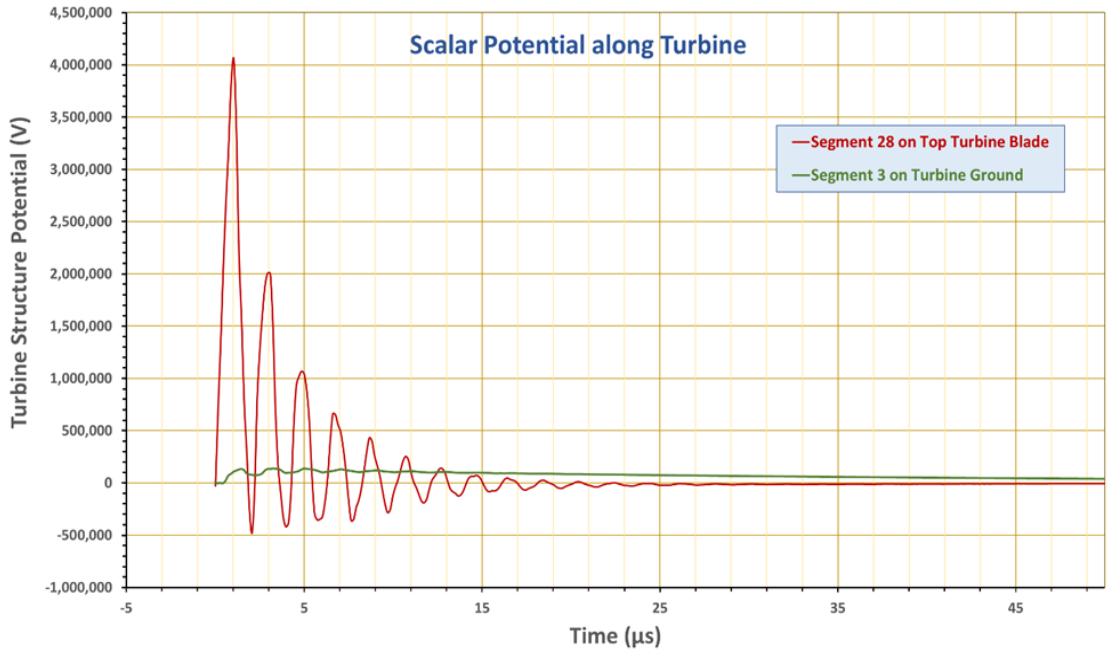

Figure 3-22: Wind turbine soil voltage response to lightning stroke potential waveform.

The scalar potential along the turbine shaft has been simulated and presented in an animation file to demonstrate the scalar potential rise along the turbine. Figure 3-23 gives the turbine response at (a) $t = 0.498534$ s, (b) $t = 1.43695$ s and (c) $t = 2.19941$ s as the strike develops. A DVD video is given in Appendix A for the developing lightning strike from which the screen captures in Figure 3-23 are taken.

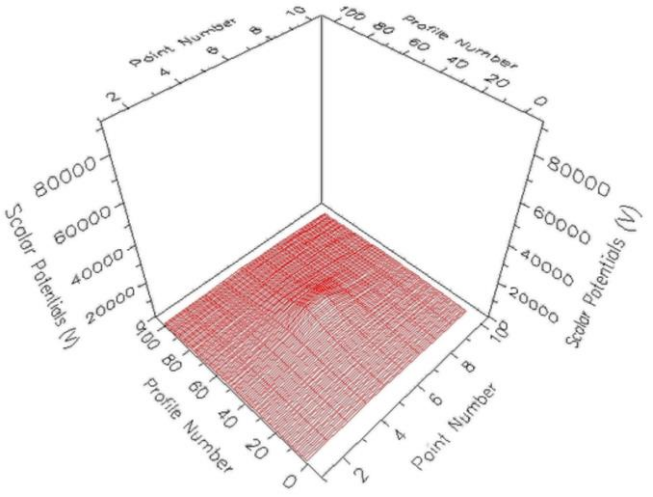

(a) t = 0.498534 s

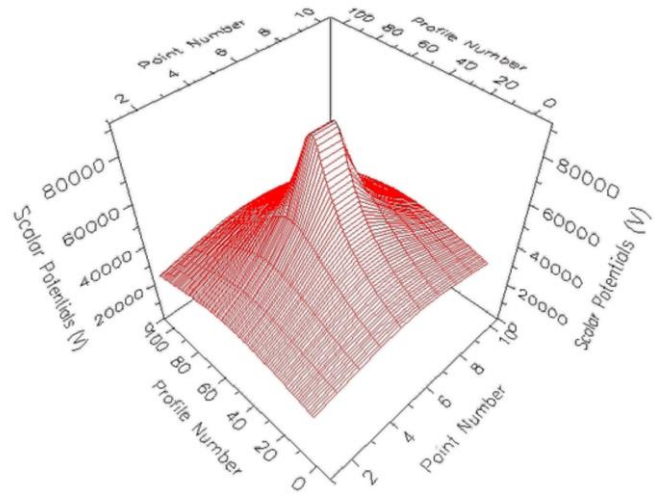

(b) t = 1.43695 s

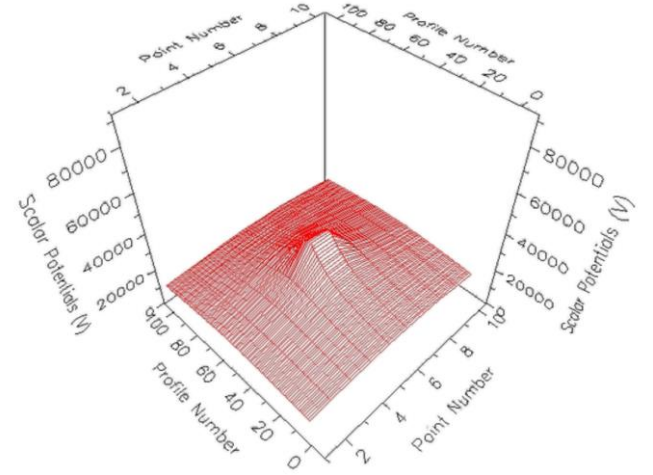

(c) t = 2.19941 s

Figure 3-23: Wind turbine soil voltage response to lightning stroke at (a) t = 0.498534 s, (b) t = 1.43695 s and (c) t = 2.19941 s.

3.3.3 Step and Touch Voltage of Wind Turbine

The earthing system of wind farms normally includes the following elements:

- Individual wind turbine earth grid and foundation (Figure 3-9);
- Turbine base kiosk;
- 33 kV cable screen; and
- Transmission substation.

During the turbine design development, the earthing system should be designed to limit prospective step and touch potential exposure of people and farm animals, however since the wind turbines are located in remote locations, the earthing system is often overlooked.

3.3.3.1 Step and Touch Voltage for Humans

In this research the guide lines of IEC 60479.1 [50] and ENA EG1 were used to calculate safe step and touch potentials. The method in IEC60479.1 is to calculate a prospective body touch potential and then to determine the safety of the resulting body current. However, here it is required to determine the safe touch voltage level. Therefore, the method from IEC 60479.1 will be reversed.

Referring to IEC 60479.1 (Figure 20 - Conventional time/current zones of effects of a.c. currents) for all earth faults and lightning situations, compliance must not exceed the AC-3 region on the figure. Thus, the upper limits of body current from hand-to-feet are as in Figure 3-24.

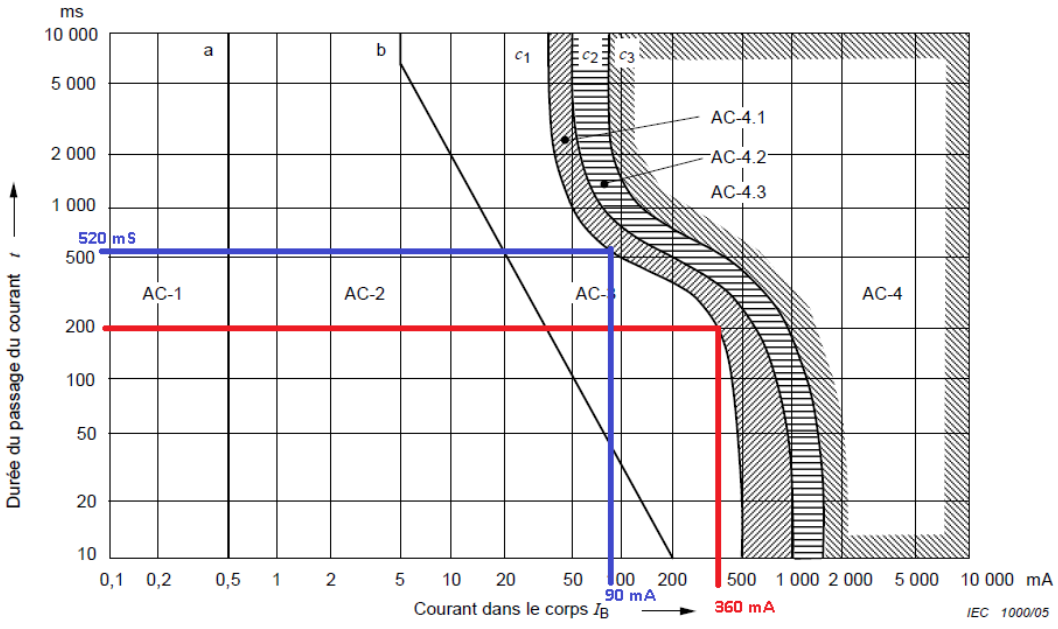

Figure 3-24: Conventional time/current zones of effects of AC currents [50] (courtesy of IEC).

In adapting the results from animal experiments to human beings, an empirical curve C1 in Figure 3-24 (labelled at the top of the figure) was conventionally established for a current path left hand to both feet, below which fibrillation is unlikely to occur. Curves C1, C2 and C3 apply for left current path to both feet. The high level for short durations of exposure between 10 ms and 100 ms was chosen as a descending line from 500 mA to 400 mA. On the basis of information on electrical accidents, the lower level for durations longer than 1 s was chosen as a descending line from 50 mA at 1 s to 40 mA for durations longer than 3 s. Both levels were connected by smooth curves. By statistical evaluation of animal experiments, curve C2 and curve C3 were established, defining a probability of fibrillation of about 5 % and 50 % respectively.

Table 2 of IEC 60479.1 defines hand-to-hand impedances, note 1 gives the estimate of 70 to 90 % to convert to hand-to-foot impedance. Annex D Example 1 in this standard confirms that this is to be interpreted as one hand to one foot. The safest value requires 70 % conversion factor form to convert the hand-to-foot impedance into the equivalent for one hand to two feet, which from AS60479, Figure 2 is a factor of 74.25 %. Combining these two factors gives an overall impedance factor of 52 %. The internal path for a hand-to-foot path is given in Figure 3-25.

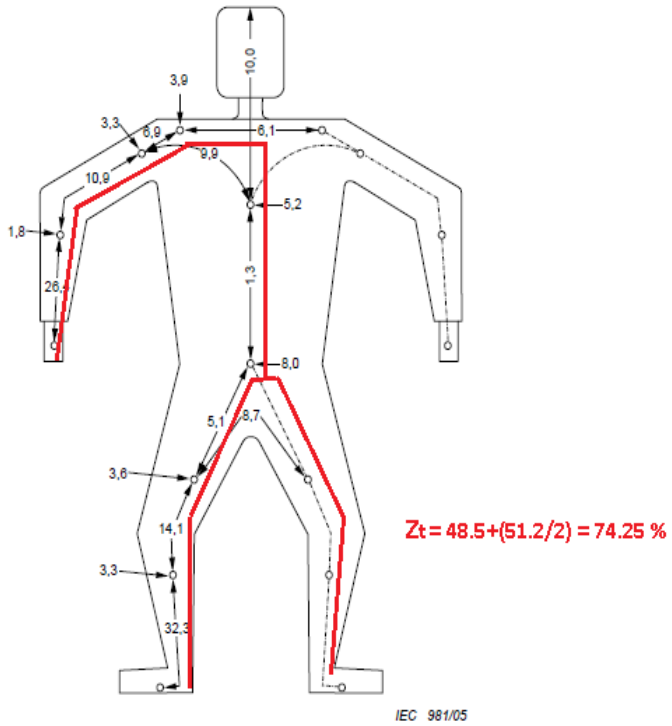

Figure 3-25: Internal partial impedances Z_t of the human body during one hand to two feet touch [50] (courtesy of IEC).

The numbers shown in Figure 3-25 indicate the percentage of the internal impedance of the human body for the body parts concerned, in relation to the hand to foot path. Interpolating the data in IEC 60479.1 (Table 2, Column "5% of the population") offers the revised hand-to-two-feet impedances and the current ratio of:

4.1 Primary protection with 0.2 s clearance time: safe body current limit of 360 mA and impedance $Z_{T(H\text{-}2F)}$ = 438 Ω gives E_B = 157.5 V.

4.2 Back-up protection with 0.52 s clearance time: safe body current limit of 90 mA and impedance $Z_{T(H\text{-}2F)}$ = 569 Ω gives E_B = 51.3 V.

For a person in a farm area, a shoe impedance of 1,100 Ω is considered. Thus, the total impedance for a person is:

$$Z_{Tstaff} = Z_{T(H-2F)} + \left(\text{shoe impedance}\right)/2 \tag{3-12}$$

To compare with previous safe touch voltage levels, the top-layer resistivity ρ_s and mutual impedance between parallel feet (including the surface layer reduction factor C_s) are also included, as per ENA EG1, and IEEE Std 80 . Thus, for a person:

$$E_{Tpublic} = I_B\left(Z_{T(H-2F)} + 1.5C_s\rho_s\right) \qquad \left(\text{for } C_s <= 1\right) \tag{3-13}$$

$$E_{Spublic} = \left(116 + 0.696C_s\rho_s\right)/\sqrt{t} \tag{3-14}$$

And the safe touch level for a staff person is:

$$E_{Tstaff} = I_B\left(Z_{Tstaff} + 1.5C_s\rho_s\right) \qquad \left(\text{for } C_s <= 1\right) \tag{3-15}$$

$$E_{Sstaff} = \left(157 + 0.942C_s\rho_s\right)/\sqrt{t} \tag{3-16}$$

The soil resistivity model as discussed in Section 3.3.1 was used for step and touch calculation. This is tabulated in Table 3-6.

Table 3-6: Selected soil resistivity method.

Layer	Resistivity [Ωm]	Depth [m]
Top	163	11
Bottom	553	infinite

3.3.3.2 Step and Touch Voltage for Animals

The IEC 60479.1 values are mainly based on experiments with animals as well as on information available from clinical observations. Animals are common around wind turbines and wind farms also double up as grazing land (Figure 3-26). Only a few experiments with shock currents of short

duration have been carried out on living human beings. However, it does not define the safe limit for animals.

Figure 3-26: Wind turbine during the construction and animal exposure (courtesy of Aurecon).

Therefore, in this research available test results are used to calculate a prospective body resistance of farm animals then to determine the safety of the resulting body current. Similar to human safe limit calculations, the allowable body current limit method will be used for step and touch voltage calculations.

Fibrillation data for dogs, pigs and sheep from experiments and for persons calculated from statistics of electrical accidents with transversal direction of current flow and body impedances are shown in Figures 3.27 and 3.28.

The lightning discharge current has a high frequency component which can impact the body impedance as per Table 3-7. Frequency dependence of the total body impedance of a population for a percentile rank of 50 % for touch voltages from 10 V to 1 000 V and a frequency range from 50 Hz to 2 kHz for a current path hand to hand or hand to foot, large surface areas of contact in dry conditions is shown in Table 3-7.

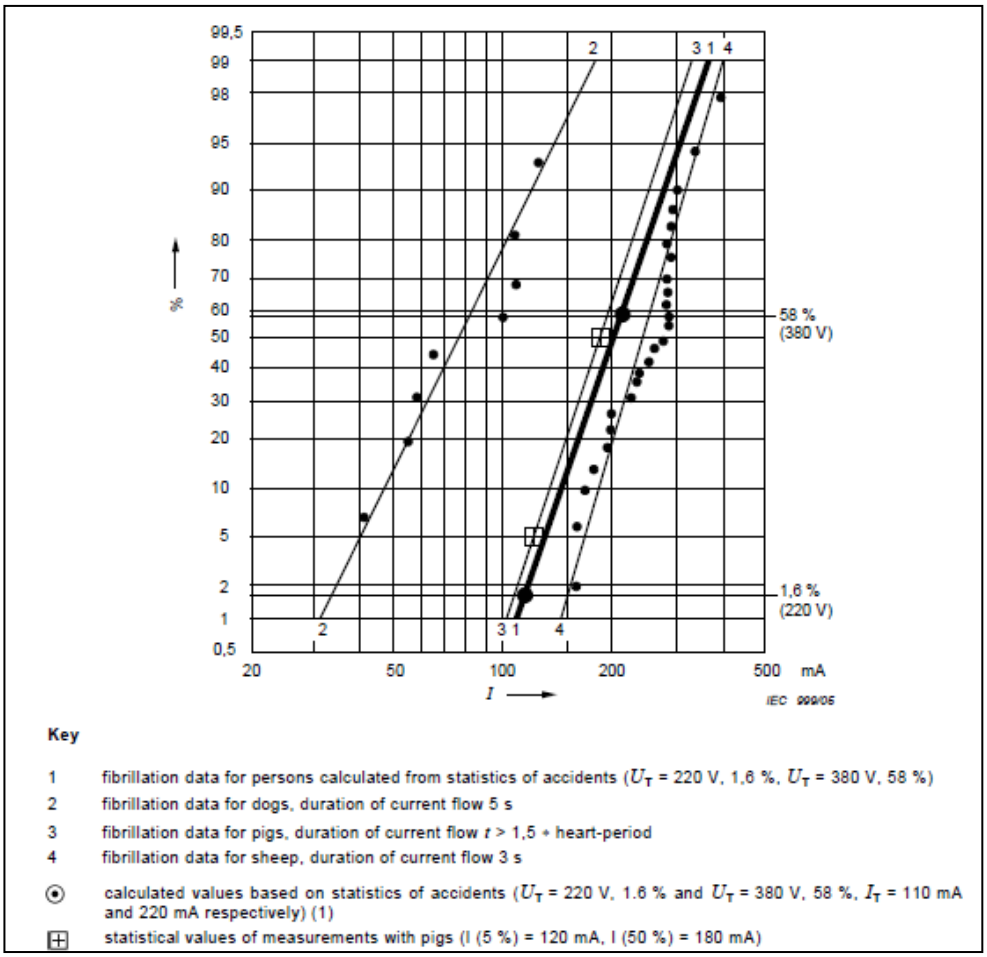

Figure 3-27: Fibrillation data for dogs, pigs, sheep and persons [50] (courtesy of IEC).

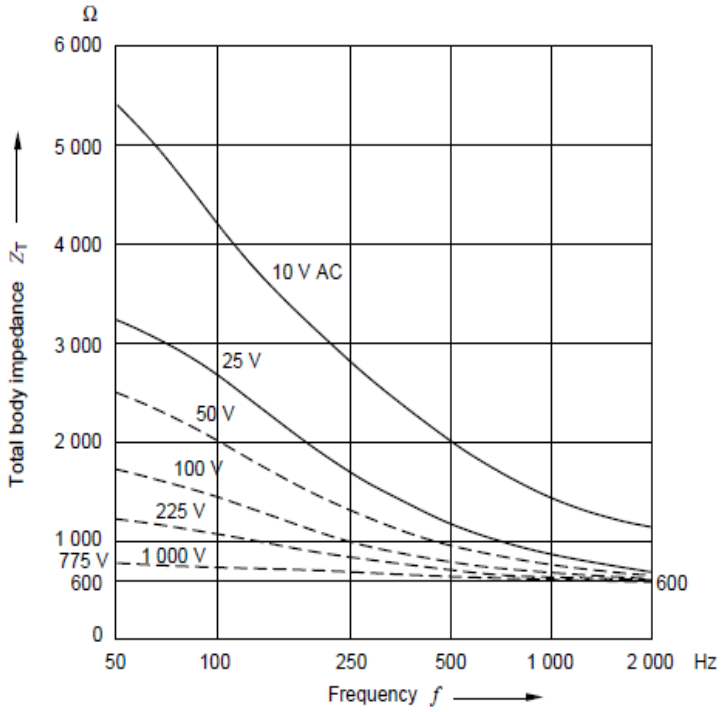

Figure 3-28: Body impedance dependence to different frequency [50] (courtesy of IEC).

The body impedance of cattle with average weight range of 750 kg can be calculated by multiplying the allowable current limit of a person by a factor of 10 for 50 Hz fault condition but for lightning condition we cannot use exposure time factor since the impedance of body will change. So for the purpose of this research the same safe voltage level for a 50 Hz earth fault with 0.2 s will be used as safe lightning protection analysis.

Therefore, from IEC 60479.1, the safe touch potential levels are presented in Table 3-7.

Table 3-7: Touch Potential Levels to IEC 60479.1.

Fault duration	Top Layer	Resistivity	Reduction factor C_s	E_{step70}	$E_{touch70}$	E_{step50}	$E_{touch50}$	$E_{step\ Cow}$
Primary protection with 0.2 s	Natural Soil	163 Ωm	0.96	1499 V	431 V	513 V	233 V	5 kV
	Wet concrete	21 Ωm	1	1116 V	354 V	292 V	156 V	3 kV
Back-up protection 0.52 s	Natural Soil	163 Ωm	0.96	909 V	380 V	318 V	181 V	3 kV
	Wet concrete	21 Ωm	1	724 V	302 V	181 V	104 V	1.8 kV

3.4 Earth Potential Rise (EPR) Simulation

3.4.1 EPR during Lightning

Wind farm Case Study 1 with more than fifty wind turbines was modelled in CDEGS software and a lightning strike of 30 kA with duration of 300 μS, as discussed in Section 3.2 was applied to one of the turbines. The simulation results are presented in Figures 3-29 to 3-35. In Appendix A a video is provided for the Ground Potential Rise (GPR – same as EPR) during a lightning strike on a wind turbine. Two observation surfaces were included in the model to simulated soil surface profile at turbine base and step up transmission substation.

The step and touch voltages of wind turbines under lightning can be calculated by measuring the voltage between two points on the soil for step and touch voltages. The voltage between tower and soil is one meter away from the tower.

The simulation plots for wind turbine with step and touch voltages for humans (Figure 3-33), and cows (Figure 3-34).

As shown in Figure 3-33, the touch voltage hazard of 3160 V will exist around wind turbine for humans coming into contact with turbine hand rails of the padmount during a lightning strike. The most hazardous situation occurs at the tower base with 31.57 kV touch voltage for humans.

The lightning strike hazardous situation for farm animals with 3 m touch/step distance is presented in Figure 3-34.

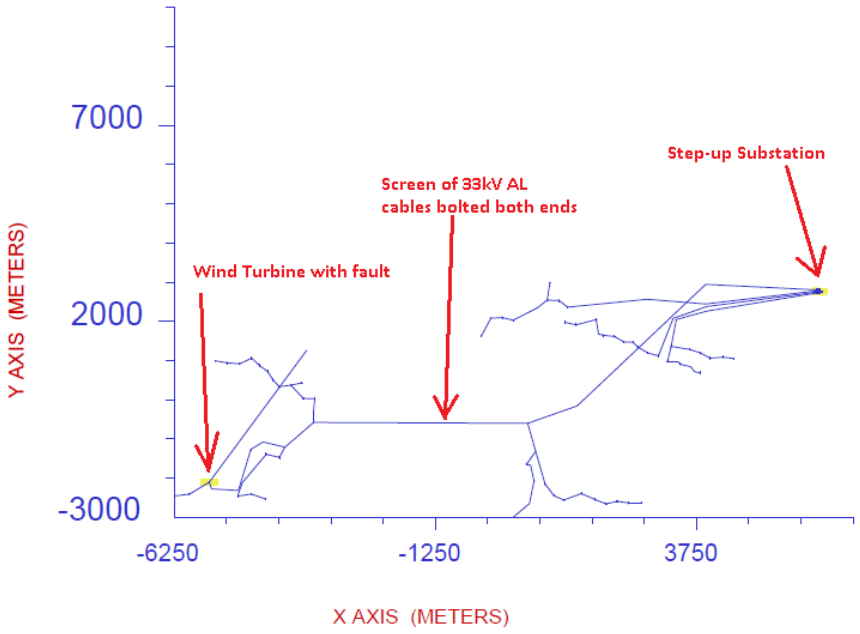

Figure 3-29: Wind farm Case Study 1 earth grid.

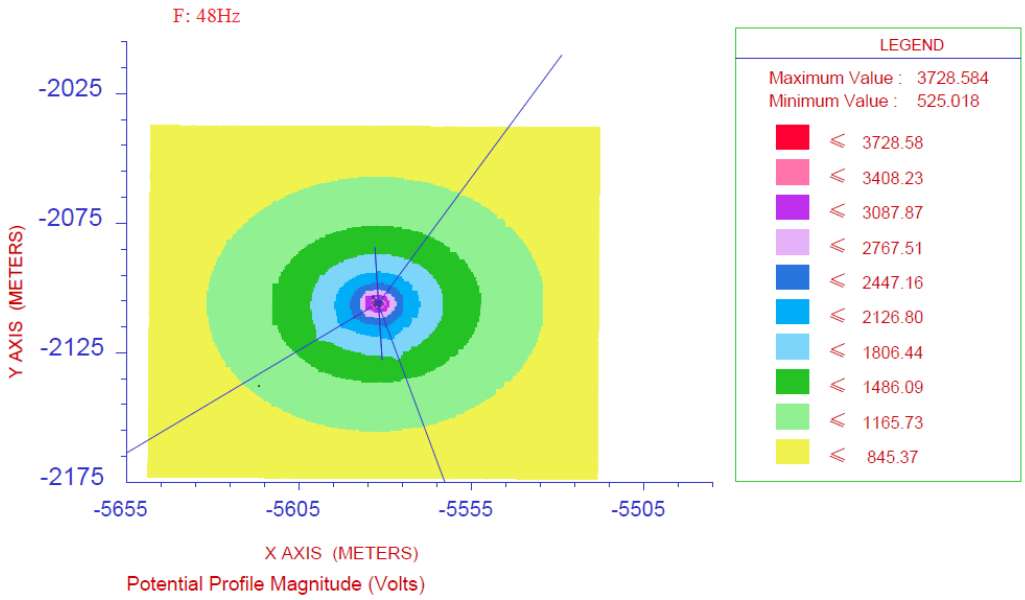

Figure 3-30: Wind turbine soils voltage profile.

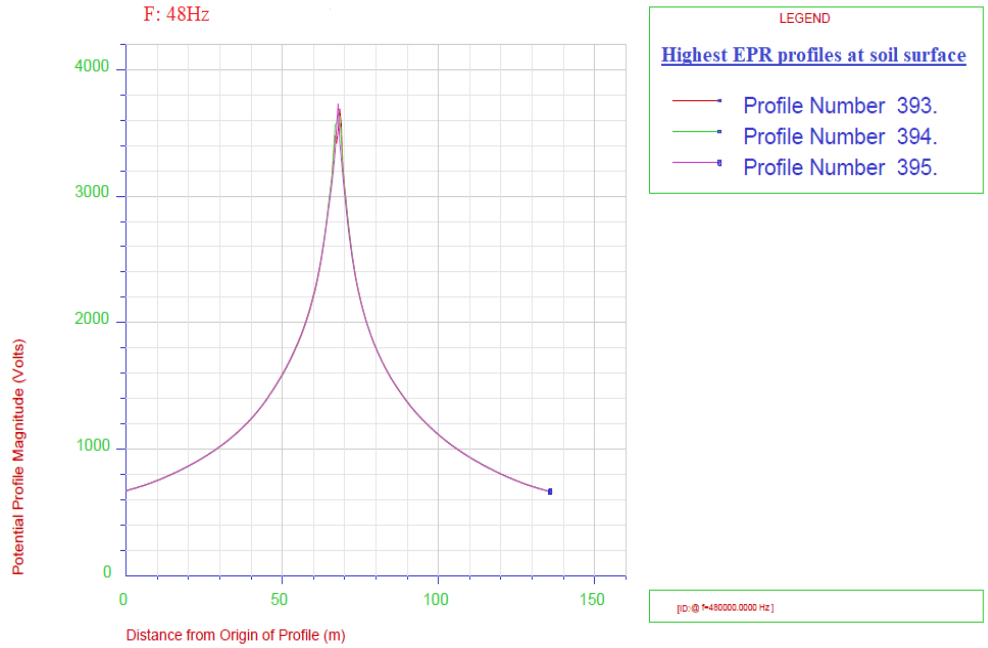

Figure 3-31: Wind turbine fall of potential.

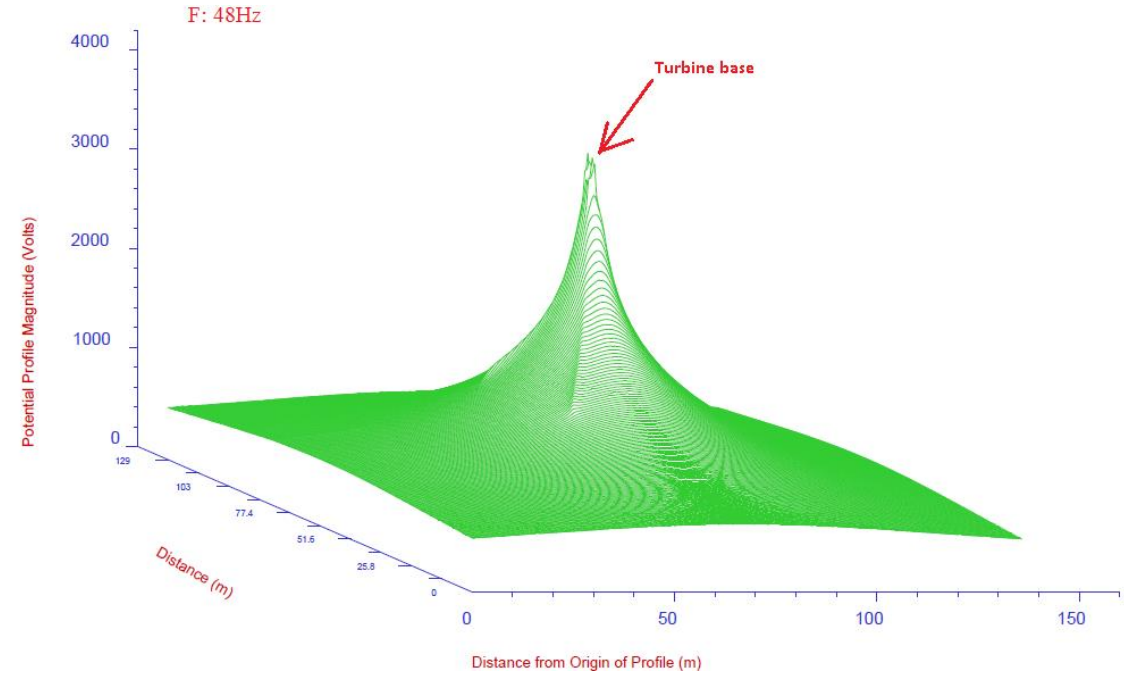

Figure 3-32: Wind turbine base contour potential profile.

The scalar potential curves in Figure 3-31 show the potential of observation surface (located at the ground level). The profile number 393, 394 and 395 are extracted from observation surface as they represent the highest EPR .

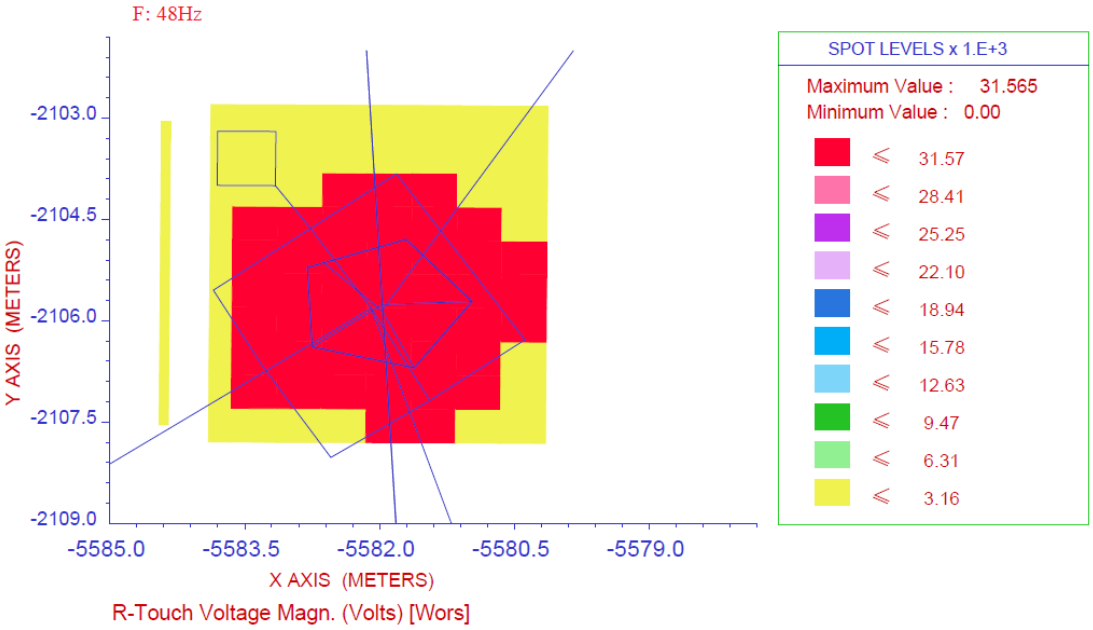

Figure 3-33: Human Touch Voltage (1 m distance) profile.

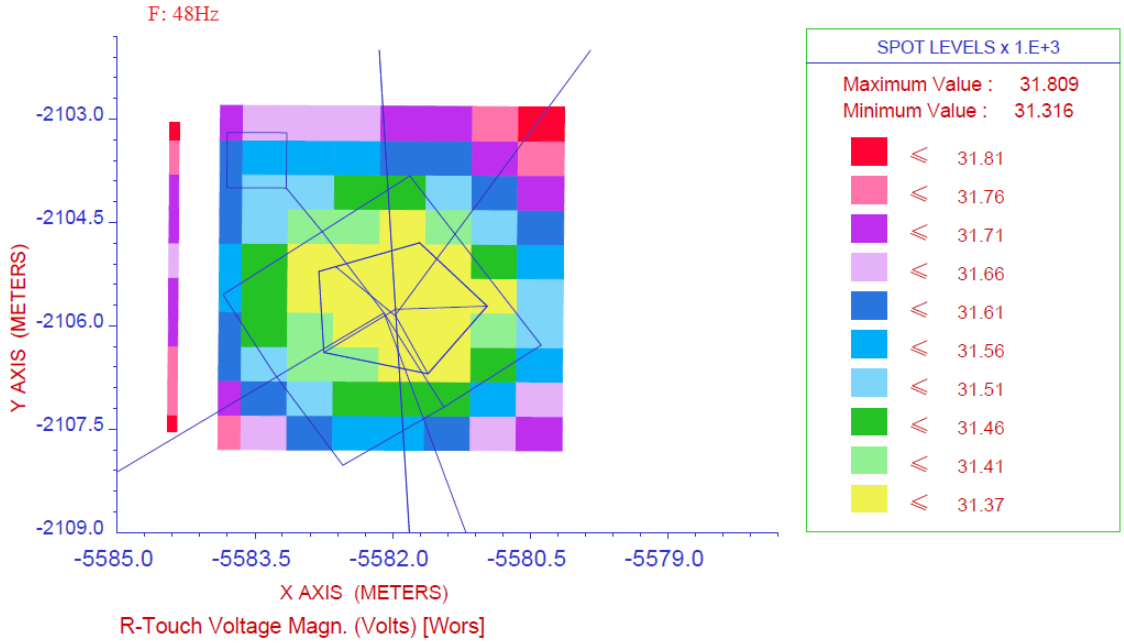

Figure 3-34: Animal Reach Voltage (3 m distance) profile.

As shown in Figure 3-34, the hazardous voltage of 31.8 kV can impact farm animals near a wind turbine. Simulation results (Figure 3-35) indicate that the worst-case step voltage of 765 V can present for humans with step distance of 1 m.

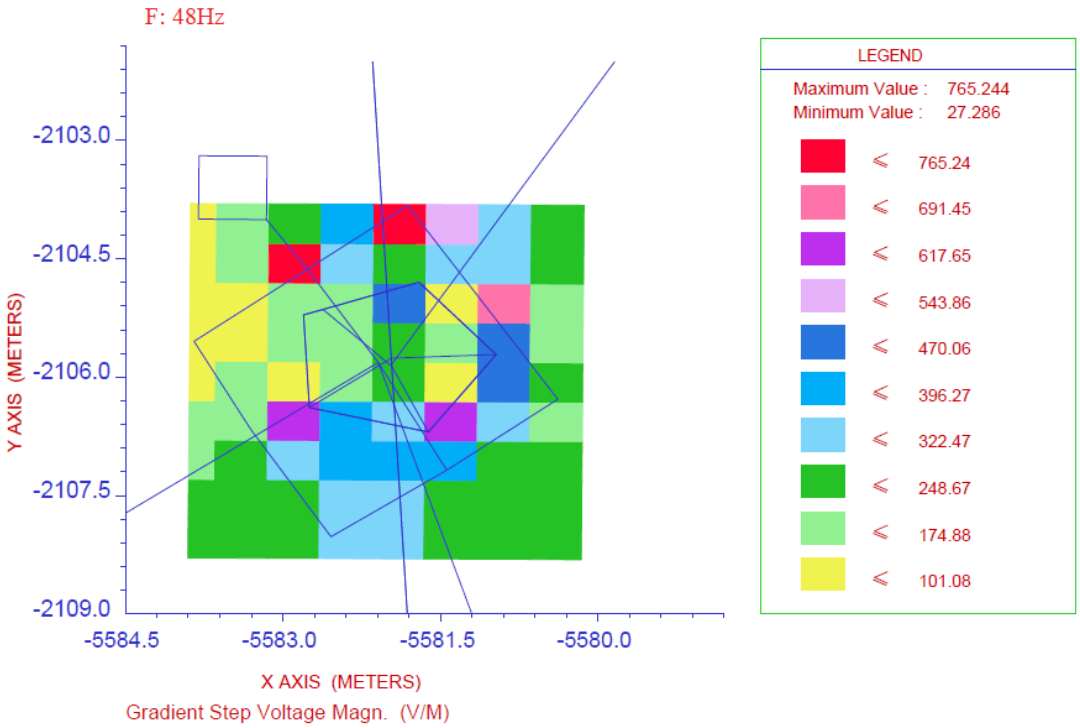

Figure 3-35: Wind turbine base Step Voltage (1 m distance) profile.

3.4.2 Low Frequency Earth Fault Study

In this section, the Case Study 1 earthing system is simulated for 50 Hz earth fault conditions using CDEGS software (HiFREQ module). The simulation is based on the soil resistivity model in Section 3.3.1 and a calculated fault current of 9582 A. A summary of the soil voltage profile at a step and touch voltage which will occur due to the 33 kV earth fault is presented in this section. An optimized method is proposed after existing earth grid performance assessment.

3.4.2.1 Existing System Simulation

The existing earthing system for wind turbines in Case Study 1 includes turbine foundation reinforcement and tower base padmount earth electrodes, which are linked to other turbines via the 33 kV cable screen. Therefore, the impedance of the interconnection cable will impact on the current spilt and earth potential rise. As shown in Figure 3-36, the earth fault current of 9582 A is applied to the wind turbine base which shows the current split result.

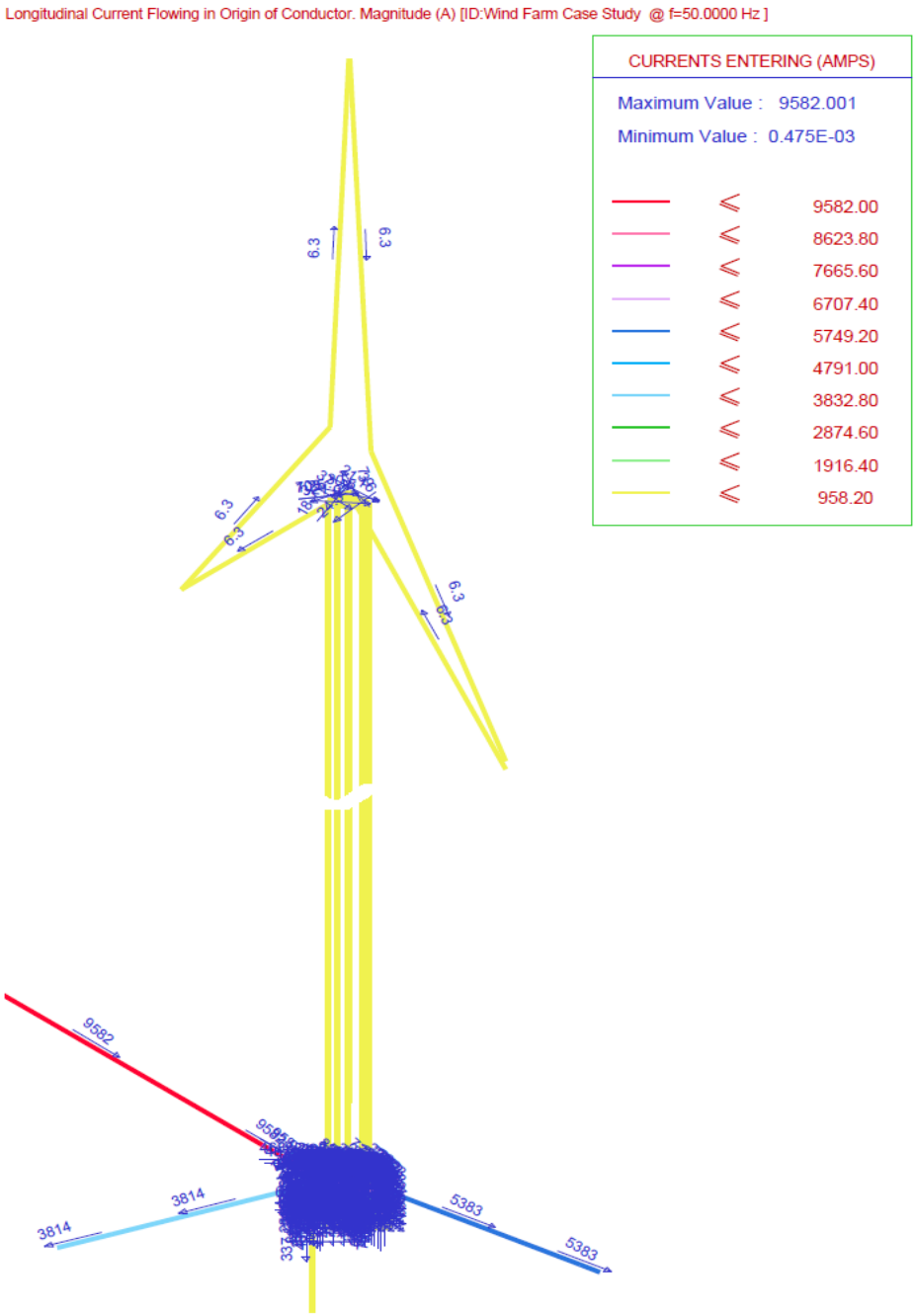

Figure 3-36: Wind turbine earth fault current split analysis.

The earthing system of wind turbine contribution to return the earth fault can be calculated from

$$I_{(WT)} = I_{EF} - \left(I_{\text{Screen 1}} + I_{\text{Screen 2}}\right) \tag{3-17}$$

$$I_{(WT)} = 9582 - (5383 + 3814) = 385 \quad [\text{A}]$$

The earthing system of the wind turbine will dissipate 4 % of the fault current. The earth potential rise can appear on the conductive parts of the wind turbines as shown in Figure 3-37. The soil voltage profile is given in 2D in Figure 3-38 and 3D in Figure 3-39. The earthing system resistance of each wind turbine can be calculated based on the above current split and EPR values so that:

$$Z_{WT} = \frac{\text{EPR}}{I_{WT}} \tag{3-18}$$

$$Z_{WT} = \frac{15750}{385} = 40.9 \quad [\Omega]$$

The wind farm earthing system total impedance considering all wind turbines earth mats, cable screens and step-up substation earth grid can be calculated by:

$$Z_{WindFarm} = \frac{15750}{9582} = 1.6 \quad [\Omega]$$

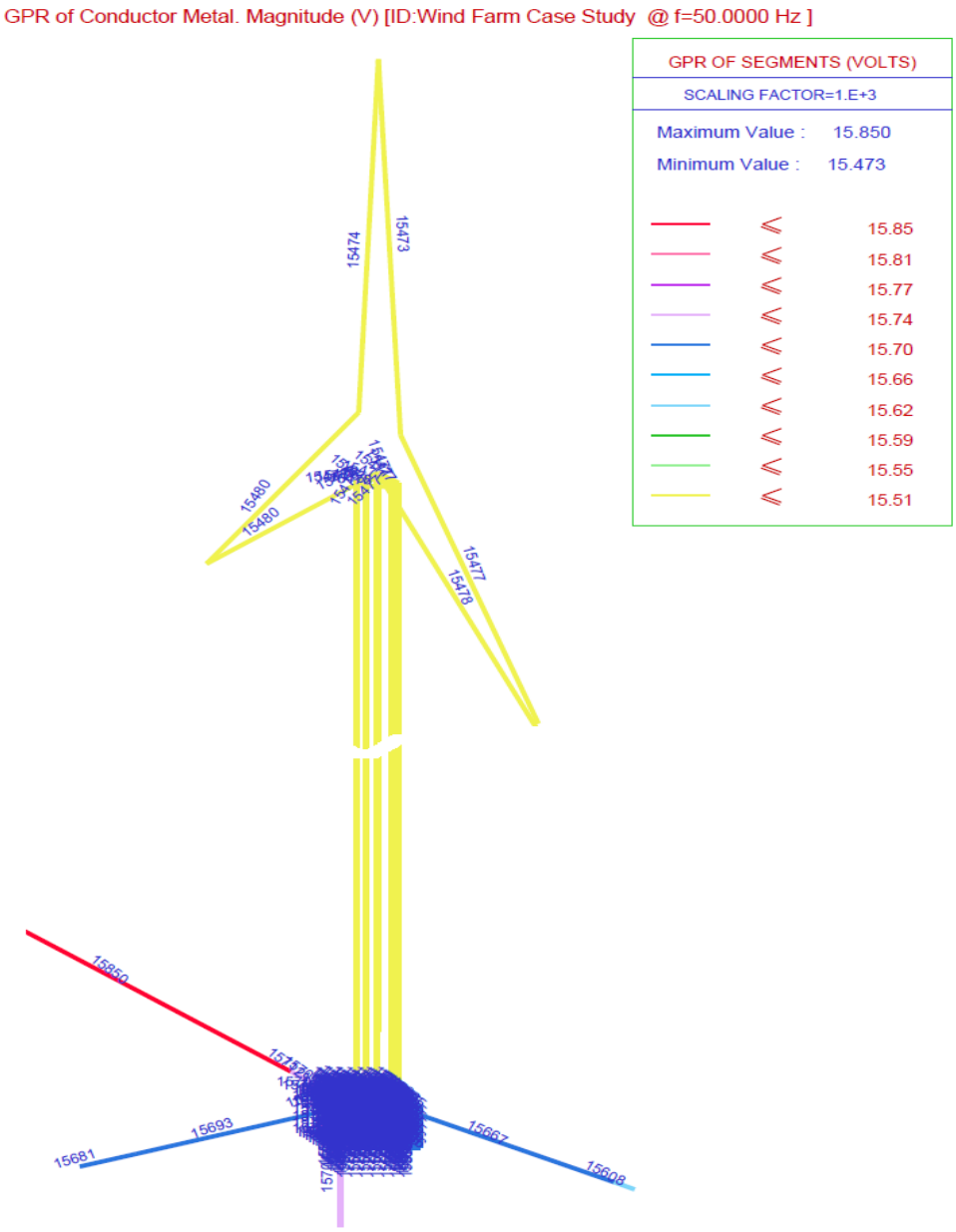

Figure 3-37: Wind turbine EPR during earth fault.

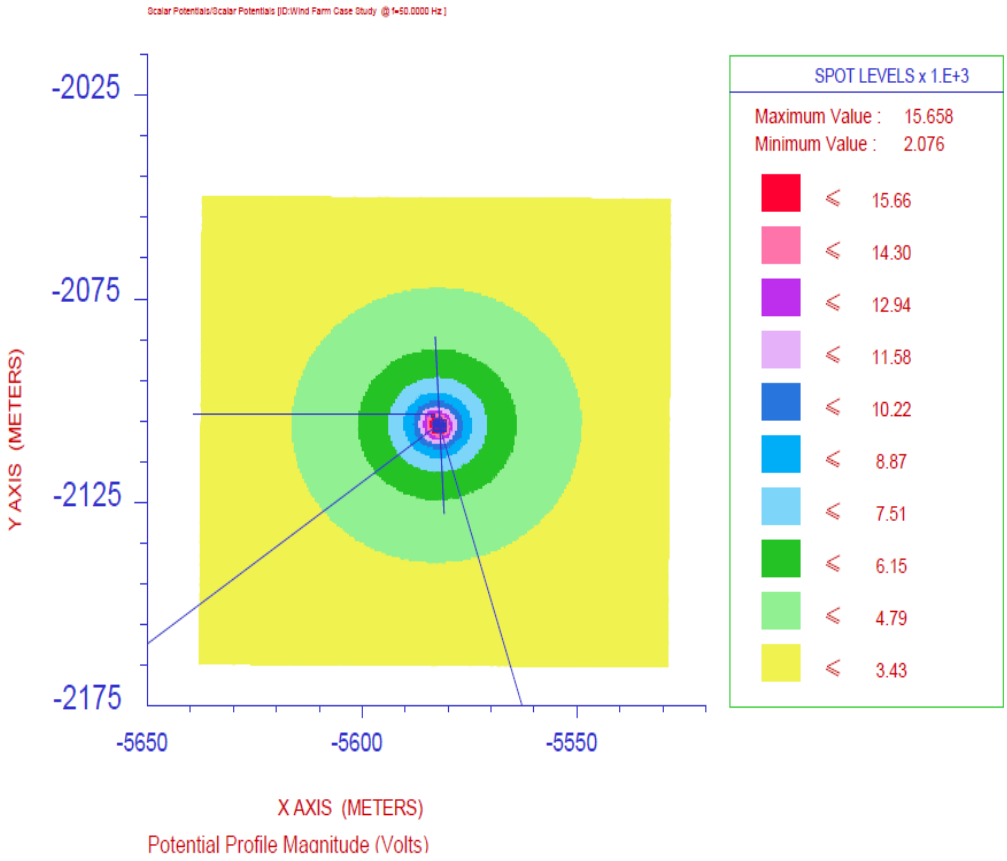

Figure 3-38: Wind turbine soil voltage profile during earth fault (values in kV).

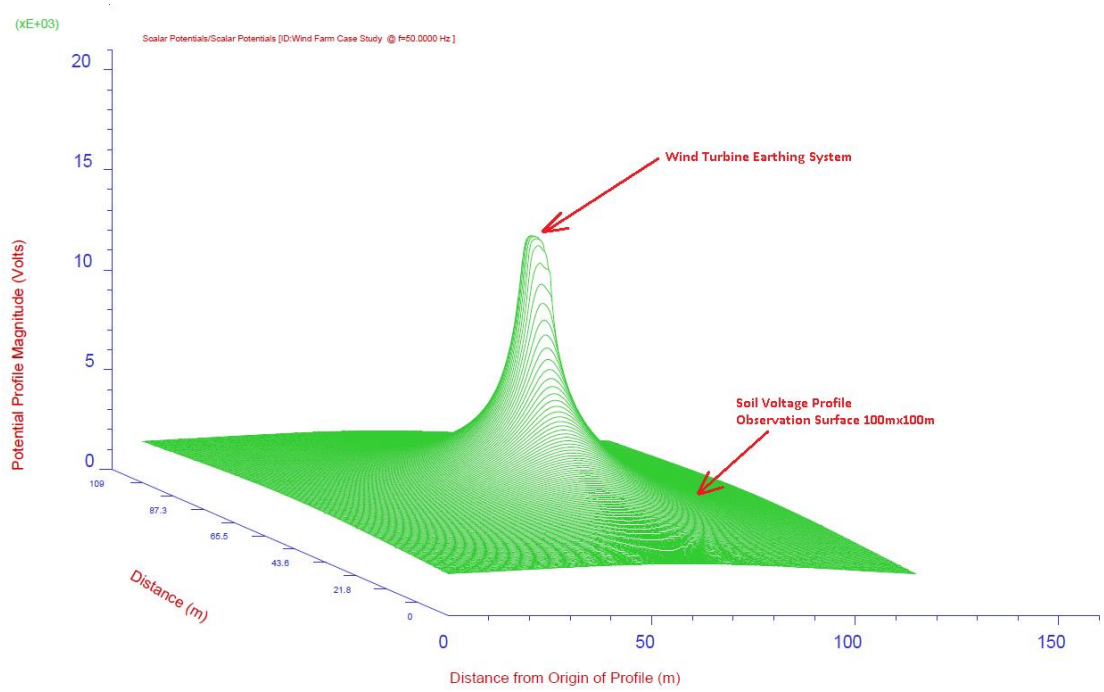

Figure 3-39: Wind turbine soil voltage 3D profile during earth fault (vertical axis in kV).

The soil voltage profile shown in Figure 3-40 is used for step and touch voltage analysis for humans and farm animals.

The step voltage for animals and touch voltage for humans have been calculated from simulation plot and calculated as:

$$E_{Touch} = 15660 - 12760 = 2900 \text{ V}$$

$$E_{SAnimals} = 15660 - 11310 = 4350 \text{ V}$$

Simulated touch voltage and step voltage (for animals) are above the allowable safe limit presented in Table 3-7. Therefore, a layer of gravel as shown in Figure 3-41 can be used as a mitigation method to reduce the risk of electrocution for humans and animals.

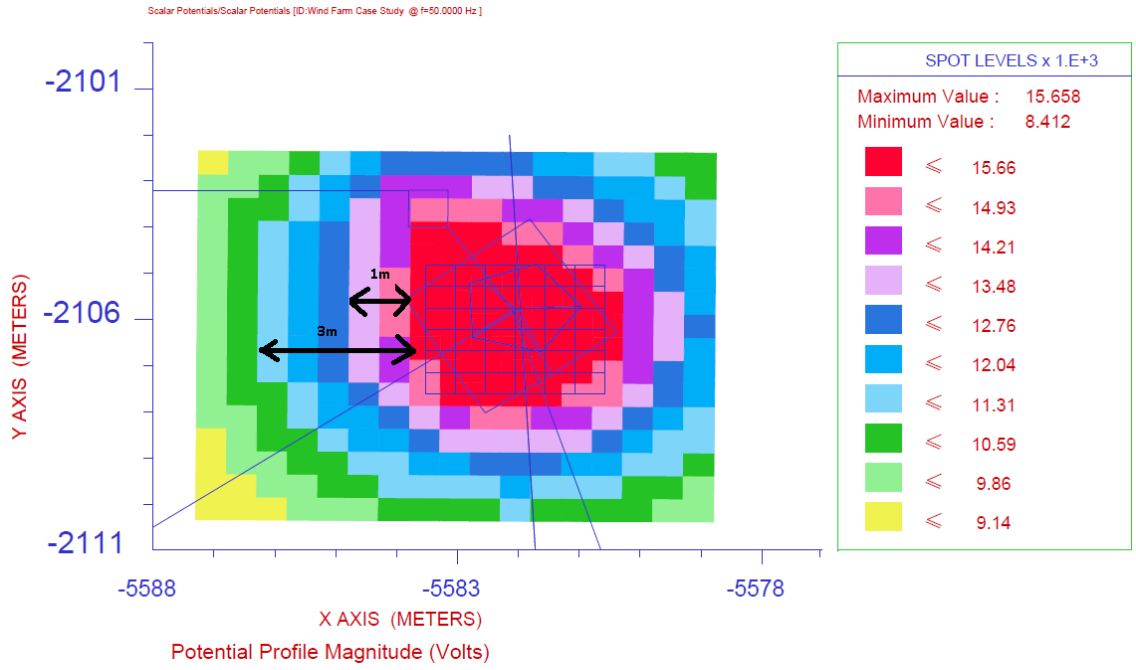

Figure 3-40: Wind turbine soil voltage zoomed (voltages in kV).

Figure 3-41: Wind turbine base (courtesy of Aurecon).

The step-up substation earth grid EPR and soil voltage profile are presented in Figure 3-42. The simulation results indicate that a portion of the fault current will return via cable screens to the main substation.

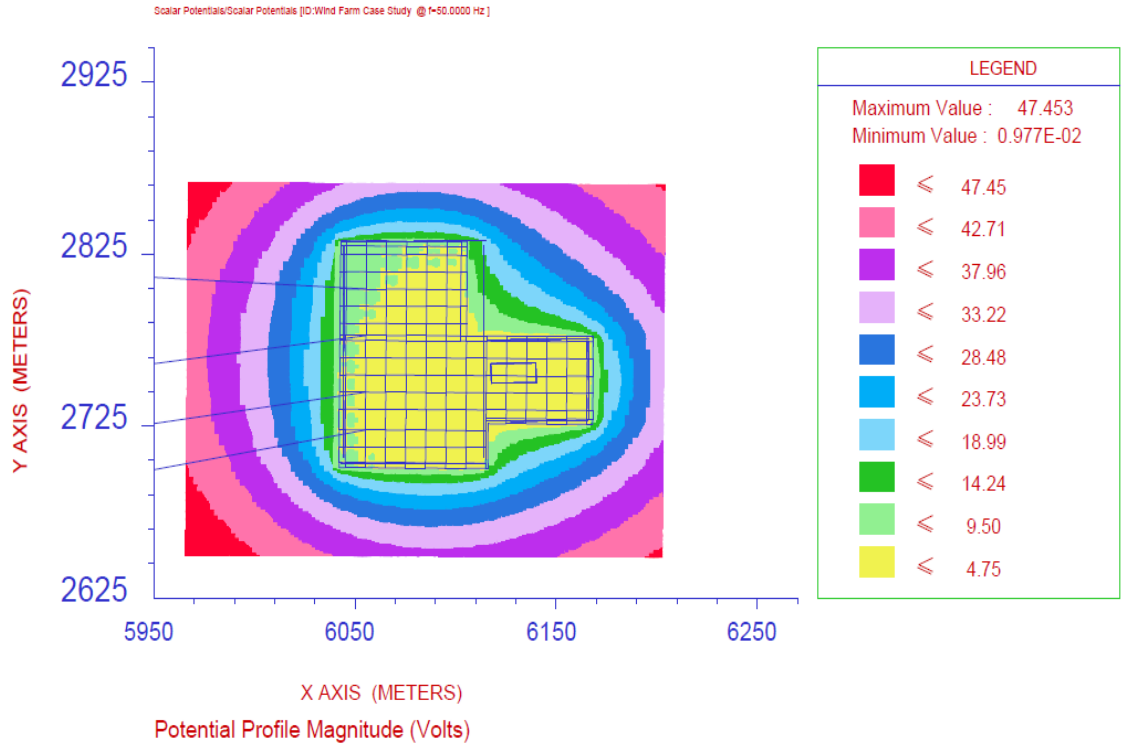

Figure 3-42: Step-up substation soil voltage profile and EPR.

3.4.2.2 Earthing System Simulation

The above simulation indicates high earth potential rise during the earth fault. In this, it is proposed to run bare aluminium conductors along the 33 kV cable to improve the performance of wind farm earth grid and lower the total impedance of earthing system. Figure 3-43 shows the soil voltage profile of proposed solution. Figure 3-43, shows that by using additional bare conductors alongside the HV cables then the earth potential rise can be reduced significantly.

A current injection test on one of the wind turbines is explained in Section 3.4.3. This can be carried out to validate the simulation in Figure 3-43.

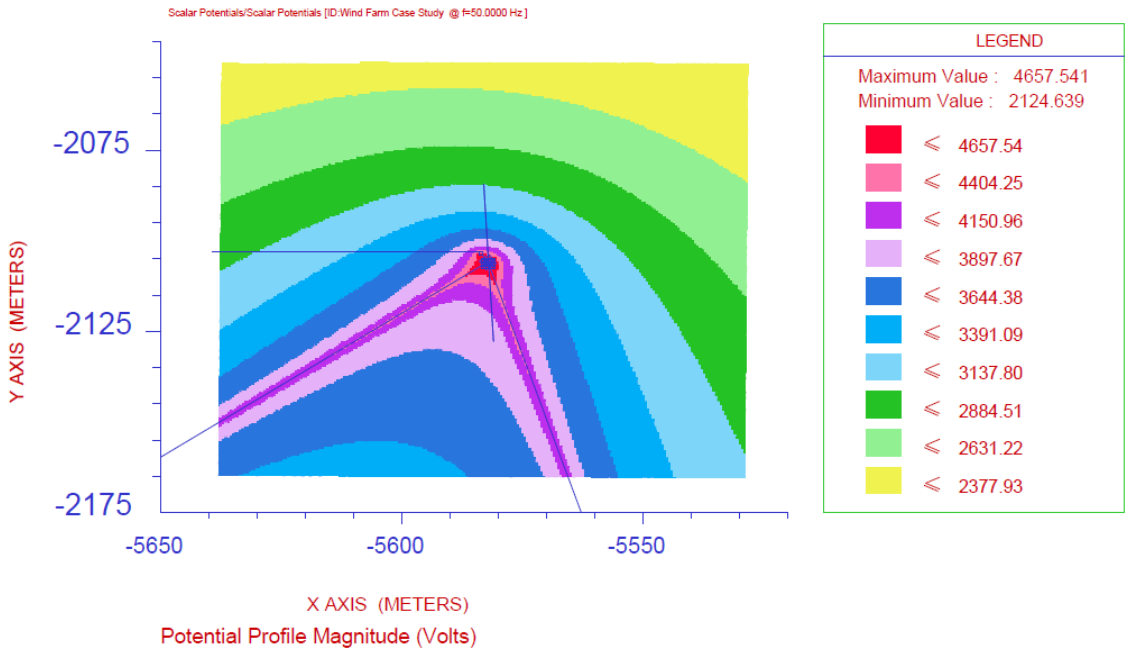

Figure 3-43: Wind turbine soil surface voltage profile during 33 kV earth fault.

3.4.3 Current Injection Test

The wind turbine earthing system requires testing to measure the prospective earth grid potential rise and impedance to validate the above simulation, together with step, touch and transfer potentials at wind turbine and the surrounding areas. Measurements of the distribution of current returning to the earth grid between cable screens and the general mass of the earth are included to determine wind turbine earth grid impedance.

In this research it is proposed to conduct the following tests:

- off-power-frequency injection; and
- High frequency (MHz) injection.

The IEEE Std 81– 2012 [26] method was proposed for 50 Hz current injection test. The major diagonal of the turbine earth grid is 6 m. Guidelines suggest that the remote current injection point should be at a distance of three to ten times the maximum diagonal of the earth grid under test, which would be 60 m in this case. The remote injection test is another wind turbine earthing system, approximately 200 m away from wind turbine under test.

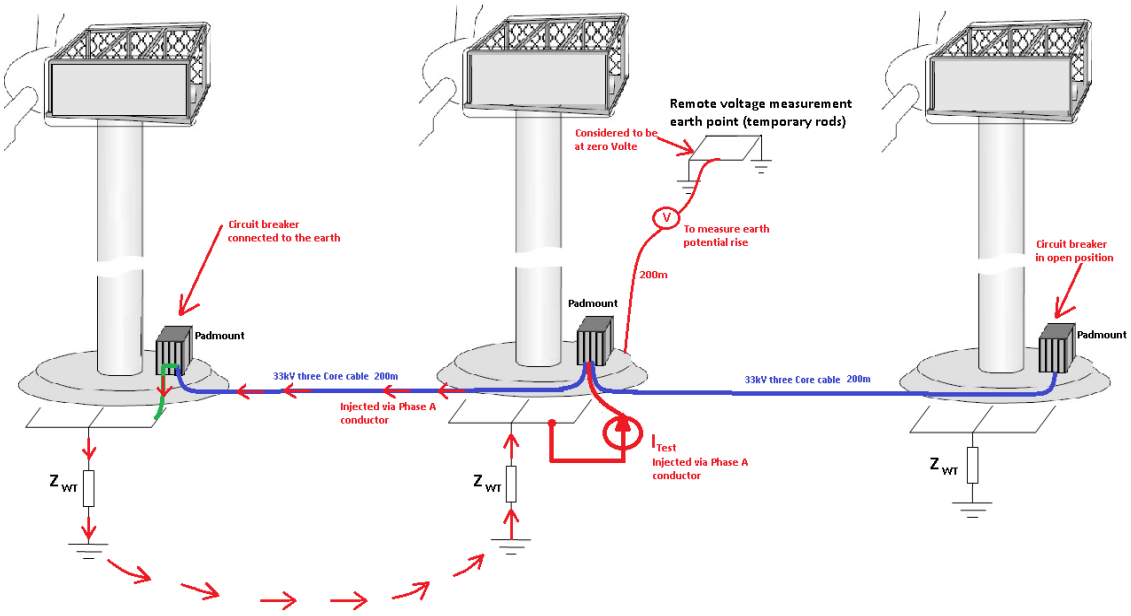

Figure 3-44: Wind turbine current injection test.

The wind turbines are in operation therefore the CIT can be conducted while two adjacent wind turbines are scheduled for maintenance. The CIT circuit is shown in Figure 3-44.

Sources of current injection could be either a signal generator plus power amplifier, a portable power generator, or an auxiliary matching transformer energized from a wind turbine low-voltage distribution board or portable power generator. The standard signal generator source allows test frequencies to range from 50 to 600 Hz with a current rating from 1 to 100 A but are restricted to the power system frequency or frequencies close to the power system (50 to 70 Hz).

Two or four temporary earth electrodes perpendicular to injection path with a 200 m distance can be used as remote earth location. Remote earth will be used as a reference point to measure the EPR of the test grid. A fall-of-potential test can be conducted to validate remote earth location.

The current level of 10 to 100 A can be used for CIT as per industry practice between two wind turbines with a suitable off-power-frequency such as 55 to 60 Hz. A Rogowski coil and frequency-selective multi-meter can be used to measure current distributions, including through the cable screens.

For high frequency tests the same CIT test circuit can be used with a Recurrent Surge Generator with a low voltage impulse generator (up to 90 V). The principle of operation of the recurrent surge generator is to discharge stabilised voltage via the charging control circuit. The firing and chopping times are adjusted with the two thyristors “surge” and “chop” in the timing control circuit. The entire event can be recorded with an oscilloscope as a stationary image and moved along the time base with the aid of the adjustable trigger signal.

A current injection test was proposed as part of this work which was rejected by the wind farm authorities and maintainer.

3.5 Conclusion

In this section, wind turbine earthing and lightning protection systems were discussed. The earthing and lightning protection of wind farms are not power quality aspects but can impact on the quality of the generated power with causing interruption, voltage dips and fluctuations.

To simulate earthing and lightning protection systems, a comprehensive discussion from soil resistivity testing, turbine foundation and surrounding soil response to high frequency lighting impulse and earth potential rise condition was presented.

A discussion about safe step and touch voltage for humans and farm animals is put forward.

3.6 Future Work

The lightning strikes have high frequency components as discussed. The high frequency electrical energy can change soil and earthing system characteristics and impedances which is not well known. Therefore, further research should be conducted on this subject. This research can be followed by site tests and measurements according to the current injection test circuit proposed in this work.

Chapter 4: Wind Farm Failures

In this section some of the practical issues which lead to wind turbine or wind farm failure and generation interruptions are presented. Presented issues can cause electrical faults; therefore, mitigating the hazard will improve the reliability of wind farms.

4.1 Power System Failure

In this section, the recent black-out event in South Australia (SA) which occurred at 16:18 on Wednesday 28 September 2016 is assessed. An AEMO preliminary report reflects that the South Australian region electrical supply consists of thermal (synchronous) generation, wind generation and imports energy during peak hours from Victoria region (another states) across both the Heywood Interconnector and Murraylink DC cable as shown in Figure 4-1 [51].

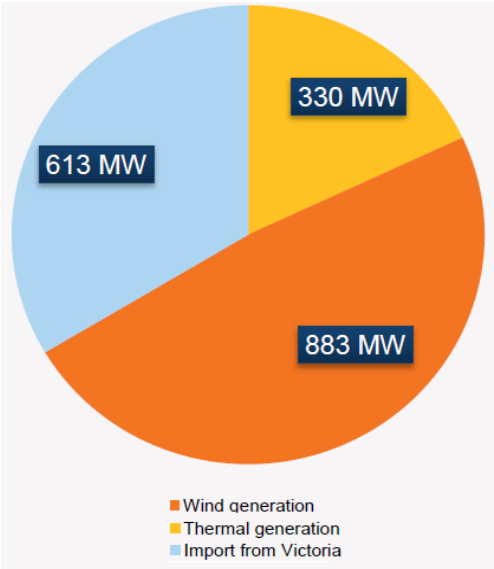

Figure 4-1: South Australia generation graph pre-event [51].

Prior to the black-out event, two main transmission lines were out of service; one of them is normally out of service but the second line was out due to a planned outage (scheduled maintenance). During the storm, the following events occurred which resulted in the state black-out:

1. Fault on a 66 kV feeder - No significant change in generation or load observed (at 16:16:46).
2. A two phase to ground fault on a 275 kV transmission line - No significant change in generation or load observed (at 16:17:33).

3. A single phase to ground fault on another 275 kV transmission line - No significant change in generation or load observed (at 16:17:59).
4. A single phase to ground fault on another 275 kV transmission line - No significant change in generation or load observed (at 16:18:08).
5. Wind farm outage due to wind gust - 123 MW reduction in power generation (at 16:18:09).
6. A single phase to ground fault on another 275 kV transmission line (at 16:18:13).
7. Another wind farm outage due to wind gust - 192 MW reduction in power generation (at 16:18:15).
8. Interconnection over load from 613MW to 850MW (at 16:18:15).
9. Supply lost to whole South Australia region (at 16:18:15).

Based on the AEMO report the above chain of events managed to result in SA state black-out in 90 seconds. Since 2007 National Electricity Rules (NER) requires generating units to remain on line for a Rate of Change of Frequency (RoCoF) of 1 Hz/s for 1 s as a minimum, and up to 4 Hz/s for 0.25 s. RoCoF must be maintained within this limit to prevent damage to generating units and effective operation of protection relays and emergency control schemes such as the automatic Under Frequency Load Shedding (UFLS) scheme [50].

The UFLS scheme in SA is designed to trip customer load to restore the balance of supply and demand following a non-credible event. The current UFLS design in SA is capable of restoring the balance of supply and demand when RoCoF is up to 3 Hz per second. The sudden loss of around 850–900 MW of supply to SA due to the tripping of the interconnector resulted in a rapid reduction in the power system frequency. AEMO analysis indicates that the RoCoF was between 6 and 7 Hz per second. Note that generating units are unable to operate, (and are not required to do so) where frequency is below 47 Hz [51]. It seems that the ‘voltage ride-through’ function of nine wind farms (of 13 refer to Figure 4-2) did not operate since there were six voltage disturbances in the system during the event. The ‘voltage ride-through’ settings were set to disconnect or reduce turbine output when between three and six ‘voltage ride-through’ events were detected within a given time frame [53]. The power flow and frequency are given in Figures 4-3 and 4-4 for this event.

Wind farm	Pre-set limit to ride-through events in 120 seconds	Number of times wind turbines activated ride-through mode	Last state of wind turbines prior to system voltage collapse	Output pre-event at 16:18:07 [MW]	Output just prior to separation at 16:18:15.4 [MW]
Canunda	9	1	Operational	27.7	27.2
Lake Bonney 1	5-9	0	Operational	77.7	76.5
Lake Bonney 2,3	9	0	Operational	171.9	158.7
Waterloo	9	5	Operational	96.6	72.9
				Expected MW Reduction	**38.6**
Clements Gap	2	3	Disconnected	14.5	-0.5
Hallett	2	3	Most turbines disconnected	34.5*	1.7*
Hallett Hill	2	3	Most turbines disconnected	41.3*	19.5*
Mt Millar	Not known	5	Stopped Operation	67.0**	2.8**
North Brown Hill	2	3	Most turbines disconnected	85.5	11.0
Hornsdale	5	6	Stopped Operation	83.9	-1.1
Snowtown North	5	6	Stopped Operation	65.5	-0.8
Snowtown South	5	6	Stopped Operation	42.1	-1.2
The Bluff	2	3	Most turbines disconnected	41.9	-0.3
				Unexpected MW Reduction	**445.1**
Total MW output				**850.1**	**366.4**
Total MW Loss					**483.7**

Figure 4-2: Wind farms voltage ride-through status [53].

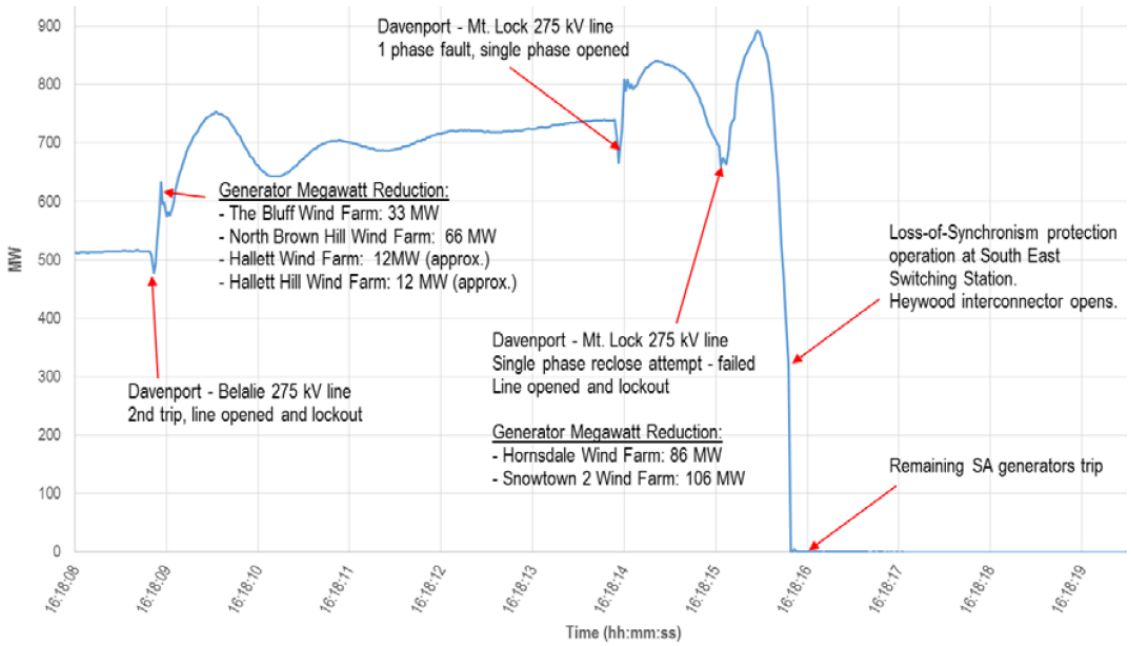

Figure 4-3: SA interconnection power flow record [51].

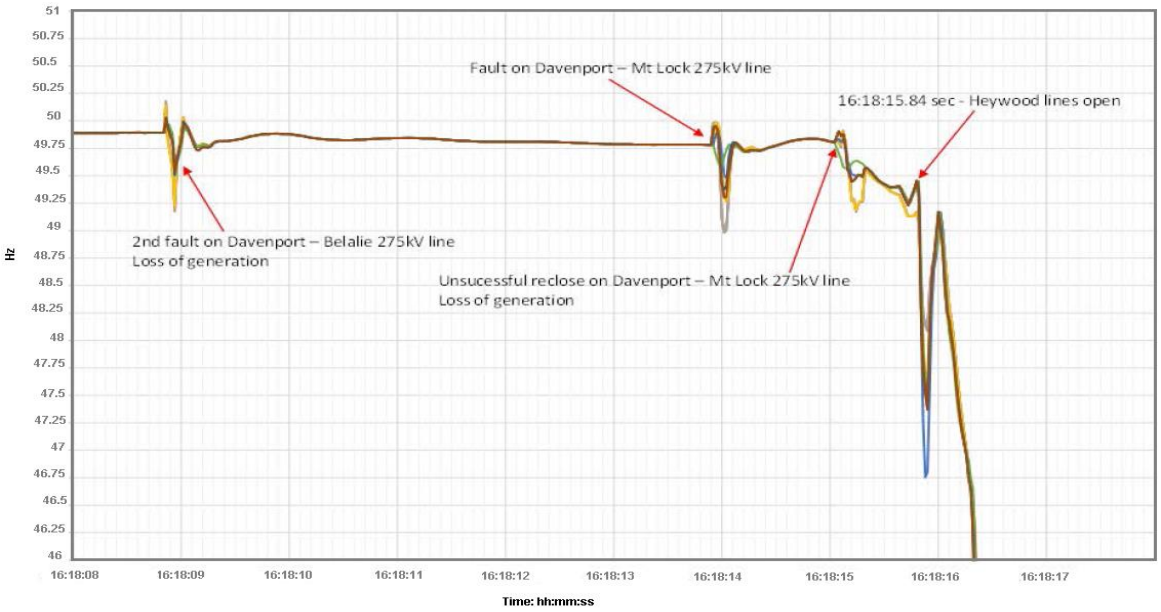

Figure 4-4: SA frequency record [51]

A simplified model of the above event is modelled in PSCAD/EMTDC as a part of this research. In this model, South Australia's power network parameters from National Transmission Network Development (2010 version) have been used and the impact of Events 4, 5 and 6 on the 132 kV network are simulated and voltage, active power curve and reactive power curve are presented in Figure 4-5.

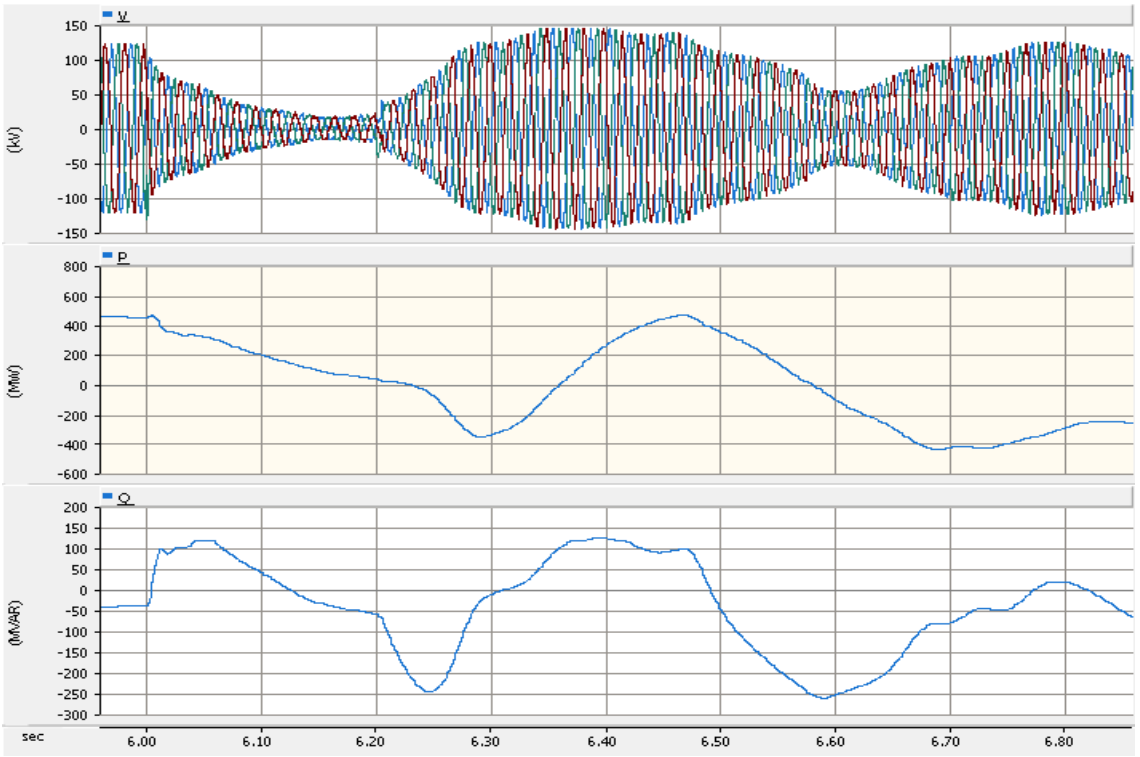

Figure 4-5: SA Black-out interconnection simulation.

4.2 Wind Farm D-VAR Failure

A dynamic Volt-Amp Reactive (D-VAR) compensation system is an industry practice to stabilize and regulate voltage and power factor on transmission and distribution networks during operations. The system detects and rapidly compensates for voltage disturbances by injecting leading or lagging reactive power at key points of transmission and distribution grids. Each D-VAR solution is tailored to meet specified requirements for each project such as wind farms.

Since the D-VAR operation is dependent on system real time condition, any modification on the system or D-VAR termination should be done with advanced planning. There was a failure alarm generated by D-VAR on one of the in-service wind farms in Australia and consequently the circuit breaker of the main step up transformer is tripped which impacts on the power quality of the wind farm at the 33 kV busbar as shown in Figure 4-6.

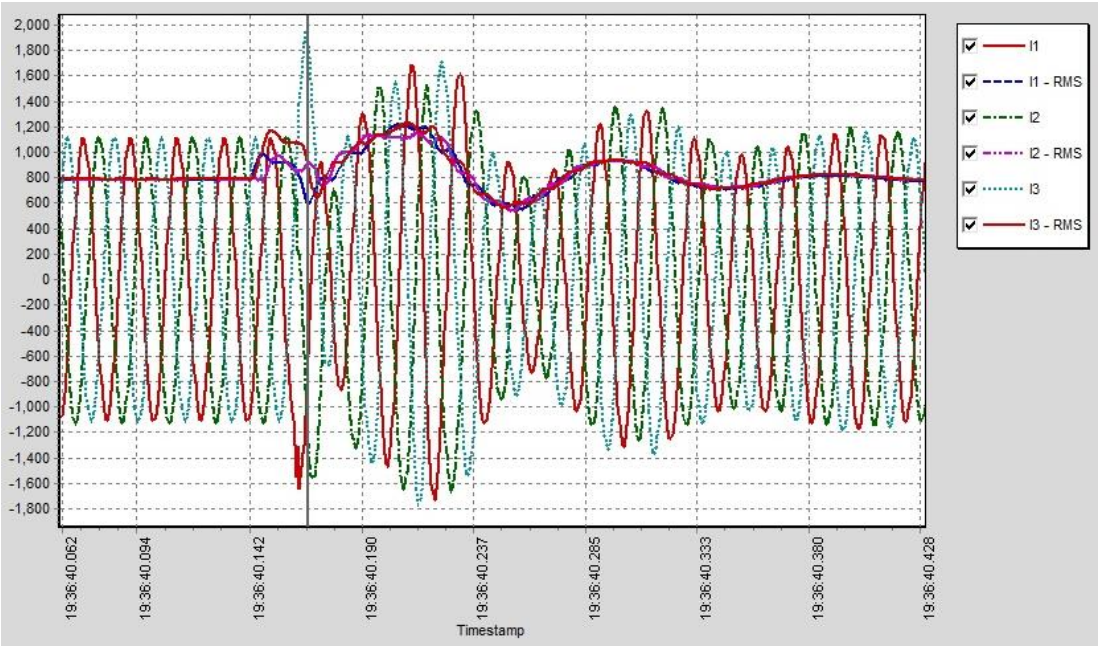

Figure 4-6: D-VAR nuisance operation record at 33 kV busbar (courtesy of Aurecon).

After investigation it is confirmed that a zigzag transformer had been taken out for maintenance. This caused a floating neutral connection at the D-VAR unit in the substation and results in D-VAR nuisance operation.

4.3 Mast Failure

Mechanical failure is a common issue in wind farms; therefore in this section of research some of the common points of failures are discussed. The first and most important mechanical aspect is the integrity of wind turbine design. The wind turbines should be designed to withstand the severe weather conditions, cyclones and storms. Figure 4-7 illustrates possible storm damage. This

shows a collapsed wind turbine due to a heavy storm on 14 January 2007 in the north of Hamburg, northern Germany.

Figure 4-7: Wind turbine mast failure (Photo: https://www.flickr.com/photos),

4.4 Blade Failure

The blades of wind turbines are normally subject to three common damage modes:

- Lightning strikes;
- Storm damage; and
- Birds.

4.5 Gearbox Failure

Gearboxes in wind turbines have a critical role in the process of conversion of mechanical power to electrical power. They are subject to different mechanical stresses during different wind conditions. Figures 4-8 displays some damaged gearboxes.

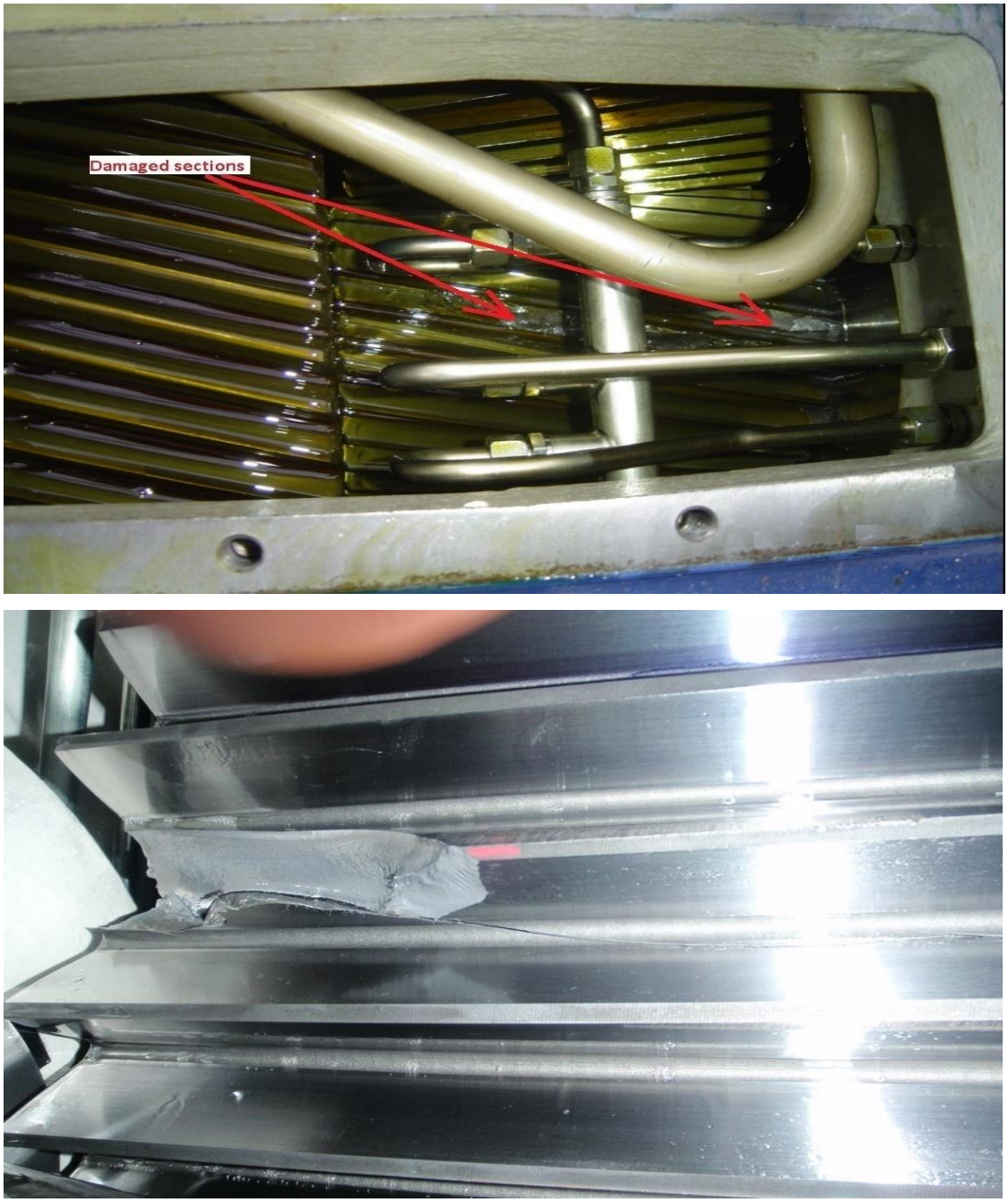

Figure 4-8: Damaged gearboxes (courtesy of Aurecon).

4.6 Generator Failure

4.6.1 Slip Ring Failure

The slip rings and brushes in synchronous and asynchronous generators are a common point of failure. Figure 4-10 represents a recorded failure in one of the in-service wind farms. Wind turbine operation and wind speed are shown in Figure 4-9, The generator failed at 20:48 and the wind speed was around 14m/s with generated power of around 1550 kW. Initial inspection revealed

burnt /melted rotor cable terminals interface to generator. The rotor cables have six current studs. The current studs were connected to the rotor windings with flexible cables. As shown in Figure 4-11, the rotor pig tail lugs failed at the soldered joint.

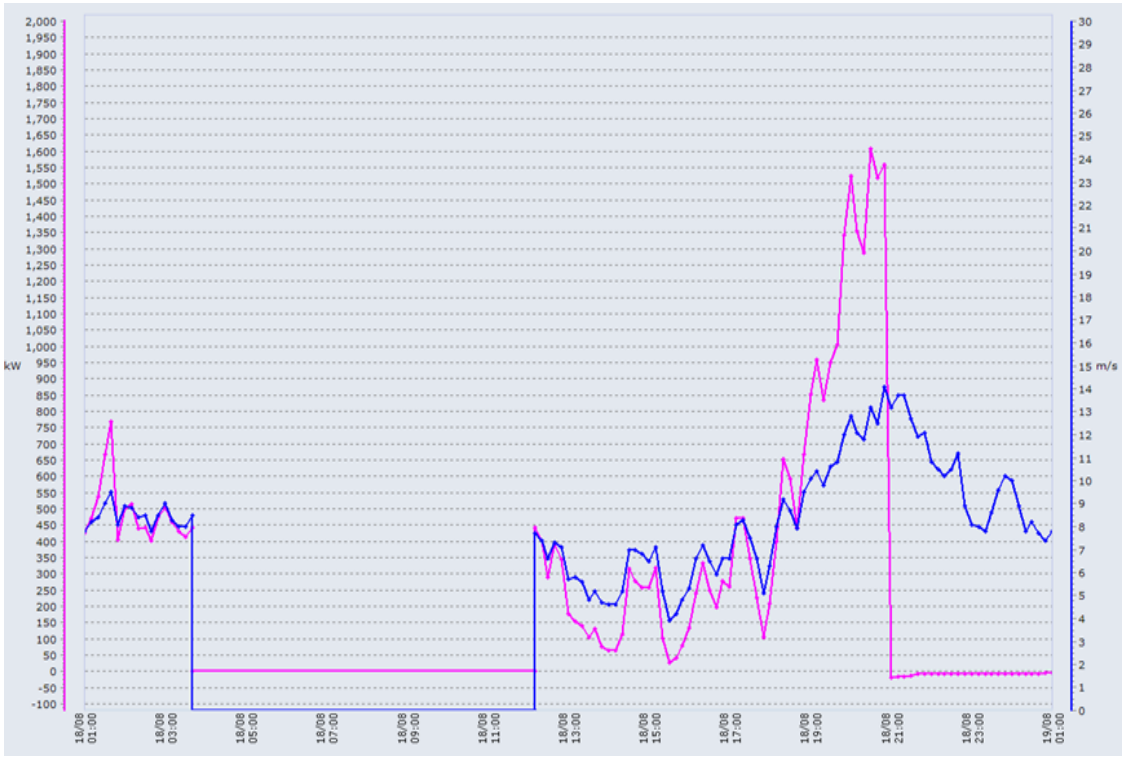

Figure 4-9: Wind speed records (courtesy of Aurecon).

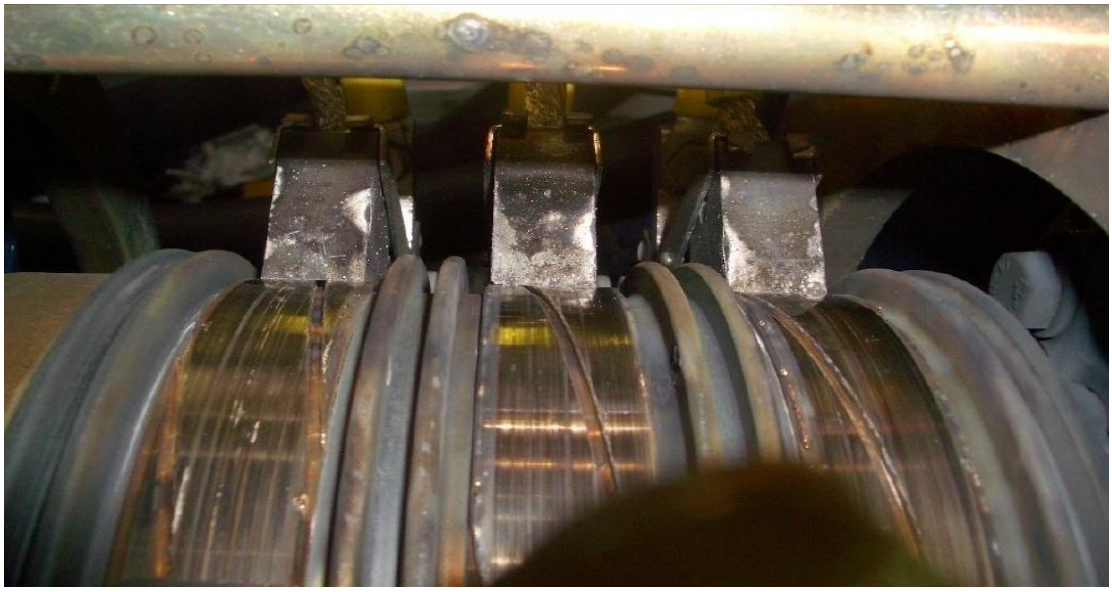

Figure 4-10: Slip ring and brushes after failure event (courtesy of Aurecon).

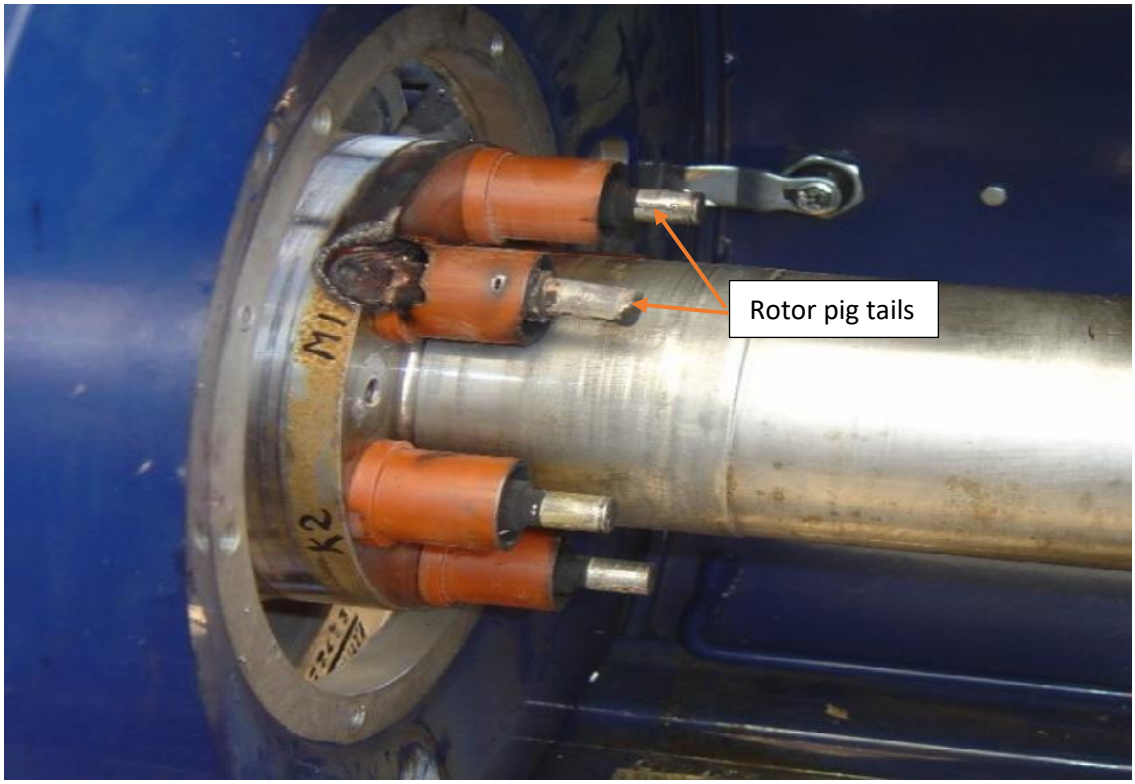

Figure 4-11: Slip ring and brushes after failure event (courtesy of Aurecon).

4.6.2 Stator Winding Failure

There have been several cases of asynchronous generator stator winding failures. Turbine manufactures have investigated these issue. The root cause analysis was to identify and investigate the reasons for the magnetic slot wedge dislodgement resulting in the failures. The magnetic slot wedges get dislodged from the wedge groove in the slot. These then migrate and come into contact with the spinning rotor and become heated. The heat from the wedges burns away the insulation of the stator coils resulting in an earth fault and failure of the generator.

Manufacturer investigations indicated that the reddish-brown dust surrounding the loose wedges was as a result of fretting. Fretting can only occur if the wedge is already loose. The loosening of the wedge is most likely related to lack/loss of adhesion along the wedge/core interface and/or inadequate back pressure from the coils and spacer. As shown in Figure 4-12 corrosion appears in the areas with incomplete corrosion protection from the resin and around the loose wedges as a result of released metal particles.

The analysis into the wedge design revealed that the wedge strength was adequate to withstand the magnetic forces acting on them. Lack of resin penetration and retention in the wedge groove was observed by tap testing all wedges along the entire length of a failed stator. The field solution

was to apply two additional coats of resin over the entire inner surface of the existing stator core to ensure bonding of the wedge in the wedge groove and thereby preventing dislodgement.

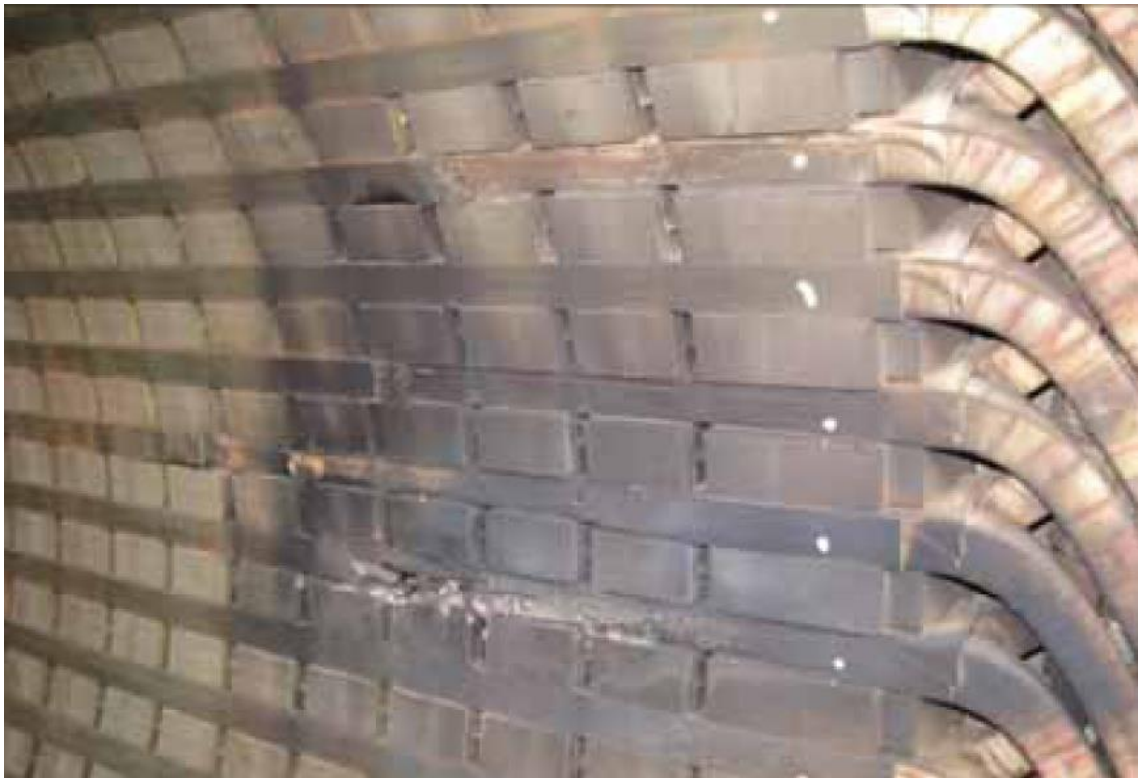

Figure 4-12: Stator winding has an earth fault just below the slot wedge (courtesy of Aurecon).

The bonding strength was verified by the maintenance team conducting destructive testing and Highly Accelerated Life Cycle Tests. The stator winding with proposed "field solution applied" is subject to a hot and cold temperature and humidity cycle. The temperature and humidity conditions are more severe than in the field to accelerate the impact. This is carried out on stator windings both with and without the field solution. The stator was subject to 21 days (126 hot and cold cycles) of environmental tests.

4.7 Transformer Failure

Normally wind turbines have a transformer to step-up generated power (normally from 690 V) to the distribution system voltage level (22 kV or 33 kV). The following failure cases presented here are based on real cases. Lessons can be learnt by industry from these failures.

Case 1: After receiving a short circuit fault from an in-service turbine, the base transformer investigation indicated that the HV winding of a transformer had failed (Figure 4-13). Once the failed HV-coil was observed, foreign material could be seen between two single windings (Figure 4-14). This foreign material is a spacer. It was used to keep the required distances between the

single windings during preparation of the coil for casting. Unfortunately, the block had not been removed before doing the casting.

Figure 4-13: 690 V / 33 kV transformer failed HV coil (courtesy of Aurecon).

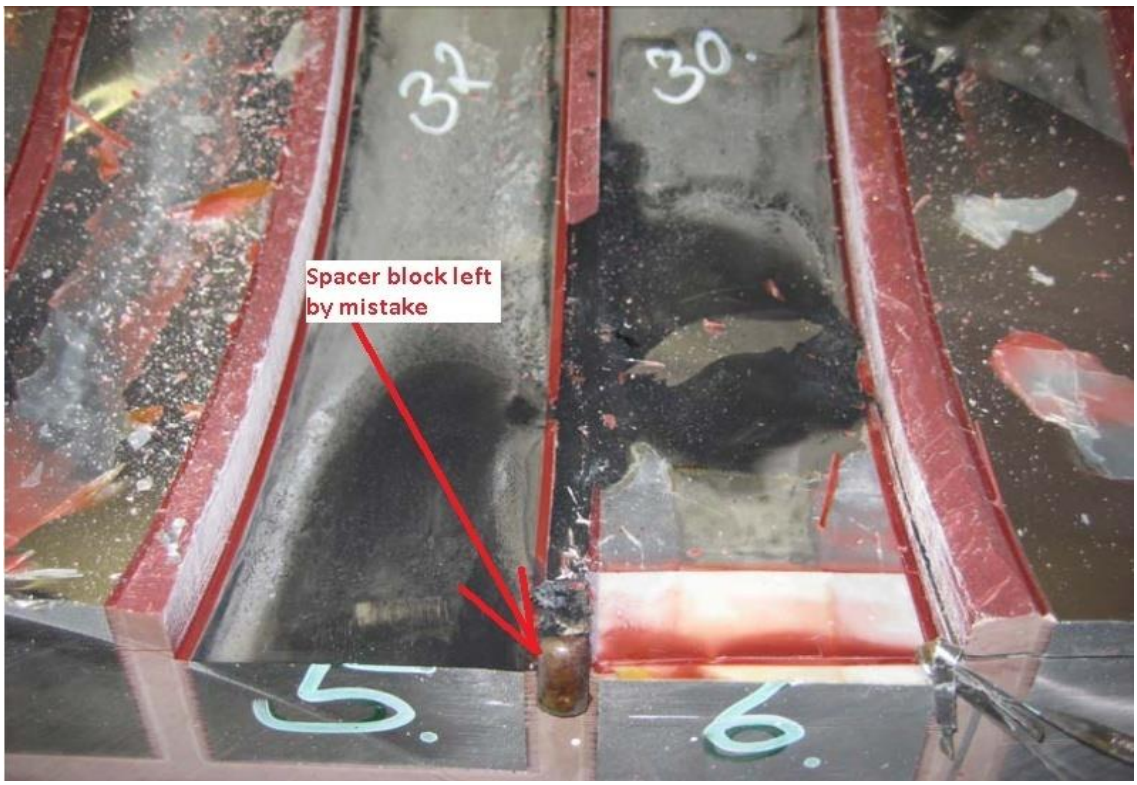

Figure 4-14: Damages in both single 33 kV windings beside the foreign material (courtesy of Aurecon).

Case 2: In this case a wind turbine transformer was energised and failed, reportedly after 10 minutes of operation. Failure was detected visually. A puff of smoke appeared from a pressure relief valve accompanied by a dark oily compound. Damage was judged to be too serious for a site repair and the transformer was returned to factory.

After stripping the transformer, it was noted that the oil was black, full of carbon particles. All insulation was contaminated. Inner surfaces were covered by granules of melted aluminium. Parts of the winding were burnt. This faulty portion was on the A phase and on the inner part of the coil which is the physical start of the winding, under the inner loop. This is shown in Figure 4-15.

Figure 4-15: Damages in 33kV windings failure on the knee of interconnected star leg (courtesy of Aurecon).

It appears that internal gasses released from the winding tend to collect under the yoke which did not react during the 52 kV site test. However, after energization the electrical stress and internal discharge shift bubbles damaged the electrical insulation strength of winding which resulted in a heavy partial discharge.

4.8 HV Cable Failure

It is a common practice to use 22 kV or 33 kV distribution systems with aluminium cables for wind farms due to the nature of wind farms with several hundred meters distance between turbines. One of the common failure points are the cable joints. An example of cable joint failure is shown in Figure 4-16.

Figure 4-16: Three core 33kV cable joint failure (before and after) (courtesy of Aurecon).

A failure shown in Figure 4-16 can create a system unbalance, voltage sags, and depending on the location of the failure, it can result in a major interruption. Another lesson learnt which can be included in this research is that the inline joint, as shown in Figure 4-16, should not be used in wind farms since the failure of one joint will result in failure in two joints. This is because some parts of the cable should be removed resulting in shorter length. Each cable joint should have a jointing bay similar to Figure 4-17.

As shown in Figure 4-17, in the case of cable failure, a cable loop can be used to recover the lost section.

Figure 4-17: Three core 33 kV cable joint bay (courtesy of Aurecon).

4.9 Termination Failure

Cable termination in the underground to overhead installation is always subject to lightning impulse damage. If the lightning discharge occurs nearby a termination point, the result will be similar to Figure 4-18.

In this situation the discharged cloud-to-ground energy will punch through the insulation. Lightning protection masts and shielding wire can be used if the damage becomes frequent as some locations are hot spots for discharge paths. In Figure 4-18 all three phases (2 conductors per phase) were damaged.

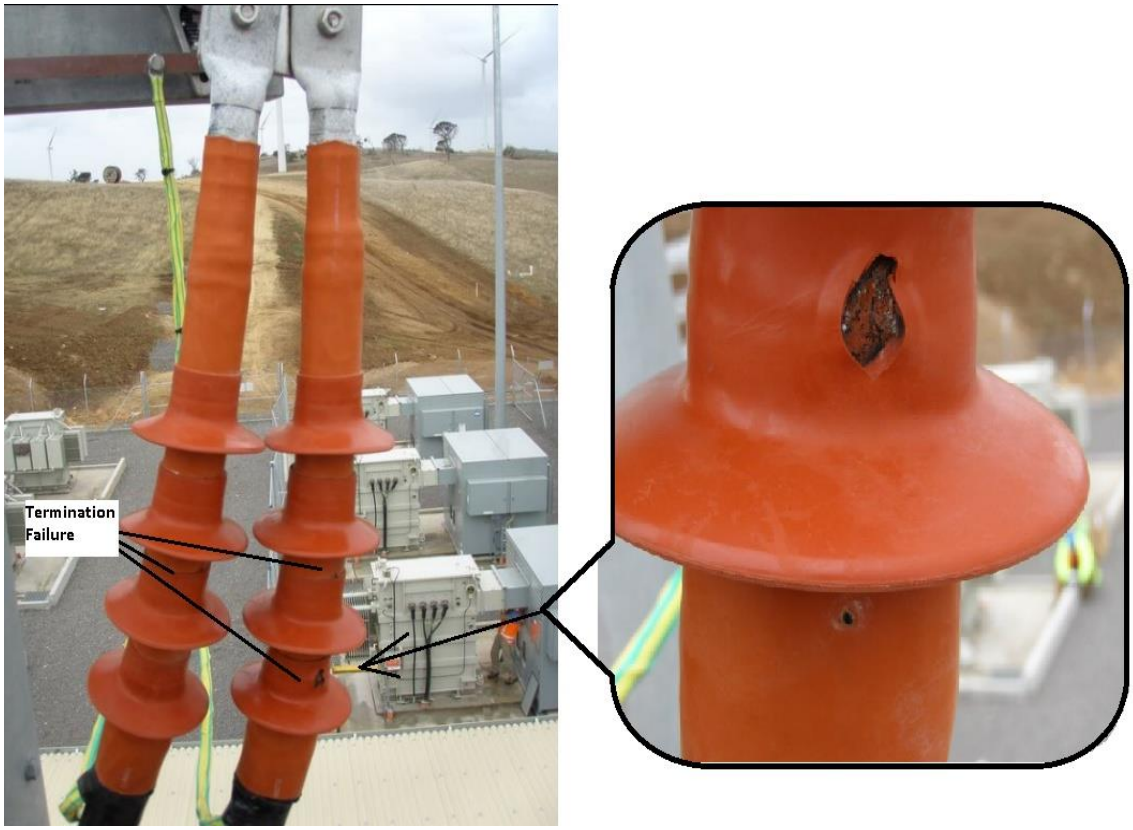

Figure 4-18: 33kV cable Termination failure due to lightning (courtesy of Aurecon).

4.10 Capacitor Bank Failure

An event record showed that a D-VAR unit in one of the wind turbines was attempting to remove the capacitor bank at the time of the fault. It appears that the D-VAR inverter outputs were transitioning from a high inductive command to a low capacitive command at the time of the fault. Event files recorded by the D-VAR indicate that the capacitor bank failure appeared due to the inability of the dynamic switch to affectively isolate the capacitor bank during the opening transient. The event resulted in the failure of six capacitor cans and the neutral CT of the affected bank. Two additional capacitors have suffered mechanical damage as a result of initial damage. This is shown in Figure 4-19.

Figure 4-19: Capacitor bank failure (courtesy of Aurecon).

4.11 Conclusion

In this chapter several actual failure cases are discussed. The above cases indicate that there is room for improvement of wind farm components, specifically during the design. Power system study and transient analysis is crucial to wind farm and power system design.

Based on discussion provided in Section 4.1, wind farm power outages due to storms or extreme high speed wind is unavoidable but their outage should not result in a major black out. Some methods such as high speed hybrid emergency power generation system with energy storage and gas turbine units can be used to recover loss of wind farms.

This section also presented some workmanship issues which can be taken as a lesson learnt by the industry.

4.12 Future Work

As mentioned in this section there are good opportunities to improve wind farms and their power system. Some critical components such as D-VAR units and harmonic filters and operational algorithms can improve. High speed hybrid emergency power generation system with energy storage and gas turbine units can be used to increase system reliability. The 'voltage ride-through' settings can also be improved with adding a dynamic simulation response to disconnect or reduce turbine output of wind turbines.

Chapter 5: Conclusions

In this chapter the work carried out in this study on power quality aspects of wind farms are assessed.

The impact of cable or transmission line installation and other components have been discussed through the project. It is demonstrated that manual calculation can be used by consideration of the positive and negative Sequence impedances of the cable in order to validate the developed models and load flow simulation. These can be used as a validation method for future research studies or actual wind farm design.

The validated model was used and behaviour of the wind turbines under steady-state and transient condition were assessed. The excitation voltage of a DFIG doubly-fed generator configuration (Type 3) and asynchronous generator with external variable resistor generator (Type 2) were simulated for different operational scenarios. Simulation results indicate that during significant network load variation the voltage and frequency of the point of common coupling (PCC) can change due to the DFIG generator dynamic response.

Future general harmonic emission limit for wind farms will be defined by AEMO or NSP. Based on simulation, generated wind farm harmonics from a 2MW asynchronous generator with external variable resistor (Type 2 with the harmonic characteristics presented in the work) will be higher than a similar wind farm with the same size of DFIG.

In this research a manual flicker calculation method was proposed according to the IEC standard method. The sequence and method of calculation has not been presented in similar research or guideline. The flicker simulation results indicate that the generated flicker, when all the 2MW Case Study 2 wind turbines start at the same time at the cut-in wind speed, is not acceptable according to the IEC and local service provider standards.

The wind turbine, wind farm and high voltage network responses during switching, steady-state operation and fault location scenarios were presented in the ferroresonance assessment and the simulation plots presented accordingly. Each component (turbine, wind farm substation and nearby transmission) was assessed in term of its transient behaviour. This can be used for protection system design and current transformer (CT), and capacitor voltage transformer (CVT) saturation studies. It was reported that the implication of ferroresonance include problems in protection systems, overheating in transformers and reactors, and excessive sound. Some of these effects could lead to equipment explosion. It can also cause thermal overloading in insulators as well as problems in transmission and distribution systems [54].

Simulation result indicates that ferroresonance occurs for certain system configurations. Therefore, to avoid experiencing the ferroresonance phenomenon in a wind farm grid, similar simulations are recommended at the wind farm design stage.

References

[1] IEEE Std 519:2014, “Recommended Practice and Requirements for Harmonic Control in Electric Power Systems”, 11 June 2014.

[2] Standard: AS/NZS 61000.3.6:2001, “Electromagnetic compatibility (EMC) – Limits – Assessment of emission limits for distorting loads in MV and HV power systems”, (IEC 61000-3-6:1996), 2001.

[3] Standard: AS/NZS 61000.3.7:2001, “Electromagnetic compatibility (EMC) – Limits – Assessment of emission limits for fluctuating loads in MV and HV power systems”, (IEC 61000-3-7:1996, MOD), 2001.

[4] Standard: IEC/TR 61000-3-13-2008, “Electromagnetic compatibility (EMC) - Part 3-13: Limits – Assessment of emission limits for the connection of unbalanced installations to MV, HV and EHV power systems’, 2008.

[5] HB 264-2003, “Power quality – Recommendations for the application of AS/NZS 61000.3.6 and AS/NZS 61000.3.7”, Standards Australia International, 2003.

[6] S. Heier, “Integration of Wind Energy Conversion Systems”, 2nd Edition, John Wiley & Sons, April 2006

[7] M. Leporace, “Harmonic Design Considerations”, GE Consumer & Industrial, on-line publication, 2015.

[8] Standard: IEC 61400-12-1:2017, “Wind energy generation systems - Part 12-1: Power performance measurements of electricity producing wind turbines”, 2017.

[9] ABB Technical Application Papers No.13, “Wind power plants”, 10/2011

[10] P. W. Carlin, A. S. Laxson and E. B. Muljadi, “The History and State of the Art of Variable-Speed wind Turbine Technology”, NREL/TP-500-28607, National Renewable Energy Laboratory, Feb 2001.

[11] S. Muller, M. Deicke and R. W De Donker, “Doubly Fed Induction Generator systems for wind farms”, IEEE Industry Applications Magazine, vol. 8, no. 3, pp 26-33, 2002.

[12] A. A. Hussein and M. H. Ali, “Comparison among series compensators for transient stability enhancement of doubly fed induction generator based variable speed wind turbines”, IET Journal on Power Generation, vol. 10, no 1, pp 116-126, 2015

[13] J. Fletcher and J. Yang, “Introduction to Doubly-Fed Induction Generator for Wind Power Applications”, Paths to Sustainable Energy, Intech Open Access, Dec, 2010.

[14] U. Vargas and A. Ramirez, “Harmonic Domain Model of a Wind Turbine Generator for Steady-State Analysis”, North American Power Symposium (NAPS), 3-6 Oct. 2015.

[15] M. de Prada Gil, A. Sumper and O. Gomis-Bellmunt, “Modeling and control of a pitch-controlled variable-speed wind turbine driven by a DFIG with frequency control support in PSS/E”, IEEE Power Electronics and Machines in Wind Applications, 16-18 July 2012.

[16] C. S. Rawal and A. M. Mulla, “An AC-AC Converter for Doubly Fed Induction Generator Driven By Wind Turbine”, International Journal of Scientific and Research Publications, Volume 4, Issue 12, pp 1-7, Dec. 2014.

[17] H. El-Helw and A. Khaled, “Comparison Study Between two Dynamic Breaking Resistor Techniques in Protecting the Doubly Fed Induction Generator”, 12th International Conf. on Environment and Electrical Engineering, May 2013.

[18] K. Lima, Ã. Luna, E. H. Watanabe and P. Rodríguez, “Control strategy for the rotor side converter of a DFIG-WT under balanced voltage sag”, IEEE Power Electronics Conference, COBEP, Brazil, Nov. 2009.

[19] J. B. Ekanayake, L. Holdsworth, X.G. Wu, and N. Jenkins, “Dynamic Modeling of Doubly Fed Induction Generator Wind Turbines”, IEEE Transactions on Power Systems, vol. 18, no. 2, pp 803-809, May 2003

[20] A. Parsotam, “Fundamentals of calculation of earth potential rise in the underground power distribution cable network”, Companion Document to NZCCPTS Application Guide for Cable Sheath Bonding, 2003

[21] M. Leporace, “Harmonic Design Considerations”, GE Consumer & Industrial, on-line publication, 2015.

[22] S. Yu, K. Emami, T. Fernando, H. H. C. Iu and K. P. Wong, “State Estimation of Doubly Fed Induction Generator Wind Turbine in Complex Power Systems”, IEEE Transactions on Power Systems, vol. 31, no. 6, pp 4935-4944, 2016.

[23] A. Wang, S. Shu and Y. Wang “Dynamic Behaviour of DFIG during Asymmetrical Voltage Dips in a Coupled Simulation”, 18th International Conference on Electrical Machines and Systems (ICEMS), October 2015.

[24] P. P. Khera, “Applications of Zigzag Transformers to Reduce Harmonics in Distribution System”, IEEE Industry Applications Society Annual Meeting, 7-9 Oct. 1990.

[25] Standard: IEEE C57.3-2015, “IEEE Standard for Requirements, Terminology, and Test Procedures for Neutral Grounding Devices”, 2015.

[26] Standard guide: 81-2012, “IEEE Guide for Measuring Earth Resistivity, Ground Impedance, and Earth Surface Potentials of a Grounding System”, revision of IEEE Std 81-1983, 2012.

[27] Standard guide: IEEE 80-2013, “IEEE Guide for Safety in AC Substation Grounding”, revision of IEEE Std 80-2000, 2013.

[28] S. Schostan, K.-D. Dettmann, I. Purellku and D. Schulz, “Harmonics and powers of doubly fed induction generators at balanced sinusoidal voltages”, International School on Nonsinusoidal Currents and Compensation, 15-18 June 2010.

[29] D. P. Kothari, I. J. Nagrath, “Modern Power Systems Analysis”, third edition.

[30] National Electricity Rules Version 82, Australian Energy Market Commission (AEMC), July 2016

[31] Standard guide: Australian Energy Market Operator (AEMO), “Guidelines for the assessment of generator performance standards”, 20 Dec. 2011.

[32] Australian Energy Market Operator (AEMO), “Wind Turbine plant capabilities report, 2013 wind integration studies”, 2013

[33] Standard: TR IEC 61000.3.7:2012, “Electromagnetic compatibility (EMC) - Part 3.7: Limits for the connection of fluctuating installations to MV, HV and EHV power system”, Standards Australia 2012.

[34] Standard: IEC 61400-21:2001, “Wind Turbines – Part 21: Measurement and assessment of power quality characteristics of grid connected wind turbines”, 2001.

[35] K. Redondo, A. Lazkano, P. Saiz, J.J. Gutierrez, I. Azcarate and L.A. Leturiondo, “Influence of the Fictitious Grid on Flicker Assessment of Grid Connected Wind Turbine”, International Conference on Renewable Energies and Power Quality Bilbao (Spain), 20-22 March, 201.

[36] Standard: AS 3851-1991, “The calculation of short-circuit currents in three-phase a.c. systems”, Australian Standards 1991.

[37] N. Vilsboll, A. L. Pinegin, T. Fischer and J. Bugge “Analysis of Advantages of the Double Supply Machine with Variable Rotation Speed Application in Wind Energy Converters”, DEWI Magazine, no. 11, pp 50-59, Aug. 1997

[38] Standard: IEC 61800-3, Ed.2.0 (2004), “Adjustable speed electrical power drive systems, Part 3: EMC requirements and specific test methods”, 2004

[39] H. Nguyen-Thanh, “Improved Control of DFIG during Grid Voltage Distortion for Reduction of Current Harmonic Using PI-Fuzzy”, International Journal of Computer and Electrical Engineering, Jan. 2015

[40] I. C. Evans and M. J. Richards, “The Price of Poor Power Quality”, American Association of Drilling Engineers, AADE-11-NTCE-7, 2011.

[41] M. Bahramipanah, S. Afsharnia and A. Aslani, “A Study on Power System’s Transient Stability in Determination of the Appropriate Generator Type for Wind Turbines”, 10th International Conference on Environment and Electrical Engineering, 2011.

[42] Australian Energy Market Operator (AEMO), “Wind Integration: International Experience, WP2: Review of Grid Codes”, 2011.

[43] T. Blalock, R. Cummings and R. Bauer, “Frequency Response Initiative, Industry Advisory - Generator Governor Frequency Response”, North American Electric Reliability Coro. (NERC), on-line, April 2015.

[44] H. R. Chamorro, M. Ghandhari and R. Eriksson, “Wind Power Impact on Power System Frequency Response”, North American Power Symposium (NAPS), 22-24 Sept. 2013.

[45] H. Berndt, M. Hermann, H. D. Kreye, et al, “Transmission Code 2007, Network and System Rules of the German Transmission System Operators”, Verband der Netzbetreiber (VDN), 2007.

[46] Standard: IEC 61400-24:2002, “Wind turbine generator systems, Part 24: Lightning protection”, 2002.

[47] Standard: AS/NZS 1768:2007, “Lightning protection”, Australian/New Zealand Standards, 2007.

[48] Troels S. Sorensen et al, “The update of IEC 61400-24 Lightning protection of wind turbine”, 29th International conference on lightning protection, Uppsala, Sweden, 2008.

[49] P. Ferracci, “Ferroresonance”, Application Note, [online] Cahier Technique Merlin Gerinno. 190, 1998.

(http://www.schneider-electric.com/cahier_technique/en/pdf/ect190.pdf)

[50] Standard: IEC TS 60479-1:2007, “Effects of current on human beings and livestock – Part 1: General aspects”, 2007.

[51] AEMO SA “Preliminary Report – Black System Event in South Australia on 28 September 2016”, on line 5 Oct 2016

[52] AMSC, “Dynamic Volt-Amp Reactive (D-VAR®) Compensation Solution”, on-line, 2016.

[53] AEMO SA “Update Report – Black System Event in South Australia on 28 September 2016”, on line 19 Oct 2016.

[54] S. A. Khan, “Ferroresonance in Capacitive Voltage Transformer (CVT) Due To Breaker,” M. Phil Dissertation, Institute of Graduate Studies, University of Malaysia, Kuala Lumpur, 2015.

[55] Y. Yao, Y. Tan, M. Li, D. Wang and Feng Zhang, “Study on methods for solving the divergence of power flow with small impedance branches”, International Conference on Sustainable Power Generation and Supply, 6-7 April 2009.

[56] Standard: AS 60038:2012, “Standard Voltages”, Australian Standards, 2012.

Appendix A: Simulation Videos

This DVD has two videos showing developing simulations in time.

The first is for the GPR (same as EPR) rise for a wind turbine during a lightning strike. This is GPRAlongTurbineShaft.avi

The second is for the soil potential during a lightning strike. This is SoilPotentialAlongProfilesResponse.avi

Appendix B: List of Publications

The following papers have been published as part of this work:

[1] M. K. Siahpoosh, D. G. Dorrell and L. Li, “Ferroresonance assessment in a case study wind farm with 8 units of 2 MVA DFIG wind turbines,” International Conference on Electrical Machines and Drives (ICEMS), Sydney, 11-14 Aug. 2017.

[2] M. K. Siahpoosh, L. Li and D. G. Dorrell, “Wind Farm Grounding System Analysis,” IEEE Energy Conversion Conference and Exposition (ECCE), 1-5 Oct., 2017.